University of Nottingham Malaysia

Department of Mechanical, Materials and Manufacturing Engineering

Synthesis of Starch Nanocrystals with Natural Rubber Derivatives in Smart Rubber for Energy Storage

by

Tan Yi Wei

Thesis submitted to the University of Nottingham for the fulfillment

of the degree of Doctor of Philosophy

September 2024

Abstract

The ever-increasing human population has raised concerns about the need for environmentally friendly, sustainable and reliable energy storage system. Natural rubber (NR) is an elastomer which exhibits unique properties such as reversible deformation, excellent mechanical strength and large strain storage capacity rendering it as a promising prospect to be developed as a smart material with energy storage potential. However, a few drawbacks of NR for instance poor oil resistivity had raised the use of synthetic rubbers produced from petrochemicals that caused environmental and health issues. To counter this circumstance, the development of novel specialty natural rubber (SPNR) have been garnering tremendous interest due to the importance of green concept of rubber. However, the physical and mechanical characteristics of epoxidized natural rubber (ENR) and deproteinized natural rubber (DPNR) both belong to the class of SPNR fabricated in the form of rubber latex (RL) films are rarely investigated. This research work aims to analyse temperature-triggered biobased smart rubber with enhanced mechanical strength for energy storage application. More precisely, the emphasis of this research is to discover the compatibility of starch nanocrystals (SNC) as reinforcement nanofiller in NR and its derivatives such as ENR and DPNR for wide range of working temperatures. Moreover, the shape memory effect (SME) of SNC reinforced RL films is yet to be explored. Majority of the current research works related to smart materials are shape memory alloys and other electro-responsive material which are seldom 100% biodegradable and possessed less flexibility. From the engineering perspective, it is also crucial to analyse and demonstrate the feasibility of a novel material before any specific application. Therefore, the physical and mechanical characteristics, shape memory behaviour as well as evaluating the energy storage capability of the fabricated smart rubbers are presented in this research.

To this end, the research was divided into three objectives: (i) experimental investigations which included characterization of SNC, physical and mechanical characteristics of sulphur-cured rubber films and SNC reinforced rubber composite films (ii) evaluation of the shape memory behaviour of sulphur-cured rubber films and SNC reinforced rubber composite films (iii) quantifying and demonstrating the energy storage potential of rubber nanocomposite films. The optimized acid hydrolysis technique was adopted to synthesize SNC from native waxy maize starch while latex casting is used to fabricate the temperature triggered smart rubber films. A series of characterization works were done to the synthesized SNC, sulphur-cured rubber films and SNC reinforced rubber composite films. For the second objective, shape memory testing was performed with a special elongation device to quantify the shape fixity (S_f) and shape recovery (S_r) of the smart rubber films. The energy stored within the smart rubber was quantified by cyclic loading-unloading test and manual experiment was performed to demonstrate the energy storage capability of the rubber nanocomposite films by lifting a load which then concludes the third objective.

In characterization of SNC, the synthesized SNC was found to be well dispersed and possessed a spherical shape with nano-dimension determined through morphological study and particle size analyser. Native waxy maize starch and SNC showed a typical A-type crystalline structure with 35% and 44% of relative crystallinity respectively. In terms of thermal behaviour, SNC displayed higher endothermic temperature peak than native starch as SNC was found to have a higher degree of crystallinity. For sulphur-cured rubber films, the following results were observed: (i) the crosslink density and tensile stress were found to increase while elongation at break decreases with higher loading of sulphur, (ii) increasing content of sulphur resulted in a decrease of swelling percentage in toluene, (iii) the samples exhibited a trend of maintaining in glassy state below its glass transition temperature (T_g) with decreasing storage modulus while T_g of ENRLs-based rubber films is higher than its NRLs counterpart. As for SNC reinforced rubber composite films, (i) SNC is well dispersed in the rubber matrices (ii) crosslink density and tensile stress increased with SNC content while incorporation of SNC maintained the deformability of the rubber nanocomposites films, (iii) water and toluene

uptake of the rubber nanocomposites films were found to be in contrast with addition of SNC, (iv) comparable T_g was found in their respective RL types with incorporation of SNC, (v) two weight loss steps corresponding to degradation of SNC and rubber matrix were found from the thermogram.

For the second objective, in terms of shape memory behaviour, the most lightly crosslinked rubber films (0.2phr sulphur) was determined to exhibit the best overall SME. Therefore, all rubber nanocomposites films were crosslinked with 0.2 phr sulphur with varying SNC contents. The results suggested that incorporation of 8% SNC into the rubber composite films achieved S_f of the 93.3% while retained 100% S_r of the material. This outcome suggested that the rubber nanocomposite film is capable of storing strain at the elongated state which translated to the storage of certain amount of elastic deformation energy. Thus, from the findings of SME, third objective of the work investigate the energy storage potential of the rubber nanocomposite films. The greatest attained energy stored was calculated to be 20.91 MJ/m^3 while manual experiment showed that the smart rubber was able to perform work by lifting a load in the vertical direction which is similar to the application of one-way actuator. This fabricated smart rubber is expected to possess environmentally friendly green energy storage capabilities and can be considered as an option for future energy storage.

It can be concluded that the smart rubber fabricated in this study possessed high mechanical properties, excellent SME and green energy storage potential. The SME and energy stored during the deformation process can be harnessed in various ways, broadening its potential application across multiple fields including soft robotics, self-deployable structures, medical devices and implants as well as energy storing devices. In all of these applications, smart rubber enables not only shape transformation but also the storage and release of mechanical energy making them highly versatile for both mechanical tasks and energy management solutions across various industries.

Acknowledgement

First and foremost, I would like to express my greatest appreciation to my principal supervisor, Associate Professor Ir. Dr. Chai Ai Bao for her continuous guidance, technical supervision and insightful critiques throughout my research works. She is always being available for meetings and discussions whenever I encountered problems and complexity during my study. Her deep commitment to academic excellence, meticulous support and valuable suggestions in every stage of my project have significantly helped me on completing the thesis on time. I am equally thankful to my co-supervisors Associate Professor Dr. Tshai Kim Yeow, Associate Professor Dr. Ho Jee Hou both from the University of Nottingham Malaysia, Dr. Shamsul Kamaruddin from the Malaysian Rubber Board and Professor Dr. Andri Andriyana from Universiti Malaya for their constructive advice and comments that enhanced the quality of my work. I am totally grateful and could not have asked for a better supervision team for my PhD endeavour.

Besides, I would like to thank the technical staffs from the Faculty of Science and Engineering whose expertise in managing laboratory equipment for their assistance in the crucial data collection of my experiments. A special thanks to the Ministry of Higher Education Malaysia which provided me with financial support under the Fundamental Research Grant Scheme that covered all study related expenses during the period of my PhD journey.

Also to mention my deepest gratitude to my parents Mr Tan Ong Kiat and Ms Lau Chin Huey for their endless love, inspiration and encouragement that provided me with positivity to complete my study. Without their unwavering emotional support, it would have almost impossible for me to go through the entire study smoothly. Last but not least, not to forget the optimism imparted from my late grandmother Madam Chua Swee Geok who nurtured the never say no attitude and enthusiastic personality in my ownself. I would have never become who I am today without the aid of my family members. To all who have indirectly contributed in my research work, thank you very much.

List of Publications and Contributions

Journal

1. Y. W. Tan, A. B. Chai, K. Y. Tshai, J. H. Ho, S. Kamaruddin, and A. Andriyana, "Mechanical characteristics epoxidised natural rubber latex film," *AIP Conf. Proc.*, vol. 2925, no. 1, p. 020019, 2024, doi: 10.1063/5.0183151.

2. Y. W. Tan, A. B. Chai, K. Y. Tshai, J. H. Ho, S. Kamaruddin, and A. Andriyana, "Effectiveness of Starch Nanocrystals on Mechanical and Shape Memory Behaviour of Smart Rubber," *Int. J. Nanoelectron. Mater.*, vol. 17, no. June, pp. 61–68, Jun. 2024, doi: 10.58915/ijneam.v17iJune.836.

3. Y. W. Tan, A. B. Chai, K. Y. Tshai, J. H. Ho, S. Kamaruddin, and A. Andriyana, "Energy Storage Capacity of Shape Memory Natural Rubber Nanocomposite Films," in *Material Strength and Applied Mechanics*, IOS Press, 2024, pp. 277-283.

4. Y. W. Tan, A. B. Chai, K. Y. Tshai, J. H. Ho, S. Kamaruddin, and A. Andriyana, " Evaluation of Physical and Mechanical Characteristics of Specialty Natural Rubber Latex Films". Paper accepted to Scopus indexed journal.

5. Y. W. Tan, A. B. Chai, K. Y. Tshai, J. H. Ho, S. Kamaruddin, and A. Andriyana, "Evaluation of Energy Storage Potential within Rubber Nanocomposite Films". Paper submmited to *Journal of Rubber Research* and currently under review. Manuscript ID: JRUR-D-24-00082.

Conference

1. Yi Wei Tan, Ai Bao Chai, Kim Yeow Tshai, Jee Hou Ho, Shamsul Kamaruddin and Andri Andriyana. Mechanical characteristics epoxidized natural rubber latex film. Full paper was presented at Advanced Materials Characterization Techniques (AMCT 2022). Universiti Tun Hussein Onn Malaysia, Johor, Malaysia. Virtual Conference / 23 – 24 August 2022.

2. Yi Wei Tan, Ai Bao Chai, Kim Yeow Tshai, Jee Hou Ho, Shamsul Kamaruddin and Andri Andriyana. Physical and Mechanical Characteristics of Specialty Natural Rubber Latex Films. Full paper was presented at International Conference on X-Rays & Related Techniques in Research & Industry 2023 (ICXRI 2023), Universiti Teknologi Malaysia, Johor, Malaysia. 23 - 24 August 2023.

3. Yi Wei Tan, Ai Bao Chai, Kim Yeow Tshai, Jee Hou Ho, Shamsul Kamaruddin and Andri Andriyana. Effectiveness of Starch Nanocrystals on Mechanical and Shape Memory Behaviour of Smart Rubber. Full paper was presented at International Conference on Nanotechnology & Material Research (ICONMAR), Universiti Malaysia Perlis, Perlis, Malaysia. 9 – 10 October 2023.

Poster

1. Yi Wei Tan, Ai Bao Chai, Kim Yeow Tshai, Jee Hou Ho, Shamsul Kamaruddin and Andri Andriyana. Stretching the Boundaries: Enhancing Performance with Smart Rubber. Poster was presented in Postgraduate Showcase 2023, University of Nottingham Malaysia, Selangor, Malaysia. 20 July 2023.

2. Yi Wei Tan, Ai Bao Chai, Kim Yeow Tshai, Jee Hou Ho, Shamsul Kamaruddin and Andri Andriyana. Mechanical characteristics of Starch Nanocrystals Filled Specialty Natural Rubber Latex Nanocomposites. Poster was presented at International Conference on X-Rays & Related Techniques in Research & Industry 2023 (ICXRI 2023), Universiti Teknologi Malaysia, Johor, Malaysia. 23 – 24 August 2023.

Table of Contents

List of Tables

List of Figures

Nomenclature

List of Abbreviations

SMAs	shape memory alloys
SMPs	shape memory polymers
NR	natural rubber
ENR	epoxidized natural rubber
DPNR	deproteinized natural rubber
SPNR	specialty natural rubber
RL	rubber latexes
SMR	shape memory rubber
SMNR	shape memory natural rubber
T_g	glass transition temperature
SIC	strain induced crystallization
S_f	shape fixity
SME	shape memory effect
T_m	melting temperature
SNC	starch nanocrystals
NRL	natural rubber latex
ENRL25	epoxidized natural rubber latex 25
ENRL50	epoxidized natural rubber latex 50
DPNRL	deproteinized natural rubber latex
S_r	shape recovery
HANR	high ammonia rubber latex
PEG	polyethylene glycol
NBR	nitrile butadiene rubber
SBR	styrene butadiene rubber
CAGR	compound annual growth rate
HCL	hydrochloric acid
H_2SO_4	sulphuric acid
T_{trans}	transition temperature
T_m	melting temperature

IEA	International Energy Agency
IRENA	International Renewable Energy Agency
ESS	energy storage systems
TESS	thermal energy storage systems
MESS	mechanical energy storage systems
FESEM	Field Emission Scanning Electron Microscope
XRD	X-Ray Diffraction
DSC	Differential Scanning Calorimeter
TGA	Thermogravimetric Analysis
PSA	Particle Size Analysis
DMA	Dynamic Mechanical Analysis
TSC	total solid content
ZDBC	zinc dibutyl dithiocarbamate
ZnO	zinc oxide
SG	specific gravity
TU	toluene uptake
WU	water uptake
DTG	Differential Thermal Gravimetry
Log (E′)	logarithm of storage modulus
tan δ	tangent of the loss angle

List of Parameters

ε_i	initial strain
ε_f	fixed strain
ε_l	loading strain
ε_r	recovery strain
Y	yield of SNC
X_c	degree of crystallinity
A_c	area of crystalline region
A_a	area of amorphous region
E'	storage modulus
η	crosslink density

R	universal gas constant
T	absolute temperature
m_0	initial weight of the sample before any immersion
m_t	final weight of the sample after removing from toluene
E'_{25}	rubbery storage tensile modulus at 25 °C
b_1	base length of one side of the tan δ curve
b_2	base length of the other side of the tan δ curve
h	height of the individual trapezoid
ε_{stored}	stored strain
$E_{applied}$	applied energy
E_{stored}	stored energy
$E_{retract}$	elastic retraction energy
$E_{efficiency}$	energy storing efficiency
l_1	base length of one side from loading curve
l_2	base length of the other side from loading curve
l_3	base length of one side from unloading curve
l_4	base length of the other side from unloading curve
W	specific work output
m_1	mass of load
m_r	mass of rubber films
g	gravitational acceleration
d	lifted distance of load by rubber films
T_α	peak of temperature
I_α	magnitude of the tan δ peak
T_{on}	onset temperature
T_{50}	temperature at which 50% decomposition
T_p	peak degradation temperature

Chapter 1

1.0 Introduction

1.1 Research background

As reported by Bloomberg New Energy Finance, 137 GW/ 442GWh of new energy storage capacity will be added globally by the end of this decade to accommodate the ever-increasing energy output (Nsitem, 2024). Population growth, industrial advancement, technology development and economic upturn have led the demand for sustainable energy storage system. The growing demand for energy has caused environmental impacts such as global warming and climate changes, air pollution that affects health condition , and threats of water and soil contamination (Riffat SB, 2015; Guney and Tepe, 2017; Osman *et al.*, 2023). The effect can be clearly noticed by the increasing atmospheric carbon dioxide concentration of 360 ppm to 400 ppm between 1995 and 2015 (Heard *et al.*, 2017). Therefore, energy insecurity and environmental consciousness have motivated researchers to develop green, high abrasion and sustainable carbon-free energy storage system for improvement of this situation (Dehghani-Sanij *et al.*, 2019). Smart material as a family member that is listed in advanced materials are material that gives responses in controllable and reversible fashion to external stimuli such as pressure, temperature, electric field, light, or chemical substances can be an interesting option for energy storage application when their characteristics undergo reversible changes (KÖK *et al.*, 2019). In fact, a material that is able to response to its surrounding with outstanding mechanical properties presents a great opportunity for the development of smart material-based energy storage system.

The types of smart materials developed through previous research comprised of shape memory alloys (SMAs), shape memory polymers (SMPs), magneto-rheostatic fluid, piezoelectric, thermo-responsive, magneto-restrictive, chromic and pH-sensitive materials (Mishra, 2017; Bahl *et al.*, 2020; W. Wang *et al.*, 2023). SMAs are smart materials that have at least two different phases which can be transformed from one to another by changing temperature and stress. They are able to transform to certain shape and return to their original structure upon presence of external stimuli (Dye, 2015). Out of all of the SMAs, the most crucial discovery of SMA is nitinol alloy system which possesses great functionality and wide range of commercial purposes (Huang, 1998). SMAs possess several features such as thermoelasticity (Aydoɨdu *et al.*, 2016; Qader, Kök and Dağdelen, 2019), superelasticity (Santoro, Nicolay and Cangialosi, 2001; Ou *et al.*, 2023) and damping capacity (Van Humbeeck and Kustov, 2005; Pan and Cho, 2007). In these works, only specialty features of the developed SMAs were discussed. Moreover, other types of smart materials were being used in various applications such as actuators (Olabi and Grunwald, 2008; Crəciunescu and Ercuta, 2015; Spanner and Koc, 2016), aeronautical technology (Toozandehjani, 2018), intelligent textiles (Thakur, 2016; Júnior *et al.*, 2022)

and energy harvesting device (Cramm *et al.*, 2011; Davino, 2021; Ali *et al.*, 2023). Nonetheless, it is worth noting that the works focusing on fabrication of smart materials showed novel functionality, but research encompasses SMPs and the storage of energy are less common. Hence, the focus of this work will be on developing SMPs with enhanced properties while exploring its energy storage capabilities.

SMPs as a member of smart materials are an emerging class of intelligent polymer gained tremendous interest among researchers in recent years due to its possibility of innovative applications and mechanical functionality. SMPs are one of the most up and coming stimuli-responsive materials that have the ability to memorize a permanent (original) macroscopic shape, be manipulated and "settled" (fixed) to a temporary shape under certain condition of temperature and stress (Jahid, Hu and Zhuo, 2018; Zende, Ghase and Jamdar, 2023). Under the influence of thermal, electrical or environmental stimulus, it can then return to the original stress-free condition. SMPs particularly shape memory natural rubber (SMNR) were claimed to be a superior smart material to SMAs because of their relatively lower processing cost, greater efficiency, biodegradability and by far offering better mechanical properties (Barik and Rao, 2019). Due to their nature of being biodegradable, a more economical and effective after life treatment of SMPs can be offered without raising any environmental concerns.

Malaysia as the fifth or sixth largest producer of natural rubber (NR) globally has registered a record spike of RM 71 billion in total export at 2021, an increment of 46.3% when compared to the year before (Low, 2022). NR is an elastic polymer which has the ability to stretch several times from its original length without breaking while imparting excellent tensile strength. Owing to the excellent properties of rubber, the physical and mechanical characteristics of this material are crucial in developing final products for various applications. Extensive research have been done on evaluating the mechanical properties of NR (Schaefer, 2002; Sasitaran *et al.*, 2016). However, NR has low resistance towards oil penetrability which gives rise to the development of novel natural rubber derivatives such as epoxidized natural rubber (ENR) and deproteinized natural rubber (DPNR) to compete with synthetic rubber while maintaining its advantage of being biodegradable (Tanrattanakul *et al.*, 2003; Ramli *et al.*, 2022). These natural rubber derivatives also known as specialty natural rubber (SPNR) are potential candidates to replace synthetic rubber produced from petroleum that caused environmental and health issues (Musto, 2013). ENR is acclaimed to exhibit improved oil and gas permeability with enhanced toughness when compared with its predecessor NR (Zhu *et al.*, 2022). DPNR a kind of NR derivative with low extractable protein content and less smell of rubber is more commonly adopt in manufacturing hypoallergenic material (Ariyawiriyanan *et al.*, 2013). Nevertheless, ENR and DPNR are normally used in the form of dry rubber with many undiscovered product

applications at this point. The physical and mechanical characteristics of these SPNR in rubber latexes (RL) form are also very much unexplored.

With the concept of sustainability in mind, the emphasis should be laid on fabricating green smart materials with outstanding mechanical properties. Therefore, with the availability of biodegradable raw material and high resistance to crack growth at large deformation, the development of shape memory rubber (SMR) will be an interesting area to explore. The major benefits of shape memory SMNR are their exceptional capability of storing large strain, cold and mechanical energy (Heuwers *et al.*, 2013), generating mechanical stress when exposed to solvent vapour (Quitmann *et al.*, 2013), programmable under different environmental conditions (Quitmann *et al.*, 2014), triggerable under mechanical and chemical stimulus with discrete trigger range (Quitmann *et al.*, 2015) and tunable trigger temperature after programming (Heuwers *et al.*, 2012; Quitmann *et al.*, 2015). Despite the magnificent properties shown by SMNR, the development of this smart material is not common because of their low glass transition temperature (T_g) which proved to be an obstacle to induce SME at room temperature (Koerner *et al.*, 2004; Zhang *et al.*, 2009; Yin *et al.*, 2022).

SMR as one of the SMPs depends on strain induced crystallization (SIC) that occurs whenever cross-linked rubber is stretched to large deformation for shape memory behaviour (Reghunadhan *et al.*, 2021). Shape fixity (S_f) then quantifies the ability of a SMP to fix the temporary shape upon mechanical deformation when releasing the stretching force (Saadoun Al Azzawi, 2023). Under the influence of external stimuli, decrystallization occurs where permanent net-points of crosslinked rubber pull the rubber molecules back to their original shape. Recently, a few strategies have been developed to induce shape memory effect (SME) on rubber. Firstly, SIC in lightly crosslinked NR where crystals do not vanish after releasing the stretching force at room temperature (Heuwers *et al.*, 2013). Secondly, the blending of additives such as fatty acid soaps in NR compound to increase the melting temperature (T_m) of the rubber composite (Wee, Chai and Ho, 2017; Kow, Chai and Ho, 2020a, 2020c, 2020b). Thirdly, the increment of T_g in ENR by using novel curing and crosslinking agent (Zhang *et al.*, 2015; Zou *et al.*, 2023). However, in majority of the studies, only different fabrication methods to induce SME in SMR had been investigated. It can be noted that considerably minimum studies that explicitly deal with improving the mechanical properties while maintaining or enhancing the SME of SMR had been conducted.

SMPs especially SMR are well accepted as smart polymetric materials due to their intriguing characteristics for instance biocompatibility, large deformation and various fabrication methods (Rousseau, 2008). However, the major limitation of SMPs are their relatively low tensile strength and stiffness when compared with metal (Pradhan *et al.*, 2022). Incorporation of effective nanofillers has

been manifested to be the most conducive approach to overcome this concern because nanoparticles can be well dispersed in polymer matrices and develop strong physical interactions while serving as multi-functional netpoints (Wu *et al.*, 2019). A number of studies regarding mechanical properties of reinforced SMP nanocomposites are available (Sessini, Brox, *et al.*, 2018; Sessini, Navarro-Baena, *et al.*, 2018; Hassanzadeh-Aghdam, Ansari and Mahmoodi, 2019; Gopinath *et al.*, 2021; Kausar, 2022; Namathoti and Vakkalagadda, 2023). The unique benefits of shape memory polymer nanocomposites include their abilities to reform under an active drive at a specific trigger, ease of transport, and their lightning production capacity further validated their potential in solving problems in many applications.

In recent years, with increasing environmental awareness, replacement of conventional inorganic fillers like carbon black, silica and clay with nanoparticles synthesized from polysaccharides has been the topic for intensive research due to its nature of being totally biodegradable (Bel Haaj *et al.*, 2016). Starch nanocrystals (SNC) were formed as distinct crystalline platelets due to the disruption of semi-crystalline phase resulting from acid hydrolysis of amorphous region (LeCorre, Bras and Dufresne, 2011). The synthesized SNC had been incorporated into NR matrix for improvement of mechanical performance and barrier properties. It was revealed that the addition of SNC as reinforcement filler appeared to be an effective reinforcing agent for NR (Gao *et al.*, 2014; Rajisha *et al.*, 2014, 2015; Anand *et al.*, 2018). In spite of these efforts, there are minimum research works regarding the incorporation of SNC in rubber matrix for fabrication of SMR while evaluating its energy storage capability and mechanical properties. Moreover, the effect of adding SNC as filler in SPNR remained trivial at this point.

This research work can be regarded as first step towards integrated analysis of temperature triggered biobased smart rubbers with improved mechanical properties for energy storage application. Moreover, the emphasis of this research is to discover the compatibility of SNC as reinforcement nanoparticles in natural rubber latex (NRL), epoxidized natural rubber latex 25 (ENRL25), epoxidized natural rubber latex 50 (ENRL50) and deproteinized natural rubber latex (DPNRL) for wide range of working temperature to induce SME while observing its potential as novel energy storage system. For these purposes, a series of characterization techniques such as the determination of crosslink density, swelling behaviour, morphological analysis, tensile testing as well as mechanical and thermal behaviour were done to evaluate the physical and mechanical characteristics of the fabricated smart rubber films by latex casting method. A self-made elongation device is developed to quantify the SME such as S_f and shape recovery (S_r) under the determined working temperature. Furthermore, experimental analysis and manual demonstrations were undergone to quantify as well as demonstrating the energy storage capabilities of the smart rubbers.

1.2 Problem statement

Smart materials especially SMR have been a compelling material for research interest among researchers and industrialists due to its unique combination of mechanical flexibility, durability and shape memory properties. These attractive characteristics allow SMR to boost its appeal for prospective cutting-edge applications ranging from medical devices to robotics and energy storage. However, the development of SMR remains uncommon due to the extremely low T_g of rubber. Moreover, rubbery materials are commonly incorporated with fillers to enhance its mechanical strength as unfilled rubber matrix possessed relatively low tensile strength and stiffness. Lately, with raising environmental consciousness given by the rise of fossil fuel depletion and global warming it is essential to replace inorganic filler with green sustainable sources. SNC is an abundant polysaccharide that can be derived from many kinds of plants which could be used as a substitute for traditional fillers to enhance the mechanical properties of the rubber matrix. Several drawbacks of NR have encouraged the development of green SPNR such as ENR and DPNR that counter the limitations of NR. To date, information about the physical and mechanical characteristics of SPNR films as well as SNC reinforced rubber composites films remain largely unknown. Further to that, little to no work has been conducted to investigate the effectiveness of SNC on SME of the rubber nanocomposite films. The SME on rubber films is the fundamental attribute required for any energy storage within the smart rubbers. Additionally, quantification and demonstration of energy stored within the SMR should be done to provide critical insight and elemental understanding towards the future development of energy storing SMR over a wide array of potential applications.

1.3 Objectives

The objectives of the research works are summarized as below:

1. To synthesis and characterize SNC as well as evaluating the physical and mechanical characteristics of sulphur-cured rubber films and SNC reinforced rubber composites films.
2. To induce SME in sulphur-cured rubber films and investigate the effectiveness of SNC on SME of the rubber nanocomposite films.
3. To evaluate the energy storage potential of smart rubbers through experimental analysis and validates the energy stored within smart rubber through manual demonstration.

1.4 Layout of the thesis

The thesis is organized as follows: Chapter 1 provides an overview on the background and motivation of this research, while the objectives and scope of the work are also highlighted in this section. Chapter 2 presents a thorough literature review related to the work. This section begins with the general review of NR and its derivatives. Subsequently, the review focuses on rubber nanocomposite with emphasis towards the incorporation of SNC as nanofiller in NR. The research-related works including general aspects of SMP and development of SMR are also included. The chapter ends with the review on the potential of SMR as an energy storage alternative. Research methodology is described in Chapter 3. The materials involved, samples preparation, a series of characterization techniques, experimental procedures and design of the manual experiment are detailed in this section. The successfully synthesized SNC is characterized accordingly. Rubber films with and without the incorporation of SNC are evaluated on their physical and mechanical characteristics before investigating their shape memory behaviour. The shape memory result is obtained to show the energy storage potential of the rubber specimen. Experimental analysis and manual demonstration are done to evaluate the energy stored within the rubber films. Chapter 4 shows the results and discussion based on the data attained from the characterization and experimental works. Chapter 5 summarizes the outcomes of the current research work and suggests improvements as well as directions for future research.

1.5 Scope of the research

This thesis first focuses on the physical and mechanical characteristics of four different RL: NRL, ENRL25, ENRL50 and DPNRL with varying sulphur loading and SNC content. The morphological study, crosslink density, swelling characteristics, dynamic mechanical behaviour, mechanical properties and thermal stability are evaluated by conducting a series of characterization tests. The emphasis is then shifted to investigating the SME of the smart rubbers through performing thermomechanical test by using self-made elongation device. Special attention is given to SNC reinforced rubber composite films on shape memory behaviour and energy storage as these rubber nanocomposite films show improved mechanical properties. The experimental data is analyzed before conducting cyclic loading-unloading test to quantify the energy storage capacity of the smart rubbers. A self-designed manual demonstration is then done to validate the energy storage in smart rubber and make evident to potential practical application.

Chapter 2

2.0 Literature Review

This chapter provides background information for the entire thesis developed in the following chapters. The contents discussed in this chapter are as followed:

1. General overview of natural rubber and its derivatives
2. An overview of rubber nanocomposites with emphasis on the incorporation of starch nanocrystal as filler in natural rubber
3. General aspects of shape memory polymers with prominence of the development of shape memory rubber
4. Potential of shape memory rubber as energy storage alternative

2.1 General overview of natural rubber and its derivatives

2.1.1 Rubber as an elastomer

Rubber is an elastomer, a term that is commonly used to describe any material with rubber-like properties. Elastomer refers to any rubbery material consists of long chain polymers that have the capability to recover to their original shape after being stretched to a certain extent (Ibrahim, 2022). Therefore, elastomer is also defined as “elastic polymer”. Elastomeric materials are often structured with physical or lightly cross-linked chemical bonds (Owen, 2001). Physical cross-links are the interactions of coordination bonding, hydrogen bonding, ionic bonding or van der Waals forces (Wang, Guo and Sun, 2019). These cross-links are natural entanglement without the addition of any cross-linking agent. Under the presence of solvent or stimuli such as heating/cooling, physical cross-links can be reversibly dissociated and recombined (Oyama, 2014). Meanwhile, chemical cross-links are usually formed by covalent bonding. Chemical cross-linking is done by cross-linking of water-soluble polymers by irradiation and co-polymerization of a monomer with cross-linking agent (Wang, Guo and Sun, 2019). Therefore, rubber latex is often compounded with cross-linking agents such as sulphur to undergo vulcanization for improvement of mechanical properties. Permanent deformation will happen when stress is applied without the presence of cross-linkages. The effect of these processes on rubber will be discussed in Section 2.1.3.

Elastomer molecules can be categorized into glassy, crystalline or rubbery state according to the glass transition temperature, T_g of the material which is usually measured in terms of modulus or stiffness. The physical properties of an elastomer will be at the glassy or crystalline region at temperature below T_g and behave like a rubbery material at temperature above T_g (Ebnesajjad, 2016). As shown in Figure 2.1, rubber behaves like an amorphous material which has a defined rubber plateau

region above T_g that enables it to have considerable segmental motion. Elastic modulus is low for an elastomer when they are in amorphous state which is also frequently defined as glassy state (Özdemir, 2020). T_g of an elastomer is significantly lower than room temperature (-70 °C for NR and – 27 °C for ENR-50 (Sisanth *et al.*, 2017). Therefore, at room temperature rubber possesses the ability to regain its original length after stretching to several times when the applied stress is removed.

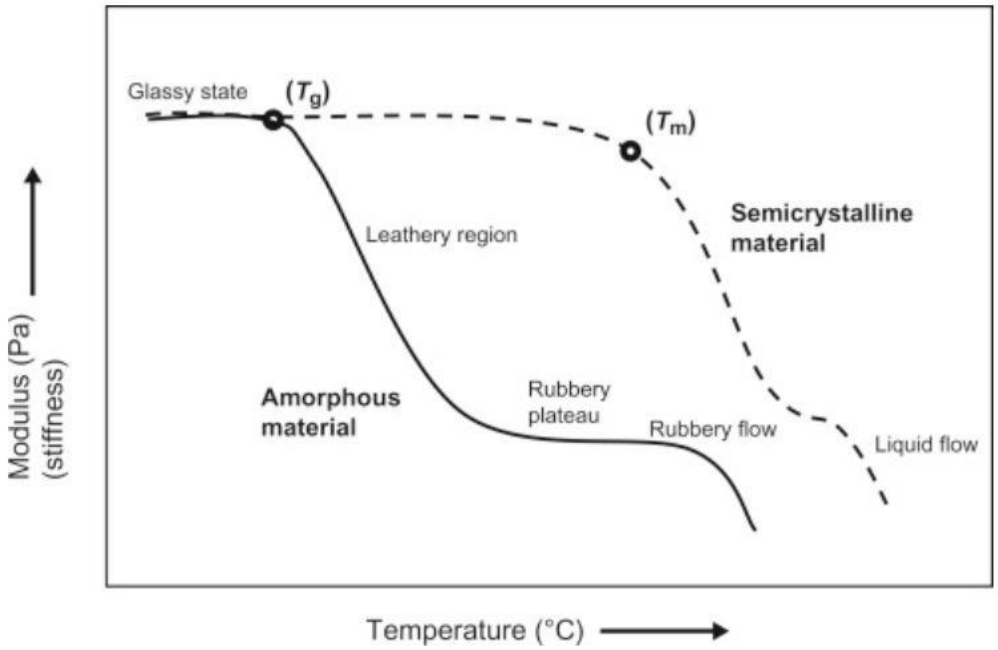

Figure 2.1: Modulus versus temperature plot for amorphous material (Shrivastava, 2018)

2.1.2 Introduction to natural rubber and its derivatives

2.1.2(a) Natural rubber (NR)

Natural rubber (NR) is a polymer produced from the milky liquid called latex of the rubber tree *Hevea Brasiliensis* (Heng and Joo, 2017). Latex is a milky white colloid that circulates in the latex vessels or barks of the rubber producing plant. The extraction process of latex known as “tapping” is done by making an incision into the bark of the rubber tree. Rubber tree is considered ready to harvest approximately 5-6 years from the date of planting while the economic life of a rubber tree is around 25-30 years (Krukanont and Prasertsan, 2004). South East Asia is the main producing region of NR with 92% of the global production due to its equatorial climate while Africa and Latin America with 6% and 2% respectively (Correa-Pinilla *et al.*, 2022). NR is a polymer mainly consisting of cis 1,4 polyisoprene as shown in Figure 2.2. Mechanically, NR is known for its ability to elongate several times without breaking, excellent tear resistance, high green and tensile strength due to the effect of SIC which set it apart from most synthetic rubbers (Schwartz, 2016). Therefore, NR can also be classified as an elastomer because of its capability to be stretched and recover to its original length. Upon compounding and vulcanization with chemicals such as sulphur, zinc oxide and accelerator, there will

be formation of crosslinks between the polymer chains of rubber molecules which improves the resistance, elasticity and tensile strength of NR (Bülbül, 2020). NR is often reinforced with filler for example carbon black to further improve its physical properties while also increasing the volume of rubber which proves to be an important step towards cost saving. Owing to the outstanding properties of NR, NR capitalizes the global rubber market with roughly 40% from the total rubber production (Shoji and Masui, 2015). NR has been widely used in the automotive and medical industry to produce car tires and gloves because of its low hysteresis properties and good abrasion resistance which is difficult to be replicated by synthetic rubber.

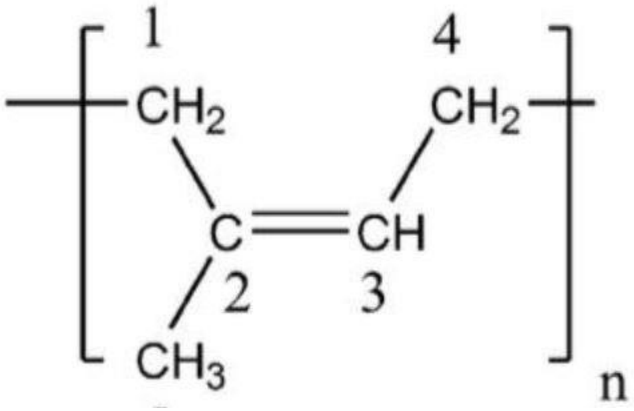

Figure 2.2: Chemical structure of NR

2.1.2(b) Epoxidized natural rubber (ENR)

Epoxidized natural rubber (ENR) is one form of the modified NR. Although NR has superior mechanical quality to most of the synthetic rubber, NR cannot compete with certain specialty synthetic rubber due to their low resistance towards oil penetrability and high gas permeability (Dieu *et al.*, 2023). Chemical modifying of NR is becoming popular to improve its stability towards these external factors. Epoxidation which produces ENR is done by establishing hydrophilic groups with regards to the isoprene backbone of NR. Synthesis of ENR involves the reaction between hydrogen peroxide and formic acid to form the in-situ performic acid. The epoxidation reaction then substitutes the C=C double bond in NR to structure the epoxy group and formic acid is the by-product (Fatimah Rubaizah *et al.*, 2018). Figure 2.3 shows the epoxidation reaction of NR. ENR has high oil resistance, low gas permeability properties and improved toughness when compare to its predecessor NR due to the presence of epoxy group randomly distributed along the isoprene backbone which increases its hydrophilicity as well as the reduced number of double bond (Zunic and Peter, 2018). Therefore, ENR has properties resembling synthetic rubber rather than NR. The three common ENRs available in the market are ENR-10, ENR-25 and ENR-50 which refers to the degree of epoxidation apropos of mole percent. For instance, 50% mole ENR will produce ENR-50. As the mole percent of epoxide level

increases, the properties of the rubber will shift from general elastomer to those of specialty elastomer (Wan, Chin and Saad, 2010). ENR-50 undergoes SIC like NR but with gas permeability similar to butyl rubbers and oil resistance comparable to medium acrylonitrile rubber (Baker and Gelling, 1989). ENR can be used in many applications where NR is needed with improved thermal, oil and gas resistances serve as a requirement. These applications include tires, the sole of footwear and adhesives.

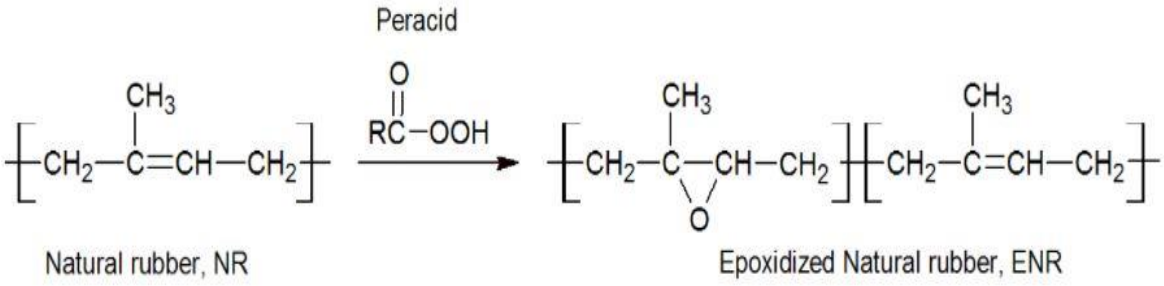

Figure 2.3: Epoxidation of NR

2.1.2(c) Deproteinized natural rubber (DPNR)

Deproteinized natural rubber (DPNR) is a type of NR derivative where the protein layer covering the rubber particles is removed. Investigations on DPNR are launched due to the issues of protein allergies caused by NR products especially gloves. Allergy reactions such as skin rashes, hives, flushing, itching and sinus symptoms were reported (Alenius, Turjanmaa and Palosuo, 2016). Studies suggested that the mean occurrence of latex allergy among individual in the healthcare industries, patients and general personnel worldwide are 9.7%, 7.2% and 4.3% respectively (Wu, McIntosh and Liu, 2016). The presence of non-rubber content particularly allergenic proteins in NR has hindered its continuous usage in existing products and potential in new applications. DPNR generally contains no substantial protein along with excellent film-forming property and impart outstanding green strength (Tanaka *et al.*, 1996). When compared with ENR, DPNR is more commercially available due to its consumption in the glove manufacturing industry. DPNR can be prepared either by centrifugation, enzymatic degradation or irradiation. Surfactant is always added during deproteinization because of the role of protein layer as stabilizer in NR. Figure 2.4 shows the schematic diagram of protein layer removal from High Ammonia Rubber Latex (HANR). Deproteinized of NR by centrifugation and hydrolysis is the most common method to prepare DPNR (Hashim and Ong, 2017). In centrifugation, polyethylene glycol (PEG) is used as surfactant for the extraction of protein from NR latex with a constant speed of 1000 rpm and processing time of 5 to 30 minutes (Danwanichakul *et al.*, 2014). The application of DPNR is mainly in the production of protein free gloves, medical and pharmaceutical industry where protein allergies have become an emerging problem.

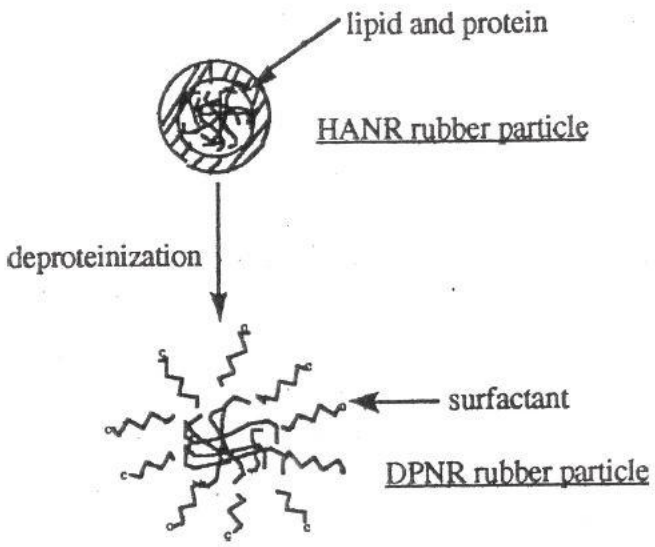

Figure 2.4: Schematic diagram of protein removal from HANR (Hashim and Ong, 2017)

2.1.3 Key terms involved in rubber manufacturing process

2.1.3(a) Compounding

Rubber or latex compounding refers to the addition of certain chemicals in raw rubber under a definite proportion to obtain a uniform mixture for the desired physical and chemical properties in order to meet the requirements of end users and to achieve low processing cost (Sisanth *et al.*, 2017). Unformulated rubbers behave like a high weight polymer with low elasticity and strength (Ramezani and Ripin, 2012). The main core chemicals used in rubber compounding are rubber matrix, filler, cross-linking agent, accelerator, activator and antioxidant. The purposes of the chemicals are listed in Table 2.1. Through vulcanization and curing, long chain rubber network will transform from a viscous like material to an elastic solid.

Table 2.1: Purposes of chemicals addition in rubber compounding (Onions, 2020)

Chemical	Purpose
Natural Rubber (rubber matrix)	Serve as the rubber matrix to be compounded
Carbon Black (filler)	Acts as a reinforcing material and to reduce the overall cost of the compound
Sulphur (cross-linking agent)	To enhance the cross-linking between rubber monomers for better mechanical properties
Thiazoles (accelerator)	To increase the speed of vulcanization and to allow vulcanization to occur at lower temperature and higher efficiency
Stearic acid (activator)	To activate the action of accelerator for vulcanization process
Amines (antioxidant)	To lower the rate of free-radical oxidation reactions for extending the service life of the rubber

2.1.3(b) Vulcanization

Vulcanization is the process involving the curing of elastomers usually by heat (Bin Samsuri and Abdullahi, 2017). Originally, rubber is a very soft and elastic material which could limit its performance in certain applications. Therefore, vulcanization is needed to maximize the potential of rubber in various industries. It is a chemical process that turns NR and other elastomers into cross-linked polymers as shown in Figure 2.5. Vulcanizing agents such as sulphur or hydrogen peroxide is added into the rubber matrix to improve the elasticity, tensile strength, viscosity and tear resistance of NR (Tang *et al.*, 2019). The cross-linking reaction between sulphur and the rubber matrix usually happens at the C=C double bond with excess amount of sulphur. Vulcanization of rubber by only sulphur consumed a huge amount of time (up to several hours) and is prone to rubber degradation due to the long exposure to heat as well as oxygen. Therefore, maximum efficiency is achieved by mixing sulphur with accelerator and metal oxides or fatty acid which acts as the activator for the cross-linking process (Nair and Joseph, 2014). The selection of suitable chemicals strongly depends on the rubber properties and application requirements. The mechanism of vulcanization and speed is a rather complicated process. It depends on the nature of rubber, type of chemicals, cure time and thermodynamics of each particular reaction (Manaila, Daniela and Craciu, 2012). It is presumed that sulphur vulcanization proceeds in three stages. The first stage forms the active-crosslinking agent from the interaction of curing systems (sulphur, accelerator and activator) and rubber. The second stage is dominated by polysulphidic cross-link from the formation of primary vulcanized network. During the third stage, the network is restructured into di and monosulphidic crosslinks with macromolecules of rubber which eventually forms the final vulcanized rubber network (Kruželák, Sýkora and Hudec, 2016). The degree of crosslinking in rubber vulcanizate can be determined through the mechanical measurements or the swelling experiments that involves Mooney-Rivlin equation (Mooney, 1940)(Rivlin, 1948) and Flory-Rehner equation (Flory and Rehner, 1943) respectively. Recently, the crosslink density of rubber specimen determined by dynamic mechanical analysis and low-field nuclear magnetic resonance proved to show great accuracy (Hiranobe *et al.*, 2021).

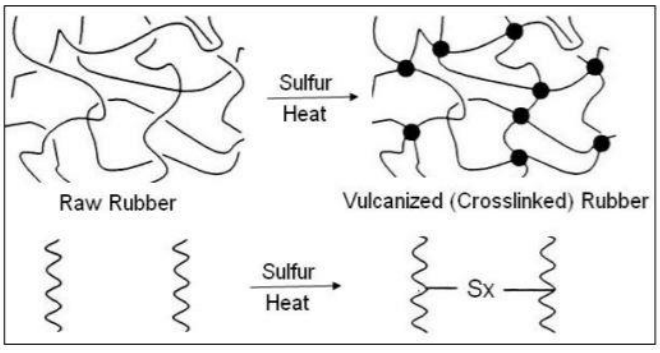

Figure 2.5: Cross-linking of rubber (Whitby and Simmons, 1925)

2.1.3(c) Reinforcement

Reinforcement of rubber refers to the addition of reinforcing material which is also commonly termed as filler in the rubber matrix for improvement of stress to strain ratio. This simple action improves the overall properties of rubber. The most prevalent type of filler used in the automotive and other rubber applications is carbon black. Carbon black is a fine black powder mainly consisting of carbon produced from the incomplete combustion of heavy petroleum products such as tar. Reinforcement of rubber by carbon black increases the rubber strength, modulus, stiffness and elongation at break as shown in Figure 2.6. The improvement in mechanical properties is attributed to the formation of networks, bound rubber and entanglement between rubber matrix and carbon black (Seo *et al.*, 2017). With the development of nanotechnology, many different types of nanoparticles are introduced as filler for rubber matrix and substantially novelty research about the regarding topic has been widely investigated (Ponnamma *et al.*, 2013). An overview about rubber nanocomposites will be discussed in Section 2.2.

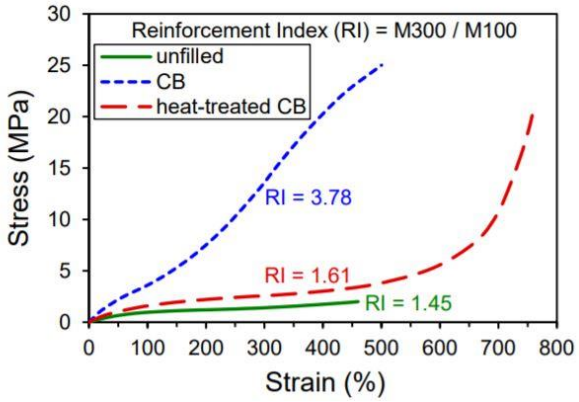

Figure 2.6: Stress-strain curve for unfilled and filled rubber (Robertson and Hardman, 2021)

2.1.3(d) Rubber shaping

When it comes to the production of rubber products, there are a few existing manufacturing processes depending on the final application of the rubber products. Once the dry rubber or latex arrives at the processing facilities, processing steps such as compounding, mixing, shaping and vulcanizing will be done individually or collectively. Compounding and mixing of rubber with other additive chemicals are key for achieving the demanded chemical and physical properties. Figure 2.7 shows the flow chart of rubber products manufacturing process. Some of the most common rubber shaping processes are calendaring, extrusion, moulding, latex dipping and casting.

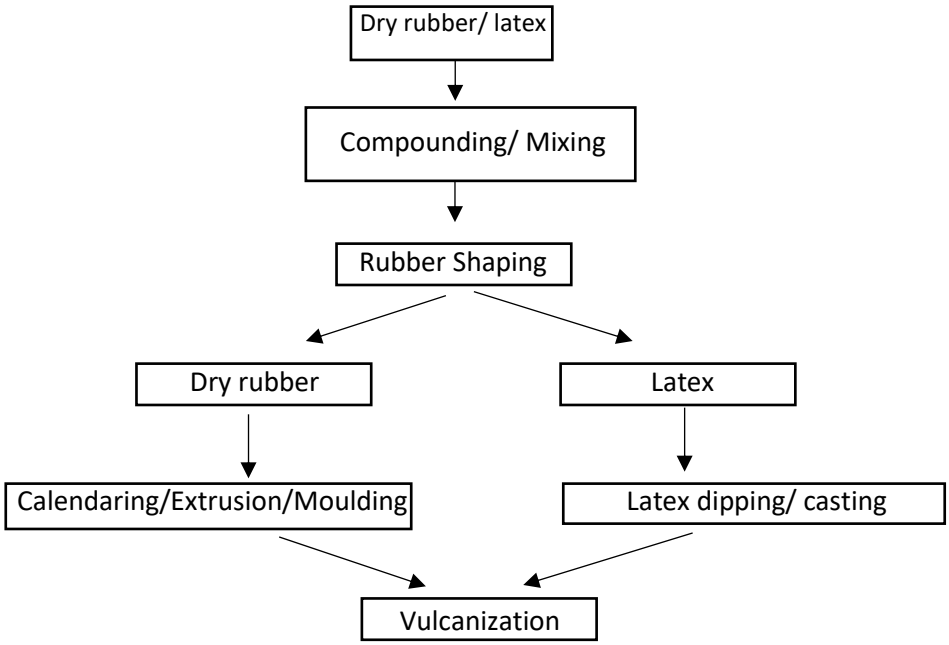

Figure 2.7: Rubber manufacturing process

2.1.3(e) Moulding

Moulding is favoured for bulk production of products with closed dimensional tolerances. Rubber products like shoe soles, seals, suction cups and bellows are typical products of moulding. Moulding is also one of the steps in making tyres. Moulding and curing are done in the same process where moulding is the process where rubber fills the cavity of the mould while curing is done next by applying heat to the rubber in the mould. The moulding operation must compromise between the necessity of viscous flow and degree of cross linking by exploring their dependence on the curing temperature. Moulding comprised of three main types which are compression moulding, transfer moulding, injection moulding and their variations. Table 2.2 shows the characteristics and applications of the moulding techniques. The selection of the most appropriate technique relies on the size, shape, function and precision needed of the rubber products as well as the amount of products to be produced (Princi, 2019). In the general rule of thumb, mass scale production will justify the need of a more sophisticated and reliable techniques while low volume production should minimize the capital on mould and equipment. The capital expenditure of the moulding techniques increases from a minimum for compression moulding then transfer moulding to a maximum for injection moulding. The advantages for moulding process include better accuracy in terms of rubber dimension, versatility and efficiency for high volume production.

Table 2.2: Characteristics and applications of moulding techniques (Princi, 2019)

Technique	Characteristics	Applications
Compression moulding	Pressing pre-shaped rubber compound in the mould High tool costs Low manufacturing costs	Small series, large parts, prototypes, samples
Injection-compression moulding	Pressing pre-plastified rubber compound High compound division without canals Less tool that can be used	Large surface membranes and sealings, small precision parts, high number tool parts
Transfer moulding	Transfer of rubber compound to cavities Improved tolerance Less compound waste	Complex precision parts, no secondary finishing
Injection moulding	Injection of pre-plastified material High manufacturing cost Low cost of tools	Medium to large series part, rubber metal part, automated manufacturing
Transfer injection moulding	Transfer of pre-plastified rubber compound High constant flow stream Low tool costs	Large series of small parts, also in rubber metal, no secondary finishing

2.1.3(f) Latex dipping

Latex dipping is a completely different process compared to the methods mentioned above when dry rubber is used. Latex refers to a stable suspension of tiny polymer particles in aqueous medium and is generally a two-phase system where water acts as the continuous phase while rubber molecules is the discontinuous phase. It is in the liquid form before it is converted to solid upon processing. NR latex is the largest volume of materials used although synthetic polymer such as nitrile butadiene rubber (NBR) and styrene butadiene rubber (SBR) are also named latex. Latex dipping process starts by immersing the former into compounded latex then slowly withdrawn from the latex in order to leave a uniform film on the former. Processes such as leaching, beading, vulcanization cooling and stripping are then done subsequently prior to the formation of final products.

The thickness of the rubber product can be increased by repetitive latex dipping (single-dip, double-dip) or by dipping the former into coagulant which is normally a solution of calcium nitrate before immersing it into latex (Groves and Routh, 2017). Calcium nitrate causes the latex to aggregate onto the former forming a weak rubber film known as wet gel. Beading is an important steps to strengthen the thin gel film against tearing at the edge of the open end and to prevent the final rubber article from distorted configuration (Blackley, 1997). Figure 2.8 shows the basic flowchart of latex dipping process. Formers are usually produced from aluminium, ceramic or stainless steel for better

sustainability for production in the long run. The surface of the formers must be polished to a smooth finish to prevent defects on the rubber products. Some of the common latex dipping products are rubber gloves, balloons and condoms.

Figure 2.8: Basic flowchart of latex dipping (Poh, Chew and Tan, 2019)

2.1.3(g) Latex casting

Latex casting is somewhat similar to the dry rubber moulding technique mentioned above where both processes require a mould to fill the material. However, casting is by pouring of liquid into the mould cavity for the formation of solid (or hollow) objects from latex compound by gelation whereas moulding involved the usage of pressure and heat to fill the mould cavity with dry solid rubber. In dipping process, the latex is placed outside of the mould (former) but latex is poured into the mould for casting technique although both involved the use of liquid latex. The products from latex casting are typically toys and rubber films where high dimensional precision and blueprints are made necessary. The internal design of the mould and surface finish will define the sharp impression of the finished articles (Mudzviti and Matai, 2019).

Generally, there are two types of mould materials: Plaster of Paris Mould (chemically named as calcium sulphate dihydrate) and metal alloy (aluminium or magnesium). The gelation mechanism for the aforementioned mould is through the absorption of water by porous mould surface and the diffusion of calcium ions into latex that lowers the latex stability (Lazim *et al.*, 2015). Therefore, a gradual deposition will develop on the internal mould surface. For metal alloys moulds, the deposition build-up depends on the temperature of the mould, heat capacity and sensitivity of the latex compound. An illustrative diagram of casting process to produce films is shown in Figure 2.9. It will serve as a useful guidance for lab-scale film preparation. Big-scale production of rubber products from

casting technique usually uses metal alloy moulds as plastic moulds must be discarded for every 25-30 castings (Nocil, 2010).

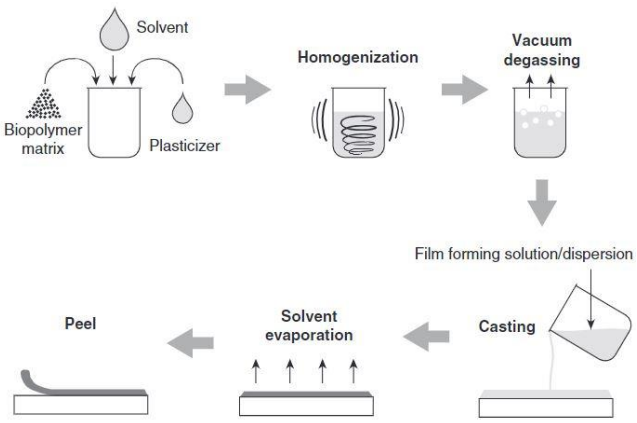

Figure 2.9: Steps of casting process for the production of films (De Azeredo *et al.*, 2014)

2.2 An overview of rubber nanocomposites with emphasis on the addition of starch nanocrystal as filler in natural rubber

2.2.1 Generalities on rubber nanocomposites

A rubber matrix with well dispersed nanoparticles in a cross-linked elastomeric polymer is defined as rubber nanocomposite. The filler can be classified as nano-filler when the average particle size is within the range of 1-100 nm (Khan, Saeed and Khan, 2019). Nano-fillers are known to improve the strength and stiffness of the rubber matrix as they will impart high elastic modulus and durability to the elastomers which are always the criteria required for practical applications. Incorporation of nano-filler also plays an important role in alternative properties such as thermal stability, electric conductivity, flame retardancy, gas and oil permeability other than the enhancement of mechanical properties (Das, Basu and Heinrich, 2020). However, the extent of properties betterment depends on size and shape of the nano-filler, degree of dispersion, aspect ratio of nano-filler, arrangement of nano-filler in the rubber matrix and interfacial adhesion between nano-filler and rubber chain (Bokobza, 2007; Wongvasana *et al.*, 2022). In this case, finer dispersion of nano-filler in the rubber matrix will develop a larger surface area which means more interfacial adhesion between the nano-filler and rubber chain resulting to the overall improvement of rubber quality.

Amidst the outstanding properties emerged by the addition of nanoparticles, fine single particle dispersion into rubber matrix proved to be difficult as most of the nanoparticles exist in agglomerate form owing to the van der Waals and strong intermolecular forces (Henry *et al.*, 2013). Several methods have been proposed to improve the dispersion of nanoparticles in polymer matrices. Parameters such as filler properties (surface area, crystallinity and structure), elastomer properties (chemical structure and molecular weight), mixing time, temperature and total shear strain are the

important factors to be considered when fabricating the rubber nanocomposites (Lacayo-pineda, 2015). The use of solvent-free powder and in-situ polymerization technique had also proved to improve the dispersion of nanoparticles in polymer matrix (Kim, Noh and Yu, 2014). Nano-fillers can be categorized into three types based on the number of dimensions at nano scale. One dimensional (plates or laminar layer silicates and layered double hydroxides), two dimensional (nanotubes and nanofibers) and three dimensional (nanogranules, nanocrystals and nano-silica) (Kumar *et al.*, 2009). Since the interfacial interaction between nanoparticles and polymer matrices is crucial in determining the composites properties, comparative study of nano-filler dimension and interfacial volume of polymer is done as shown in Figure 2.10. The plot of volume fraction of interfacial polymer against volume fraction of filler shows increasing interfacial volume with decreasing nano-filler size.

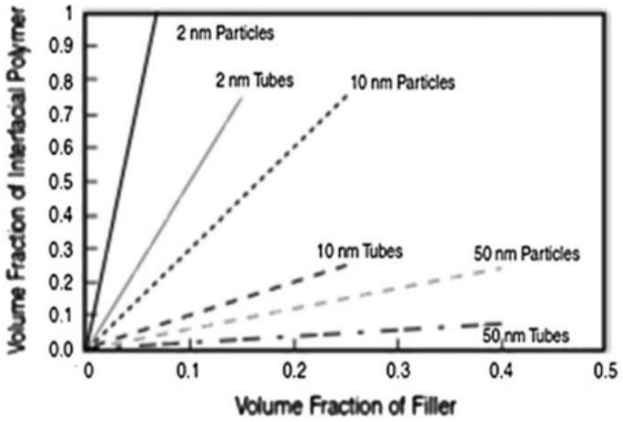

Figure 2.10: Plot of volume fraction of interfacial polymer against volume fraction of filler (Ponnamma *et al.*, 2013)

2.2.2 Starch nanocrystals as reinforcement material

2.2.2(a) An overview of starch

Starch is a naturally occurring, renewable and biodegradable polysaccharide found in almost all flora in the world. The most abundant carbohydrates found in food is polysaccharide. Polysaccharides are long polymer chains composed of monosaccharide or disaccharide units joined by glycosidic bonds (Mager and Thomas, 2011). Starch is the second most abundant biomass material on earth used in the food and beverage industry as well as starch-based adhesive industrial products which includes packaging and coating. Low density, cost effectiveness, non-toxicity, biocompatibility and the increasing world population escalates the demand of starch. The global starch market is expected to reach 160.3 million metric tons by 2026 growing at a Compound Annual Growth Rate (CAGR) of 5% over the period (GlobeNewswire, 2021). Starch consists of two polysaccharides, amylose and amylopectin. Amylose is a primarily linear or slightly branched (1 -> 4)–α–D–glucan polysaccharide while amylopectin is a highly branched polysaccharide composed of (1 -> 4)–α–D –glucan short chain

linked through α-(1->6) linkages (Paris *et al.*, 1999). Generally, starch contains 20-30% of amylose and 70-80% of amylopectin (Svihus, Uhlen and Harstad, 2005). The conventional model of starch granules are form through the amorphous (amylose) and crystalline (amylopectin) regions of starch granules that are arranged alternately circling the initiation point called hilum as shown in Figure 2.11. (Jenkins *et al.*, 1994).

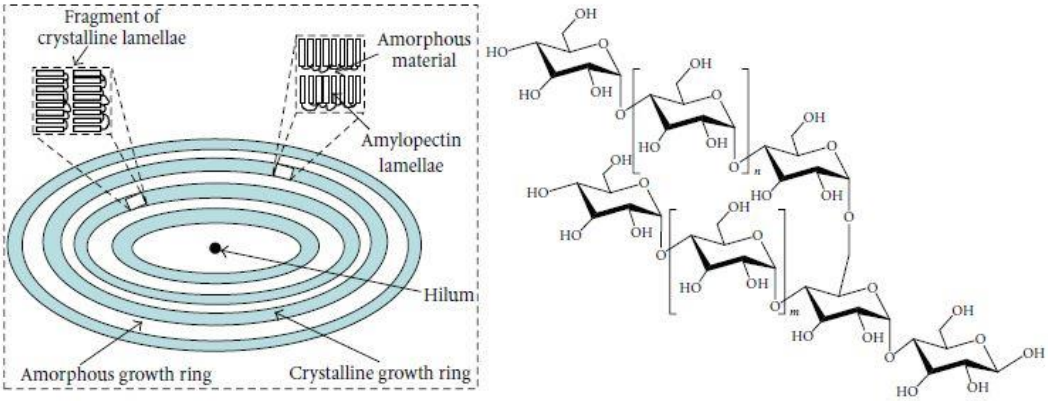

Figure 2.11: Schematic diagram of starch granule and chemical structure of amylopectin (Lin *et al.*, 2011)

Starch presents as white granules in various locations of a plant for instance grains (corn, rice and wheat), roots (sweet potatoes and cassavas), tubers (potatoes) and seeds (peas and beans) (Swinkels, 1985). The granular size, shape, morphological structure, composition of amylose and crystallinity differ considerably between the origin sites of each starch. In general, plant starches are classified into A, B and C according to the X-ray diffraction diagram produced from the amylopectin crystal lattices of starches by evaluating the peak locations in the diffractogram. Grain starches have A type crystalline structure, roots and tubers starches show B-type crystalline structure while legume (plants that produce a pod of seeds) appears as C-type crystalline structure (Buléon *et al.*, 1997; Dome *et al.*, 2020). X-Ray diffraction pattern of C-type starches showed a combination polymorph of A and B-types, thus C-type starches can be considered as a mixture of the two. The crystalline type of native starches can also be well differentiated by their amylopectin chain length. In most cases, A-type starches have shorter average chain length than B-type starches (Li *et al.*, 2018). Difference between A and B-type starches can also be explained through the double helices packing configuration. The structure of A-type starches are closely packed with water molecules in between each double helices packing while the water molecules in B-type starches are at center cavity formed by six double helices (Imberty and Perez, 1988; Ouyang *et al.*, 2021). Figure 2.12 shows the double helices packing structure of A and B-type starches.

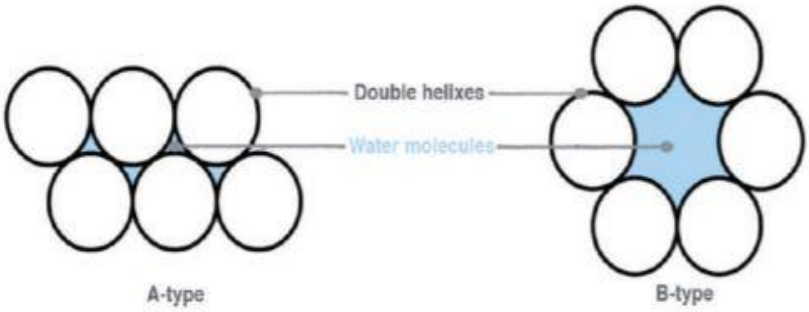

Figure 2.12: Double helices structure of A and B-type starches (Le Corre, Bras and Dufresne, 2010)

Crystallinity is the degree of long-range structural order and regularity of crystal lattice within a solid material. The relative crystallinity of a solid has a big effect on the density, hardness and diffusivity of the material. The relative crystallinity of native starches can be quantified with a two-phase method by using X-Ray Diffraction pattern. Basically, a curve between the 2Θ angle of 4° and 40° is plotted in the diffractogram. The area above the curve is defined as crystalline while the area below the curve and linear baseline is defined as amorphous (LeCorre, Bras and Dufresne, 2011). Figure 2.13 shows the X-ray diffraction pattern of waxy maize (type A), potato (type B) and peas (type C) starches. The relative crystallinity of the starches can then be calculated by Equation 2.1 (Nara and Komiya, 1983).

$$X_c = \frac{A_c}{A_c + A_a} \tag{2.1}$$

where X_c is the relative crystallinity, A_c is the area of the crystalline region, A_a is the area of the amorphous region.

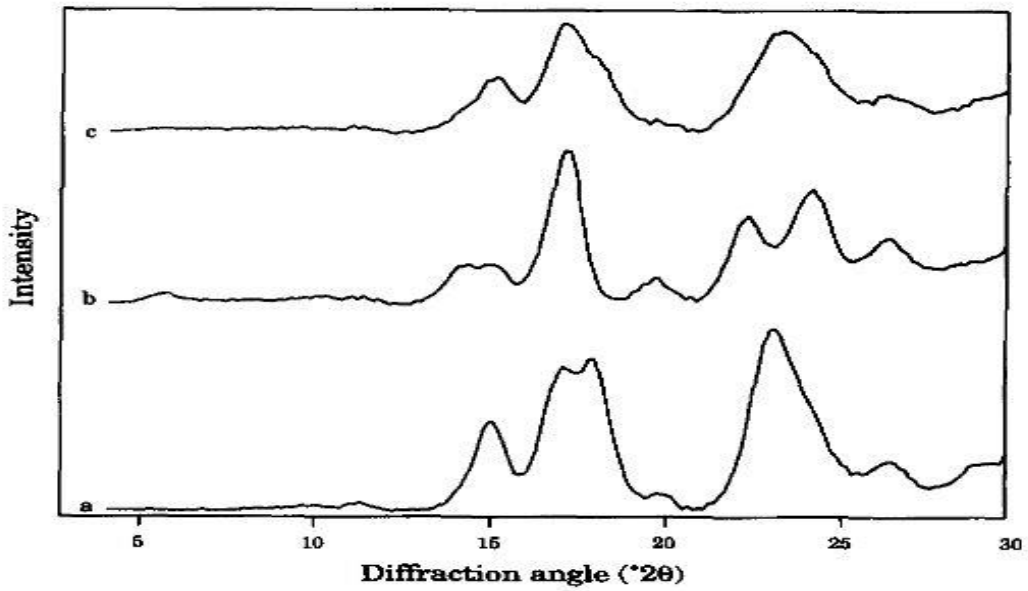

Figure 2.13: X-ray diffraction pattern from the starches (a) waxy maize (b) potato and (c) peas (Cairns *et al.*, 1997)

2.2.2(b) Preparation of starch nanocrystals

SNC are the crystalline platelets from the semicrystalline structure (amylopectin) of starch granules following the removal of amorphous region (amylose) (Lecorre, Bras and Dufresne, 2011a). The most common and established way to prepare SNC is by acid hydrolysis while some researchers proposed the production of SNC by enzymatic hydrolysis. In acid hydrolysis, the regions of low lateral order and amorphous phases are dissolved while the water-insoluble crystalline regions are obtained as SNC. In the case for enzymatic hydrolysis, the less organized amorphous regions are more susceptible to enzymatic attack while semicrystalline amylopectin regions are more resistant to enzymatic erosion (Kim, Park and Lim, 2008). Therefore, the crystalline regions are retained as SNC.

Literatures regarding the preparation of SNC by acid hydrolysis and characterisation techniques are summarized and gathered in Table 2.3. From Table 2.3, the acids used are hydrochloric acid (HCL) and sulphuric acid (H_2SO_4), the temperature of hydrolysis shows little variation which is between 30 °C – 40 °C while the duration of hydrolysis varies from 5 days – 40 days. The main reason for low hydrolysis temperature is to prevent the gelatinization of starch and destruction of starch crystalline under extreme temperature. The use of HCL and H_2SO_4 shows distinct difference for the hydrolysis period, namely, approximately 5 days for H_2SO_4 while more than 15 days is required for HCL. Angellier et al (2004) proposed an optimized process for the preparation of SNC, most of the methods listed in Table 2.3 were adopted from the optimized technique. Starch granules of approximately 36.725g is mixed with 3.16 M, 250mL of H_2SO_4 in Erlenmeyer flask with stirring speed of 100 rpm at 40 °C for 5 days. After that, the suspensions were washed by distilled water using Centrifuge Sigma 6K15 for 10 minutes at 10000 rpm until neutral pH is achieved. Stable starch suspension is attained by dispersing aggregates using mechanical treatment with homogenizer Ultra Turrax for a duration of 2 minutes at 13000 rpm. The suspensions were added with chloroform and kept at 4 °C to avoid the growth of bacteria (Angellier *et al.*, 2004).

Table 2.3: Prepare conditions of SNC and its characterization techniques

Starch		Acid		Duration (days)	T (°C)	Characterization	Reference
Type	W (g)	Type	C (M)				
Potato	50	HCL	2.2	15	30	-	(Dufresne and Cavaillé, 1998)
Waxy Maize	50	HCL/H_2SO_4	-	-	35	TEM, SEM	(Dufresne, 2000)
Waxy Maize	10	HCL	2.2	40	36	TEM, XRD	(Putaux *et al.*, 2003)
Waxy Maize	14.7	H_2SO_4	3.16	5	40	TEM	(Angellier *et al.*, 2005)
Potato	37	H_2SO_4	3.16	5	40	TEM	(G. Chen *et al.*, 2008)
Pea	37	H_2SO_4	3.16	5	40	TEM	(Hua *et al.*, 2008)
Pea	15	H_2SO_4	3.16	5	40	SEM	(Y. Chen *et al.*, 2008)
Potato	50	HCL	2.2	15	35	SEM, TEM, XRD, TGA, FTIR, DSC	(Namazi and Dadkhah, 2008)
Waxy Maize	15	H_2SO_4	3.16	5	40	TEM, XRD, TGA, FTIR, DSC	(Namazi and Dadkhah, 2010)
Rice/ Potato	25	H_2SO_4	3.16	5/7	40	DSC, XRD, SEM, particle size, swelling power	(Martins, Latorres and Martins, 2022)

Remarks: W = Weight, C = Concentration, T = Temperature, TEM = Transmission Electron Microscope, SEM = Scanning Electron Microscope, XRD = X Ray Diffraction, TGA = Thermogravimetric Analysis, FTIR = Fourier Transform Infrared Spectroscopy, DSC = Differential Scanning Calorimetry

As discussed, the botanical origins of starch granules will affect the granular size, crystalline type, morphology as well as the yield of SNC. Xu et al (2014) investigated the yield of SNC, amylose content, granular size, crystallinity type and degree of crystallinity of starches from different botanical sources. The findings of the investigation are presented in Table 2.4. Xu et al (2014) adopted the optimized acid hydrolysis technique as per discussed in Section 2.2.1(b) for the preparation of SNC. From Table 2.4, following 5 days of hydrolysis period, it can be found that the yield of SNC ranged between 8.8% for potato starch to 35.7% for mungbean starch. Furthermore, the SNC yield of corn, barley, tapioca and chickpea starch were 14.1%, 18.2%, 15.1% and 16.8% respectively. The swollen structure of potato starch is the main reason for the lowest yield of potato SNC as the swollen condition is more prone to acid hydrolysis (Kim *et al.*, 2012). In the other hand, the highest yield of SNC for mungbean starch indicates its greater resistance towards acid hydrolysis process. However, the synthesizing technique for waxy maize starch is the most established as shown in Table 2.3 and optimized acid hydrolysis technique was reported (Angellier *et al.*, 2004). Moreover, no amylose content is detected for all SNC showed that the amorphous regions of native starches are completely hydrolysed. The crystalline type for each native starch and its respective SNC were determined by the 2Θ diffraction peaks from the X-Ray Diffractogram. The result presented in Table 2.4 are also consistent with the findings from

previous literature. The degree of crystallinity is calculated using Equation 2.1. As shown in Table 2.4, the degree of crystallinity for every SNC increased when compared to its native form. This further proved that the amylose regions were dissolved during the acid hydrolysis process.

Table 2.4: Results of investigation (Xu *et al.*, 2014)

Origin of starch	Yield of SNC (%)	Amylose (%)	Granular Size (nm)	Type and degree of crystallinity (%)
Corn	14.1 ± 0.6	nd	47.0 ± 10.5	A, 44.0 ± 0.6
Barley	18.2 ± 1.7	nd	54.6 ± 10.8	A, 39.0 ± 0.6
Tapioca	15.1 ± 0.2	nd	25.5 ± 2.0	A, 51.1 ± 2.8
Potato	8.8 ± 0.6	nd	117.1 ± 13.1	B, 32.0 ± 1.0
Mungbean	35.7 ± 2.3	nd	81.4 ± 7.1	C, 45.8 ± 0.5
Chickpea	16.8 ± 1.5	nd	61.7 ± 11.7	C, 46.7 ± 0.2

Remarks: Data are presented as mean value ± standard deviation, nd = not detected

2.2.2(c) Use of starch nanocrystals as reinforcing filler in various polymer

In the past decades, research works have shifted its focus to the development of other reinforcing materials to replace carbon black in rubber compounding. It was due to the fact that the production of carbon black from partial combustion of hydrocarbon will cause pollution as well as harmful effects. Silica is also a commonly used reinforcing agent in rubber tread compounds but its reinforcing properties such as abrasion resistance are lower than those obtained in carbon black (Flanigan *et al.*, 2012). Therefore, the search for alternative filler that implies similar or better reinforcing properties than carbon black remained a field to be explored. In recent years, starch nanocrystals have attracted substantial attention among researchers and industrialists as synthetic nanomaterials lack the ease of processability and biodegradability when compared to natural nanomaterials. It is also a step to promote the use of environmentally friendly materials for sustainable development in the rubber industry. The most prominent use of starch in rubber industry is witnessed when a patented innovation called Biotred is developed. Novamont (Novara, Italy) working in partnership with Goodyear Tire and Rubber has produced tires using nanoparticles derived from corn starch to replace the conventional carbon black and silica (Materne, Corvasce and Leitz, 2000). This patented innovation not only presented environmental supremacy but also reduced the rolling resistance of tires. Moreover, the innovation also provides new ideas and possibilities for research in the scope of using natural nanofiller for the development of environmentally friendly strong rubber nanocomposites.

Numerous attempts have been made to incorporate SNC in polymetric matrices. The resulting polymer nanocomposite often displays outstanding mechanical properties and thermal stability. Table 2.5 summarized the characterisation techniques and effect on mechanical properties for polymer nanocomposite when NR acts as the polymer matrix and SNC as the reinforcing material. From Table

2.5, it was found that SNC brought great reinforcing effect on NR matrix especially at temperature above T_g which is at the rubber plateau region. This observation was confirmed by most of the authors from their experimental investigations. However, the data obtained should be carefully compared as the amount of SNC incorporated in NR matrix are different depending on the author. Some authors expressed the dosage of SNC in weight percentage (the ratio of SNC to the total content of the rubber nanocomposite) while some authors prefer to express SNC in the unit phr (per hundred rubber). Nonetheless, the introduction of SNC in NR matrix showed increment in tensile strength and tensile modulus with a decrease in elongation at break. For most authors, the optimum dosage of SNC as filler in NR is approximately 20% wt. This SNC content effectively reinforced the NR matrix without significantly decrease the elongation at break.

Table 2.5: Characterization techniques of rubber nanocomposite and mechanical properties of SNC filled nanocomposite

Type of SNC	Rubber matrix	Characterization techniques of rubber nanocomposite	Mechanical properties of SNC filled nanocomposite	References
Potato	NRL	FESEM, XRD, Water Uptake	Tensile strength and tensile modulus increased linearly with SNC content (5-20 wt%)	(Rajisha *et al.*, 2014)
Corn	NRL	Toluene Uptake	Improved tensile strength and modulus (optimum mechanical properties achieved at 1.38 phr of SNC)	(Anand *et al.*, 2018)
Corn	Dry NR	FESEM, DMA	Tensile strength and modulus increased linearly with SNC (1-7.5 phr)	(Rajisha *et al.*, 2015)
Cassava	NRL	DSC, MST, Crosslink Density, Water and Toluene Uptake	Improved tensile strength and modulus (optimum mechanical properties achieved at 6% wt of SNC)	(Gao *et al.*, 2014)
Waxy Maize	NRL	Water and Toluene Uptake, DMA	Improved tensile strength and modulus (optimum mechanical properties achieved at 20% wt of SNC)	(Angellier, Molina-Boisseau and Dufresne, 2006)
Waxy Maize	Dry NR	SEM, TGA, DSC, Water Uptake	Improved tensile strength with addition of SNC (optimum mechanical properties	(Valodkar and Thakore, 2010)

			achieved at 30 phr of SNC content)	
Waxy Maize	NRL	FESEM, particle size distribution, DMA	Tensile strength increased with SNC content (2-8%)	(Tan *et al.*, 2024b, 2024a)

Remarks: FESEM = Field Emission Scanning Electron Microscope, XRD = X Ray Diffraction, DMA = Dynamic Mechanical Analysis, DSC = Differential Scanning Calorimeter, MST = Mechanical Stability Test, SEM = Scanning Electron Microscope, TGA = Thermogravimetric Analysis

As discussed, the use of SNC as filler in NR matrix showed improved mechanical properties. Le Corre, Bras and Dufresne (2011) made a thorough investigation about the influence of different botanic origins on the reinforcing effect of SNC. Waxy maize starch with 27% and 70% amylose content, wheat starch with 28% amylose content and potato starch with 21% amylose content were used to prepare the SNC. Four conclusions can be made from the results displayed on Figure 2.16: (i) nominal stress increased with nominal strain until the breakage of the film (ii) the nominal stress evolved greatly with increasing SNC content without much affecting the elongation at break (iii) all botanic origins of starches improved the mechanical properties of NR/SNC composite film (iv) the higher the amylose content (the lower the initial crystallinity) of native starch used to prepare SNC, the lower the reinforcing effect (except for potato starch) for instance waxy maize starch of 27% amylose content showed much better reinforcing effect on NR matrix when compare to waxy maize starch of 70% amylose content. The results shown at Figure 2.14 consolidated the findings from Table 2.5 as the preparation method of NR/SNC composites and testing procedures of the fabricated films are standardized throughout the experiment. A new discovery is found where amylose content of native starches play an important role when identifying starch to prepare SNC as reinforcing filler.

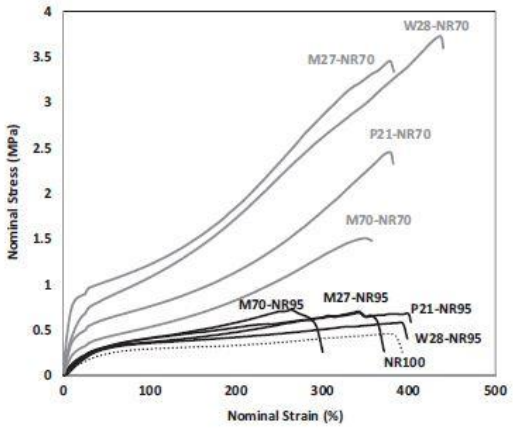

Figure 2.14: Typical nominal stress versus nominal strain curves of NR/SNC composites films where dotted line refer to unfilled NR matrix, black and grey lines correspond to 5% and 30% wt of SNC content respectively (LeCorre, Bras and Dufresne, 2011)

Various techniques had been used to characterize rubber nanocomposites as shown in Table 2.5. Angellier et al (2005) characterized NR filled waxy maize SNC in terms of morphology, toluene and

water uptake, barrier properties to water vapour and oxygen, thermal properties as well as crystallinity. The outcomes of the characterization from Table 2.5 are in agreement with the investigation done by Angellier et al (2005). The morphology of NR/SNC were evaluated by the surface fracture film using SEM. The micrographs of unfilled NR, NR with 5% and 30% SNC are shown in Figure 2.15. From Figure 2.15(a), unfilled NR film shows a smooth and uniform morphology. The presence of SNC is easily identify with the presence of white dots. As shown in Figure 2.15(b) and (c), the dispersion of SNC is homogenous for both compositions. This key aspect is important to ensure a good reinforcing effect on the NR matrix. The characterization results for other properties of NR/SNC composite is summarize as below:

- The toluene uptake for unfilled NR film is the highest whereas the addition of SNC into NR matrix displayed a dramatic decrease for the diffusivity of toluene. This observation may be due to the formation of three dimensional network for rodlike polysaccharide filler (Gopalan Nair and Dufresne, 2003). Contrary to the toluene uptake, the unfilled NR film showed the lowest water diffusivity. It proved that the incorporation of SNC favours the uptake of water.

- The addition of SNC do not affect the permeability of water vapour to NR matrix due to the hydrophilic nature of starch. The permeability of oxygen to NR matrix decreased upon the addition of SNC as the platelet like structure of starch stand in the way of oxygen diffusivity.

- DSC results showed decrease in T_g upon the addition of SNC. However, it is believed that T_g for NR/SNC composite should increase because of the hydrogen network formation.

- The addition of SNC increased the relative crystallinity of the composite film as the amorphous region of native starch is dissolved during the acid hydrolysis process.

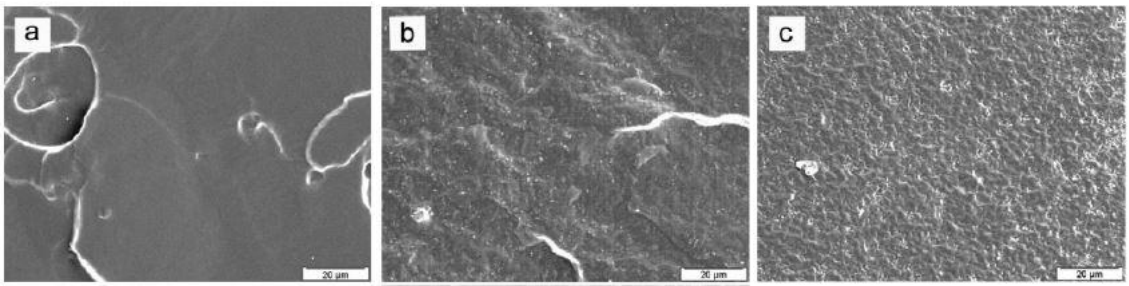

Figure 2.15: SEM of the fractured surfaces (a) unfilled NR, (b) NR filled with 5% SNC, (c) NR filled with 30% SNC (Angellier *et al.*, 2005)

SNC have also been used as reinforcing agent in other natural polymers as well as synthetic polymers. For natural polymer, starch-based materials had been used as matrix and SNC as reinforcing

filler. This combination will promote good adhesive interaction and miscibility between the matrix and filler as the chemical structure of the components are similar. Nanocomposites materials prepared by SNC as the reinforcing phase and starch plasticized by sorbitol as the matrix showed improvement on the mechanical properties (Viguié, Molina-Boisseau and Dufresne, 2007). This reinforcing effect was attributed to the increase in crystallinity of the nanocomposite material and strong interactions between SNC as well as filler and matrix which aided in occurrence of crystallization between filler and matrix interface. As for synthetic polymer, waxy maize SNC were blended with poly(styrene-co-butyl acrylate) to produce nanocomposite (Angellier *et al.*, 2005). The nanocomposite filled with different loadings of SNC (ranging from 0-50% wt) showed substantial improvement in mechanical properties upon increasing amount of filler. Another example is the inclusion of potato SNC as filler into waterborne polyurethane (G. Chen *et al.*, 2008). The incorporation of only 2% wt of potato SNC had increased the tensile strength of nanocomposite by 1.7-fold.

2.2.2(d) Reinforcement mechanism of SNC

The reinforcing capability of SNC in various polymer matrices is well discussed in the above literature. The structure of the matrices, network formed between SNC and polymer matrices, interfacial interaction, the scale of dispersion and morphology of SNC are important factors to the cooperative effects of the nanocomposites. A percolation mechanism, governed by the three-dimensional network formed between the interconnectivity of SNC and strengthen by the hydrogen bond is the main contributor to the improved mechanical properties of the nanocomposites. It has been manifested that over the percolation threshold, SNC is interconnected and form a tri-dimensional network through the nanocomposites (Favier *et al.*, 1997). Figure 2.16 shows the possible three-dimensional network formed in the nanocomposites. The formation of this network is the result of strong interaction forces between SNC such as hydrogen bond. This phenomenon can be explained through the mechanical properties spotted through a sheet of paper which result from the hydrogen bonding forces that hold the percolation network of fibres together (Dufresne, 2008b). The mechanical properties of the nanocomposites will be affected when the formation of percolation network is interfered (Dufresne, 2006). Four factors that affect the formation of the described network are morphology and dimension of nanocrystals, preparation and processing of nanocrystals, structure of the matrix and the interaction between nanocrystals and matrix. It should be taken into account that although chemical modification of SNC improves the interaction between the filler and matrix, this action will partially or totally destroy the three-dimensional network (Angellier, Molina-Boisseau, Lebrun, *et al.*, 2005). Ultimately, this will lead to a strong decrease in the mechanical

properties of the nanocomposites. A similar result is also shown in NR filled with chemically modified crab shell chitin nanowhiskers (Nair *et al.*, 2003).

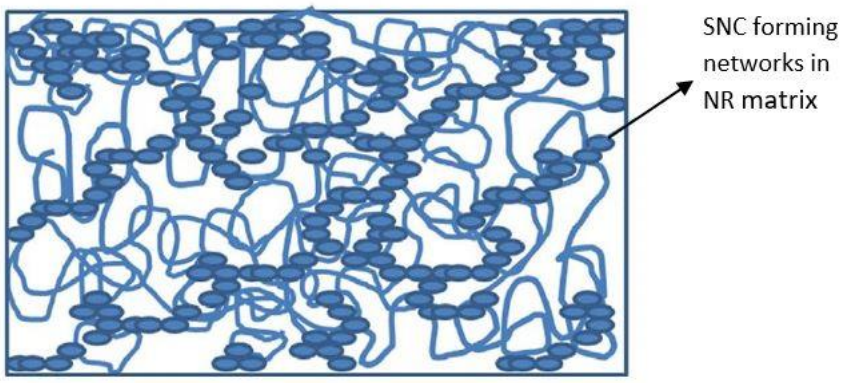

Figure 2.16: Schematic diagram of network formation between SNC and NR matrix (Rajisha *et al.*, 2014)

2.3 General aspects of shape memory polymers with prominence on the development of shape memory rubber

2.3.1 Introduction to shape memory polymers

SMPs represent a technologically important class of stimuli-responsive smart materials that can respond dynamically to external stimuli. Stimuli-responsive materials are considered as smart because of their capability to sense changes to the surrounding and provide direct response (Zhang *et al.*, 2019). There are many organisms in nature that demonstrate the stimuli-responsive phenomena. For instance, chameleons change their bodies colour when expose to changes in temperature or light intensity, sunflower bends towards the direction of the sun to increase sunlight exposure and the leaves of *Mimosa pudica* folds inwards rapidly when exposed to physical touches. The research and design of stimuli-responsive materials are done extensively to mimic the natural behaviour of the organisms. The first significant contribution to the field of SMP is the development of polynorbornene (T_g = 35-40 °C) by CDF Chimie Company, France in 1984 (Ratna and Karger-Kocsis, 2008). Despite the long history of SMP, limited scientific papers and advanced investigation had been done because of the limited processability of SMP. The invention of thermoplastic polyurethane SMP by Mitsubishi Heavy Industries Ltd., Japan reignited the interest in this field due to the easy processing and versatility of urethane in wide range of T_g (Huang *et al.*, 2010). Ni-Ti alloy (Nitinol) is the most widely used shape memory materials as it possesses desirable transition temperature (close to body temperature), great elasticity and biocompatibility (Dhanasekaran *et al.*, 2018). Despite the mentioned quality, SMAs show downside such as limited recoverable strain (less than 8%), high stiffness, high cost and complicated processing conditions. Such limitations have inspired for the search of alternative shape memory materials predominantly SMPs. Table 2.6 shows the comparison of properties between SMAs and

SMPs. SMPs offer deformation to a significantly higher degree (up to 800%) and a wider scope of varying mechanical properties when compared to SMAs in addition to their relatively cheap cost, easy processibility and biodegradable nature. Therefore, SMPs have raised mounting interest in recent times because of their applicability in numerous fields such as microelectromechanical system, 4D printing, aerospace engineering, smart actuators and biomedical devices (Xia *et al.*, 2021). Moreover, attention have been shifted to develop biodegradable and biocompatible SMPs with attractive synergic properties referring to thermal behaviour, biodegradability as well as mechanical properties due to the growing interest on the field of advanced materials (Navarro-Baena *et al.*, 2016).

Table 2.6: Comparison of properties between SMA and SMP (Liu, Qin and Mather, 2007)

Parameters	SMPs	SMAs
Density (g/cm3)	0.9-1.1	6-8
Extent of deformation (%)	Up to 800%	<8%
Young's modulus at T < T_{trans} (GPa)	0.01-3	83 (NiTi)
Young's modulus at T > T_{trans} (GPa)	(0.1-10) x 10^{-3}	28-41
Stress required for deformation (MPa)	1-3	50-200
Stress generated during recovery (MPa)	1-3	150-300
Critical temperatures (°C)	-10 - 100	- 10 - 100
Recovery time (s)	< 1s - 120	<1s
Biocompatibility and biodegradability	Yes	Part of
Corrosion performance	Excellent	Excellent
Cost ($)	10	250

SMPs are smart materials that can change their shapes upon exposure to external stimulus such as heat, light solvent, pH, magnetic field and electric field. Moreover, there are various kinds of SME discovered: one-way, two-way and three-way shape memory capability. This review primarily focuses on one-way thermally induced SMPs which have the ability to memorize a macroscopic (permanent) shape as well as fixing a temporary shape under specific temperature and stress conditions, and subsequently revert back to their original shape under stress relaxation and suitable external stimulus. The emphasis on one-way SME is due to the second objective of this research that is to investigate the effectiveness of SNC in conventional one-way SME of the rubber nanocomposite films whereas multiple-way SME requires two distinct transition temperature (T_{trans}) which diverges from the original objective. SME happens when the original shape is recovered from the deliberately fixed temporary shape. More studies about one-way thermally induced SMPs are discussed at Section 2.3.3. S_f and S_r are the two functions used to quantity SME. Shape memory functions of a polymer matrix take place below and above a (T_{trans}) which involve the freezing and activation of macromolecular chains. The extent of fixing the temporary shape upon deformation strain under T_{trans} by switching (soft) segment is known as S_f whereas the extent of recovery to the original shape upon stress relaxation above T_{trans} by hard segment is known as S_r. S_f and S_r are calculated by using Equation 2.2 and 2.3 (Sun *et al.*, 2011).

$$S_f = \frac{\varepsilon_f}{\varepsilon_l} \text{ x } 100\% \quad (2.2)$$

$$S_r = \frac{\varepsilon_l - \varepsilon_r}{\varepsilon_l - \varepsilon_i} \text{ x } 100\% \quad (2.3)$$

where ε_i is the initial strain, ε_f is fixed strain after stress is unloaded, ε_l is the loading strain upon deformation stress, ε_r is the recovery strain.

T_{trans} can be either T_g or melting temperature (T_m) of the polymer. T_g is the T_{trans} for amorphous polymers while T_m is the T_{trans} for crystalline polymers. In the case for semi-crystalline polymers either T_g or T_m can be considered as the T_{trans}. However, T_m is prefer over T_g as melting is comparatively a sharper transition (Zhang *et al.*, 2012). A shape memory cycle is defined as the progression of stress, strain and temperature during a thermomechanical cycle which involve deformation, fixing and recovery. Figure 2.17 shows the schematic illustration of shape memory cycle revealing the step-by-step development of shape memory behaviour of responsive materials.

1. Deformation: SMP is deformed to a predetermined strain under a certain stress at deformation temperature (above T_g or T_m) which often accompanied by modulus drop (material soften).
2. Fixity: The deformed polymer is cooled (temperature below T_g or T_m) under constant stress or strain for a period of time before stress relaxation. This causes the material to achieve a rigid state with the freezing of polymer chains while storing the strain as energy.
3. Recovery: The temporary deformed polymer is reheated (temperature above T_g or T_m) without any stress thus allowing the immobilized polymer chains to regain mobility and returning to its original shape. The stored strain energy is released as elastic energy to drive the recovery process.

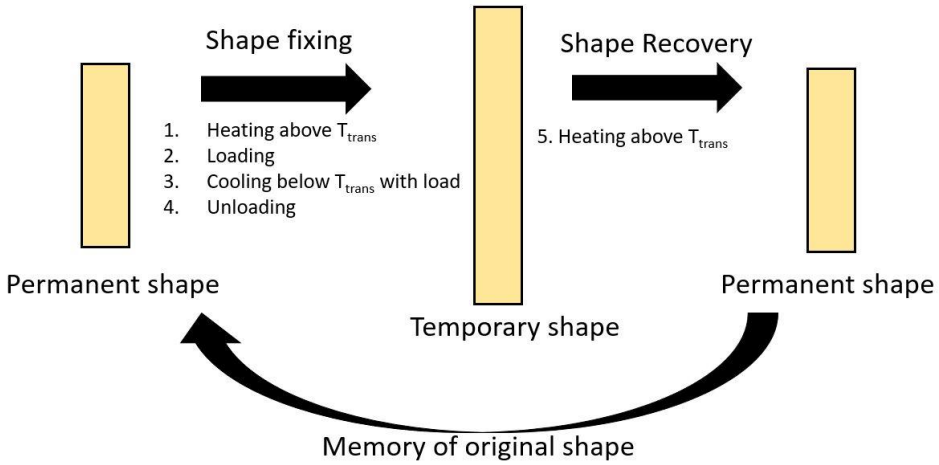

Figure 2.17: Schematic illustration of shape memory cycle

2.3.2 Mechanism for shape memory effect

The mechanism responsible for the SME of SMAs and SMPs differ dramatically although both showed similar behaviour to a certain extent. For SMAs, the existence of SME relies on the reversible thermal transition between two stable crystal structures which are the low temperature favoured (yieldable) martensitic phase and high temperature favoured austenitic phase. Pseudo-plastic fixing is realizable through the martensitic de-twinning mechanism while recovery is induced by the martensite-austenite phase transition (Liu, Qin and Mather, 2007). Contrarily, SME of SMPs is entirely an entropic phenomenon. It can be thought as the activation and freezing of molecular chain by a change in temperature from the molecular point of view. Figure 2.18 shows the molecular mechanism for heat triggered SME. In the permanent macroscopic shape, the molecular chains within the SMP networks are at the lowest energy (highest entropy) state. That is, the chains are at the thermodynamically stable state. When an external deformation stress is applied to the SMP (step 2-3 in Figure 2.18), the conformation of the chains will be changed leading to a raise in energy (lower entropy) and macroscopic deformation of the SMP. Upon cooling below the T_{trans} of the SMP (step 3-4 in Figure 2.18), the macroscopic shape of the SMP will be fixed due to the freezing of the molecular chains which led to the kinetic trap for maintaining the temporary shape (high energy state). The mobility of the molecular chains is re-activated (kinetic trap is removed) when the SMP is heated above its T_{trans} (step 4-5 in Figure 2.18). At this case, the entropic energy is released and the SMP recovers to its original shape by driving the chain to return to their highest entropy level. In short, the storing and release of the entropic energy is responsible for the shape fixing and recovery of SMP.

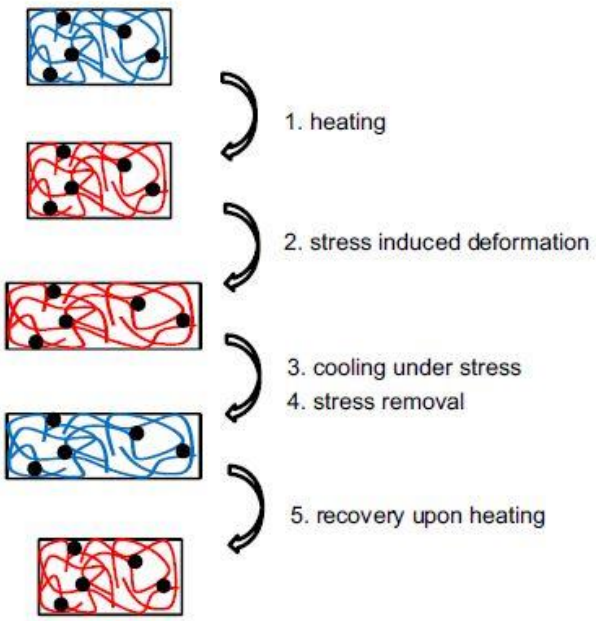

Figure 2.18: Molecular mechanism for heat triggered SME, black dots: net-points; blue line: low mobility molecular chain under T_{trans} red line: high mobility molecular chain above T_{trans} (Xie, 2011)

For a polymer to display SME, two structural requirements that must be met are the presence of crosslinks and switching (soft) segment. Crosslinks or net-points determine the permanent shape of SMP by preventing the chain slippage of macroscopic material under large deformation stress whereas switching (soft) segment allows the immobilizing of molecular chains for entropy trapping (shape fixity) to maintain the temporary shape (Behl, Razzaq and Lendlein, 2010). Without the net-points, polymer when heated with stress above its T_{trans} will undergo macroscopic shape change but with little or no change in chain conformation (entropy) that consequently caused the non-reversible macroscopic deformation of the polymer thus it shows no SME (Wu, Jin and Sun, 2011). The net-points that set the permanent shape can be in the form of physical (entanglements, crystalline network, interpenetrated network) or chemical (covalent bond) crosslinking. When the morphology of the polymer is segregated into two domains, physical crosslinking will be obtained. The domain with the highest T_{trans} acts as the hard segment while the domain associated with the second highest T_{trans} acts as the switching (soft) segment. Under certain conditions, the physical net-points may be reversible which suggests that a new permanent shape can be formed for the SMP and contribute to the re-processability. In comparison to chemical net-points, SMPs with physical net-points are more likely to unintended shape changes during shape memory cycle which leads to imperfect shape recovery. Chemical crosslinks in the other hand are obtained by the chemical reaction of two functional groups for example the vulcanization of rubber by using sulphur as the crosslinker. In contrast, most chemical crosslinking often helps in acquiring good shape recovery therefore it is non-reprocessable. A recent discovery of the incorporation of nanoparticles into polymer matrix can also serve as net-points will be discussed

in Section 2.3.4. Switching segment is usually related to the vitrification – glass transition, crystallization – melting transition, molecular cross-linking and liquid crystal clearing transition. Solidification of the switching segment via vitrification or crystallization is needed to enable the storing of entropic energy (Liu, Qin and Mather, 2007). Upon reheating, the glassy domain will become soft or the crystallites will melt with the releasing of entropic energy that recoils the molecular chain back to the original shape. Figure 2.19 shows the schematic diagram for various net-points and switching segment.

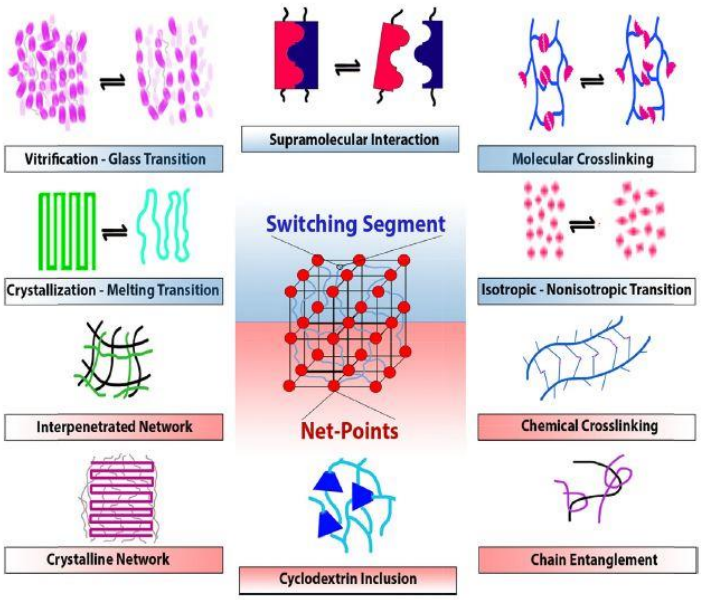

Figure 2.19: Schematic diagram for various net-points and switching segment (Zare *et al.*, 2019)

2.3.3 Classification of one-way thermally induced shape memory polymers

Based on the nature of permanent crosslinking and thermal reversible transition related to the switching domain, SMPs can be classified into four different categories namely: (i) chemically crosslinked glassy polymer ($T_g = T_{trans}$) (ii) chemically crosslinked semi-crystalline polymer ($T_m = T_{trans}$) (iii) physically crosslinked glassy polymer ($T_g = T_{trans}$) (iv) physically crosslinked semi-crystalline polymer ($T_m = T_{trans}$). These four types of SMPs can be characterized through dynamic thermomechanical behaviour as shown in Figure 2.20 where the tensile storage modulus is plotted against temperature at small oscillatory deformation of 1Hz. The elastic modulus of a material is a mechanical property that determines the stiffness and its resistance towards external loading. Elastic modulus composed of storage modulus and loss modulus, where storage modulus is a measurement for the elastic response of a material while loss modulus is the modulus for the viscous part of the material. The first type of SMP (Figure 2.20a) features a sharp T_g at the temperature of interest and shows rubber elasticity above T_g resulting from the chemically cross-linked structure. The second type of SMP (Figure 2.20b) composed of semi-crystalline structure where T_m is employed to trigger the shape recovery

which typically gives a more distinct recovery event. Here, the temporary shape is fixed by crystallization instead of vitrification which occur in the first type of SMP during the shape fixing step. The third type of SMP (Figure 2.20c) in which the crystalline or rigid amorphous domain contributes to the physical crosslinks that offer high elasticity for SME mainly in the form of phase separated block copolymers. The fourth type of SMP (Figure 2.20d) is also composed of block copolymer which soft domain crystallize while T_{m1} serve as the shape memory transition temperature instead of T_g. For both the third and fourth type of SMP, T_m and T_{m2} serve as the hard domain where the permanent shape of the polymer is characterized. However, when the temperature is above T_m or T_{m2} the material can be reshaped and reprocessed. The shape memory transition temperature is T_g (type 3) and T_{m1} (type 4) which soften to a rubbery state when $T_g/T_{m1} < T < T_m/T_{m2}$ and fixed to a temporary shape upon cooling $T < T_g/T_{m1}$.

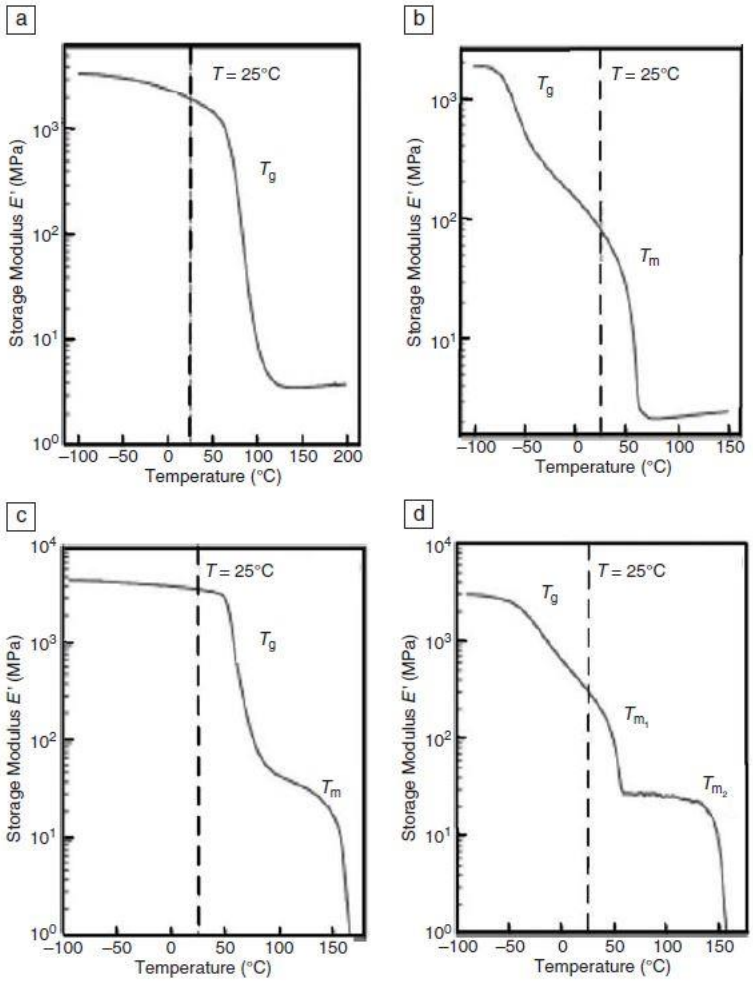

Figure 2.20: Dynamic thermomechanical behaviour for the four types of SMPs (a) chemically crosslinked glassy polymer ($T_g = T_{trans}$) (b) chemically crosslinked semi-crystalline polymer ($T_m = T_{trans}$) (c) physically crosslinked glassy polymer ($T_g = T_{trans}$) (d) physically crosslinked semi-crystalline polymer ($T_{m1} = T_{trans}$) (Leng *et al.*, 2009)

2.3.3(a) Chemically crosslinked glassy polymer

The nature of chemical (permanent) crosslinking leads to attractive attributes that include excellent degree of shape fixity and recovery, changeable working capacity that is governed by the rubbery modulus through the extent of crosslinking and a strong hold of permanent shape due to the strong chemical bonds. As discussed, once the material is processed (casting or moulding), the shape is fixed permanently as the primary shape is covalently bonded. The length and functionality of the crosslinking, switching segment and network structure define the shape memory behaviour for this type of SMP (Kalita, 2018). An example for this type of SMP is chemically crosslinked vinylidene random copolymer with methyl methacrylate and butyl methacrylate acting as the two vinylidene monomers. These two monomers showed distinct T_g values of 110 °C and 20 °C respectively (Liu and Mather, 2002). T_g of the copolymer showed a single sharp transition between the mentioned values that is tuneable by varying the composition of the two monomers while the work capacity controlled by the rubbery modulus is adjustable to fit specific application by manipulating the extent of crosslinking, in this case by copolymerization with tetra-ethylene glycol dimethacrylate. This class of SMP showed complete shape fixity ($T < T_g$) and recovery ($T > T_g$) in hot water at a short period of time. This material has the advantage of being castable to a definite dimension and optically transparent. Ultrahigh molecular weight polymer ($> 10^6$ g mol^{-1}) with T_g higher than room temperature may also be included in this type of SMP due to their lack of flow below T_g as well as excellent shape fixing by vitrification. These characteristics make the polymers behave like the example mentioned above. A summary of chemically crosslinked glassy polymer with shape recovery triggered by T_g is showed in Table 2.7.

Table 2.7: Summary of chemically crosslinked glassy polymer with shape recovery triggered by T_g (Liu, Qin and Mather, 2007)

Materials	T_g (°C)	Unique features
P(MMA-co-VP)-PEG semi-IPNs	65	Semi-IPN
Copolyester	48-66	Biodegradable
P(AA-co-MMA)-PEG	60	Wide transition
Corn oil copolymer	0-90	Biomaterial
PMMA-PBMA copolymers	20-110	Transparent
Fish oil copolymers	30-109	Biodegradable
PET-PEG copolymer	< 80	N/A
P(MA-co-MMA)-PEG	50-90	N/A
Thermosetting PU	< 56	Water swollen
Polynorbornene	40	Precise T_g
High M_w PMMA	105	Deformable at $T < T_g$

Remarks: P(MMA-co-VP)-PEG semi IPNs = poly((methyl methacrylate)-co-(N-vinyl-2-pyrrolidone))-polyethylene glycol semi interpenetrating network, P(AA-co-MMA)-PEG = poly(acrylic acid-co-methyl methacrylate)-polyethylene glycol, PMMA-PBMA = polymethyl methacrylate-polybutyl methacrylate PET-PEG = polyethylene terephthalate – polyethylene glycol, P(MA-co-MMA)-PEG =

Poly(methacrylate-co-methyl methacrylate)-polyethylene glycol, PU = polyurethane
M_w = Molecular weight, N/A = non-available

2.3.3(b) Chemically crosslinked semi-crystalline polymer

This type of SMP is similar to the first mentioned, once processed it cannot be reshaped because of the permanent setting by the strong covalent bond. Here, T_m is employed as the critical temperature to trigger SME and the temporary shape is fixed by crystallization instead of vitrification as discussed in Section 2.3.3. A comparatively lower temperature than T_{trans} can be chosen to allow a higher degree of crystallization for the improvement of shape fixing for this kind of SMP. The sharper transition zone of T_m aid in the faster shape recovery for this first order transition (Kalita, 2018). Compared with glassy materials, this class of SMP offers better compliances where its shape memory behaviour is influenced by the functionality of crosslink and degree of crystallinity which is often affected by the extent of crosslink. This type of SMP includes bulk polymers for instance semi-crystalline rubber, liquid crystals elastomer and hydrogels with phase separated crystalline microstructure. Table 2.8 shows a summary for this class of SMP associated with the hard segment, soft segment and T_{trans}. Polycyclooctene chemically crosslinked with dicumyl peroxide has been developed and showed shape memory behaviour (Liu *et al.*, 2002). Initially, the neat polycyclooctene synthesized from the ring-opening metathesis polymerization of cyclooctene and catalysed by dihydroimidazolylidene-modified Grubb's catalyst does not exhibit shape memory behaviour because of the missing of rubbery plateau region above T_m. The crosslinked polycyclooctene showed shape memory behaviour where the net-points and polycyclooctene act as the hard and soft segment respectively. This is in agreement with the previous statement where the presence of crosslinks is a compulsory requirement for the shape memory effect. The shape recovery for this SMP was found to increase with higher degree of crosslink which is closely related to the theory of rubber elasticity – network structures with high crosslink density tend to return to the lowest entropy state due to the high driving force. Another example for this type of SMP is the crosslinked poly(ethylene-co-1-octene) has been developed (Kolesov *et al.*, 2009). The switching temperature of this SMP can be designed to between 60 °C – 100 °C by varying the degree of crosslinking. The shape fixity and recovery were found to increase with the crystallinity level and extent of crosslinking. It was observed that the perfection of crystalline structure has strong influence on the stored strain energy.

Table 2.8: Examples of chemically crosslinked semi-crystalline SMP (Kalita, 2018)

Materials	Hard Segment	Soft Segment	T_{trans} (°C)
Dicumyl peroxide polycyclooctene	Crosslink	Polycyclooctene	30-60
Alkoxysilane-poly-(Ɛ-caprolactone)	Crosslink	PCL	40-60
Natural Rubber	Crosslink	Polyisoprene	0-45
LDPE	Crosslink	LDPE	60-100
PU-epoxy	TDI/1,4 butanediol	PCL	40-60

Remarks: PU = polyurethane, TDI = toluene-diisocyanate PCL = polycaprolactone, LDPE = low density polyethylene

2.3.3(c) Physically crosslinked glassy polymer

For this type of SMP, the hard or rigid amorphous domains may act as physical crosslink via Van Der Waals forces, polar-polar interactions and hydrogen bonding to afford the elasticity required for SME to take place mainly in the form of phase-separated linear block copolymers and multiblock copolymers or blends. As mentioned in Section 2.3.3, the material will flow and will be able to be reshaped and reprocessed when the temperature is raised above T_g and T_m of the copolymer. The comparatively lower T_g of the copolymer is responsible for the SME as shown in Figure 2.22(c). The possible losses of physical crosslinks due to mechanical deformation may cause a lower extent of SME for this type of SMP. Physically crosslinked MDI and PTMG soft segment polyurethane based SMP had been developed (Cho *et al.*, 2004). Two types of PTMG with molecular weight 1800 and 1000 g mol^{-1} are used as soft segments. The response of SME based on the soft segment arrangement of polyurethane SMP was investigated. The results showed that random and block copolymer exhibited shape recovery ratios of higher than 80% whereas copolymer with one kind of PTMG showed insignificant SME. Another example for this class of SMP is the blend of PCL based thermoplastic polyurethane with phenoxy resin which act as the soft segment whereas HDI/4,4'-dihydroxy biphenyl act as the hard segment (Jeong, Ahn and Kim, 2001). This blend made a single miscible domain and showed single T_g which lied between those of PCL segment and phenoxy resin. The blend showed decent shape recovery when the trigger temperature is actuated to 70 °C which is at the higher range of T_g region. Other examples of physically crosslinked glassy polymer are showed in Table 2.9. Most of the examples showed in Table 2.9 have tuneable T_g by varying the ratio of the blends. The best transition temperature can then be investigated based on the requirement needed on shape fixity and shape recovery of the SMP.

Table 2.9: Examples of physically crosslinked glassy polymer (Kalita, 2018)

Materials	Hard Segment	Soft Segment	T_{trans} (°C)
PU-phenoxy resin	HDI/4,4'-dihydroxy biphenyl	PCL/phenoxy resin miscible domain	40-70
PU-PVC	HDI/4,4'-dihydroxy biphenyl	PCL/PVC miscible domain	40-50
Poly(ethylene adipate)-PU	MDI/1,4-butanediol	Poly(ethylene adipate)	10-50
PolyStyrene-polybutadiene	PolyStyrene	Polybutadiene	70-140
Poly(acrylic acid)-co-methyl methacrylate)/PEG	Crosslink	Poly(acrylic acid)/PEG blend	45-60
PVDF/ACP	Netpoints	PVDF-ACP amorphous phase	45
Poly(L-lactide-co-Ɛ-caprolactone)-PU	TDI/1,4-butanediol	Poly(L-lactide-co-Ɛ-caprolactone)	30-55

Remarks: PU= polyurethane, HDI = hexamethylene diisocyanate, PCL = polycaprolactone,
PVC = poly(vinyl chloride), MDI = methylene diphenyl diisocyanate, TDI = toluene diisocyanate
PEG = poly(ethylene glycol), PVP = polyvinylpyrrolidone, PVDF = poly(vinylidene fluoride)
ACP = acrylic copolymer

2.3.3(d) Physically crosslinked semi-crystalline polymer

In this type of SMP, the soft segments will crystallize, instead of T_g, T_m is used as T_{trans} for SME. Such SMP shows narrow transition zone unlike the SMP discussed in Section 2.3.3(c) with amorphous reversible domain that displays a broader range of T_{trans}. The shape memory behaviour for this class of SMP can be modified through the ratio of hard and soft domains. Various SMP compositions, with crystalline soft segments and their SME are presented in Table 2.10. PCL has been extensively used for the synthesis of PU with crystalline soft segment by microphase separation of the PCL segment. The optimum shape recovery temperature is generally between 40 °C to 60 °C depending on the molecular weight of PCL as well as the composition of soft and hard segment (Kim *et al.*, 2000). However, some reports suggest the crystallization of PCL segment is obstructed by the low molecular weight of the polymer. No SME takes place when the average molecular weight of the PCL copolymer is below 2000 g mol^{-1} while the optimum molecular weight was observed to be 5000-6000 g mol^{-1} (Kim, Lee and Xu, 1996). The shape fixity of the SMP was found to increase over the number of cycles under cyclic thermomechanical measurements. This discovery is mainly attributed to the relaxation of the SMP after several cycles which resulted in the increasing orientation and crystallization of the chains. The major issues of PU based SMP are the difficulty in achieving maximum crystallization and stable hard domains. Various methods such as the addition of mesogenic segment and ionic groups have been reported to enforce the microphase separation of PCL. Partial replacement of 1,4 BD by an extender with ammonium ions as backbone for the synthesizing of PCL based PU cationomer SMP has been developed (Yong *et al.*, 2006). NMDA or BIN has been used as the extender while the

corresponding cationomers were synthesized by acetic acid neutralisation. Introduction of the cationic groups have shown improvement of both the shape fixity and shape recovery of the SMP.

Table 2.10: Examples of physically crosslinked semi crystalline polymer (Ratna and Karger-Kocsis, 2008)

HS	SS	%SS	T_r (°C)	$R_f(1)/R_f(4)$ (%)	$R_r(1)/R_r(4)$ (%)
MDI/1,4-BD	PCL	70	44-55	82/95	82/73
MDI/1.4-BD	PCL/PBC blend (6/4)	38-62	18-48	92	60
MDI/BEBP or BHBP	PCL	57-70	41-50	80/85	80/75
MDI/DMPA	PCL	70	45	95/95	66/45
MDI/NMDA or BIN	PCL	75	10-20	98	90
Aramid	PCL	78-91	14-54	78	99
MDI/1,4-BD + ODO	PBAG	75	40-45	~100	~100
TDI/1,4-BD	Trans-polyisoprene	70	65	99	85
PET	PEO	72	58	>90	-

Remarks: SS = soft segment, %SS = percentage of soft segment, T_r = recovery temperature
$R_f(1)/R_f(4)$ = values of shape fixity after the first and forth cycle,
$R_r(1)/R_r(4)$ = values of shape recovery after the first and forth cycle,
MDI = methylene diphenyl diisocyanate, BD = butanediol, PCL = polycaprolactone,
BEBP = bis(2-hydroxyethoxy)biphenyl, BHBP = bis(2-hydroxyhexoxy)biphenyl,
DMPA = dimethylol propionic acid, NMDA = N-methyldiethamine,
BIN = bis(2-hydroxyethyl)isonicotinamide, ODO = octadecanol,
PBAG = poly(1,4 butylene adipate) glycol, PET = poly(1,4 butylene adipate) glycol,
PEO = polyethylene oxide

2.3.4 Shape memory polymer nanocomposites

The demands of advanced application SMPs have leaded to continuous development of SMP nanocomposites. As discussed in Section 2.3.1, although SMPs have a few advantages over SMAs, they still imposed several limitations such as low strength, low stiffness and produce elastic modulus up to only 10 MPa (Leng *et al.*, 2009). Therefore, incorporation of nano reinforcement fillers into SMPs have attracted tremendous interest due to the significant improvement of mechanical strength, recovery stress and speed as well as thermal properties (Meng and Hu, 2009). SMPs nanocomposite are the combination of two materials where the dimension of one domain lies in the range of 1-100nm. This represents a better option than the conventional filled polymer due to the fact that nanofillers offer larger surface area to volume ratio that results in higher interfacial interaction between the SMP and nanofiller. The examples for the common nanofillers are nano-clay, carbon nanotube and carbon nanofiber.

Montmorillonite, attapulgite, saponite and synthetic mica are the common clay materials used to prepare nano-clay. Clay particles are generally formed by layered structure where each layer composed of octahedral and tetrahedral structural sheets. The effect by the addition of nano-clay as reinforcement filler on the mechanical properties and SME of polyurethane/nano-clay nanocomposites had been reported (Cao and Jana, 2007). Tensile strength and elongation at break of the nanocomposite is found to increase with the content of nano-clay. The improvement of tensile strength is because of the increment in interfacial bonding between nano-clay and polymer chain that inhibited the chain mobility while the enhancement of elongation at break is attributed to the present of ammonium ions in clay particles who acted as plasticizers that suspended the chain formation in the polymer matrix. On the other hand, the study revealed that the shape fixity of the SMP nanocomposite decreased with increasing amount of nano-clay due to the decrease in crystallinity of the overall polymer structure as shown in Figure 2.21(a). Contrarily, the shape recovery is found to increase with the incorporation of nano-clay. It had been reported that the addition of 1wt% nano-clay exhibited the best shape recovery when compared to higher composition of 3wt% and 5wt% as shown in Figure 2.21(b). It is because 1wt% of nano-clay has higher exfoliation and lower rate of relaxation resulting in higher shape recovery.

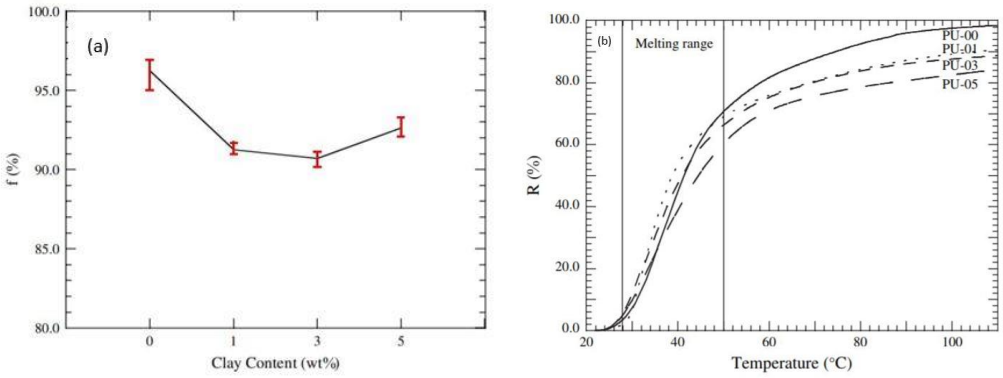

Figure 2.21: (a) shape fixity polyurethane/nano-clay (b) shape recovery of polyurethane/nano-clay where PU-00, PU-01,PU-03 and PU-05 indicate 0wt%, 1wt%, 3wt% and 5wt% of nano-clay respectively (Cao and Jana, 2007)

The incorporation of carbon nanotube into various polymer matrices displayed excellent result in the mechanical and electrical properties of the material. This has attracted immense interest for the investigation towards SMP/carbon nanotube nanocomposite. High performance shape memory epoxy/carbon nanotube nanocomposites had been developed (Liu *et al.*, 2016). The prepared materials showed a wide range of T_g (65 °C – 140 °C) with excellent mechanical properties. The wide range of T_g enable researchers to fine tune the trigger and recovery temperature to achieve the desired SME. The SMP nanocomposite showed high modulus up to 3GPa at room temperature and

tensile strength of 30 MPa. Moreover, high shape fixity (up to 98%) and shape recovery (up to 92%) as shown in Table 2.11 is achieved with 1.0 shape memory epoxy and 0.25wt% of carbon nanotube at elevated temperature of 20 °C above the highest T_g for shape recovery and cooled at 20 °C for shape fixity. Mechanical properties, thermal stability and SME of biobased polyurethane/multiwalled carbon nanotube nanocomposites were investigated in another study (Kalita and Karak, 2014). Multiwalled carbon nanotubes were modified through non-covalent technique using polyoxyethylene octyl phenyl ether for better dispersion of the nanofiller in polymer matrix. The study revealed such nanocomposite exhibited improved tensile strength and thermal stability when compared with pure polyurethane. This can be due to the homogenous distribution of nanofiller in polymer matrix that increased interfacial interaction such as physical crosslinking. Moreover, the addition of multiwalled carbon nanotube may serve as a physical barrier so that the volatile component will have to overcome a more difficult path during the thermal decomposition process, as a consequence, enhanced the thermal stability of the material. As for the SME, all samples including polyurethane showed 100% shape fixity however the shape recovery speed increased with the amount of multiwalled carbon nanotube. This can be attributed to the increased elastic stored energy in the nanocomposite because of the higher degree of physical crosslinking between nanofiller and polymer matrix.

Table 2.11: SME of SMP/carbon nanotube nanocomposite (Liu *et al.*, 2016)

Materials	S_f (%)	S_r (%)
0.5EP	96.5	86.7
0.5EP-0.25%	96.7	97.6
0.5EP-0.75%	97.6	83.7
1.0EP	97.9	96.4
1.0EP-0.25%	98.1	92.1
1.0EP-0.75%	98.0	91.4

Remarks: S_f = percentage of shape fixity, S_r = percentage of shape recovery, EP = shape memory epoxy
0.25% and 0.75% = composition of carbon nanotube

Another type of carbon-based nanofiller that significantly improve the mechanical properties and SME of SMP is carbon nanofiber. Carbon nanofibers have great effect on the crystallinity, degree of crosslinking and conductivity of SMP that lead to differ behavior of SME. By incorporation of carbon nanofibers, SME can be triggered by multiple stimuli. The performance of carbon nanofibers on the mechanical properties and SME mainly depends on the homogeneity distribution of nanofiller in the polymer matrix. Chemical surface treatment by oxidizing carbon nanofiber in a mixture of sulphuric acid and nitric acid at various temperatures is an effective method to improve their dispersion in the polymer matrix. The mechanical properties and SME by electrically trigger epoxy/carbon nanofiber nanocomposite had been investigated (Luo and Mather, 2010). As expected, the nanocomposites showed higher tensile strength and elastic modulus than the pristine epoxy. Furthermore,

nanocomposites exhibited excellent shape recovery (up to 100%) under 15V of DC voltage. This is the cause of well distributed carbon nanofiber in polymer matrix and the generation of efficient percolating conductive network. In another study, the mechanical properties and SME of thermoplastic polyurethane/oxidized carbon nanofiber had been evaluated (Jimenez and Jana, 2009). Generally, tensile strength and elongation at break of carbon nanofiber (1wt%) reinforced thermoplastic polyurethane increased 100% and 150% respectively over the pure specimen, however, both of these properties decreased when the composition of nanofiller is higher than 1wt% due to agglomeration. On the other hand, tensile strength can be increased by 200% with chemically modified oxidized carbon nanotubes attributed to better nanofiber dispersion. It was observed that shape fixity of the nanocomposites decreased dramatically with the presence of nanofiller as shown in Figure 2.22(b). It is because the soft segment crystallinity of the SMP decreased from 29% for unfilled thermoplastic polyurethane to less than 15% with 5wt% carbon nanofiber content as shown in Figure 2.22(a). Contrarily, nanocomposites exhibited higher recovery stress than pure thermoplastic polyurethane.

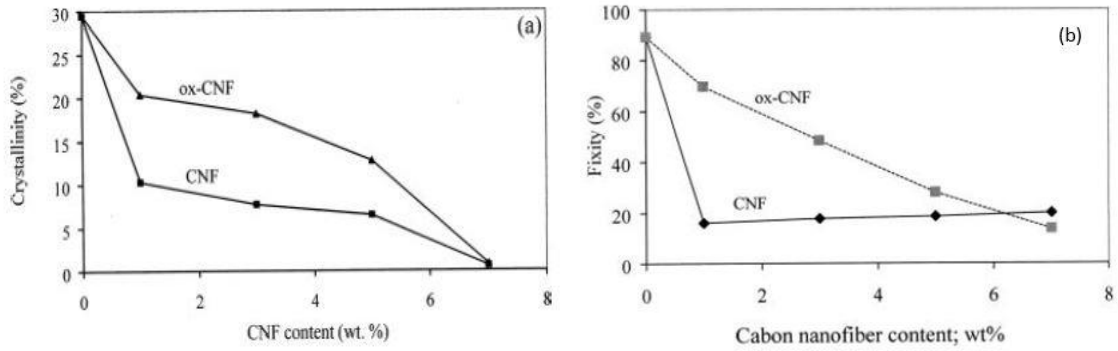

Figure 2.22: (a) crystallinity of thermoplastic polyurethane/carbon nanofiber nanocomposites (b) shape fixity of the SMP where ox-CNF represents oxidized carbon nanofiber, CNF represents carbon nanofiber (Jimenez and Jana, 2009)

Recently, cellulose nanocrystals as a more sustainable, biodegradable and renewable alternative to carbon-based nanofiller has been extensively studied. Cellulose nanocrystals have been incorporated into commercially obtainable shape memory polyester urethane (Shirole *et al.*, 2018). The shape memory behaviour was made available by formulating the nanocomposites and modifying the crystallization of soft switching segment via addition of nucleating agent. The addition of cellulose nanocrystals had increased the tensile strength by approximately 3.5-fold while shape fixity increased from 47 to 75% at a particular fixing temperature. In another study, cellulose nanocrystals were incorporated into low molecular weight polyethylene glycol based polyurethane where nanocomposites fabricated by in-situ polymerization and pre-polymer approach (Khadivi *et al.*, 2019). The addition of cellulose nanocrystals had no major impact on thermal-physical and thermal

properties of the matrix. However, the modulus, tensile strength and elongation at break of the nanocomposites were significantly improved with 0.5%wt of cellulose nanocrystals. The nanocomposites showed shape memory behaviour with the same dosage while at higher loading no shape memory effect was observed.

2.3.5 Development of shape memory rubber

SMR is a class of SMPs that possess the ability to retain the permanent shape after being programmed to a temporary shape under thermal, electrical, magnetic, light or moisture command. NR as a class of polymer that is capable of supporting large stress up to 30MPa at strain of multiple 100% (Rattanasom, Prasertsri and Ruangritnumchai, 2009). Therefore, research regarding SMNR has attracted tremendous interest because of its excellent properties. The mechanism for SME of SMNR is consistent with the statement mentioned in Section 2.3.2. SMNR consists of two phases which are switching (soft) segment and permanent net-points that serve as hard segment. SIC of NR is responsible for the shape fixity while the presence of crosslinking in NR serve as the permanent net-points that offers shape recovery (Reghunadhan *et al.*, 2021). SME of SMPs usually rely on T_g and T_m of the material, low T_g (-70 °C) of NR makes research works on SMNR uncommon. Two strategies that had been reported to develop SMNR are SIC in lightly crosslinked (<0.4%) NR network that have trigger temperature above room temperature (Katzenberg, Heuwers and Tiller, 2011) and swelling crosslinked NR with stearic acid that will form a percolated crystalline network upon cooling (Brostowitz, Weiss and Cavicchi, 2014).

A number of attempts have been made to fabricate SMR in order to investigate their shape memory behavior under different conditions. Table 2.12 shows a compiled version of fabricated SMR with trigger mechanism, SME and methods to quantify shape memory behavior. From Table 2.12, three SME trigger mechanisms have been discovered to fabricate SMR. First of all, lightly cross-linked SMNR at the borderline between thermoplastic and elastomer allow SIC to fix the rubber network that is stable at room temperature. The low surface energy of strain induced crystals have a melting point higher than room temperature promote the existence of SMNR (Cavicchi, 2015). Secondly, swelling of rubber specimens in fatty acid helps to induce SME in rubber. Swelling allows the formation of crystalline platelets upon cooling which will act as the temporary network (soft segment) and subsequently increase the trigger temperature to T_m of the fatty acid. Thirdly, chemically crosslinked rubber with non-conventional crosslinker such as zinc ferulate and 3-amino-1,2,4-triazole exhibited high strength and deformability as well as possessing T_g above room temperature that proved to be a major upside for SME. Most of the SMR triggered by the mechanisms mentioned showed excellent SME with shape fixity higher than 90% and shape recovery of 100%. The quantification methods of

SME which include self-made stretching apparatus, tensile tester and dynamic mechanical analyzer vary accordingly to the authors. As a conclusion, SMR showed promising SME with slightly affected mechanical properties makes them potentially useful in many applications.

Table 2.12: Compilation of fabricated SMR

Rubber film forming	Trigger mechanism	SME and trigger temperature	Quantify method	References
NR latex casting, solid NR mastication	Lightly crosslinked SMNR	Achieved 92% shape fixity, 100% shape recovery at room temperature (20 °C) and cooled at 0 °C	Custom made stretching apparatus operated in strain-controlled mode	(Heuwers *et al.*, 2013)
Solid NR mastication	Swelling of NR with palmitic acid	Achieved 98% shape fixity, 100% shape recovery at elevated temperature of 75 °C and cooled at 10 °C	Tensile testing machine	(Setyadewi and Indrajati, 2019)
Solid ENR mastication	ENR crosslinked by in-situ formed zinc ferulate via oxa-Michael reaction	Achieved 100% shape fixity, 100% shape recovery at elevated temperature of 30°C above T_g and cooled at 40 °C below T_g	Dynamic mechanical analyzer	(Zhang *et al.*, 2015)
ENR melt mixing	ENR crosslinked by 3-amino-1,2,4-triazole with bisphenol-A as a catalyst	Achieved 95% shape fixity, 100% shape recovery elevated temperature of 20°C above T_g and cooled at 20 °C below T_g	Dynamic mechanical analyzer	(Chang *et al.*, 2006)
NR from Malaysian Rubber Board	Swelling of NR with palmitic acid	Achieved 80% shape fixity, 83% shape recovery at elevated temperature of 75 °C and cooled at 10 °C	Modified adjustable spanner	(Wee, Chai and Ho, 2017)
NR latex molding	Swelling of NR with palmitic acid and stearic acid	Achieved 92% shape fixity, 100% shape recovery at elevated temperature of 70 °C and cooled at 0 °C	Self-made special elongation device	(Kow, Chai and Ho, 2020a)
NR rubber band	Swell crosslinked NR with stearic acid	Achieved 99% shape fixity, 88% shape recovery at elevated temperature of 75 °C and cooled at 10 °C	Modified wrench and dynamic mechanical analyzer	(Brostowitz, Weiss and Cavicchi, 2014)
Solid XNBR mastication	XNBR matrix crosslinked with ionic associations	Achieved more than 90% shape fixity, more than 90% shape	Modified wrench and dynamic	(González-Jiménez *et al.*, 2022)

	between MgO salt and the carboxylic groups	recovery at elevated temperature of 150 °C and cooled at 25 °C	mechanical analyzer	

Remarks: The summarized SME and trigger temperatures are the optimum results from the literatures

2.3.6 Applications of shape memory polymer

Since SME in polymeric materials were first discovered, potential applications for SMP almost exist in every part of our daily life ranging from traditional applications such as heat shrinkable tapes and tubes made with radiation crosslinked polyethylene (Kleinhans and Heidenhain, 1986), thermally reversible recording for information storage (Terai, 2002), temperature sensors (Osada, 1995; Asar *et al.*, 2022) and actuators (Yoo *et al.*, 2006). Furthermore, thermally induced SMPs have been developed in the field of aerospace engineering to meet current and future demand due to their attractive properties such as reasonably low cost, light weight and tunable shape memory behavior. These desirable features make SMPs well-suited for small and large applications such as hinges, versatile optical systems, antennae as well as morphing structures (Meng and Li, 2016). Figure 2.23 shows the recovery process of a prototype of solar array actuated by SMP hinge. After fixing the temporary shape at room temperature, the SMP hinge was heated to 80°C, the SMP hinge deployed from 90 ° to 0 ° in 80 seconds showing the complete shape recovery of the SMP.

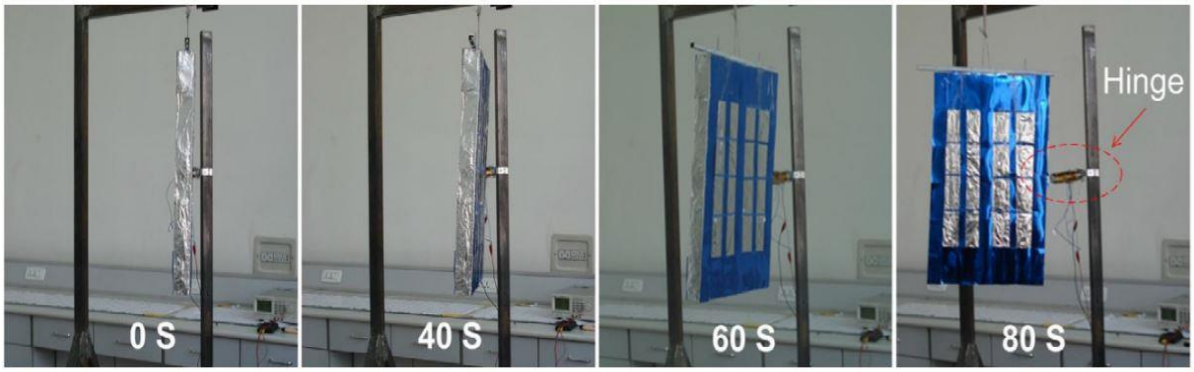

Figure 2.23: Shape recovery process of solar array prototype actuated by SMP hinge (Lan *et al.*, 2009)

The biomedical applications of SMPs have raised tremendous interest due to their nature of being biodegradable, wide range of tailorable stiffness (0.01 GPa < E < 3 GPa), tunable transition temperature with sharp transition zone, excellent shape deformation and recovery as well as being able to response swiftly to the applied stimulus. Currently in the animal testing stage, many novel medical devices using SME have been investigated to minimize the impact of invasive surgery and enhance the recovery process of patients. Large bulky medical devices could potentially be inserted into the body with a compressed temporary shape and then be expanded to the permanent shape that is required to perform the treatment. Figure 2.24(a) shows the removal of blood clot by laser-

activated SMP microactuator coupled to an optical fiber (Small IV *et al.*, 2005). The medical device is introduced into blood vessel in its temporary straight rod form and coils into its permanent corkscrew shape for blood clot removal upon laser activation. Figure 2.24(b) shows a self-tightening biodegradable suture fabricated from thermoplastic monofilament fiber based SMP (Lendlein and Langer, 2002). The development of this smart suture is inspired from the difficulty in tying a knot to close an incision or open wound during endoscopic surgery. It is extremely challenging to manipulate the conventional suture so that the wound lips are closed under the right stress. With the design of smart suture, the temporary shape of the medical device can be formed by elongating the fiber with controlled stress and would shrink while tightening the knot by applying optimum force to close the wound when raised above the transition temperature. An additional set of experiments had been done to investigate the feasibility of the concept is shown in Figure 2.24(c). The programmed smart suture was loosely stitched through rat belly and abdominal muscle. Shape recovery was triggered when the temperature was raised to 41 °C while the smart suture tighten automatically releasing an impressive force of 1.6N during the process (Lendlein and Langer, 2002). The following examples have given a solid foundation for SMP to excel in biomedical applications.

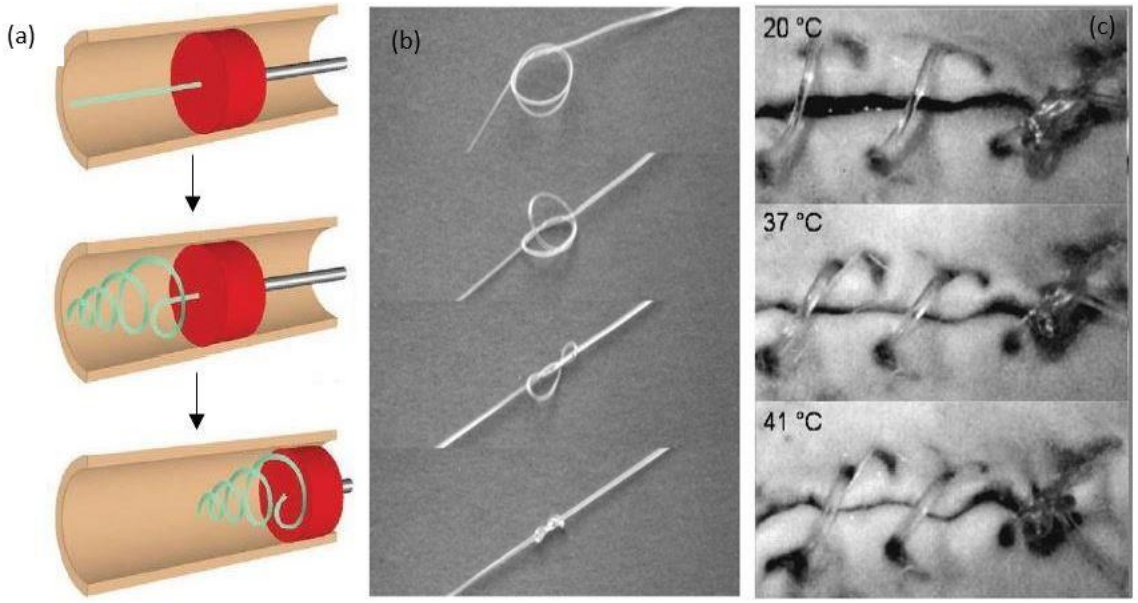

Figure 2.24: (a) SMP microactuator coupled to an optical fiber. The figure from top to bottom showed the coils forming for blood clot removal upon laser activation (Small IV *et al.*, 2005) (b) Self-tightening smart suture. The figure from top to bottom showed the knot was tighten in 20s when heated to an elevated temperature of 40 °C (Lendlein and Langer, 2002) (c) Biodegradable smart suture for wound closure. The figure from top to bottom shows the shrinkage of fiber and wound closure when temperature is increased from 20 °C to 40 °C (Lendlein and Langer, 2002).

2.4 Potential of shape memory rubber as alternative for energy storage application

2.4.1 Current state of the art for global energy

Global energy consumption has increased dramatically as a result of escalating industrialization, technological innovation, increasing demand and economic growth in developing countries. Despite the consistent surge in energy price, the needs for energy are soaring rapidly because of the increase in human population, per capita consumption, energy supply in remote areas, static large-scale machinery and portable devices. According to the recent survey released by International Energy Agency (IEA), the global energy demand will rise by 4.5% or a staggering 1000 TWh in 2021 which boosted CO_2 emission by over 5% (Grundy, 2021). Given the current situation, renewable energies are being employed at an astounding rate to counter the worldwide environmental issue of CO_2 release for the sake of no greenhouse gases is emitted during the energy production process. On the report from International Renewable Energy Agency (IRENA), the share of renewable energy sources will rise from 26% currently to 57% by 2030 and 86% by 2050 to promote sustainable growth for future energy (IRENA, 2020). However, these green energy sources may be inconsistent due to unavoidable circumstances for example: inefficiency of solar panels and wind turbines at cloudy and calm weather. Therefore, to account for these intermittencies, energy storage systems (ESS) are regarded as the most realistic choice who possesses excellent prospective to optimize energy handling and control energy spillage (Mitali, Dhinakaran and Mohamad, 2022). ESS are the set of technologies used to harvest, transform and store energy which can be then withdrawn at a later time to perform practical operations. An ESS is defined by its capability to store certain quantity of energy and power (Arcos-Vargas, Canca and Nunez, 2021). Furthermore, report suggested that 345GW/ 999 GWh of new energy storage capacity will be added globally by 2030 to accommodate the increasing energy output (Henze, 2021). Figure 2.25 shows the forecast of global cumulative energy storage installation in various countries which highlighted the dramatic increase in demand of ESS due to the rising of renewable energy sources. According to estimates, requirements for ESS will become triple the present values while the quantities of electricity supply through grids will be dominated by stationary energy (Ralon *et al.*, 2017). ESS can be used in every stage of the network that encompasses generation, storage, transmission and distribution for many stationary applications.

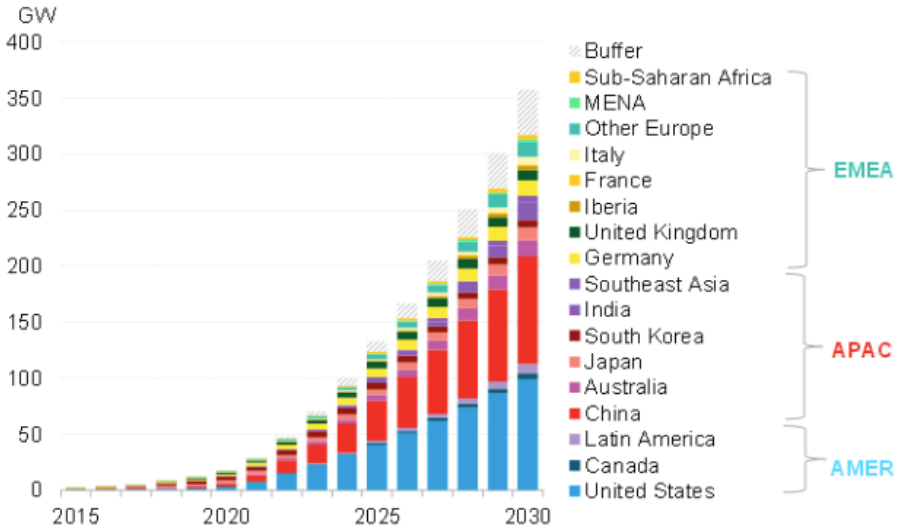

Figure 2.25: Accumulation of global energy storage installations from 2015-2030 (Henze, 2021) Note: MENA= Middle East & North Africa, EMEA= Europe, Middle East and Africa, APAC= Asia-Pacific, AMER= Americas

2.4.2 Classification and techniques of energy storage systems

As discussed in Section 2.4.1, current status of global energy suggested that the demand for ESS is expected to skyrocket in the near future while the economy is shifting towards production of greener energy. These demands are the driving force behind for researchers to develop novel methods of energy storage that are capable of delivering consistent and controlled power while being more efficient. ESS are designed to sustain unforeseen circumstances during peak and off-peak season. The integration of ESS and energy utilization significantly reduced electricity production that in turn lowered the emission of CO_2 to the atmosphere (Olabi *et al.*, 2021). Therefore, installation of renewable energy sources must be coupled with ESS to achieve the best outcome of loading and unloading of green energy (Ralon *et al.*, 2017). ESS is classified by the form of energy stored, usage of energy, storing efficiency and time. Figure 2.26 shows the classification of major ESS based on the form of energy. From Figure 2.26, energy can be stored in the form of thermal, mechanical, chemical, electrochemical and hybrid form which is a blend two different forms.

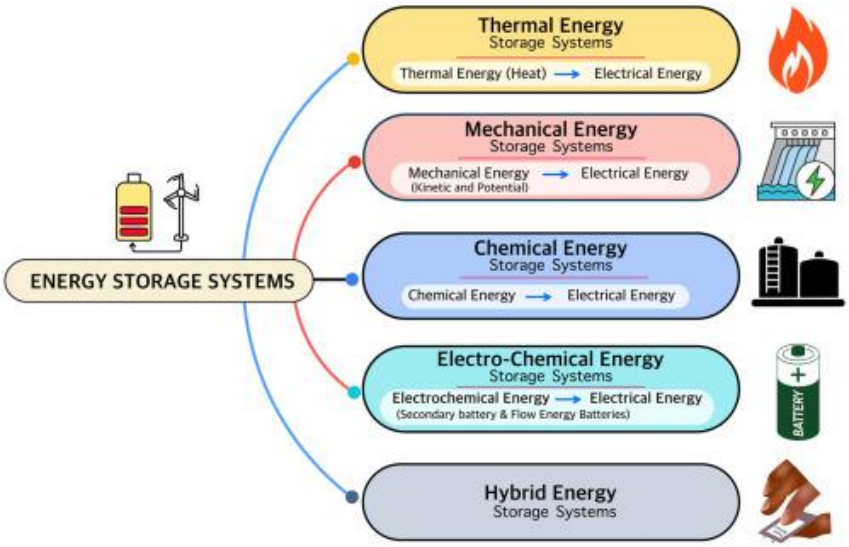

Figure 2.26: Major energy storage systems (Mitali, Dhinakaran and Mohamad, 2022)

Thermal energy storage systems (TESS) are basically dealing with the changes in temperature which specifically designed to store heat energy by heating, cooling, melting, condensing and vaporizing of a substance (Mitali, Dhinakaran and Mohamad, 2022). The materials are stored in an insulated repository of high or low temperatures where the energy from these materials are recovered at a later time for various application such as heating or cooling of a space, production of hot water and electricity generation depending on the operating temperature range (Chen *et al.*, 2009). In this case, the materials gain energy when temperature is increased and lose energy when temperature decreased. The three main types of TESS are sensible heat, latent heat and thermochemical heat energy storage. Sensible heat storage system is where the energy is contained through increasing or decreasing in temperature of the single-phase storage medium. Sensible liquid storage for energy includes aquifer (Lee, 2010; Bloemendal and Olsthoorn, 2018), hot water (Nabavitabatabayi *et al.*, 2014; Sarbu and Sebarchievici, 2016; Bespalko, Miranda and Halychyi, 2018), gravel-water (Rad and Fung, 2016) and molten salt (Bauer *et al.*, 2012; Ushak, Fernández and Grageda, 2015) thermal energy storage systems. Latent heat energy storage system deals with the phase change of storage materials when a certain amount of heat is released or absorbed. Moreover, thermochemical energy storage involves association or dissociation of molecular bonds in a completely reversible chemical reaction where the heat energy is stored by utilizing the enthalpy of reaction. Figure 2.27 shows the phase of matter for each of the involved thermal energy storage systems.

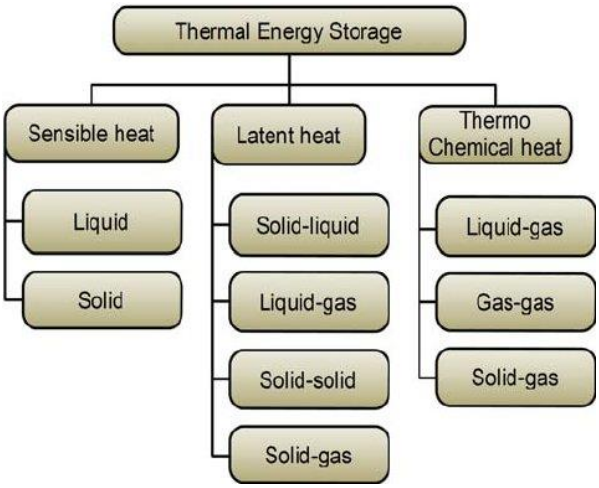

Figure 2.27: State of energy storage material for thermal energy storage system (Socaciu, 2012)

In mechanical energy storage systems (MESS), the energy stored is induced by the conversion between mechanical and electrical energy forms (Nadeem *et al.*, 2019). In this sense, mechanical energy in the form of kinetic or potential energy are stored by the conversion of electrical energy from power source during off-peak hours. During peak hours, kinetic or potential energy is transformed back into electrical energy. MESS can be classified into four categories: flywheel energy storage system, pumped hydro energy storage, gravity energy storage and compressed air energy storage as shown in Figure 2.28. Kinetic energy is stored in flywheel energy storage system while potential energy is stored in the other three types of energy storage system. MESS can be regarded as highly attractive because they offer several benefits in terms of environmental concerns, cost and sustainability when compared to other ESS (Mahmoud *et al.*, 2020). Moreover, the common advantages between different kinds of MESS are their capability to quickly convert and release stored mechanical energy while producing less contaminants in both operational and construction phase which indeed is an crucial element to improve environmental problems for avoidance of human health-related diseases (Guney and Tepe, 2017). The flywheel energy storage system is a short term mechanical energy storage device that utilized the kinetic energy for example rotating motion of massive cylinder (Hossain *et al.*, 2020) to store energy in the form of mechanical. Furthermore, pumped hydro energy storage is the most implemented MESS characterized by its huge energy storage capacity, long life cycle, long storage capacity and low maintenance cost (Rehman, Al-Hadhrami and Alam, 2015). Generally, this type of storage system comprises two large reservoirs at different elevations for initiation of potential energy, pumping system to pump water from low to high reservoir and turbine for generation of electrical energy. Sometimes, due to geological and water limitations when considering pumped hydro energy storage, there is inclination towards a new gravitational energy storage concept called gravity energy storage system (Aneke and Wang, 2016). An example of this technique is developed by Gravity Power where energy is stored by using water to lift a piston or other object with a prerequisite mass then

dropping the piston to allow water pushing through hydroelectric generator when power is needed (Gravity power, 2014). In compressed air energy storage, energy is stored in a reservoir either in an underground ground cavern or aboveground pipelines by compressing the air (Akhil *et al.*, 2015). The air is heated and expanded before using in a turbine generator to produce electricity during peak period. The amount of energy stored depends on the volume of storage space, pressure and temperature where the air is stored (Vazquez *et al.*, 2010).

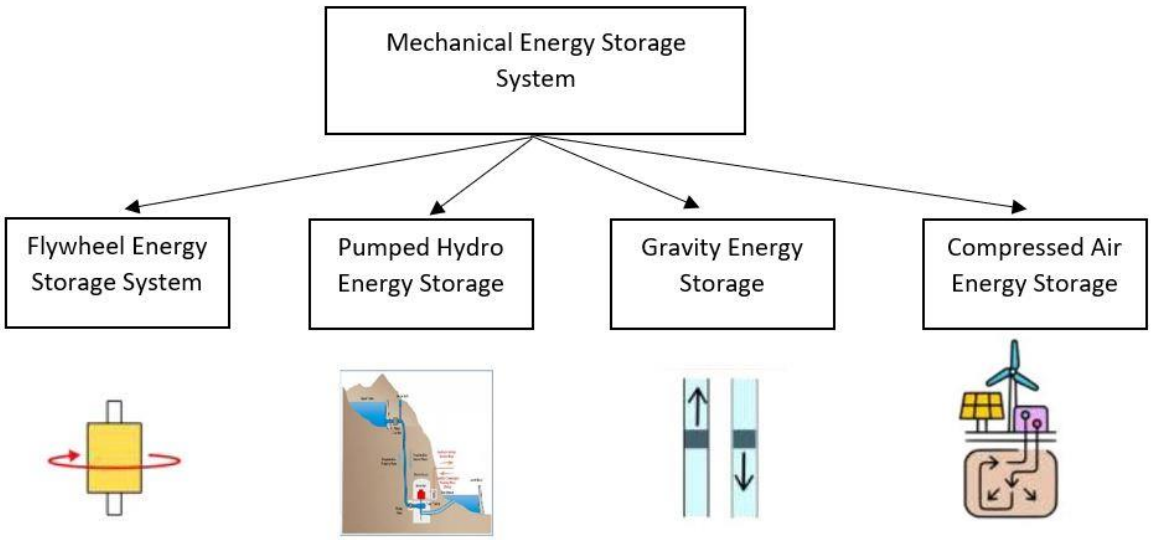

Figure 2.28: Classification of mechanical energy storage systems

2.4.3 Storage of elastic potential energy with emphasis on shape memory rubber

Elastic potential energy is the energy stored by deformation of an elastic material as a result from the force applied (Lifshitz, Kosevich and Pitaevskii, 1986). The storage of energy happens until the force is removed and the deformed object returns to its original shape doing work in the process. Stretching, compressing and twisting of the objects are examples to the type of deformations. Objects such as compressed or stretched spring, stretched bow, bent diving board and rubber band are designed specifically to store elastic potential energy to suit our daily life applications. Similar to an elastomer, objects designed to store elastic potential energy usually have high elastic limit to sustain the applied load. When the object is deformed beyond its elastic limit, it will undergo permanent deformation where the macroscopic structure of the object will no longer return to its original shape. A perfectly elastic material for instance cross-linked amorphous polymer stores all energy associated with deformation as potential energy which is a kind of mechanical energy (Ratner, 2012).

Mechanical properties of NR are mainly related to SIC (Nie *et al.*, 2017). However, several phenomena regarding SIC are still being misunderstood for example the contradicting effect of SIC on

stress. On one hand, SIC acts as network points which increase network chain density and resulting in stress hardening (Flory, 1947). On the other hand, SIC induced stress relaxation of the amorphous phase which can be observed from the plateau region of stress-strain curve upon crystallization begins (Toki, Fujimaki and Okuyama, 2000; Trabelsi, Albouy and Rault, 2003). Moreover, studies also suggested that SIC might develop due to constant strain on the amorphous region of NR (Albouy *et al.*, 2012, 2014). Strain's energy is required to generate a certain stress in the material which translates to the moment where SIC occurs. The mechanical energy brought onto the object will dissipate over a cycle referring to loading and unloading part. The difference between the strain's energy at a given stress and the material's elastic energy at the stress is called elastic hysteresis. In another word, it is the area in the centre of hysteresis loop which corresponds to the difference in area below the loading and unloading curve as shown in Figure 2.29. Experiment years ago first showed that SIC is closely related to elastic hysteresis witnessed from the kinetic differences between occurrence of crystallization and crystallite melting (Clark *et al.*, 1940). Therefore, SIC can be generally assumed to be responsible for the hysteresis loop discovered in mechanical responses of NR.

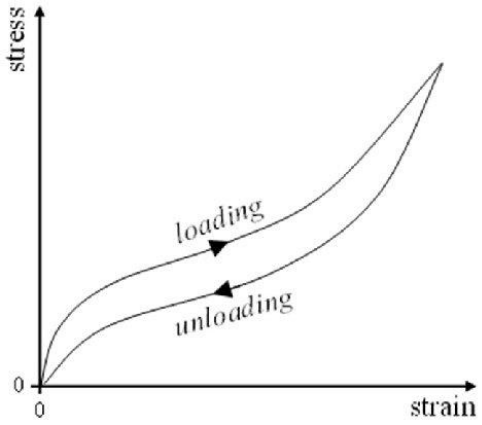

Figure 2.29: Hysteresis loop of NR (Rezende *et al.*, 2019)

As mentioned, elastic material such as NR is able to store the elastic potential energy upon deformation. A study on phase modelling of SIC suggested that storage of elastic energy is possible in the vicinity of crystal while topological constraints such as crosslinks or entanglements are accumulated (Laghmach *et al.*, 2015). Another research stated that mechanical energy dissipated by NR, which is the area in the centre of elastic hysteresis loop, is neither due to intrinsic nor thermal dissipation but is entirely consumed by the material itself to undergo microstructure changes (Le Cam, 2017). It was also showed that mechanical energy brought to deform NR is stored elastically in the amorphous region along with additional topological constraints induced close to the crystallites in the event of SIC. The crystallization / crystallite melting process stores and releases elastic part of the mechanical energy at different kinetics explained the phenomenon of changes in internal energy of

the hysteresis loop. Moreover, several studies further concreted that the elastic hysteresis of NR networks is mainly due to the formation of crystals upon deformation strain (Trabelsi, Albouy and Rault, 2003; Toki *et al.*, 2004). Therefore, the extraordinary resistance to crack growth of NR can be realistically explained through the formation strain-induced crystals and the ability of NR to store elastic part of mechanical energy without converting it into heat energy. As revealed in Section 2.3.5, SMR showed capability of fixing a temporary shape and recover to its original shape after being elongated to several 100%. In another word, the ability of SMR storing strain highlighted its potential to also store stress which corresponds to certain amount of energy. A study explored the energy storage potential of SMNR by calculating the elongation and stored energies through numerical integration of force against crosshead travel plots during the demonstrated first shape memory cycle (Heuwers *et al.*, 2013). Figure 2.30 shows the plot of force versus crosshead travel for a complete shape memory cycle of one SMNR sample. The result indicated that the values of the calculated stored elastic energy were in the range of 1.34 to 4.88 J g^{-1} with efficiencies between 26.22 and 48.32%. Ultimately, the effectively stored mechanical energy in SMNR is rightly comparable to the best value presented by spring steel (Ashby, 2016). The stored elastic energy and efficiencies both increased with increasing degree of crosslinking for SMNR. Interestingly, the storage of elastic energy happens at a minimum programming strain at this case 300%. This is because SIC in NR only happens under large deformation of several 100% strain when chain of molecules in the material become ordered under deformation process (Gent and Zhang, 2002; Huneau, 2011; Candau *et al.*, 2019; Loos *et al.*, 2020). Therefore, it is not possible to store elastic energy contributed by SME below a certain deformation strain.

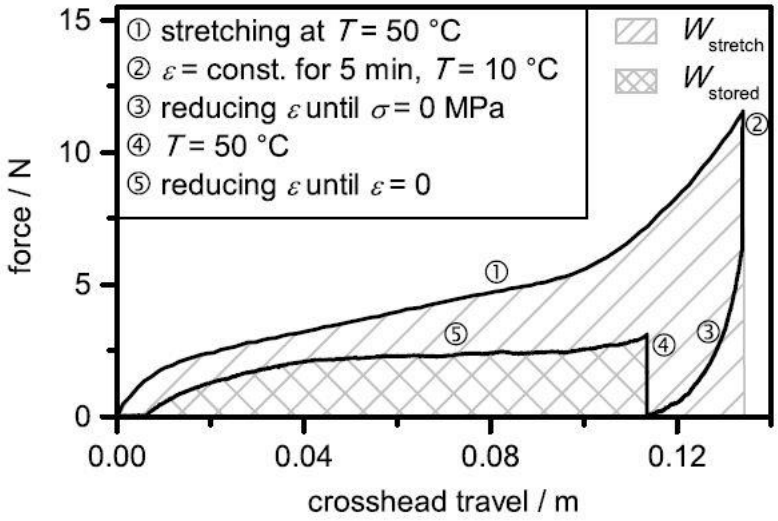

Figure 2.30: Plot of force versus crosshead travel (Heuwers *et al.*, 2013) Note: Ɛ = strain, σ = stress, $W_{stretch}$ = energy needed for stretching, W_{stored} = stored elastic energy

2.5 Thoughts and research gaps

As discussed in Section 2.2, SNC showed promising reinforcing effects on the mechanical properties of NR/SNC nanocomposites. However, minimum work about the evaluation of physical and mechanical characteristics of SNC reinforced NR derivatives had been performed. Moreover, ENR is usually used in the form of bulk rubber to produce dry rubber products. There is limited information regarding the usage of ENRL to fabricate latex-based products (Ramli *et al.*, 2020). To add on this, the characteristics of unfilled ENRL and DPNRL has rarely been investigated. This presents an opportunity to investigate the physical and mechanical characteristics of unfilled and filled NR derivatives latex in depth. It serves as a step to promote new sustainable green material which have better mechanical properties than synthetic rubber and its predecessor NR as well as having improved resistance against oil and gas attack that NR lacks. Furthermore, it will help in the search of an alternative filler that raises great research interest recently to replace the conventional carbon black which causes a certain degree of pollution during its manufacturing process.

From Section 2.3, shape memory polymers showed promising potential in various applications such as temperature sensors, actuators, biomedical products and aerospace industry. Incorporation of nanofillers into shape memory polymers had been extensively studied recently due to its larger surface area and subsequently stronger polymer-nanofiller interaction which enhanced the polymer mechanical properties. However, on behalf of shape memory behaviour, conflicting results had been presented about the influence of nanofillers on shape memory effect of polymers (Jimenez and Jana, 2009; Luo and Mather, 2010; Kalita and Karak, 2014; Shirole *et al.*, 2018). This uncertainty never stop research regarding SMP because of their capability to offer unique and outstanding characteristics. Furthermore, development of SMNR has attracted tremendous interest due to the biodegradability and amazing mechanical properties offered by NR. Nonetheless, the specific material needs to have a T_g above ambient temperature or is partially crystalline at ambient temperature to develop SME. NR lacks both prerequisite and should not show any shape memory behaviour at normal condition. This inspired an idea of research with the incorporation of SNC into NR and its derivatives for enhancement of mechanical properties while investigating its effect in shape memory behaviour of smart rubbers. Moreover, limited works have been done on developing SMR especially NR derivatives with the incorporation of SNC as nanofiller (Kalita, 2018).

As per Section 2.4, the current view of global energy is shifting towards the production of greener energy and lower cost as well as efficient design of energy storage system. This aid in the realization of Kyoto and Paris agreement which goal is to reduce the total emission into atmosphere by energy harnessed from fossil fuels commodities (Olabi *et al.*, 2021). Therefore, research is needed to develop

sustainable energy storage devices with lower cost, higher efficiency and minimum environmental impacts especially at the disposal stage after completing the life cycle of the devices. SMPs are interesting prospects for the development novel energy storage device because of their ability to fix a temporary shape and recover to its original shape after being elongated to a certain extent. During the shape memory cycle, strain is stored in the material after being deformed and energy is released when the material recovers to its original shape. This ultimately showed the capability of SMPs to store energy in one shape memory cycle. Due to the fact that most of the SMPs store fairly low strain, there have not been much effort in the determination of stored work in SMP so far (Rapp and Baier, 2010). However, SMR is an ideal candidate for energy storage since SMR is capable of storing strain up to several 100% while supporting high tensile stress. Moreover, the formation of strain induced crystals in rubber chain molecules upon deformation strain aid in energy storage of SMR. Up to date, there is minimum research quantifying the energy storage capability of SMR. Moreover, demonstration of the energy storage capability of SMR has yet to be reported so far.

In this research, NRL, ENRL25, ENRL50 and DPNRL will be used as the raw material for the fabrication of RL films. The latex casting method using petri dish and glass mould are adopted due to the inability of ENR latex to form film through typical coagulant dipping process which involves the usage of calcium nitrate solution (Darji *et al.*, 2020). The low total solid content and presence of non-ionic surfactants in ENR had proof to be the sources for this problem. The purposes of using both latex casting with different apparatuses is to fabricate rubber films with varying dimensions and thicknesses. The optimized acid hydrolysis process presented in the above literature is adopted for synthesizing of SNC from native waxy maize starch. Later, a series of characterization techniques such as FESEM, SEM, TGA, DSC and DMA were performed to evaluate the characteristics of SNC, sulphur-cured rubber films and rubber nanocomposites films. Mechanical properties such as tensile strength, elongation at break and modulus were determined by tensile test to evaluate the reinforcing effect of SNC in different types of latex. A special elongation device was then developed for the purpose of performing thermomechanical shape memory test under strain-control mode to quantify the S_f and S_r of the fabricated rubber films. Quantification of the energy stored and demonstration of the energy storage capability of the smart rubber were conducted by cyclic loading-unloading test and manual experiment. Further details of the research methodology are presented at Chapter 3 of the report.

Chapter 3

3.0 Research Methodology

The literature review has shown that very limited work had been done towards fabrication of biodegradable SMR nanocomposites with improved mechanical properties and energy storage capability. The present research has therefore been conducted to develop SMR with types of rubber latexes: NRL, ENRL25, ENRL50 and DPNRL along with a series of characterization techniques.

Section 3.1 presents the materials and chemicals required for the experimental works in this research. Experimental procedures to synthesize SNC, determination for yield of SNC, fabrication of sulphur-cured rubber films and SNC reinforced rubber nanocomposites are discussed in detail in Section 3.2. Section 3.3 layout the characterization techniques such as Field Emission Scanning Electron Microscope (FESEM), X-Ray Diffraction (XRD), Differential Scanning Calorimeter (DSC), Thermogravimetric Analysis (TGA), and Particle Size Analysis (PSA) utilized to characterize the synthesized SNC. Subsequently, a series of characterization works for the fabricated rubber film and rubber nanocomposites films including determination of crosslink density, Dynamic Mechanical Analysis (DMA), FESEM, tensile test, water and toluene uptake, and TGA were shown at Section 3.4. Lastly, the evaluation of energy storage potential which involves shape memory test, cyclic-loading-unloading test and manual demonstration are detailed in Section 3.5.

The overall flowchart of the research work is described in Figure 3.1.

Remark: *It is to note that most of the content of this and the following chapters have been either published or accepted in the list of journals as stated in the list of publications.*

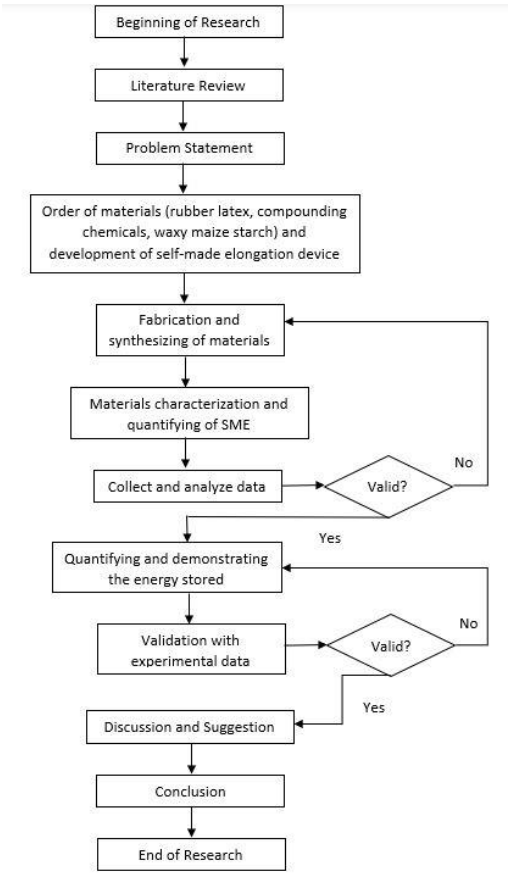

Figure 3.1: Overall flow chart of research methodology

3.1 Materials

Commercial grade concentrated low ammonia NRL and DPNRL were purchased from Getahindus (M) SDN BHD while ENRL with epoxidation level 25 and 50% were purchased from Malaysian Rubber Board. Table 3.1 shows the specifications such as total solid content (TSC), dry rubber content, alkalinity and special features of the purchased latexes. The compounding chemicals in dispersion form such as sulphur, zinc dibutyl dithiocarbamate (ZDBC) and zinc oxide (ZnO) were supplied by Aquaspersions (M) Sdn Bhd. The TSC, viscosity, specific gravity (SG), pH and particle size of the compounding chemicals are listed in Table 3.2. TSC of the chemicals were determined by evaporation at 105 °C to constant weight. Viscosity, SG and pH were measured by Brookfield Reading Viscometer Spindle No.4 at 20 revolution per minute, digital meter and pH meter respectively. All testing parameters were measured at 25 °C. The particle size of the compounding chemicals was measured in microns (μm) using particle size analyzer with particle size below the specified diameter is 95%. Furthermore, commercial grade waxy maize starch with product name RESISTAMYL (TM) 347 was supplied by Imextco (M) SDN BHD. Moisture content of the waxy maize starch ranged between 11-14% was measured using EN ISO 1666 method. The product is suitable for experimental work because it

complies with the requirements of EU Directives and Regulations in force on foods and food ingredients.

Table 3.1: Specifications of the rubber latexes

Latex	TSC (%)	Dry rubber content (%)	Alkalinity (%)	Special feature
NRL	61.84	60.16	0.30	-
ENRL - 25	62.55	61.15	0.10	25% epoxidation level
ENRL - 50	61.27	59.77	0.10	50% epoxidation level
DPNRL	60.30	59.50	0.55	Deproteinized NR latex

Table 3.2: Specifications of the compounding chemicals

Chemicals	TSC (%)	Viscosity (cps)	SG (g/cm^3)	pH	Particle Size (μm)
Sulphur	60.85	810	1.428	10.22	3.760
ZDBC	51.98	800	1.114	10.42	3.343
ZnO	52.19	850	1.727	9.750	2.690

3.2 Materials Preparation

Based on the literature review at Section 2.4.3, SNC was synthesized using the optimized technique (Angellier *et al.*, 2004). It is because this technique was proved to be the most consistent method while consuming the least time. Furthermore, low crosslinking NRL, ENRL25, ENRL50 and DPNRL films were fabricated using latex casting method. Investigation regarding the utilization of latex-based ENR for fabrication of rubber films has been absent so far. The synthesized SNC is used as a reinforcing filler in all fabricated rubber films to evaluate its effect on mechanical properties of the rubber films. Shape memory behaviour of the fabricated rubber films and SNC reinforced rubber nanocomposites were then investigated based on the formation of SIC at different deformation strain and programming temperature.

3.2.1 Synthesizing of SNC

Commercial grade waxy maize starch was used for the preparation of SNC. The optimized technique for the preparation of SNC aqueous suspension discussed in Chapter 2.2.1(b) was adopted. Waxy maize starch with a weight of 36.725g (14.69 wt%) was mixed with 250mL of 3.16 M H_2SO_4 solution (178.1 mL of 95% H_2SO_4 and 821.9 mL of distilled water) in a 500 mL Erlenmeyer flask at 40 °C, mechanical stirring speed of 100 rpm for 5 days duration. H_2SO_4 was selected ahead of HCL because of the long treatment time (more than 15 days) and low yield of HCL hydrolysis. After 5 days, the suspension was transferred into 50mL centrifuge tubes to separate the SNC from acid by centrifugations using Eppendorf Centrifuge 5430 for 12 minutes at 7800 rpm. Successive centrifugations and washing with distilled water were performed to achieve neutrality in the SNC suspension (about 8 subsequent centrifuging and washing cycles). At this stage, native starch was

believed to be broken down into nanocrystals from the noticeable opaque nature of the aqueous suspension which changes the refractive index of the starch solution. The suspension was then sent to ultrasonic treatment to disperse aggregates by using Cole Parmer ultrasonic processor at 50% amplitude for 10 minutes. The visible aggregates were completely dispersed and homogenized following the ultrasonic treatment producing SNC dispersion. Finally, several drops of chloroform were then added into the dispersion to prevent the growth of bacteria. The resulting aqueous suspension was then stored in a 4 °C refrigerator. The flow chart and step-by-step diagrams for the preparation of waxy maize SNC are shown in Figure 3.2 and 3.3.

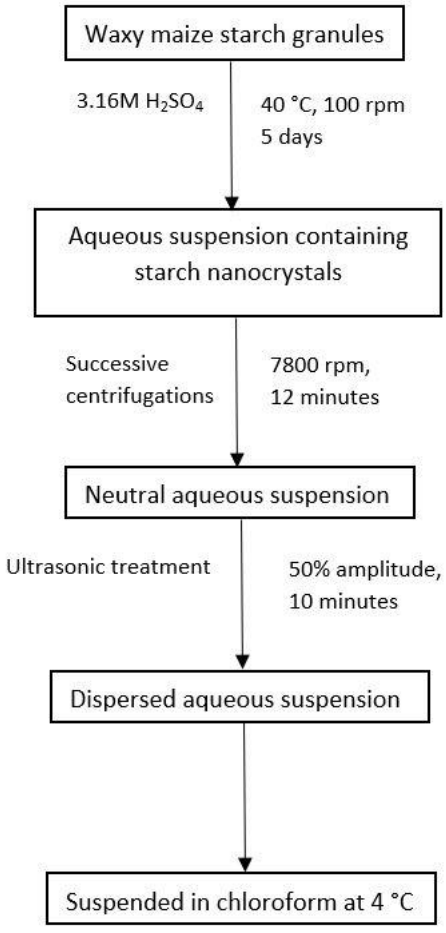

Figure 3.2: Flowchart for preparation of SNC

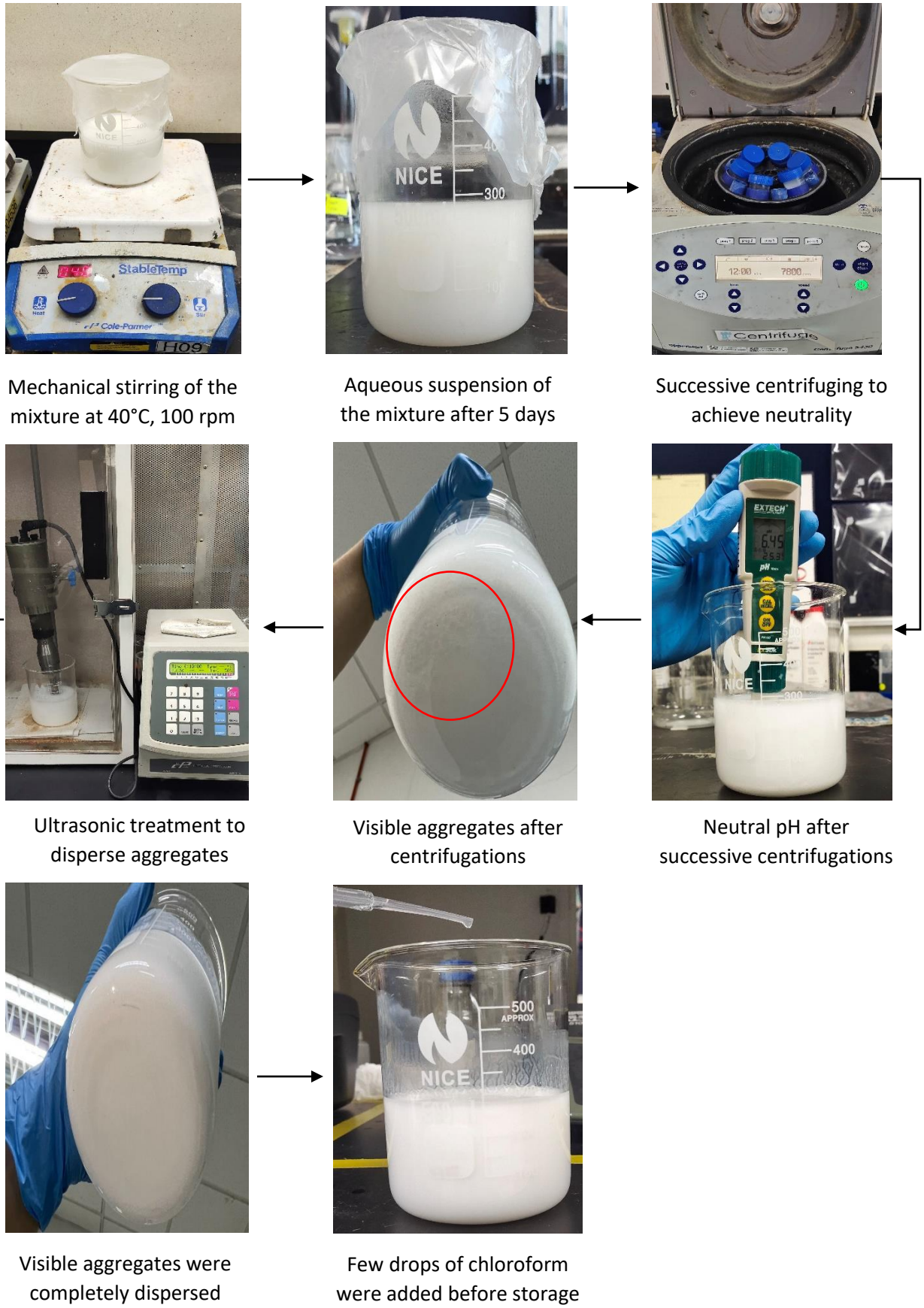

Mechanical stirring of the mixture at 40°C, 100 rpm

Aqueous suspension of the mixture after 5 days

Successive centrifuging to achieve neutrality

Ultrasonic treatment to disperse aggregates

Visible aggregates after centrifugations

Neutral pH after successive centrifugations

Visible aggregates were completely dispersed

Few drops of chloroform were added before storage

Figure 3.3: Synthesizing procedures of SNC

The obtained aqueous suspension was freeze-dried using CHRIST Alpha 1-2 LDplus freeze drier at temperature of -50 °C and vacuum pressure of 0.040 mbar for 6 hours to obtain loose SNC powder. The resulting hydrolysis yield of SNC, Y was calculated as a percentage of the dry weight of non-solubilized particles in relative to the initial dry weight of native starch as shown by equation 3.1 (Le Corre *et al.*, 2012).

$$Y(\%) = \frac{Weight\ of\ freeze-dried\ loose\ powder\ (g)}{Weight\ of\ native\ starch\ (g)} \times 100\% \quad (3.1)$$

After 5 days of SNC synthesizing, the yield of waxy maize SNC was found to be 15.7%. The result is comparable to the literature using the same duration and type of acid for the synthesizing of SNC that produce a yield of 14% (Lecorre, Bras and Dufresne, 2011b).

3.2.2 Fabrication of low crosslinking NRL, ENRL-25, ENRL-50 and DPNRL films

All RL were mixed individually with the chemical compounds listed in Table 3.3 and transferred to separate beakers prior to the stirring process. The mixtures were continuously stirred by Cole-Parmer magnetic stirrer at 200 rpm for 60 minutes at room temperature to ensure uniform dispersion. Subsequently, the homogenized mixtures were cast and dipped with petri dish to form rubber films with 1mm thickness. The mixtures were also cast on glass mould to form rubber films with larger surface dimensions for the purpose of mechanical properties testing. The step-by-step rubber films fabrication process is shown in Figure 3.4. The yellow appearance of the vulcanized rubber films is directly related to the amount of sulphur where higher sulphur dosage resulted in a more yellowish film. Firstly, the oven was pre-heated to 50 °C for 2 hours for thermal equilibrium before the drying process. Next, the rubber specimen was heated at 50 °C for 5 hours. The vulcanized rubber films were then stored at room temperature for 7 days to allow complete drying. After 7 days, the dried rubber films were removed from the petri dish and cut into rubber strips with dimensions of 10 mm x 30 mm and 20mm x 50mm both with 1mm thickness. The dried rubber films cast on glass mould occupied a dimension of 150 mm x 150 mm with 0.3 mm thickness.

Table 3.3: Rubber formulation for various kind of RL films

Sample name	Sulphur (pphr)	ZDBC (pphr)	ZnO (pphr)
RL 0.00	0.00	0.00	0.00
RL 0.20	0.20	0.40	0.25
RL 0.30	0.30	0.50	0.25
RL 0.40	0.40	0.60	0.25
RL 2.00	2.00	1.00	0.25

Continuous stirring of the rubber mixture at 200rpm for 60 minutes at room temperature

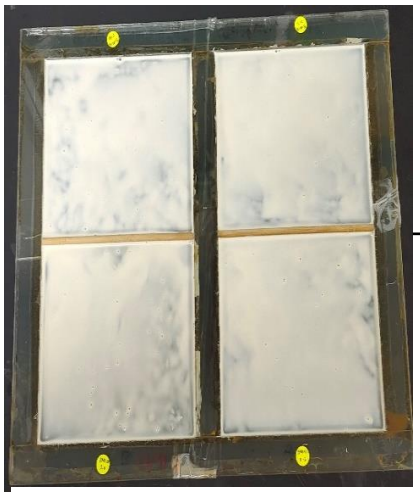

Homogenized mixture was casted on glass mould

Rubber specimen was heated at 50 °C for 5 hours

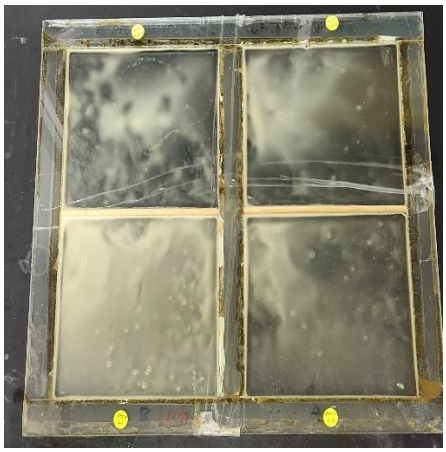

Dried rubber specimen after drying in oven

Figure 3.4: Fabrication process of sulphur-cured rubber films

3.2.3 Fabrication of rubber nanocomposites films

The aqueous suspension of waxy maize SNC were mixed with compounded RL under various proportion using magnetic stirrer to obtain nanocomposite films with weight fractions of dry SNC ranging from 0-8% wt. 0.2phr sulphur content is used for the fabrication of all rubber nanocomposites films as this dosage showed the best overall SME determined from previous shape memory tests on lightly-crosslinked rubber films (Tan *et al.*, 2024a). Therefore, the corresponding amount of ZDBC and ZnO were 0.40 and 0.25 respectively. Table 3.4 shows the varying amount of SNC incorporated into RL. The mixing process was carried out by Cole-Parmer magnetic stirrer at 200 rpm for 15 minutes to ensure uniform dispersion. After mixing, the mixtures were placed in an Elma ultrasonic bath operating under degas mode with 35kHz frequency and 60% amplitude for 10 minutes to degas the

mixture thereby avoiding irreversible bubbles formation during water evaporation. Next, the homogenized mixtures were cast on petri dishes and glass moulds to form uniform films before drying in a ventilated oven at 70 °C for 3 hours and then vulcanized at 105 °C for 30 minutes. 10g of the mixtures were poured into petri dishes and glass moulds to obtain the desired thicknesses. The resulting dry films were then conditioned at room temperature for 7 days before cutting into rubber strips that occupied similar dimensions with the fabricated low crosslinking rubber films.

Table 3.4: Amount of SNC in rubber nanocomposite films

Sample name	SNC (dry wt%)
RL/SNC 0%	0.0
RL/SNC 2%	2.0
RL/SNC 4%	4.0
RL/SNC 6%	6.0
RL/SNC 8%	8.0

3.3 Characterization techniques for SNC

3.3.1 Field Emission Scanning Electron Microscope (FESEM)

Morphology and particle size of the synthesized SNC were determined by Field Emission Scanning Electron Microscope (FESEM, FEI QUANTA 400F). Aqueous suspension of SNC samples were mounted on aluminium specimen holder before being inserted into the FESEM. The samples were examined at accelerating potential of 5 – 10kV with 3000 and 8000 times of magnification. All tests were performed under vacuum condition. The samples were observed 'as it is" without any form of metal deposition.

3.3.2 Particle Size Analysis (PSA)

Particle size distribution of native starch and synthesized SNC were measured using Malvern Panalytical Nano-Zetasizer. Dry state native starch and aqueous suspension of SNC were placed on quartz cuvette at 25 °C before running the analyzer for 60s. The refractive index of native starch and SNC were determined to be 1.50. Water having a refractive index of 1.33 and viscosity of 0.8872 mPa.s was used as the dispersant for the analyzing work.

3.3.3 X-Ray Diffraction (XRD) analysis

The crystalline structure of both native starch and SNC were characterized by Panalytical X'pert Pro MPD X-Ray diffractometer. The analysis conditions for the diffractometer were Cu K_α radiation at λ = 1.54060 Å with generator settings of 45kV and 35mA for voltage and current, respectively. The samples were scanned with scattered radiation at 2Θ ranging from 5 to 50 °, with a step size of 0.02 ° and a step time of 0.15s operating under continuous mode. Freeze-dried SNC powder and native starch were used for the X-ray scanning to avoid interference with moisture. The degree of crystallinity

of native starch and SNC can be quantitatively calculated by using the two-phase method (LeCorre, Bras and Dufresne, 2011). Basically, a curve connecting the peak baseline was plotted on the diffractogram. The area above the curve was defined as the crystalline region while the area below the curve and baseline corresponded to the amorphous region. The degree of crystallinity of the material is taken as the ratio of the upper area to the total area and was calculated as equation 3.3.

$$X_c = \frac{A_c}{A_c + A_a} \tag{3.3}$$

where,

X_c = degree of crystallinity

A_c = area of the crystalline region

A_a = area of the amorphous region

3.3.4 Differential Scanning Calorimetry (DSC)

Thermal transitions of dry state native starch and SNC were measured by research grade DSC Q2000 TA instrument. Native starch and freeze dried SNC samples weighed 3-7mg were transferred into hermetically sealed aluminium pan. Each sample were heated from 30 – 250 °C at heating rate of 10 °C/min under nitrogen environment. Endothermic peaks of native starch and SNC were determined from the DSC diagram.

3.3.5 Thermogravimetric Analysis (TGA)

Thermal stability of native starch and SNC were measured by TGA/DSC Mettler Toledo. Samples of native starch and freeze dried SNC weighed 3-6mg were heated from 60 – 600 °C at heating rate of 10 °C/min under nitrogen flow at 20ml/min. The sample weight in percentage were plotted against temperature to determine the thermal degradation of native starch and SNC.

3.4 Characterization works for rubber and rubber nanocomposite films

3.4.1 FESEM

The morphology of the rubber nanocomposites films was evaluated by FESEM. A FEI, QUANTA 500F was used to observe the morphological pattern of nanocomposites films with different SNC content. Samples of the rubber nanocomposites films were mounted on aluminium sputter holder before being sputter coated with gold to ensure conduction. The specimens were coated using Quorum Q 150 RS plus with sputter current of 20mA, sputter time of 20 seconds and tooling factor of

1.0. The samples were examined under 10000 times magnification with accelerating voltage ranging between 5 – 20kV depending on the quality of the images. The tests were performed under vacuum condition and the micrographs were analyzed “as it is” without any forms of modification.

3.4.2 Determination of crosslink density

The crosslink density of the rubber films were calculated through the obtained storage modulus (E’) from DMA tests at room temperature of approximately 25 ± 1 °C (Hiranobe *et al.*, 2021). The resulting crosslink density can then be calculated as shown by equation 3.2.

$$\eta = \frac{E'}{6\,R\,T} \times 10^{-6} \tag{3.2}$$

where,

η = crosslink density (mol cm^{-3})

E' = elastic storage modulus of the polymer (Pa)

R = universal gas constant (m^3 Pa K^{-1} mol^{-1})

T = absolute temperature (K)

3.4.3 Toluene and water uptake

The kinetics of toluene and water absorption were determined for all rubber and rubber nanocomposites films. The samples used for the absorption study were rectangular films with dimension 10mm x 30mm x 1mm. The rubber films were thin enough to ensure the happening of only unidirectional diffusion. The films were first weighted using analytical balance with 0.1mg resolution before immersing in water and toluene. Swelling experiments were carried out for a period of 48 hours as equilibrium is deemed to be reached at this time (Anand *et al.*, 2018). The samples were wiped with filter paper upon their removal from solution to ensure no adherence of toluene on the rubber surface. The toluene uptake (TU) and water uptake (WU) were calculated as shown by Equation 3.3 (Angellier *et al.*, 2005).

$$TU\ (\%) = \frac{m_t - m_0}{m_0} \times 100 \tag{3.3}$$

where,

m_0 = initial weight of the sample before any immersion

m_t = final weight of the sample after removing from toluene solution

3.4.4 Dynamic Mechanical Analysis (DMA)

Dynamic mechanical tests were performed with Dynamic Mechanical Analyzer 8000 PerkinElmer for the identification of E' and tan δ peak to relate the T_g of rubber samples. The tests were carried out under tensile mode with a frequency of 1Hz. In each test, a rectangular sample with dimension (30 x 10 x 1mm) was loaded with static force of 0.5N, force multiplier of 2.0 and strain of 0.1mm. The scanning temperature for E' against temperature was programmed from -60 to 110 °C at 2 °C/min while the scanning temperature for tan δ against temperature is -60 to 40 °C. Liquid nitrogen was purged into the system to achieve the required testing condition. Area under the tan δ curves were calculated using Equation 3.4 to evaluate the damping of the rubber samples. The rubbery storage tensile modulus at room temperature of 25 °C (E'_{25}) were determined from the test to investigate the reinforcing effect of SNC at temperature higher than T_g and to validate the results from tensile tests (Angellier, Molina-Boisseau and Dufresne, 2005). The experimental setup displayed the results through evolution of E' and tan δ between the range of programmed temperatures.

$$Area = \sum_{-60}^{40} [\left(\frac{b_1 + b_2}{2}\right) \times \mathrm{h}] \tag{3.4}$$

where,

b_1 = base length of one side of the tan δ curve

b_2 = base length of the other side of the tan δ curve

h = height of the individual trapezoid

3.4.5 Tensile test

Mechanical properties of the rubber and rubber nanocomposites samples were evaluated by Universal Tensile Machine AI 3000 (GT Instruments). All tensile tests were performed in accordance with ASTM D412 standards (ASTM D412, 2016). The dried rubber films were removed from the glass mould and subsequently cut into dumbbell shape with dimension of 115mm x 25mm with thicknesses ranging between 0.2-0.3mm as shown in Figure 3.5(a) using pressurized dumbbell specimen cutter machine. In each test, dumbbell shaped rubber sample was clamped tightly between two grips to allow elongation of the specimen as shown in Figure 3.5(b). Gauge length of 25mm was set while crosshead speed of the tensile tester was 500mm/min. The tests were conducted at an ambient temperature of approximately 25 °C. The samples were elongated until break in every of the tensile test. Stress strain curves of the rubber samples were obtained to evaluate the tensile strength and elongation at break of the rubber and rubber nanocomposites films. The tensile test was repeated

three times for each of the different formulations and the average value was calculated along with the standard deviation.

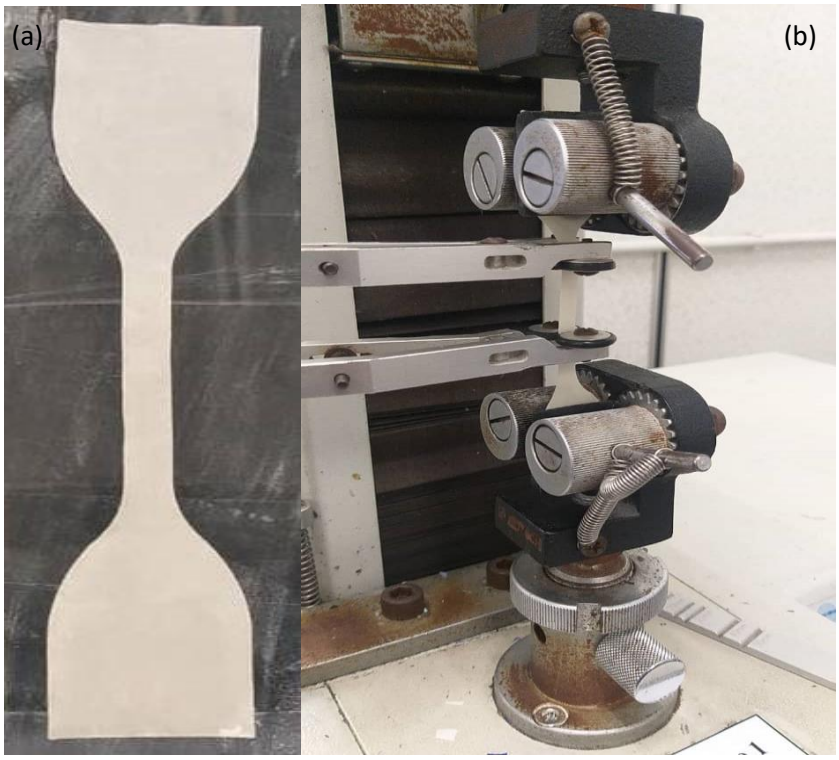

Figure 3.5: (a) dumbbell shape rubber sample (b) properly clamped rubber sample

3.4.6 TGA and Differential Thermal Gravimetry (DTG)

TGA has been widely used as the method to evaluate thermal stability and degradation of polymeric materials. The weight of the sample is measured as a function of temperature or time in a stable atmosphere while the specimen is subjected to undergo a controlled temperature program. DTG is the first derivative of TGA that analyzed the rate of material weight change upon heating. It supplies sensitive analysis that is useful to determine the relative rate of polymer degradation as well as to distinguish between the minor and major weight loss step in polymer composites. The maximum peak in DTG plot corresponds to the maximum rate of weight loss in the material. The thermal stability of rubber and rubber nanocomposites films were evaluated by using TGA/DSC Mettler Toledo. The tests were performed under nitrogen atmosphere at a rate of 20ml/min to furnish a fundamental air condition for the material of interest. Each test involving 3-8mg of rubber samples were heated from 60 – 600 °C at a heating rate of 10 °C/min under the settings of enabled synchronization.

3.5 Evaluation of energy storage capability of rubber and rubber nanocomposite films

3.5.1 Shape memory behaviour

Technique of measuring the shape memory effect for fabricated rubber films were adopted from previous literatures (Sun *et al.*, 2011; Brostowitz, Weiss and Cavicchi, 2014). Thermomechanical cycles were performed to determine the shape memory parameters of rubber vulcanizates using a self-made elongation device operated in strain-controlled mode. The rubber specimen with dimensions of 50mm x 20mm x 1mm was secured by two stainless steel clipper that acted as clamps. Ultimately, this special elongation device is the ideal tool to demonstrate the shape memory testing because of the need for rapid temperature changes of the environment when immersing the rubber specimens into water bath. The shape memory testing was carried out as follows. Firstly, each rubber specimen was marked with a 1cm gap as the initial strain, ε_i with a pen before clamping on the clipper of the special elongation device. Next, the rubber specimens were stretched at room temperature of 25 °C to an elongation strain of 600% and the elongated length is recorded as loading strain, ε_l. The loading strain is determined from tensile tests that indicated a minimum 700% elongation before fracture. As a precaution to overstretching the rubber films, 600% loading strain was used to determine the shape memory parameters. Then, the rubber specimens were immediately quenched in a 4 °C ice water bath for 120s to fix the temporary shape. The stretched samples were then unloaded from the clipper and the fixed strain, ε_f was recorded. Subsequently, the recovery process was induced at temperature of 37 °C and the recovery strain, ε_r is measured. The accuracy of the length measurement is ±0.5mm. After all data had been collected, S_f and S_r of the rubber specimens were calculated using Equation 3.5 and 3.6 (Sun *et al.*, 2011). The test was repeated twice and the average values were obtained. Figure 3.6 shows the shape memory testing process of the smart rubber film.

$$S_f(\%) = \frac{\varepsilon_f}{\varepsilon_l} \times 100 \tag{3.5}$$

$$S_r(\%) = \frac{\varepsilon_l - \varepsilon_r}{\varepsilon_l - \varepsilon_i} \times 100 \tag{3.6}$$

An additional parameter related to the strain storage capability of the specimen is recorded as stored strain, ε_{stored} (Heuwers *et al.*, 2013). This parameter identified the percentage of stored elongation after the S_f process. ε_{stored} over one shape memory cycle is calculated as Equation 3.7.

$$\varepsilon_{stored}(\%) = (\varepsilon_f - \varepsilon_i) \times 100 \tag{3.7}$$

Initial gap of smart rubber film was indicated as 1cm

Smart rubber film was stretched to an elongation strain of 600%

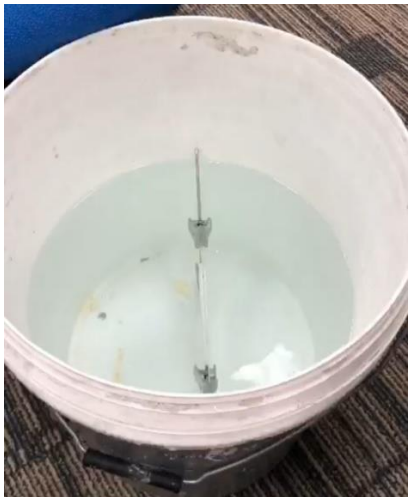

Smart rubber film was quenched in ice water of 4 °C for S_f

Smart rubber film unloaded from clipper and ε_f was recorded

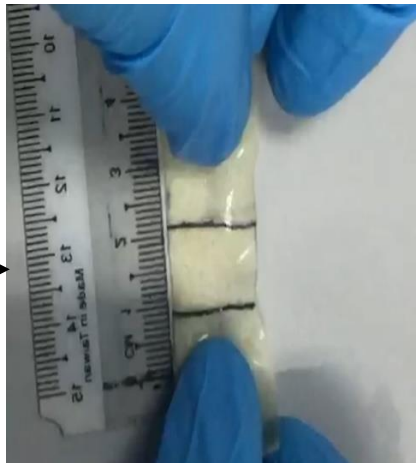

S_r of the smart rubber was initiated and ε_r was measured

Figure 3.6: Shape memory testing process of smart rubber film

3.5.2 Energy storage capacity

The evaluation of energy storage capacity of the rubber nanocomposite films was evaluated using cyclic loading-unloading tensile tests. The cyclic tests were performed using Instron Universal Tensile Machine (5566). Real image of the equipment is shown in Figure 3.7(a). Firstly, rubber specimen with dimension 50mm x 20mm x 1mm was secured by two vertically held clamps to prevent slippage of the sample during elongation as presented in Figure 3.7(b). During the loading test, the rubber sample was elongated to a strain of 600% at room temperature with a crosshead speed of 500mm/min as shown in Figure 3.7(c). The unloading test started when the rubber sample reached a strain of 600%, the applied force was reduced to zero and the rubber sample was allowed to slowly return to its original shape without any external forces. This successfully concluded a single loading-unloading tensile test. The loading-unloading tensile test was performed for three cycles and the stress-strain curves were obtained. Five parameters which included applied energy ($E_{applied}$), stored energy (E_{stored}), elastic retraction energy ($E_{retract}$), hysteresis and energy storing efficiency ($E_{efficiency}$) were determined from the obtained data. The $E_{applied}$, E_{stored} and $E_{retract}$ were determined by calculating the area under the loading and unloading curve by breaking down every interval data point into an individual trapezoid (Heuwers *et al.*, 2013; Cooper *et al.*, 2021). The summation of the area of individual trapezoid within the points of interest indicated the values of $E_{applied}$, E_{stored} and $E_{retract}$. $E_{applied}$ was determined by calculating the area under the loading curve between the point of 0% and 600% strain. The values of $E_{applied}$ were calculated by using Equation 3.8. E_{stored} was determined by calculating the area under the unloading curve between the points of ε_{stored} discovered from shape memory test and 0% strain since all investigated rubber specimens exhibited S_r of 100%. The values of E_{stored} were then calculated using Equation 3.9. $E_{retract}$ indicates the energy loss due to retraction of the rubber specimen. In another word, the non-fixation part of the rubber specimen during shape programming of a shape memory cycle. $E_{retract}$ was then determined by calculating the area under the unloading curve between the points of 600% strain and ε_{stored}. The values of $E_{retract}$ were then calculated using Equation 3.10. The hysteresis energy loss of the rubber specimen is the area between the loading and unloading curve. It was then calculated by Equation 3.11 using simple mathematical subtraction. $E_{efficiency}$ of the rubber specimen is the ratio between E_{stored} and $E_{applied}$. It was determined using Equation 3.12.

$$E_{applied}(MJ/m^3) = \sum_{0}^{600} [\left(\frac{\sigma_1 + \sigma_2}{2}\right) \times \varepsilon] \tag{3.8}$$

where,

σ_1 = tensile strength of one side from loading curve

σ_2 = tensile strength of the other side from loading curve

ε = strain of the individual trapezoid

$$E_{stored}(MJ/m^3) = \sum_{0}^{\varepsilon_{stored}} [\left(\frac{\sigma_3 + \sigma_4}{2}\right) \times \varepsilon] \tag{3.9}$$

where,

σ_3 = tensile strength of one side from unloading curve

σ_4 = tensile strength of the other side from unloading curve

ε = strain of the individual trapezoid

$$E_{retract}(MJ/m^3) = \sum_{\varepsilon_{stored}}^{600} [\left(\frac{\sigma_5 + \sigma_6}{2}\right) \times \varepsilon] \tag{3.10}$$

where,

σ_5 = tensile strength of one side from unloading curve

σ_6 = tensile strength of the other side from unloading curve

ε = strain of the individual trapezoid

$$Hysteresis\ (MJ/m^3) = E_{applied} - E_{stored} - E_{retract} \tag{3.11}$$

$$E_{efficiency}(\%) = \left(\frac{E_{stored}}{E_{applied}}\right) \times 100\% \tag{3.12}$$

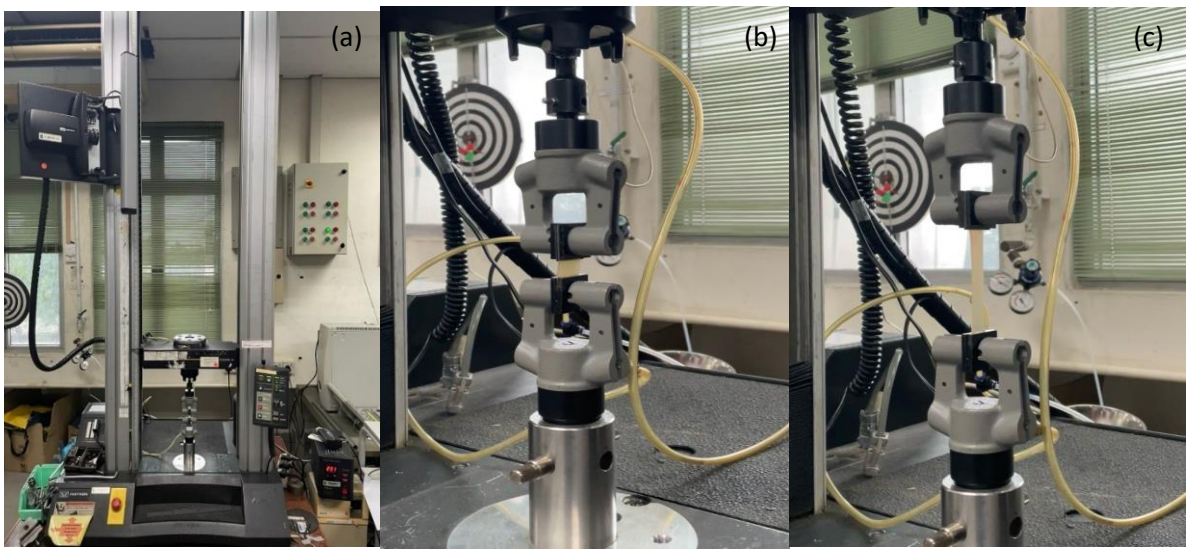

Figure 3.7: (a) Instron Universal Tensile Machine (b) Tightly held rubber specimen (c) Elongation of rubber specimen to 600% strain

3.5.3 Demonstration of energy stored within the rubber nanocomposite films

A manual demonstration was undertaken to demonstrate there is stored energy within the rubber nanocomposite films while showing its potential as a thermomechanical energy storage system. The demonstration was done by showing the rubber nanocomposite films capable of lifting a weight during a shape memory cycle. More specifically, the stored energy was utilized during the recovering of its original shape after exhibiting fixation of the temporary shape. DPNRL/SNC 8% was selected ahead of the other rubber nanocomposite films to conduct the manual experiment as it showed the highest E_{stored} during the cyclic loading-unloading test. Before undergoing the thermomechanical manual experiment, rubber film weighing 1g with dimensions of 50mm x 20mm x 1mm was fixed firmly between steel plates weighing 20g as shown in Figure 3.8(a) and (b). A 1cm gap was marked on the rubber films to aid with the experiment process during elongation of the rubber films. Next, a standard weight of 20g acting as additional load was attached by nylon string to the bottom of the steel plates be seen in Figure 3.8(c). The manual demonstration was carried out by using a modified self-made elongation device operating in strain-controlled mode. The elongation device was modified from the piece of equipment used in shape memory tests by adding a retort clamp to prevent slippage during elongation of the rubber nanocomposite films. The step-by-step manual experiment processes were shown in Figure 3.9. Initially, the rubber film was carefully secured by two stainless steel clippers which acted as clamps before tightening the retort clamp located at the top side of the clipper. Then, the rubber film was elongated to 600% strain at room temperature where the gap between the two lines was measured as 7cm. Next, the elongated rubber film was quenched in 4 °C ice water for 2 minutes to induce fixation of the temporary shape. Subsequently, the rubber film was removed from the ice water and unclamped from the bottom clipper. The recovery process was then initiated and the lifted distance, d of the metal plates and standard weight induced by stored energy within the rubber films were measured. Specific work output, W can then be calculated directly from Equation 3.12.

$$W = \frac{m_1}{m_r} \times \mathrm{g} \times \mathrm{d} \tag{3.12}$$

where,

W = specific work output (J/g)

m_1 = mass of loads (g)

m_r = mass of rubber films (g)

g = gravitational acceleration (m/s^2)

d = lifted distance of load by rubber films (m)

Figure 3.8: (a) Rubber films fixed between steel plates (b) Weight of the steel plates and (c) Additional standard weight on rubber films

Rubber film was secured on the modified special elongation device

The rubber film was elongated to 600% strain

Rubber film was quenched in 4 °C ice water

Rubber film was unclamped from the bottom clipper

Figure 3.9: Manual demonstration of rubber nanocomposite film

3.6 Summary of Chapter 3

Chapter 3 presents a comprehensive methodology encompassing all materials preparation, characterization techniques and the evaluation of energy storage potential of sulphur-cured rubber films and SNC reinforced rubber composite films. Section 3.1 presents the materials and chemicals required for the experimental works in this research. Experimental procedures to synthesize SNC, determination for yield of SNC, fabrication of sulphur-cured rubber films and SNC reinforced rubber nanocomposites are discussed in detail in Section 3.2. Section 3.3 layout the characterization techniques such as FESEM, XRD, DSC, TGA, and PSA utilized to characterize the synthesized SNC. Subsequently, a series of characterization works for the fabricated rubber film and rubber nanocomposites films including determination of crosslink density, DMA, FESEM, tensile test, water and toluene uptake, TGA and DTG were shown at Section 3.4. These characterization works are done to investigate the physical and mechanical characteristics of sulphur-cured rubber films and SNC reinforced rubber composite films. Lastly, the evaluation of energy storage potential which involves shape memory test, cyclic-loading-unloading test and manual demonstration are detailed in Section 3.5. Important figures and equations involved in calculating any parameter are listed in a sequential manner in the above sub-sections.

Chapter 4

4.0 Characteristics and Properties of SNC, Sulphur-Cured Rubber Films and SNC/Rubber Composites Films

4.1 Characterization of SNC

4.1.1 Morphology and particle size of native starch and SNC

The morphology structures and particle size of SNC evaluated by FESEM were presented in Figure 4.1(a) and (b) while the particle size distribution of native starch and SNC were presented in Figure 4.2(a) and (b). From Figure 4.1(a), the synthesized SNC have spherical shape. Furthermore, no aggregate nor impurities are found in the material. This suggested that the SNC were well dispersed and the method to synthesize it does not create any impurities. However, irregular spherical morphology and rough surface are observed on some of the SNC. The heterogeneity and surface roughness of SNC can be recognised as the adhesion between starch granules and surface fracture caused by rigorous stirring during acid hydrolysis process and ultrasonic treatment (Utrilla-Coello *et al.*, 2014). From Figure 4.1(b), the size of individual SNC is ranging from 368.4 to 563.4nm with an average size of approximately 450nm. This is in agreement with the findings from previous literature (LeCorre, Bras and Dufresne, 2011). The size of SNC in nanoscale was further proven with particle size distribution determined by zetasizer. It can be clearly seen from Figure 4.2 (b) that most of the size distribution of SNC is in the range of approximately 600nm. Moreover, from Figure 4.2(b), some of the SNC size are at 6µm which is equivalent to the size of native starch as shown in Figure 4.2(a) reflects the presence of native starch in SNC suspension. The presence of SNC in microscale might be due to incomplete hydrolysis of the native starch. This circumstance can be improved by using a filter paper before any usage of SNC. From the results of FESEM and zetasizer, the synthesizing method of SNC is reckoned to be successful because of the obvious size reduction and well dispersed particles. SNC can therefore be considered as a potential reinforcement nanofillers in rubber matrix because of its demonstrated ability to distribute homogeneously in aqueous suspension.

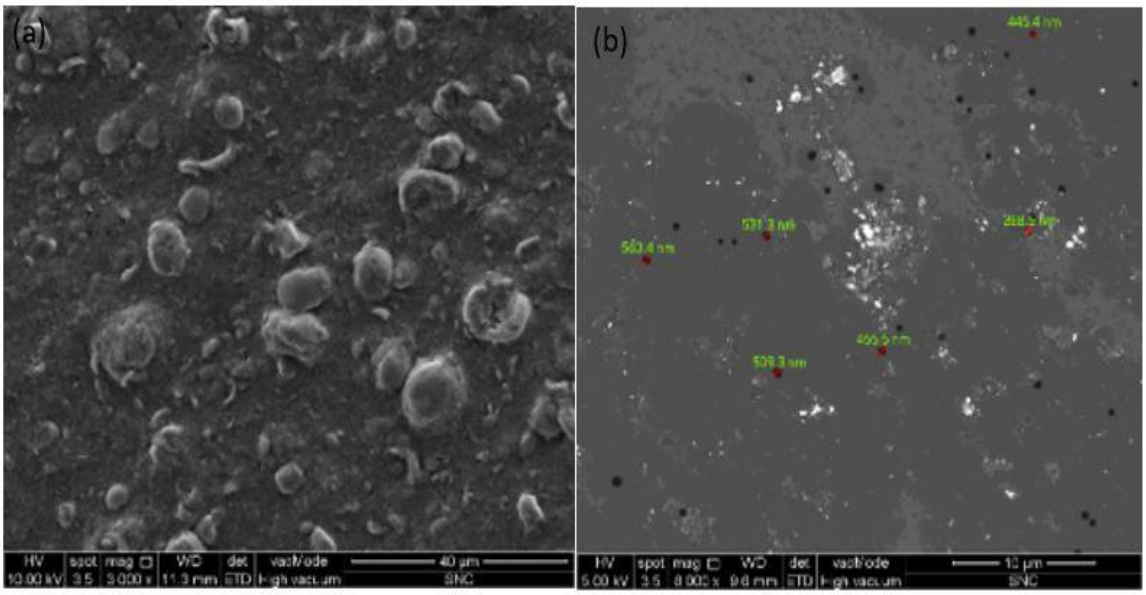

Figure 4.1: (a) morphology structure of SNC (b) particle size of SNC

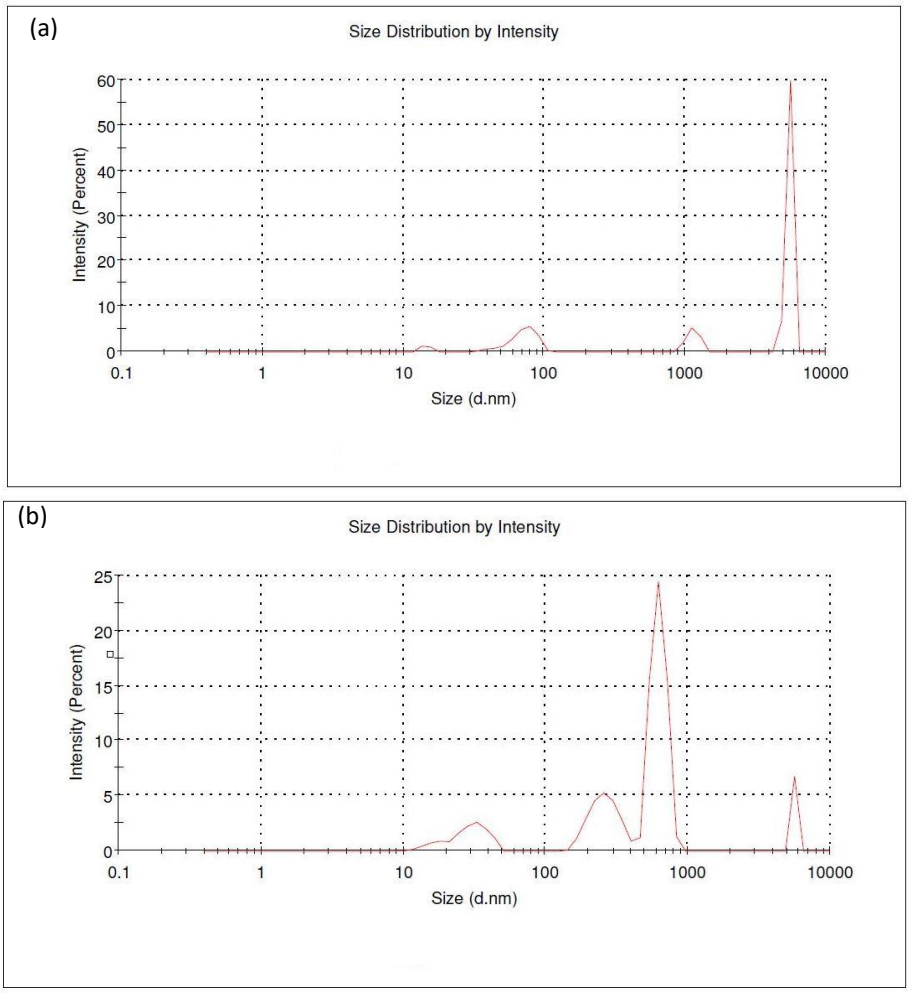

Figure 4.2: particle size distribution of (a) native starch (b) SNC

4.1.2 Crystallinity of SNC

X-Ray Diffraction pattern of native starch and SNC was presented as Figure 4.3. Both native starch and SNC showed a typical A-type crystalline structure notable from the 2Θ diffraction peaks. The native starch and SNC exhibited diffraction peaks where 2Θ of the first peak was at around 15°, second peak at near 17° and third peak at approximately 23°. The peak at 2Θ = 23° is more prominent when compared with the other. The results related to the type of crystalline structure and locations of the peaks were in accordance with the findings from other literature (Bel Haaj *et al.*, 2016). The sharper peaks and increment in area of the peaks after acid hydrolysis were due to higher relative crystallinity in SNC. The two curves corresponding to native starch and SNC were simply vertically shifted after hydrolysis treatment suggesting that the amylopectin content in SNC was higher. In another word, the amorphous region of the native starch was being hydrolyzed leaving a higher relative crystallinity in SNC. After 5 days of acid hydrolysis, the relative crystallinity of native starch and SNC were 35% and 44% respectively. This was consistent with the result published in previous literature (LeCorre, Bras and Dufresne, 2011). The relative gain in crystallinity of SNC was limited as native starch had already possessed a high crystallinity. This study in crystallinity further proved that acid treatment enables the dissolving of low lateral order in native starch and high crystalline region may be converted into stable suspension even with the action of vigorous mechanical shearing (Wang *et al.*, 2010).

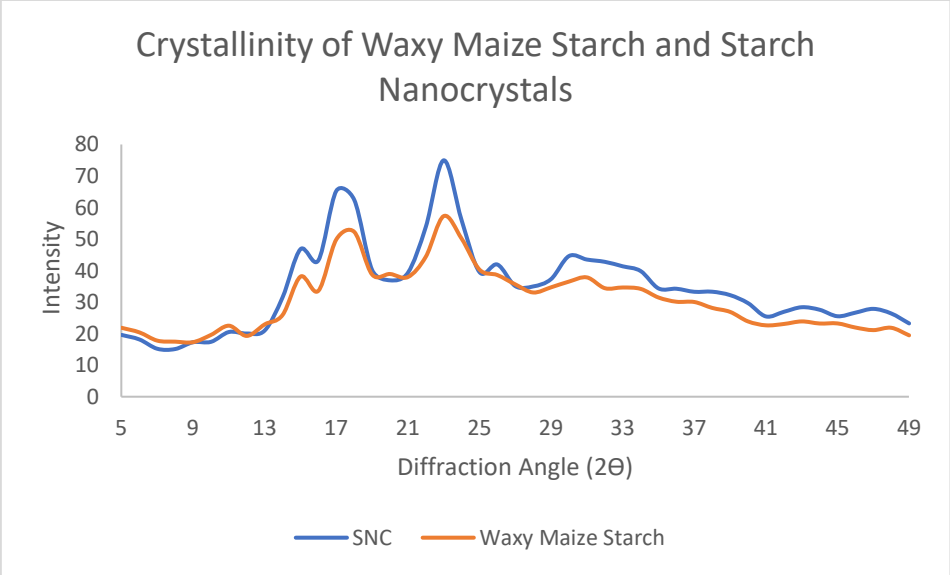

Figure 4.3: X-Ray Diffraction pattern of native starch and SNC

4.1.3 Thermal properties of SNC

Figure 4.4(a) indicates the characteristics temperature observed for the endothermic transition of native starch and SNC. The measurement for native starch shows two endothermic peak instead of one which is not in agreement with the findings from previous literature (D. Lecorre, Bras and Dufresne, 2012). The first unusual peak found in the diagram for native starch is due to the melting of unstable crystallites that absorbed water while the second peak reflects the melting of stable crystallites at higher temperatures. Another explanation for the appearance of two endothermic peaks suggested that the first and second peak are related to the partial and final melting of the crystals where recrystallization occurred in between the melting processes (Biliaderis *et al.*, 1985). Furthermore, this case can also be attributed to the melting of amylose lipid complexes and crystallites respectively (Zhong and Sun, 2005). It was revealed that the maximum endothermic peak for native starch is ranged between temperature of 175 to 185 °C. This is aligned with the initial expectation as the theoretical melting point of perfect crystallites without any presence of water is estimated between 160 -210 °C (Colonna and Buleon, 2009). Therefore, this reassured the freeze-drying process in SNC synthesizing removed residual moisture in the samples.

Based on Figure 4.4(a), to postulate mechanism the thermal behaviour of SNC had been characterized and analysed. Two observations can be made from the diagram shown: (i) two endothermic peaks was observed in dry state SNC, (ii) an obvious shift to the right in temperature when compared with native starch. From the thermogram, the first maximum peak is located at temperature of around 155 °C while the second peak is at approximately 200 - 210 °C. The result is in agreement with the findings from previous literatures (Thielemans, Belgacem and Dufresne, 2006; D. Lecorre, Bras and Dufresne, 2012). The first peak observed might be attributed to the gelatinization of SNC and the increase in temperature of both the peaks is due to the more crystalline nature of SNC. The existence of two endothermic peaks correspond to the presence of weak crystallites that melt earlier and more stable crystallites that melt at a higher temperature (Evans and Haisman, 1982). It is important to ensure that no depolymerization and degradation occurs under these conditions to confirm the postulated mechanism. Therefore, TGA measurements are carried out to determine the authenticity of this interpretations. Moreover, it should be noted that no consensus thermal transition temperatures for SNC is established due to limited number of research work and different in botanic origin of the native starch. Considering a classic polymeric approach, a few factors might increase the melting temperature of semi-crystalline polymer, in this case SNC (i) increase in crystallinity, (ii) a more perfect crystals with less plasticizer content. In the case of SNC, the increase in crystallinity when comparing with its native counterpart was demonstrated through XRD pattern shown in Section 4.1.2. This is because the amylose region of native starch is hydrolysed during synthesizing of SNC leaving

the more crystalline amylopectin region behind limiting its effect as a plasticizer. Moreover, because of the freeze-drying process, it is highly possible that the crystalline parts in SNC are more closely arranged and bonded via hydrogen bonding forming a perfect crystal.

Thermal degradation behaviour of native starch and SNC were evaluated by TGA in the temperature range of 50 – 550 °C under oxygen flow. Figure 4.4(b) shows the weight loss percentage of native starch and SNC. It was revealed from the thermogram that there are two major similar weight loss steps for both samples. The initial weight loss of approximately 5% is attributed to the evaporation of adsorbed water that starts immediately upon temperature rises and ends at around 110 °C for both native starch and SNC. The second weight loss step which commences at around 300 °C represents the thermal degradation of native starch and SNC which involves the depolymerization of saccharide rings. It should be noted from the thermogram that the secondary weight loss of SNC begins at a lower temperature of 200 °C. This corresponds to the presence of sulphate groups at the surface of SNC that are thermally decomposed at 200 – 250 °C (Jiang *et al.*, 1999; Angellier, 2005). The weight loss related to the decomposition of sulphonic acid groups reduces the depolymerization rate of SNC as observed from the delay in ending of degradation pertaining to SNC. Therefore, the depolymerization of SNC ends at 400 °C which is approximately 50 °C higher than native starch. This further suggested that SNC has stronger crystal structure and higher crystallinity contributed by the more crystalline amylopectin region. The thermogram also showed that the solid residue left behind by SNC (28.46%) is higher than native starch (19.75%). This result indicated that the thermal stability of SNC is higher that its native counterpart. In spite of this, the result is mutual with the findings of many authors that studied the thermal decomposition of various native starches using TGA (Soliman, El-Shinnawy and Mobarak, 1997; Aggarwal and Dollimore, 1998; Šimkovic and Jakab, 2001; Liu *et al.*, 2010). The first weight loss is related to evaporation of abounded water and the second weight loss resembles the thermal decomposition of native starch while remains with 20% of solid residue after the whole heating process (Liu *et al.*, 2010). Furthermore, the thermal degradation behaviour of SNC showed by TGA is in agreement with the previously reported results (D. Lecorre, Bras and Dufresne, 2012; Piyada, Waranyou and Thawien, 2013; Wei *et al.*, 2015). Indeed, depolymerization of SNC starts earlier than native starch due to the presence of sulphate groups while having greater thermal stability observed from the higher amount of remaining solid residues. In comparison, SNC has three different weight loss steps pertaining to the evaporation of water at beginning of the curve, the decomposition of sulphate groups at surface of SNC which starts at 200 °C contributes to the secondary weight loss and the degradation of SNC at higher temperature of 300 °C. On the other hand, native starch possessed two weight loss steps related to the evaporation of water and degradation of native starch both occurring at similar temperature to SNC.

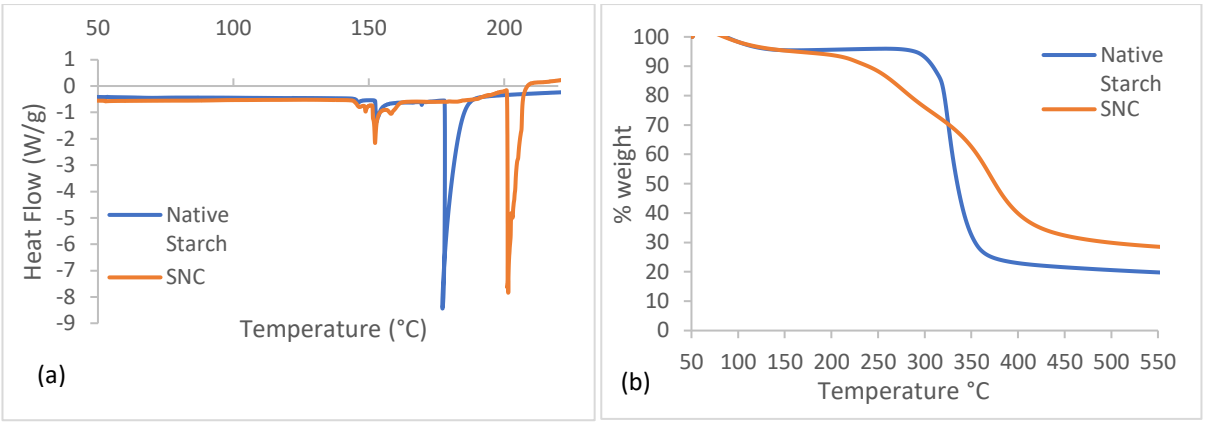

Figure 4.4: (a) DSC thermograms (b) TGA curves for native starch and SNC

Additionally, validation for melting of crystallites in dry condition reflected by the endothermal peaks displayed in Figure 4.4(a) can be assessed with TGA measurements (D. Lecorre, Bras and Dufresne, 2012). Table 4.1 shows the temperature of endothermic peaks and degradation for native starch and SNC. The postulated mechanism regarding the presence of weak crystallites that melt earlier and more stable crystals that melt at a higher temperature reflected through the two endothermic peaks is verified through a much higher degradation temperature than both the endothermic peaks for native starch. Similar result was obtained concerning the evaluation on SNC. It is shown that the two endothermic transitions of SNC displayed by DSC thermogram happens before the thermal degradation temperature observed in TGA. This consolidated that no depolymerization and degradation occurs before the temperatures of endothermic peaks. Although trace amount of initial water evaporation is discovered for freeze-dried SNC, early stage depolymerization is absented as observed from the TGA curve. This reaffirmed that the two endothermic peaks recognized from DSC thermogram reflected the melting of weak and more stable crystallites of native starch and SNC.

Table 4.1: Temperature of endothermic peaks and degradation for native starch and SNC

Samples	Temperature of endothermic peaks (°C)	Degradation temperature (°C)
Native starch	155 (first), 175 – 185 (second)	300
SNC	155 (first), 200 – 210 (second)	300

4.2 Physical and Mechanical Characteristics of Sulphur-Cured Rubber Films

4.2.1 Crosslink densities of sulphur-cured rubber films

Crosslinking of rubber involves the linkages of rubber molecules via chemical bonding that forms three-dimensional network structure prior to the vulcanization process. The crosslink densities of sulphur-cured rubber films comprised of NRL, ENRL25, ENRL50 and DPNRL were calculated with equation 3.2 aforementioned at section 3.3.1. This method involves the use of storage modulus in the rubber plateau region at room temperature of 25 °C determined experimentally by DMA. The

calculated crosslink densities of all sulphur-cured rubber films expressed in mol cm^{-3} were tabulated in Table 4.2. As expected, the crosslink densities of the rubber films increased with higher sulphur loading. In another word, higher loading of crosslinking agent promotes the formation of crosslink between rubber chains. It is because higher sulphur loadings give more available sulphur atoms to react with the unsaturated C=C bonds in rubber. This is in agreement with the findings from previous literature regarding NR where higher loading of crosslink density promotes the increment in polysulphidic linkages within the rubber vulcanizates (Coran, 2013; Boonkerd, Deeprasertkul and Boonsomwong, 2016). In the rubber chain, monosulphide, disulphide and polysulphide structures were formed through the crosslinking reaction. The most stable polysulphide structure formed through the ring-opening reaction with rubber was the most constituted crosslinking found in the rubber vulcanizates (Rabiei and Shojaei, 2016).

Crosslinking in rubber chains through vulcanization gives the material a more rigid and better-defined structure thus improving the mechanical properties involving tensile strength and modulus of the rubber material. With this, the overall performance of the rubber will be enhanced complementing the usage of rubber in various applications. These crosslinks tie the rubber molecules together developing a net-like structure and forming a stiffer material while preventing the intermolecular movement of rubber chains. The reduction in mobility of the rubber molecules leads to an increment in T_g of the sulphur-cured rubber films (Marković *et al.*, 2020). It is because with increasing crosslink densities, there will be higher intermolecular forces, interchain attraction and cohesion between rubber chains that subsequently leads to a decrease in free volume causing an increase in T_g of the rubber films. This interpretation is proven by the slight shift to the right of tan δ peaks for all rubber matrices with the highest sulphur loading as shown in Figure 4.6(a), 4.6(b), 4.6(c) and 4.6(d) in Section 4.2.3. Furthermore, from Table 4.2, it was manifested that ENRLs based films have lower crosslink density when comparing to NRLs films. This is because epoxide groups developed a bulky side group that reduced the accessibility of curing agent to C=C which eventually lowered the number of available sites for event of sulphur crosslinking. However, the crosslink densities of ENRLs increased as more unsaturated bonds were converted to epoxide groups. The ring-opening reactions between epoxy groups and activation of double bonds by adjacent epoxy groups of ENRLs are the factors behind this circumstance (Poh and Tan, 1991). These reactions happen during the vulcanization process when curing agent is added to the rubber leading to the opening of epoxide ring and formation of reactive hydroxyl group as well as a C=C bond. The reactive groups can then react with crosslinking agent to form covalent bonds. Therefore, the crosslink densities of ENRL50 are comparatively higher than ENRL25 as observed from Table 4.2.

Table 4.2: Crosslink densities of sulphur-cured rubber films

Samples	Crosslink Density ($x10^{-4}$ mol cm^{-3})	Samples	Crosslink Density ($x10^{-4}$ mol cm^{-3})
NRL 0.2	1.20	ENRL25 0.2	0.72
NRL 0.3	1.40	ENRL25 0.3	0.80
NRL 0.4	1.58	ENRL25 0.4	1.23
NRL 2.0	2.59	ENRL25 2.0	1.96
DPNRL 0.2	1.64	ENRL50 0.2	1.02
DPNRL 0.3	1.68	ENRL50 0.3	1.23
DPNRL 0.4	1.99	ENRL50 0.4	1.72
DPNRL 2.0	2.59	ENRL50 2.0	2.25

4.2.2 Swelling measurement of sulphur-cured rubber films

As mentioned in Section 4.2.1, crosslinks are essential to improving the overall performance of rubber. Swelling measurement is an indicator directly related to the crosslink density of rubber films as the swelling percentage is inversely proportional to the amount of crosslinks. In another word, an increase in crosslink density stipulates the decrease in toluene uptake and vice versa. Therefore, the rubber films were immersed in toluene until equilibrium to authenticate the interpretation relating crosslink density and swelling behaviour as well as evaluating the oil resistance of ENRLs to solvent. Figure 4.5(a) and (b) shows the condition of the NRL films at initial and final stage of swelling in toluene. However, the difference in colours of the two figures was not investigated in this study as the purpose of the swelling experiments are to relate the toluene uptake to crosslink density of the rubber films. The calculated crosslink densities for each rubber films were presented in Table 4.2. From Table 4.3, it showed clear evident that increasing crosslink density in all types of rubber films resulted in decreasing swelling percentage. Similar findings accounting for NR were also discovered in other literatures (Surya, Sukeksi and Hayeemasae, 2018; Kim *et al.*, 2020). The toluene uptake for DPNRL 0.0 calculated as 571.43% was the highest swelling percentage recorded while ENRL50 2.0 which recorded a reading of 305.00% had the lowest swelling percentage within the investigated range of sulphur-cured rubber latexes. This is because increasing crosslink density in the rubber network indicates that there are more covalent bonds between the rubber chains that develops a more compact and tighter structure. This tighter structure reduces the free volume available in the rubber matrix meaning less space between the rubber chains, therefore reducing the availability of solvent molecules to penetrate into the rubber network resulting in less swelling (Hiemenz and Lodge, 2007; Fried, 2014; Darko, 2022; Tsai and Chiu, 2022). Therefore, rubber films with high crosslink density can accommodate fewer number of solvent molecules by immobilization of their rubber chains due to the rigidity of the structure. The reduction of toluene uptake between neat rubber and RL crosslinked with 2.0 phr sulphur is determined to be 26.67%, 28.41%, 28.90% and 30.10% accounting for NRL, DPNRL,

ENRL25 and ENRL50 respectively. Hence, the highest reduction in toluene uptake is ENRL50 as it is well known that epoxidation of NR improves the oil and solvent resistance. From Table 4.3, it was manifested that ENRLs based rubber films exhibited better toluene resistance than its NRLs counterpart analogous to the same sulphur loadings. Owing to the fact that epoxidation reaction increases the polarity of NR, this allows the rubber molecules to be less susceptible to swelling in non-polar solvents such as toluene and benzene. This is due to the presence of oxirane groups that contain oxygen atoms in epoxide groups which reduced its affinity towards non-polar solvents leading to improved resistance against them (Ahmad, Ismail and Rashid, 2017). Moreover, increasing the fraction of epoxide groups that means higher polarity of rubber films result in decreasing solvent penetrability which in turn improve the oil resistance making ENRLs possessed comparable properties to synthetic rubber such as NBR. ENRL with higher degree of epoxidation also contributed to lower solvent sorption and equilibrium mol uptake (Kinasih, Fathurrohman and Winarto, 2017). These statements are in agreement with the finding discovered where ENRL50 has better oil resistance than ENRL25. Similar outcomes have also been uncovered in other literatures (Burfield, Lim and Law, 1984; Alakrach *et al.*, 2018).

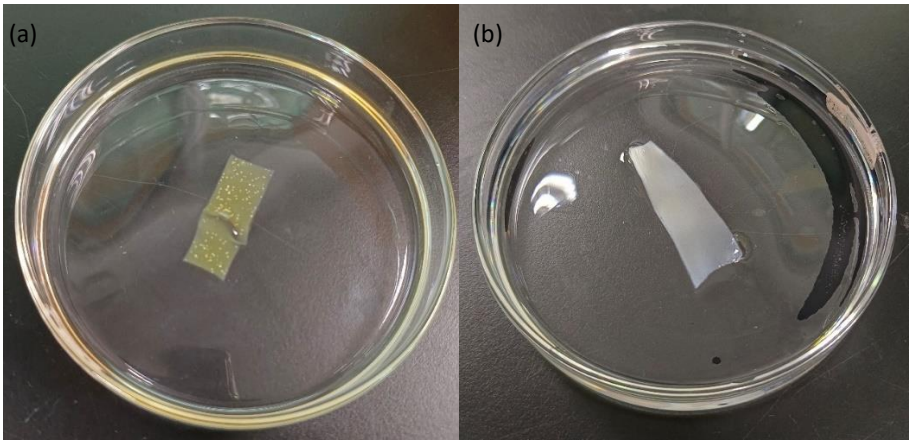

Figure 4.5: Condition of NRL films at (a) initial and (b) final swelling stage in toluene

Table 4.3: Toluene uptake of various rubber films after immersion for two days

Samples	Toluene uptake (%)	Samples	Toluene uptake (%)
NRL 0.0	540.00	ENRL25 0.0	464.00
NRL 0.2	503.85	ENRL25 0.2	451.61
NRL 0.3	481.82	ENRL25 0.3	408.82
NRL 0.4	445.83	ENRL25 0.4	381.82
NRL 2.0	396.00	ENRL25 2.0	329.63
DPNRL 0.0	571.43	ENRL50 0.0	436.36
DPNRL 0.2	520.00	ENRL50 0.2	416.67
DPNRL 0.3	504.00	ENRL50 0.3	382.35
DPNRL 0.4	482.76	ENRL50 0.4	360.87
DPNRL 2.0	409.09	ENRL50 2.0	305.00

4.2.3 Dynamic Mechanical behaviour of sulphur-cured rubber films

Dynamic mechanical measurement was performed for sulphur-cured rubber films with different sulphur loadings. Plots of the logarithm of storage modulus Log (E') and tangent of the loss angle (tan δ) against temperature at 1Hz are shown as Figure 4.6 and 4.7. All curves of Log (E') correlated with the rubber matrices showed a typical fully amorphous high molecular weight thermoplastic behaviour. All samples exhibited a similar trend of maintaining in the glassy state at temperatures below T_g with decreasing storage modulus against temperature but remained roughly constant above 1GPa. The state of materials is hard and brittle at this condition. From Figure 4.6(a) and (b), a sharp decrease of storage modulus of approximately 3 decades is observed at temperature around -60°C accounting for NRL and DPNRL. In fact, an obvious glass-rubber transition zone is not clearly shown for NRL and DPNRL as the horizontal glassy region of the materials are not reflected through the figures. This observation is aligned with the certainty surrounding T_g of pure NRL films being -65 °C (Ho and Khew, 2000). The same magnitude of storage modulus decrease is noticed from Figure 4.6(c) and (d) at temperature of -40 and -25 °C for ENRL25 and ENRL50 respectively. The clear increment of temperature for ENRLs at the initial sharp decrease of storage modulus is because epoxidation improves the homogeneity of the polymer with narrower molecular weight distribution that enhanced the rotational hindrance of ENRLs and reduced the free volume of chain sections (Ren *et al.*, 2022). Similar phenomenon is reported on epoxidized solution polymerized styrene-butadiene rubber (Liu *et al.*, 2020). This drop in storage modulus of all rubber latexes indicated that the rubber matrices underwent primary relaxation process correlated with the glass-rubber transition. Moreover, this plunge is related to an energy dissipation phenomenon showed in the concomitant relaxation process where tan δ reaches a maximum peak. Moving on, the storage modulus of all rubber matrices reached a plateau stage at around 1-5MPa. At this stage, the material behaves as an elastomer which gives softness and flexibility to the polymer. This also corresponds to the rubbery state of the material. The broad temperature range between -20 °C to 110 °C of the rubbery state is due to the high molecular weight of the polymer eventuating in a highly entangled state of the macromolecules.

Furthermore, the storage modulus is an indication of a polymer's ability to store deformation energy. This is directly related to the extent of crosslinking, where a higher degree of crosslinking signifies the greater storage modulus. A higher storage modulus also denotes a more solid like property which means higher strength or mechanical rigidity (Ahmed, 2017). Figure 4.7(a), (b), (c), (d) and (e) show the zoomed in plots of Log E' against temperature for rubber films with different sulphur loadings. All figures apart from Figure 4.7(a) showed consistent data where DPNRL possessed the highest storage modulus followed by NRL, ENRL50 and ENRL25. Moreover, the storage modulus increased with sulphur loading which is in agreement with the aforementioned statement. This is also

aligned with the findings shown at Table 4.4 where DPNRL films have the highest mechanical strength among the other investigated rubber films.

From Figure 4.8(a), (b), (c) and (d) the evolution of tan δ with temperature displayed a peak located at T_g of NRLs and ENRLs. The peak of tan δ often indicates the glass-transition region of rubbery material where the material has the most viscous response to deformation. It is the most common way to identify the T_g of a material using DMA in accordance with ASTM D4065 (A.J. Jeffrey, 2020). This relaxation process is associated with the anelastic manifestation of the glass-rubber transition of the polymer and engaged collective movements of the long chain sequences. All NRL and DPNRL films with varying sulphur loadings showed T_g at temperatures between -50 and - 40 °C. ENRL25 and ENRL50 films displayed T_g at approximately -30 and -15 °C revealing that ENRLs displayed higher T_g than NRLs. This is because the epoxidation of cis 1,4 polyisoprene which introduced the presence of epoxide groups reduced the conformational flexibility of the polymer chains that gives rise to the increment in T_g of NR (Chuayjuljit *et al.*, 2006; Kaewsakul *et al.*, 2021). Indeed, per degree % of epoxidation caused around 0.9 °C of escalation in T_g of NR (Roberts, 1988; Cataldo, 1992). Hence, the T_g of ENRLs can be manipulated by just controlling the degree % of epoxidation. In this case, the T_g of ENRL50 is higher than ENRL25 while ENRLs have obviously higher T_g than NRLs. In all cases, the rubber networks possessed a homogenous phase at the molecular level which can be observed from the single peak of the curves. As revealed, the curves of tan δ for all types of rubber films shifted slightly to the right when comparing rubber films with 2.0 phr and no sulphur loadings. This event suggested that T_g of rubber films are increased by the structural modification of rubber chains via crosslinking. This increment is also due to the consistently increased limitations of chain motion due to higher crosslink density. Furthermore, tan δ represents the ratio of viscous to elastic response of a viscoelastic material and it is often called damping. In another word, the energy dissipation potential of a material. It was observed that NRL and DPNRL have comparatively higher tan δ peaks than ENRLs based rubber films. Moreover, Table 4.4 showed the area under tan δ curves of each specimen. It was realized that the areas under the tan δ curves of NRLs based rubber films are larger than its ENRLs counterpart, indicating that NRLs have greater damping coefficient which translated to better efficiency in accomplishing energy absorption and dispersal. In summary, NRLs have better damping coefficient whereas ENRLs based rubber films have higher T_g than NRLs while the appreciable increase in T_g of all rubber films with higher sulphur loadings symbolized the increment in stiffness of the network.

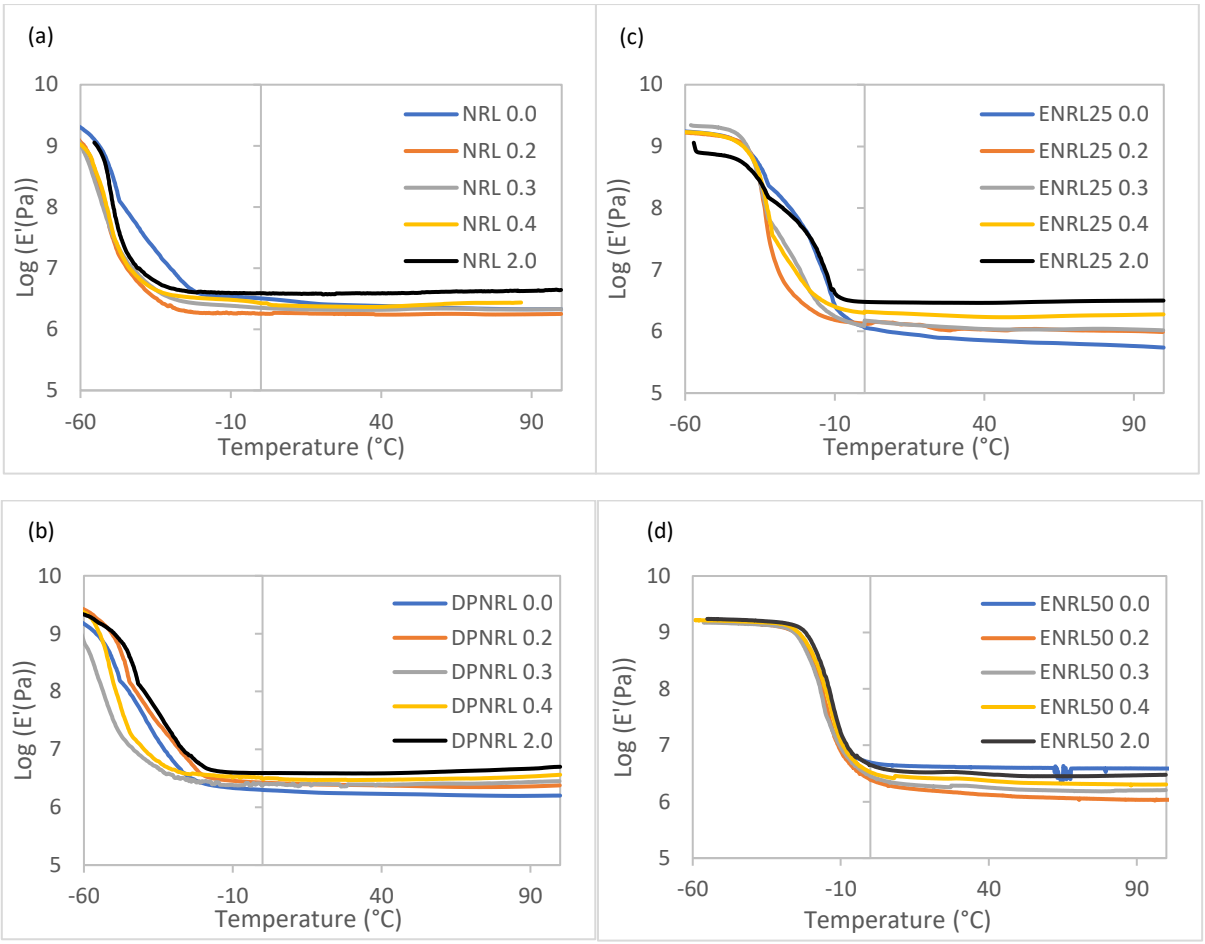

Figure 4.6: Plot of logarithm of storage modulus against temperature for (a) NRL (b) DPNRL (c) ENRL25 and (d) ENRL50

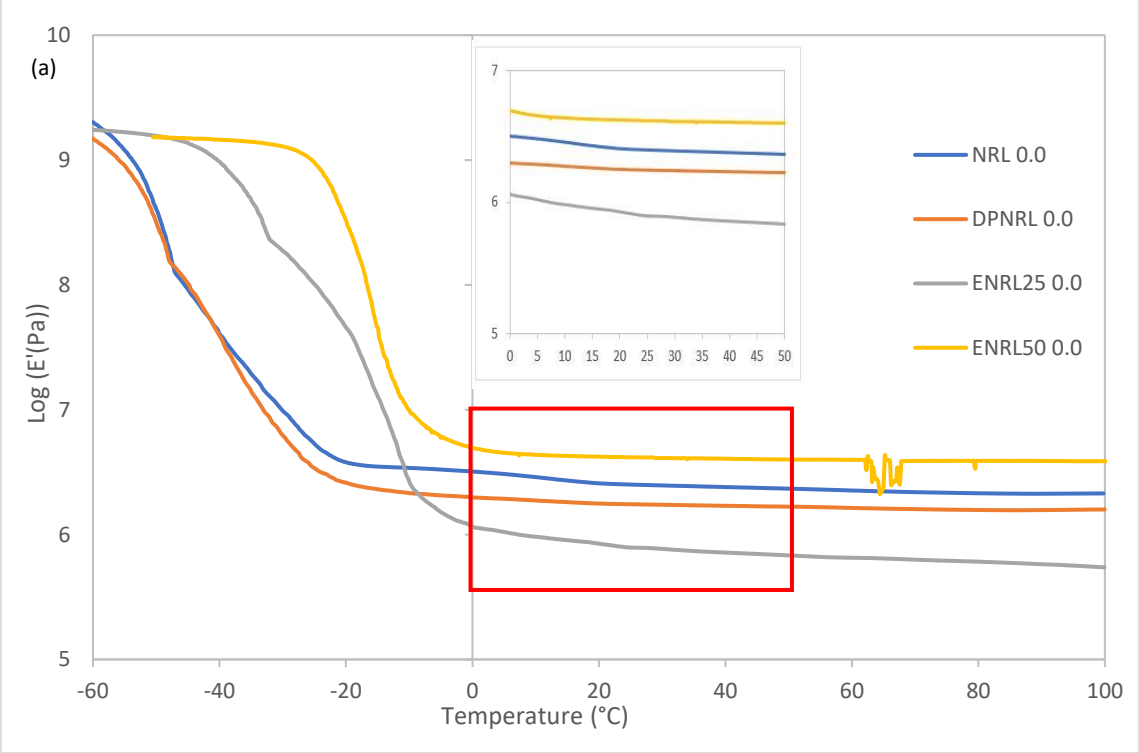
(a)
Log (E'(Pa))
Temperature (°C)
NRL 0.0
DPNRL 0.0
ENRL25 0.0
ENRL50 0.0

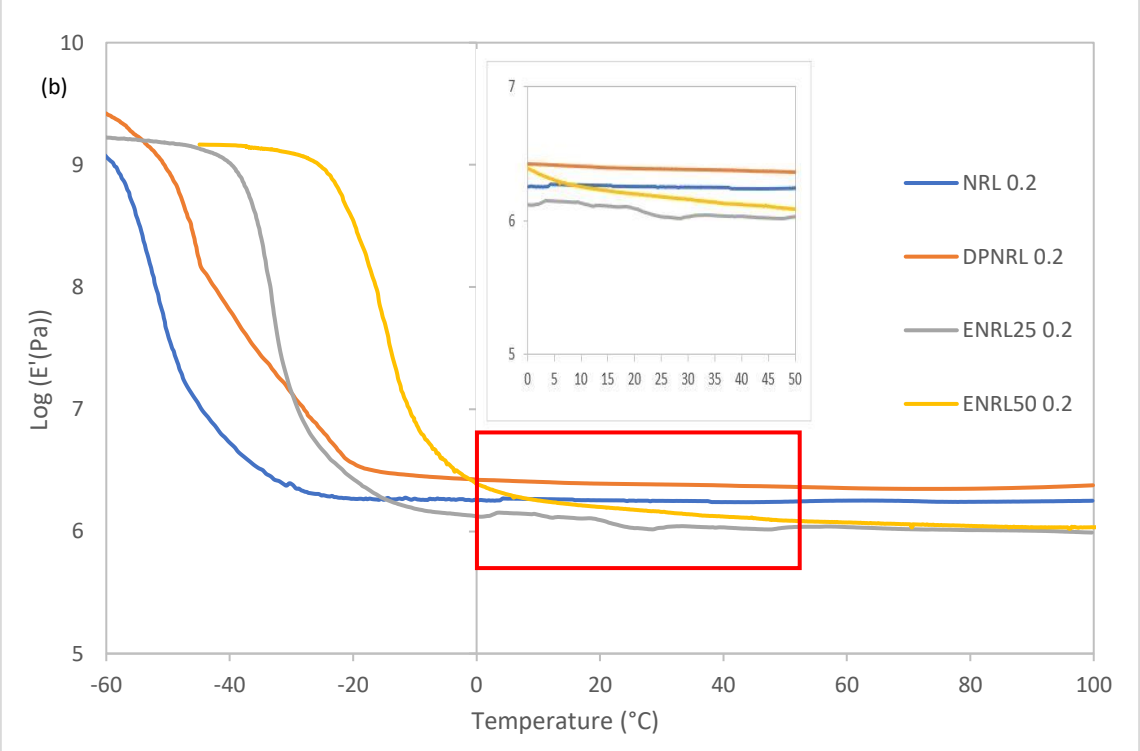
(b)
Log (E'(Pa))
Temperature (°C)
NRL 0.2
DPNRL 0.2
ENRL25 0.2
ENRL50 0.2

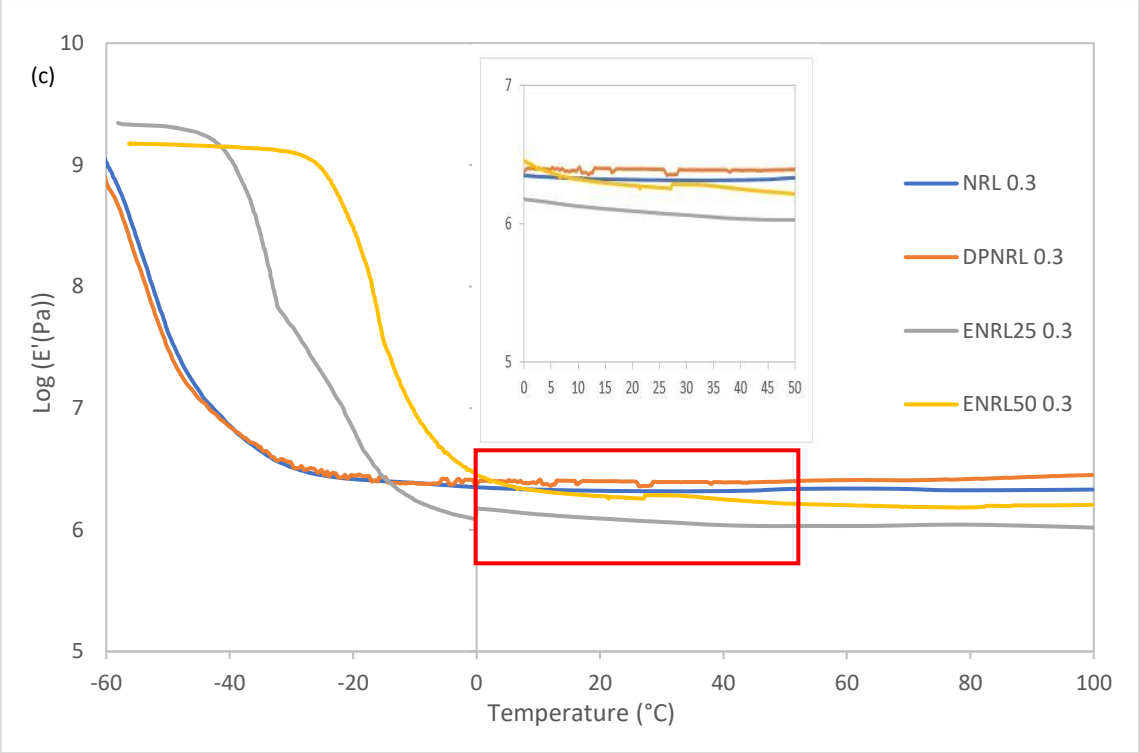
(c)
Log (E'(Pa))
Temperature (°C)
NRL 0.3
DPNRL 0.3
ENRL25 0.3
ENRL50 0.3

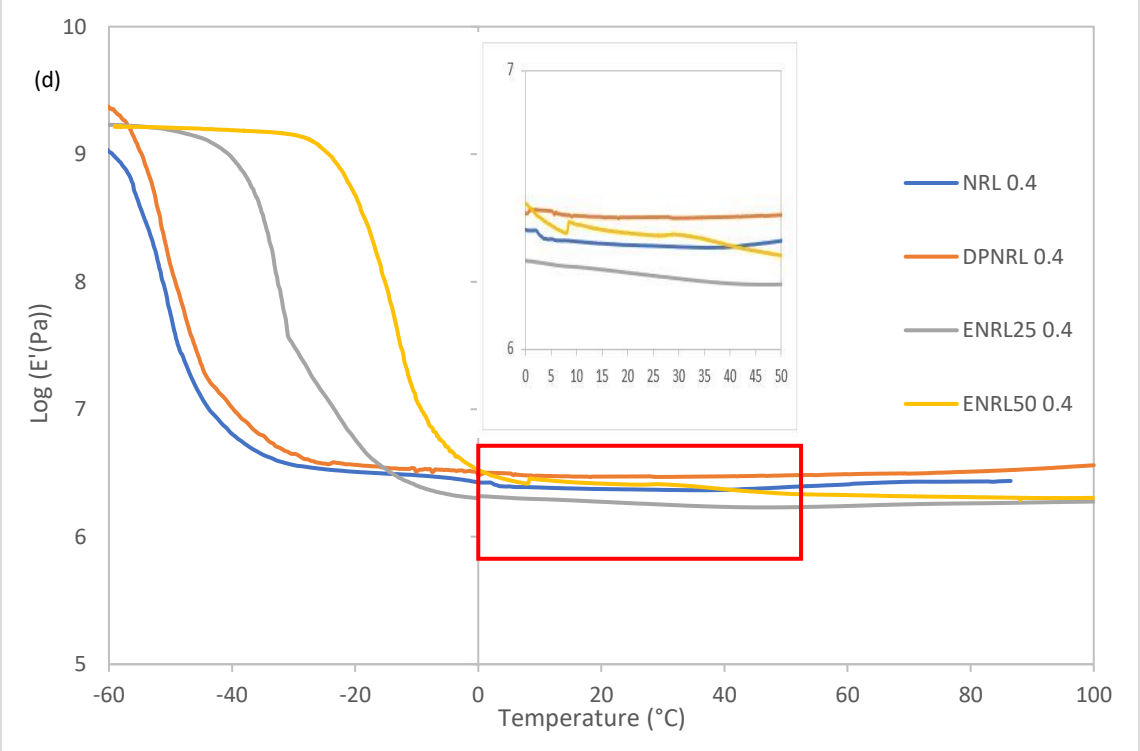
(d)
Log (E'(Pa))
Temperature (°C)
NRL 0.4
DPNRL 0.4
ENRL25 0.4
ENRL50 0.4

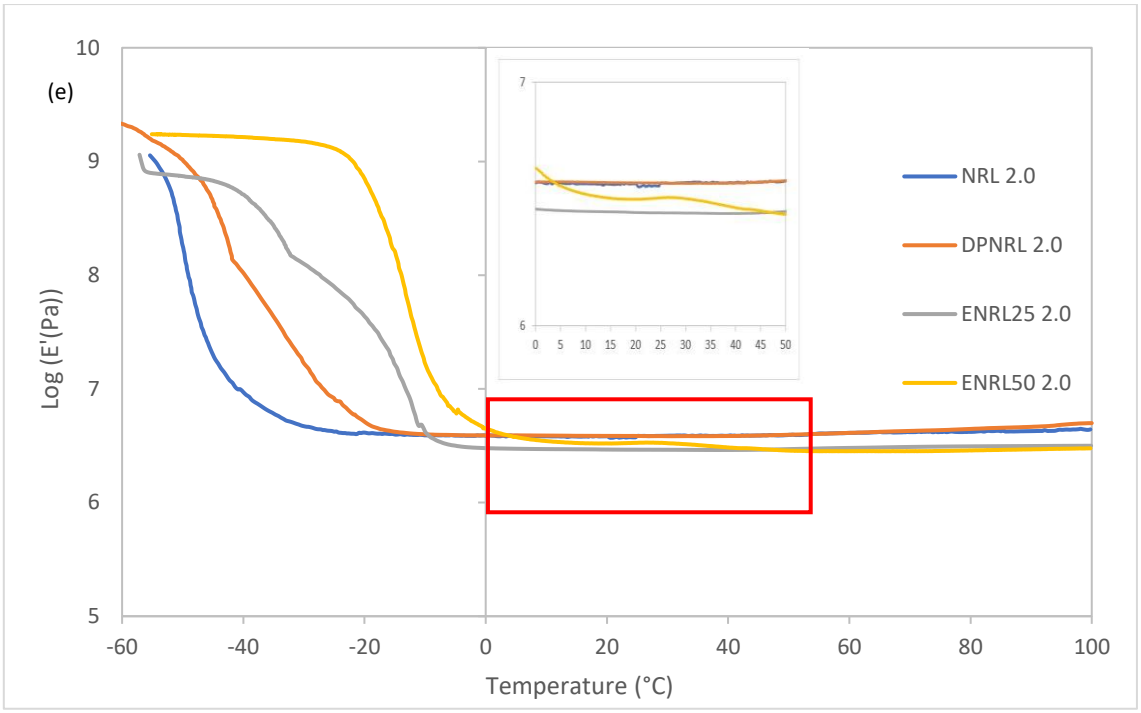

Figure 4.7: Logarithm of storage modulus against temperature with zoomed in images for rubber films with (a) 0.0 phr (b) 0.2 phr (c) 0.3 phr (d) 0.4 phr and (e) 2.0 phr sulphur content

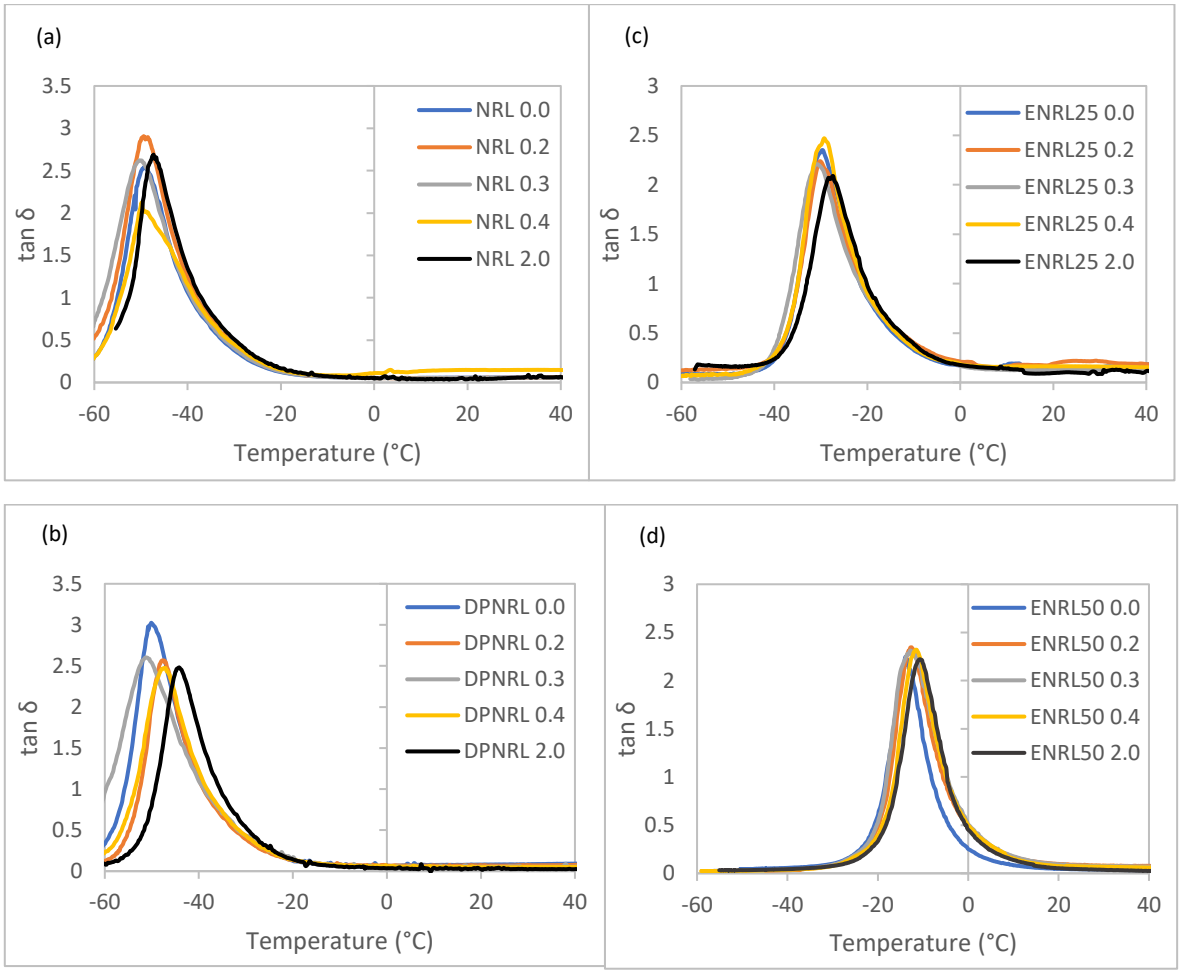

Figure 4.8: Plot of tan δ against temperature for (a) NRL (b) DPNRL (c) ENRL25 and (d) ENRL50

Table 4.4: Area under tan δ curves

Samples	Area under tan δ curve	Samples	Area under tan δ curve
NRL 0.0	43.19	ENRL25 0.0	38.66
NRL 0.2	49.54	ENRL25 0.2	40.25
NRL 0.3	48.90	ENRL25 0.3	39.30
NRL 0.4	44.55	ENRL25 0.4	36.90
NRL 2.0	42.57	ENRL25 2.0	33.91
DPNRL 0.0	49.89	ENRL50 0.0	34.06
DPNRL 0.2	45.05	ENRL50 0.2	35.77
DPNRL 0.3	48.91	ENRL50 0.3	37.64
DPNRL 0.4	43.52	ENRL50 0.4	33.84
DPNRL 2.0	40.50	ENRL50 2.0	31.22

4.2.4 Mechanical properties of sulphur-cured rubber films

The tensile mechanical properties of four different types of sulphur-cured rubber films (NRL, ENRL-25, ENRL-50 and DPNRL) with different sulphur loadings were evaluated at room temperature. Elastic non-linear behaviour of a typical amorphous polymer was found for all rubber films after studying the result from tensile tests at $T > T_g$. Figure 4.9(a), (b), (c) and (d) shows the stress-strain relationship of the rubber films with different sulphur loading. It was found that the tensile strength constantly increased with amount of sulphur until breaking of the rubber films. As expected, tensile modulus and tensile strength increased with higher sulphur loading. The tensile strengths were increased by 236% (NRL), 388% (ENRL25), 315% (ENRL50) and 333% (DPNRL) when sulphur loading rose from 0.0-2.0phr accounting to an increment of 200% in crosslinking agent. This result is mutual with the findings presented at Section 4.2.1 where higher sulphur loading developed rubber films with higher crosslink density that subsequently formed stronger rubber films. Ultimately, low loading of sulphur produces shorter crosslinks with a smaller number of sulphur atoms making the rubber softer. Conversely, high loading of sulphur gives longer crosslinks and a larger number of sulphur atoms makes the rubber harder with improved physical durability and tensile stress (Joseph *et al.*, 2015; Tan *et al.,* 2024b). It is because the vulcanization process hardens rubber by forming crosslinks between their individual rubber molecules where the resulting rubber chains were permanently linked together to increase its strength. Therefore, vulcanization with sulphur increases viscosity, hardness, modulus, tensile strength and abrasion resistance while decrease elongation at break, compression set and solubility in solvents (Miguel Martín-Martínez, 2002). Furthermore, the increase in T_g of rubber film will tend to increase its tensile strength if the fraction of crystallinity remain constant and compensate for any drop if the crystallinity decreased (Davies *et al.*, 1983). This interpretation is constant with the discussion at Section 4.2.3 where increasing sulphur loading caused a shift to the right of tan δ peaks of all rubber films as shown in Figure 4.8(a), 4.8(b), 4.8(c) and 4.8(d).

From Table 4.5, it was noted that all rubber films with no addition of sulphur (NRL 0.0, ENRL25 0.0, ENRL50 0.0 and DPNRL 0.0) possessed the lowest tensile strength while rubber films with the most sulphur loading (NRL 2.0, ENRL25 2.0, ENRL50 2.0 and DPNRL 2.0) have the highest tensile strength among their respective rubber types. In fact, it is worth to note that NRLs based films displayed higher tensile strength when compared with its ENRLs counterpart. This is because NR has many double bonds in its molecular chains that react with sulphur to form continuous network that makes the rubber stronger while ENR converts part of the C=C double bonds in NR structure to epoxide groups. Moreover, the presence of crosslink network enhanced the behaviour of SIC as there are more entanglements within the rubber chains, this improved the tensile strength of NRLs films since crystallization occurred upon stretching (Toki *et al.*, 2009). This statement is proved by Table 4.2 where ENRLs films have relatively lower crosslink density when comparing with NRLs films. Furthermore, reports suggested that epoxidation of NR has suppressed the ability of NR to exhibit SIC at high elongation (Cataldo, 2002; Chuayjuljit, Mungmeechai and Boonmahitthisud, 2017). Therefore, cis 1,4 configuration with higher capability to strain crystallize upon elongation aided in the slightly higher tensile strength of vulcanized NRLs films. Similar observations about the effect of SIC to tensile properties of rubber vulcanizates had also been revealed elsewhere (Sadequl, Poh and Ishiaku, 1999; Cataldo, 2002; Raksaksri *et al.*, 2017; Ngudsuntear *et al.*, 2022). Out of all rubber films with highest sulphur loadings, DPNRL and ENRL25 showed the highest and lowest tensile strength at 15.1 MPa and 9.9 MPa respectively. The upper bound value of tensile strength at 2.0phr sulphur loading for NRLs based film is measured to be 15.1 MPa while ENRLs based films recorded a value of 10.2 MPa. DPNRL 2.0 and ENRL50 2.0 are the specimens behind these upper bound tensile strength values. When comparing ENRLs based films within themselves, the tensile strength of the rubber films is relatively the same at similar sulphur loadings. ENRL50 showed slightly better tensile strength than ENRL25, this is due to the greater polarity of ENRL50 that contributed positively to mechanical properties.

On the other hand, the brittleness of the material increased with sulphur content as the movement of chain is restricted which in turn reduced the flexibility of the rubber films (Al-Maamori and Hamza, 2018). This is shown when all rubber films with 2.0 phr sulphur loading have the lowest elongation at break when compared with the other rubber films. In spite of this, the decrement in elongation at break is less than 100%, thus, this drop in fracture strain is deemed to be insignificant. Interestingly, lightly crosslinked ENRLs in this case from 0.2-0.4 phr sulphur loading appeared to have higher elongation at break than their respective neat rubber. The reason could be the weaker adherence of sulphur to ENRLs polymer matrix hence leading to less stiffening of the rubber chains. However, the improvement in elongation at break is trivial as the increment is less than 100% in contrast to ENRL25 0.0 and ENRL50 0.0. From Table 4.5, all rubber films exhibited excellent flexibility

that is manifested by elongation at break higher than 700%. Therefore, it is safe to postulate that sulphur loading between 0.2-2.0 phr showed overall good mechanical properties. Considering the ultimate properties, a good compromise must be made to select the rubber formulation to achieve the desired strength and hardness.

Table 4.5: Tensile strength and elongation at break of sulphur-cured rubber films

Samples	Tensile Strength (MPa)	Elongation at break (%)	Samples	Tensile Strength (MPa)	Elongation at break (%)
NRL 0.0	4.1 ± 0.3	812.6 ± 20.1	ENRL25 0.0	2.0 ± 0.3	863.0 ± 54.4
NRL 0.2	5.9 ± 0.7	817.7 ± 25.4	ENRL25 0.2	3.2 ± 0.1	924.4 ± 24.9
NRL 0.3	6.6 ± 0.5	793.8 ± 16.9	ENRL25 0.3	5.0 ± 0.4	917.3 ± 22.1
NRL 0.4	8.3 ± 0.2	757.6 ± 36.1	ENRL25 0.4	6.5 ± 0.5	933.9 ± 20.4
NRL 2.0	13.8 ± 0.4	742.7 ± 20.3	ENRL25 2.0	9.9 ± 0.1	847.2 ± 10.2
DPNRL 0.0	3.5 ± 0.3	981.5 ± 15.5	ENRL50 0.0	2.5 ± 0.3	938.8 ± 32.1
DPNRL 0.2	6.3 ± 0.3	942.3 ± 28.5	ENRL50 0.2	4.3 ± 0.5	958.2 ± 34.8
DPNRL 0.3	7.6 ± 0.5	942.4 ± 36.7	ENRL50 0.3	5.5 ± 0.4	945.1 ± 11.6
DPNRL 0.4	9.4 ± 0.2	940.8 ± 11.6	ENRL50 0.4	6.9 ± 0.3	973.2 ± 15.9
DPNRL 2.0	15.1 ± 0.4	937.2 ± 12.2	ENRL50 2.0	10.2 ± 0.5	886.3 ± 29.6

Remarks: Data were presented as average value ± standard deviation

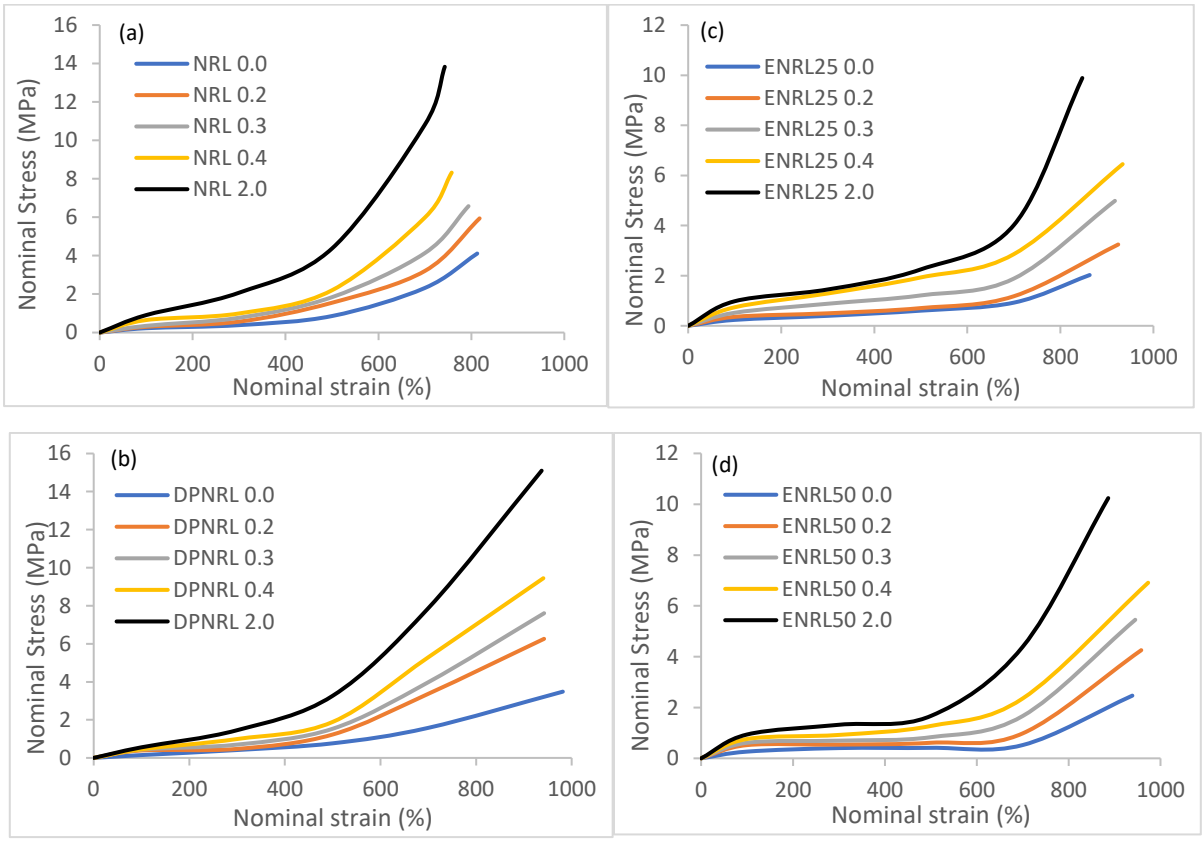

Figure 4.9: Plots of nominal stress against nominal strain for sulphur-cured (a) NRL films (b) DPNRL films (c) ENRL25 films (d) ENRL50 films

4.3 Characteristics and Mechanical Properties of SNC/Rubber Composites Films

4.3.1 Morphology of SNC/rubber composites films by FESEM

The morphology of SNC reinforced rubber nanocomposites films were evaluated by FESEM analysis. The insights regarding distribution level of varying SNC content in RL were identified by the surface morphology patterns of the rubber nanocomposite films as presented in Figure 4.10, 4.11, 4.12, 4.13 and 4.14. The presence of SNC is easily evidenced by the appearance of white dots in the micrographs whose concentration is a direct function of the SNC content. A rather homogenous distribution of SNC is observed for all rubber nanocomposites films. The micrographs also showed that there was no significant difference accounting for the homogeneity in dispersion between NRLs and ENRLs based films. However, a tendency to agglomerate is seen for increasing SNC content ranging from 6-8%. Such scenario is also reported elsewhere on potato and corn SNC filled NR rubber matrix (Bouthegourd *et al.*, 2011; Rajisha *et al.*, 2014, 2015). In fact, the reason that SNC can be spotted throughout these micrographs suggested that some small parts of the SNC are "homogenously aggregated" in the rubber matrices (D. S. Lecorre, Bras and Dufresne, 2012). Therefore, it is convinced that there was coexistence of micro and nano-scaled SNC in the suspension which aligned with the findings from particle size distribution analysis discussed at Section 4.1.1. Thus, even though micro-scaled SNC is spotted in the 6-8% micrographs due to its higher loading, a huge part of SNC presence in nano-scaled are still well dispersed. This uniform distribution of SNC plays a big role in ensuring the reinforcement effect on rubber matrices. Apart from this, it was revealed that no particular sedimentation of SNC had occurred within the thickness of the investigated rubber nanocomposites films from micrographs and small angle light scattering analysis of the other study (Angellier, Molina-Boisseau, Lebrun, *et al.*, 2005). Furthermore, Figure 4.15 shows the side view of rubber nanocomposites films with 8% SNC content. The micrograph clearly unveiled the homogenous dispersion of nano-scaled SNC in the rubber matrix with very slight specific "site agglomeration" consisting of larger spherical SNC which agrees with the discussion above.

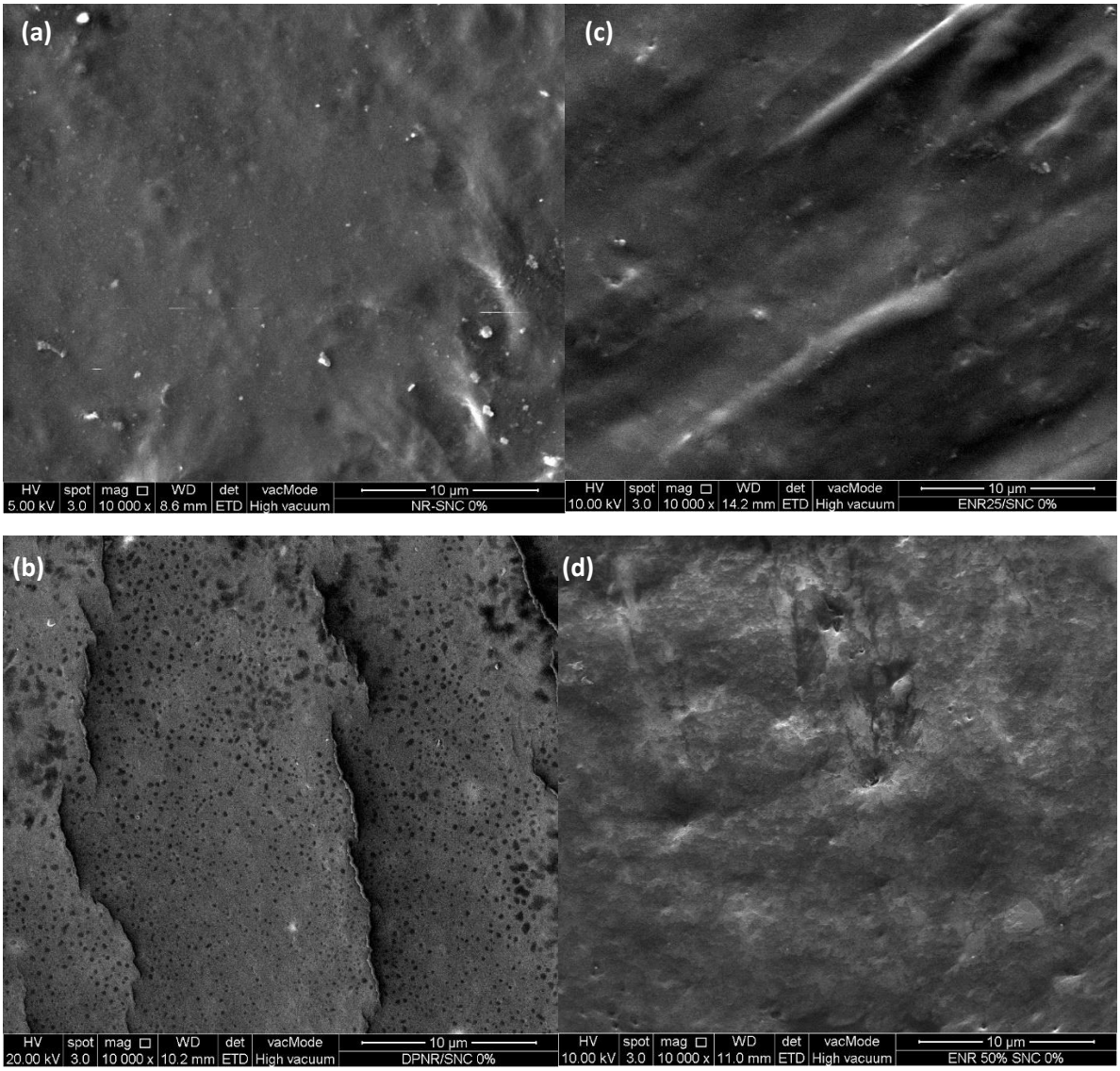

Figure 4.10: FESEM images (a) NRL/SNC 0% (b) DPNRL/SNC 0% (c) ENRL25/SNC 0% (d) ENRL50/SNC 0%

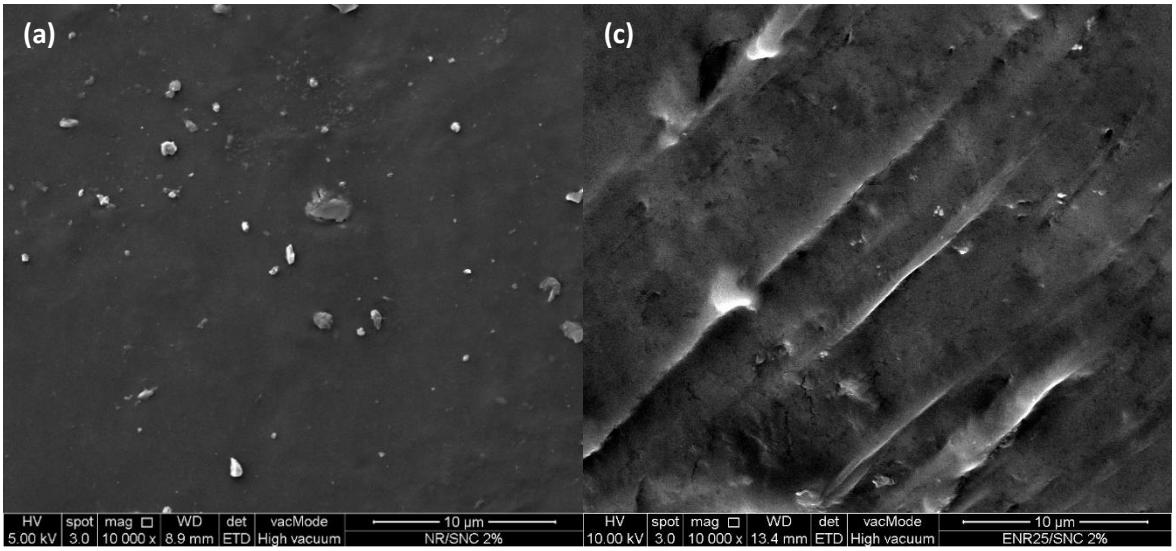

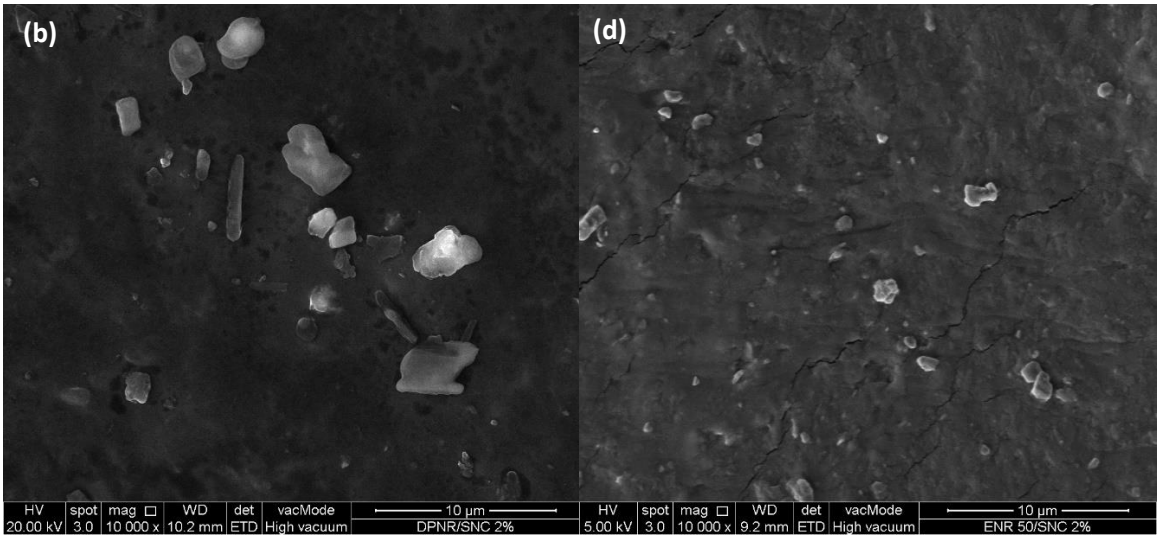

Figure 4.11: FESEM images (a) NRL/SNC 2% (b) DPNRL/SNC 2% (c) ENRL25/SNC 2% (d) ENRL50/SNC 2%

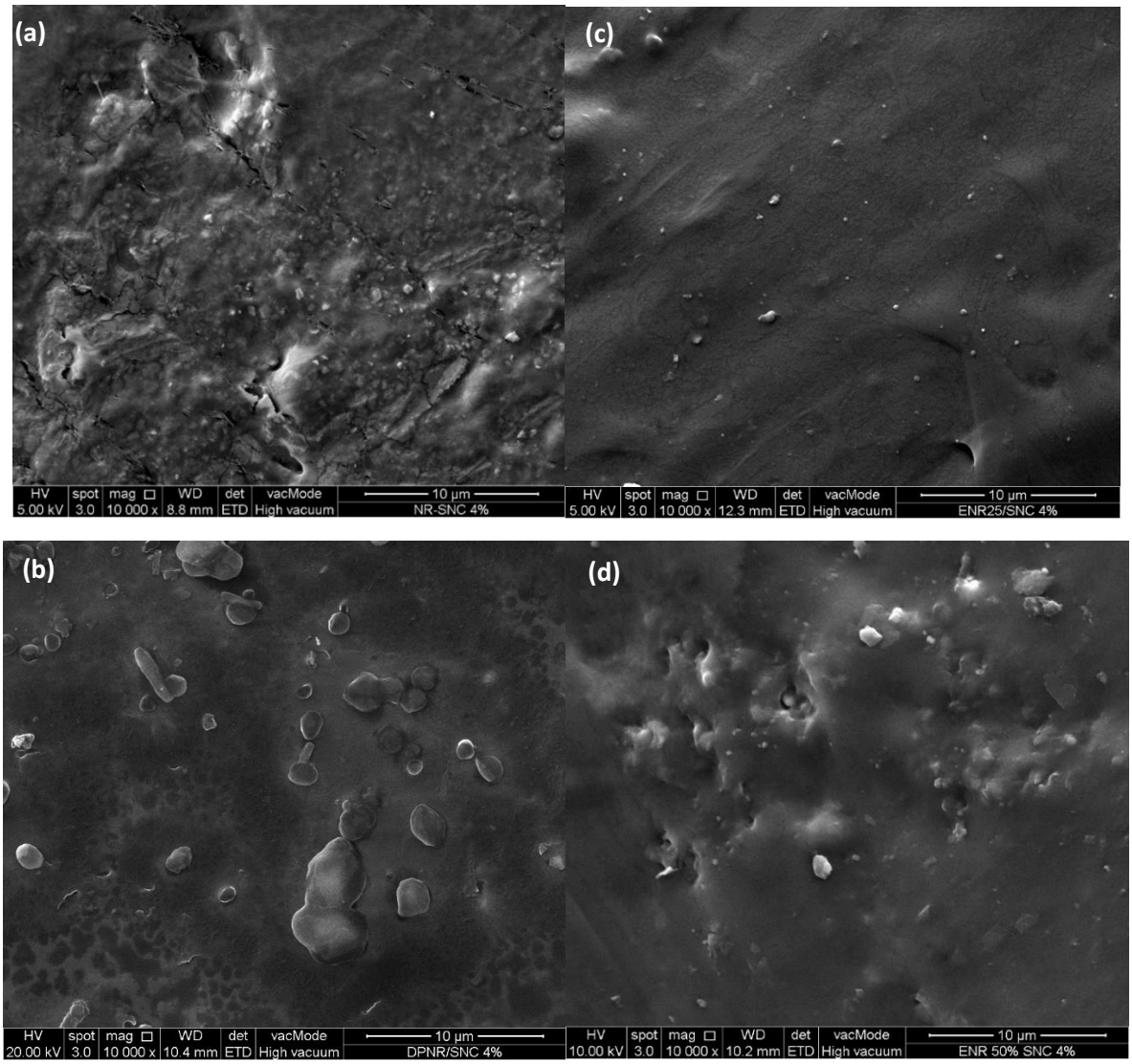

Figure 4.12: FESEM images (a) NRL/SNC 4% (b) DPNRL/SNC 4% (c) ENRL25/SNC 4% (d) ENRL50/SNC 4%

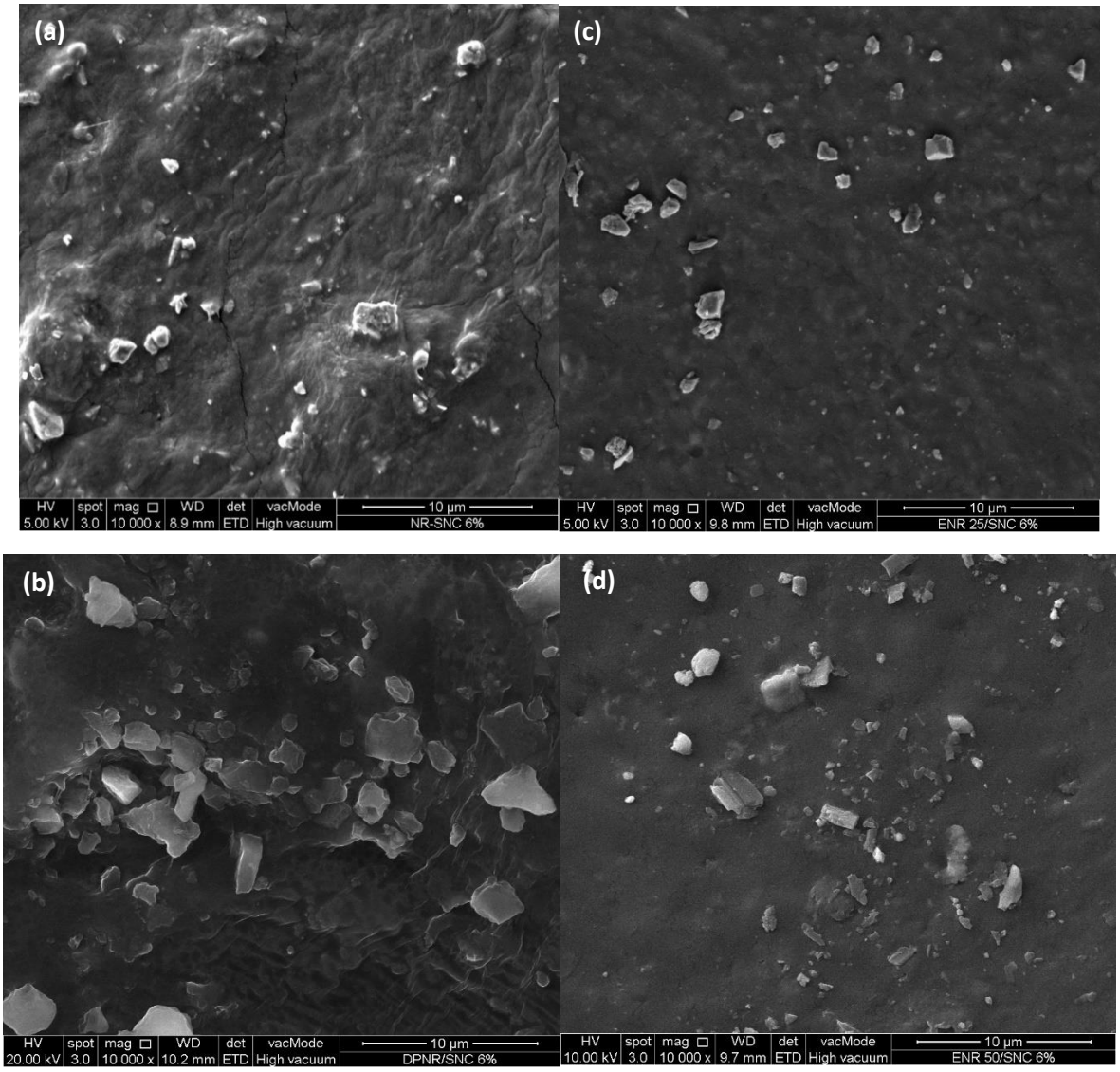

Figure 4.13: FESEM images (a) NRL/SNC 6% (b) DPNRL/SNC 6% (c) ENRL25/SNC 6% (d) ENRL50/SNC 6%

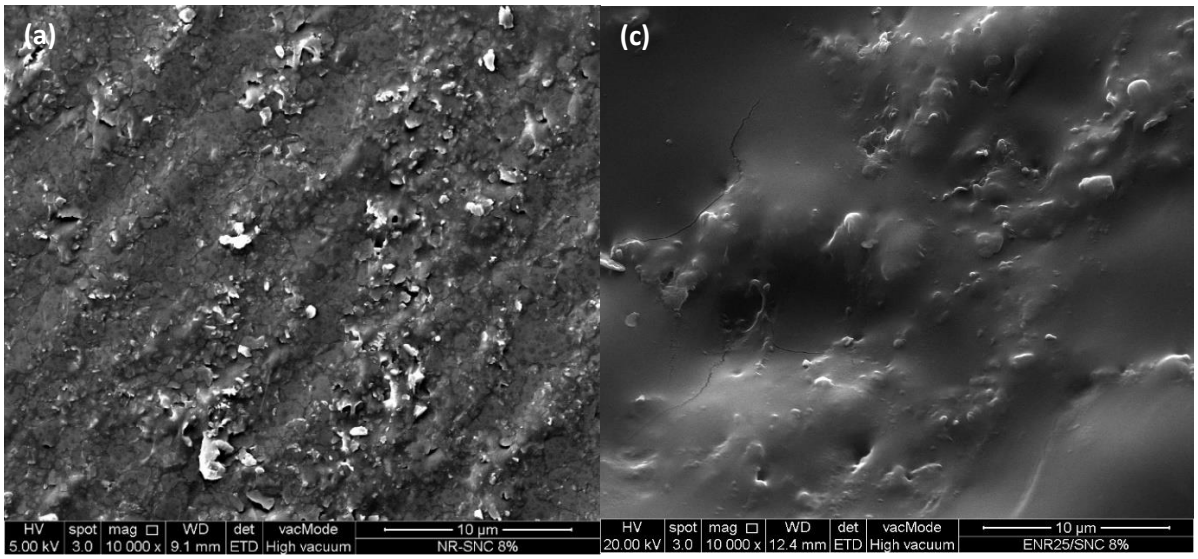

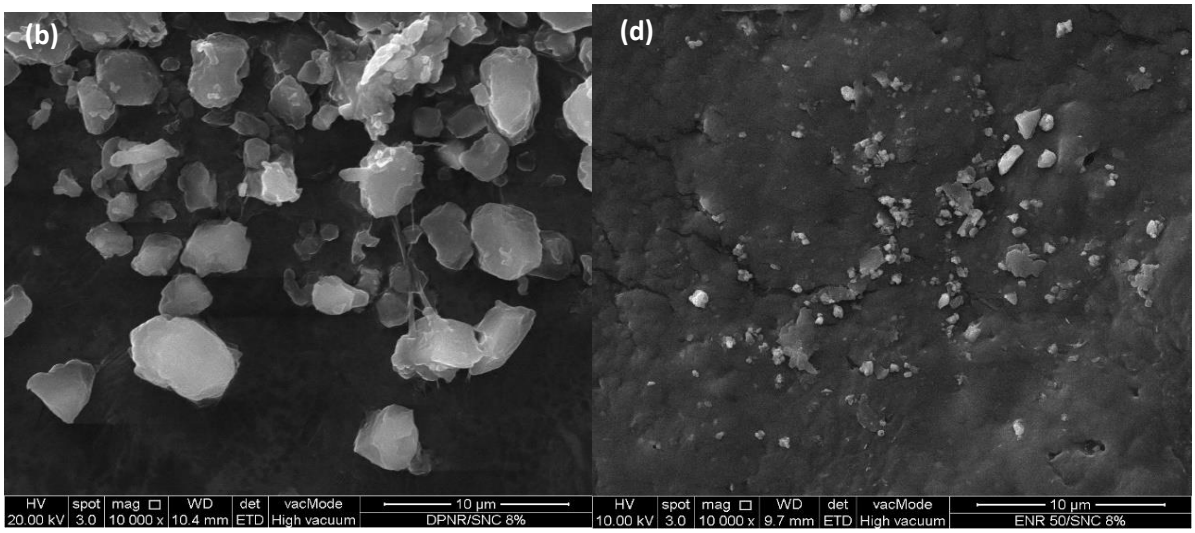

Figure 4.14: FESEM images (a) NRL/SNC 8% (b) DPNRL/SNC 8% (c) ENRL25/SNC 8% (d) ENRL50/SNC 8%

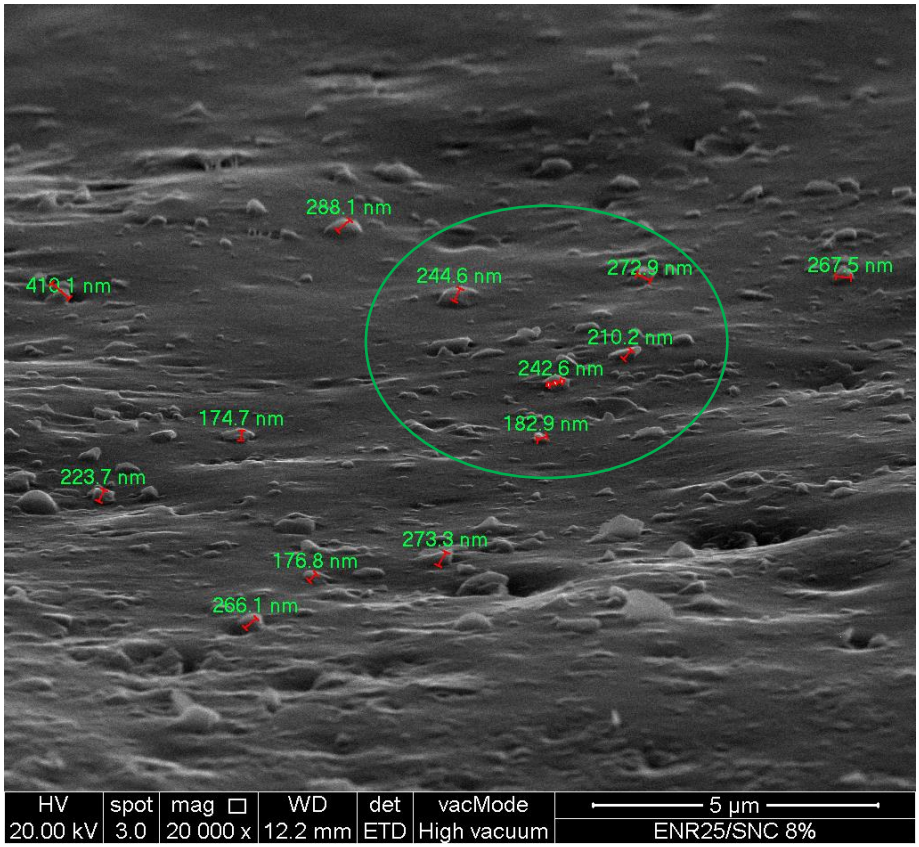

Figure 4.15: Side view of FESEM image for rubber nanocomposites film with 8% SNC content

4.3.2 Crosslink densities of SNC/rubber composites films

The effect on crosslink density of rubber nanocomposite films upon incorporation of SNC were evaluated through the obtained storage modulus by DMA tests. Crosslink density of the rubber nanocomposites films is an important parameter to investigate because of its strong influence in mechanical properties and solvent absorption of the material. The crosslink densities of the rubber/SNC nanocomposite films were calculated as described in Section 4.2.1. Thereby, the calculated crosslink densities of the rubber nanocomposite films were tabulated in Table 4.6. As shown in Table 4.6, the crosslink densities of rubber nanocomposites films increased with SNC content. Similar observation had been realized in graphene and calcium carbonate NR nanocomposites, carbon black NBR nanocomposites and cellulose nanocrystals ENR nanocomposites (Saeb, Ramezani-Dakhel and Esteki, 2012; Kang *et al.*, 2017; Habib *et al.*, 2021; Somseemee *et al.*, 2022). The crosslink density is significantly increased by at least 3.5-fold for all types of rubber nanocomposites films when the SNC content increased from 0-8% which strongly substantiates that the crosslinked supramolecular network was enhanced with SNC content. This is attributed to the good dispersion of SNC within the incorporated range as revealed in Section 4.3.1 that formed effective interaction with the rubber matrix. Furthermore, the increase in crosslink density might be also due to (i) the presence of SNC that enhanced the physical entanglements with rubber chains which eventually formed network structure, (ii) the increase in chemical crosslink as SNC contains hydroxyl groups that can participate in crosslinking reactions with the rubber chains, (iii) the high surface area of SNC that creates nucleation effect which provides favorable sites for initiation and propagation of crosslinking reaction (Q. Wang *et al.*, 2023; Yadav, Pal and Poonia, 2024)

As discussed in Section 4.2.1, increasing crosslink density tends to develop a stiffer rubber nanocomposites film where the movement of the polymer chains are restricted thereby increasing the T_g of the rubber films. This case is not reflected by SNC reinforced rubber nanocomposites films through the result from DMA in Figure 4.17 in Section 4.3.4. It was affirmed that tan α peak of the rubber nanocomposites films within their respective RL type do not simply shift to the right although their crosslink densities were determined to be higher with addition of SNC. It is because the incorporation of SNC appeared to have good interaction with rubber matrix leading to enhanced mechanical properties as evident in Section 4.3.5. However, the presence of SNC does not significantly influence the chain mobility of the rubber nanocomposites films that governs T_g of the material. This leads to the comparable T_g between unfilled rubber films and rubber nanocomposites films. From Table 4.6, it was shown that ENRLs based rubber nanocomposites films exhibited higher crosslink density than NRLs. This is due to the hydroxyl groups present on SNC which can react with epoxy group in ENR facilitating the formation of additional crosslinks within the rubber nanocomposites films.

Subsequently, ENRL50 based nanocomposites films have higher crosslink density than ENRL25 because of the greater number of epoxy groups.

Table 4.6: Crosslink densities of SNC reinforced rubber composites films

Samples	Crosslink Density ($x10^{-4}$ mol cm^{-3})	Samples	Crosslink Density ($x10^{-4}$ mol cm^{-3})
NRL/SNC 0%	0.49	ENRL25/SNC 0%	0.49
NRL/SNC 2%	0.80	ENRL25/SNC 2%	0.91
NRL/SNC 4%	1.22	ENRL25/SNC 4%	1.35
NRL/SNC 6%	1.59	ENRL25/SNC 6%	1.57
NRL/SNC 8%	2.19	ENRL25/SNC 8%	2.29
DPNRL/SNC 0%	0.72	ENRL50/SNC 0%	1.11
DPNRL/SNC 2%	1.08	ENRL50/SNC 2%	1.62
DPNRL/SNC 4%	1.60	ENRL50/SNC 4%	1.94
DPNRL/SNC 6%	1.84	ENRL50/SNC 6%	2.54
DPNRL/SNC 8%	2.58	ENRL50/SNC 8%	4.16

4.3.3 Swelling behaviour of SNC/rubber composites films

The swelling behaviour of rubber/SNC composites films were evaluated after immersion in water and toluene until equilibrium. Toluene is known to be a good solvent for rubber matrices while water has a high affinity for polysaccharides. The respective water and toluene uptake of rubber nanocomposites films were calculated using Equation 3.3. The toluene uptake of all rubber nanocomposites films was higher than 380% whereas the highest reading for water uptake is only slightly more than 10%. This is due to the hydrophobic nature of rubber latexes. Figure 4.16(a) showed that the water uptake increased with the introduction of SNC for all rubber films. The microstructure of nanocomposites films has a significant influence on the diffusion of water molecules whereas the amount of SNC present had an observable impact on this process. It was revealed that the unfilled rubber matrix displayed the lowest water uptake while swelling in water increased with the amount of SNC until weight fraction of 8% within this context. Similar observation on NR nanocomposites was also being reported in other literatures (Gao *et al.*, 2014; Rajisha *et al.*, 2014). Water uptake of the vulcanized rubber nanocomposites was escalated due to the high hydrophilicity of the hydroxyl groups in starch molecules, this allowed them to easily attract and bind with water molecules. With the increment of SNC contents, there are more capacities for swelling of starch domains which weakens the interface between rubber matrix and nano-filler leading to the creation of free volumes at interfacial areas that increased the water uptake. Moreover, the addition of SNC that dispersed homogenously in rubber matrix verified by FESEM developed additional surface area for water molecules to penetrate due to their high surface area to volume ratio. The increased surface area leads to a surge in the number of interfacial regions between rubber matrix and water molecules that

promotes the formation of hydrogen bonds between them, causing an increase in water uptake. Therefore, the formation of continuous polar network of SNC with increased surface area and hydrogen bonding within the rubber matrices encouraged the nanocomposites films to swell up when exposed to water.

The swelling behaviour of rubber nanocomposites films in toluene was displayed as Figure 4.16(b). It was observed that the unfilled rubber matrices displayed the highest toluene permeability while the addition of SNC inhibited the toluene uptake in almost linear fashion with increasing SNC contents. Comparable findings were reported on SNC filled NR (Angellier, 2005; Gao *et al.*, 2014; Anand *et al.*, 2018). This is due to the formation of three-dimensional network of SNC that act as a physical barrier which hindered the diffusion of toluene molecules into the rubber nanocomposites films. Moreover, this network will develop tortuous pathways for the permeability of toluene molecules thus lowering the swelling percentage. The formation of this network had already been reported for other polysaccharide based fillers (Neus Angles and Dufresne, 2000). Similarly to the network effect of SNC, the incorporation of SNC increased the crosslink densities of rubber nanocomposites films as shown in Table 4.6 which developed good interfacial interaction with rubber matrix that enhanced the physical barrier thus resulted in less swelling. Contrarily to swelling in water, the homogeneity in dispersion of SNC in rubber matrices that increased the interfacial interaction between them reduced its susceptibility to toluene uptake but increased the mechanical properties of the rubber nanocomposites films as shown in Section 4.3.5. Also, the formation of hydrogen bonds improves the adhesion between SNC and rubber matrices which reduced the tendency of the rubber nanocomposites to swell when exposed to toluene. As displayed by Figure 4.16(a) and (b), SNC reinforced ENRL nanocomposites films have lower water and toluene uptake compared to NRL nanocomposites films. This discovery and reason are analogous to the result reported in Section 4.2.2 where sulphur-cured ENRL films were less prone to toluene swelling due to its polar nature that exhibited improved oil resistance. The reduced water uptake of ENRL nanocomposites is due to the presence of cyclic structures such as oxirane rings that act as physical barrier towards any penetrating molecules. Similar finding had also been reported where blending of ENR into wheat gluten improved the water resistance of the blends with respect to pure wheat gluten (Hemsri *et al.*, 2015).

Table 4.7: WU and TU of rubber nanocomposites films at swelling equilibrium

Samples	WU (%)	TU (%)	Samples	WU (%)	TU (%)
NRL/SNC 0%	2.60	515.38	ENRL25/SNC 0%	0.88	471.43
NRL/SNC 2%	6.06	495.24	ENRL25/SNC 2%	2.58	456.56
NRL/SNC 4%	8.11	468.08	ENRL25/SNC 4%	4.52	435.09
NRL/SNC 6%	8.86	446.67	ENRL25/SNC 6%	5.94	426.32
NRL/SNC 8%	11.96	424.23	ENRL25/SNC 8%	7.05	404.31
DPNRL/SNC 0%	1.42	525.00	ENRL50/SNC 0%	0.78	442.31
DPNRL/SNC 2%	4.31	511.61	ENRL50/SNC 2%	2.43	424.53
DPNRL/SNC 4%	5.31	491.49	ENRL50/SNC 4%	4.14	405.58
DPNRL/SNC 6%	8.15	477.41	ENRL50/SNC 6%	5.35	398.19
DPNRL/SNC 8%	10.65	436.89	ENRL50/SNC 8%	6.03	378.63

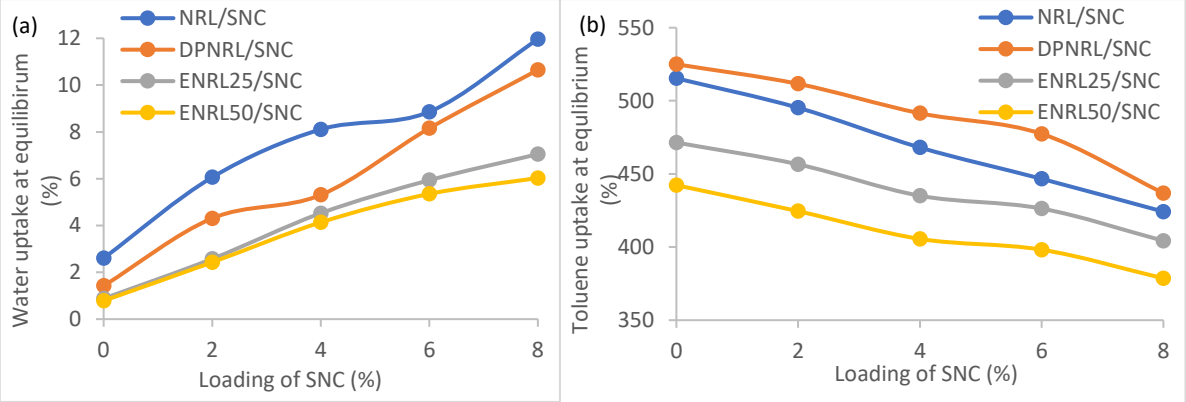

Figure 4.16: Swelling behaviour of SNC reinforced rubber composites films (a) water uptake at equilibrium (b) toluene uptake at equilibrium

4.3.4 Dynamic Mechanical behaviour of SNC/rubber composites films

DMA was performed for the rubber nanocomposites films with varying SNC content over temperature ranging between -60 – 100 °C. It measures the viscoelastic response of the rubber nanocomposites films under periodic stress as a function of temperature. Storage modulus and damping ratio often denoted by tan δ are measured in a DMA test. The plots of Log E' and tan δ against temperature for SNC reinforced rubber nanocomposites films were presented in Figure 4.17 and 4.18. All curves of Log E' for the unfilled rubber matrices displayed a typical high molecular weight thermoplastic behaviour as revealed in Figure 4.17. Since NRL 0.2 and NRL/SNC 0% shared the same formulation, the curves of Log E' against temperature exhibited similar trend among one another when comparing Figure 4.6(a) and 4.17(a). Indeed, SNC filled rubber matrices showed a similar pattern to the unfilled matrices corresponding to the storage modulus curve. This event suggested that the incorporation of SNC in RL maintains the elastomeric properties with viscoelastic behaviour within the material. At temperature below T_g, all rubber nanocomposites films are in their glassy state where they become rigid and brittle with decreasing storage modulus against temperature but remains

above 0.1 GPa. A sharp decrease in storage modulus of over 2-3 decades was observed through Figure 4.17 for both NRLs and ENRLs based nanocomposites films corresponding to the primary relaxation process related with the glass-rubber transition which resulted in a damping phenomenon as shown in Figure 4.18. This sharp decrease in storage modulus occurred at -60 °C for NRLs based nanocomposites films while it happened at -40 °C and -25 °C for ENRL25 and ENRL50 nanocomposites films. Similarly to the findings discussed at Section 4.2.3, no clear horizontal glassy region is observed for NRLs based nanocomposites films and the glass-rubber transition of ENRLs based nanocomposites films occurred at a higher temperature. Then, the modulus reached a plateau rubbery region at 0.7 – 6.2MPa for all rubber nanocomposites films. The broad rubbery region implied that the material is flexible, elastic and capable of returning to its original shape after deformation over a wide span of temperature.

Interestingly, all drops in storage modulus at glass-rubber transition zone of SNC filled rubber nanocomposites films is lesser than the unfilled rubber matrix which eventuated a higher storage modulus for the rubber nanocomposites films at the rubbery region. Therefore, the incorporation of SNC to rubber matrices helps to retain stiffness while enhancing the energy storage capability reflected through the higher storage modulus of the material. This advocated that SNC possessed significant reinforcing effect at temperature above T_g. For instance, the E'_{25} of rubber nanocomposites films containing 2%, 4%, 6% and 8% of SNC is at least 1.5, 2.0, 2.5 and 3.5 times higher respectively than the unfilled rubber matrix as shown in Table 4.8. This reinforcing effect is usually attributed to the development of robust network of SNC interconnected through strong hydrogen bonds (Dufresne, 2008a, 2010). It was also demonstrated that the reinforcing effect of SNC could be ascribed to the filler/rubber matrix interactions (Mélé *et al.*, 2011).

The evolution of tan δ against temperature shown in Figure 4.18 displayed a peak located at T_g of the rubber nanocomposites films. This relaxation process referred to as α is associated to the anelastic behaviour observed during the glass-rubber transition of the polymer. It involves coordinated movements of long chain segments within the material. It was revealed that the T_g for NRL and DPNRL nanocomposites films are at around -50 °C whereas T_g of ENRL25 and ENRL50 nanocomposites films are at approximately -30 °C and -10 °C. Reasons for the higher T_g showed by ENRLs based rubber nanocomposites films are clearly discussed at Section 4.2.3. In fact, SNC filled rubber matrices have comparable T_g to pure rubber matrix as presented through the peak of temperature (T_α) in Table 4.8. This outcome is identical to the findings of other literature where addition of varying SNC loading from different botanical origin to NR matrix resulted in similar T_g (LeCorre, Bras and Dufresne, 2012). Thus, it is in agreement with the discussion at Section 4.3.2 where incorporation of SNC within the range of 2-8% do not directly affect the chain mobility which governs T_g of a material but aided in mechanical

properties enhancement through good filler/rubber interactions. Moreover, the magnitudes of tan δ peak (I_α) and area under the tan δ curves of the rubber nanocomposites films are listed in Table 4.8. These values provided an insight to the energy dissipation potential of a material as rubbers possessed viscoelastic behaviour that are capable of storing part of the energy applied upon deformation and dissipate the other part through viscous dissipation. It was realized that I_α and area under than tan δ curves of SNC filled rubber nanocomposites films are lower than pure rubber. Similar observations had been reported on carbon nanotubes reinforced polycarbonate composites (Babal *et al.*, 2015). This is due to the lower energy loss caused by the diminished molecular motion of polymer chains resulted from good intermolecular interactions between filler and matrix (Haris *et al.*, 2022). Therefore, rubber nanocomposites films act more elastic and have more potential to store energy rather than dissipating it. Ultimately, this makes rubber nanocomposites films a suitable candidate to be developed as smart rubbers for energy storage application if the temporary deformed shape can be fixed when the applied force is removed. Further discussion about the development of rubber nanocomposites films for this characteristic is done in Section 5.

Table 4.8: E'_{25}, T_α, I_α and area under tan δ curves of rubber nanocomposites films

Sample	E'_{25} (MPa)	T_α (°C)	I_α	Area under tan δ curve	Sample	E'_{25} (MPa)	T_α (°C)	I_α	Area under tan δ curve
NRL/SNC 0%	0.73	-46.45	2.75	44.98	ENRL25/SNC 0%	0.73	-29.29	2.11	42.65
NRL/SNC 2%	1.20	-50.42	2.45	43.72	ENRL25/SNC 2%	1.35	-28.80	2.19	41.81
NRL/SNC 4%	1.81	-49.10	2.06	41.67	ENRL25/SNC 4%	2.01	-30.14	2.23	40.03
NRL/SNC 6%	2.37	-49.86	2.41	40.32	ENRL25/SNC 6%	2.34	-29.16	2.05	39.77
NRL/SNC 8%	3.25	-49.78	2.08	38.86	ENRL25/SNC 8%	3.40	-29.75	1.82	37.51
DPNRL/SNC 0%	1.08	-50.93	2.56	46.18	ENRL50/SNC 0%	1.65	-13.20	2.42	41.58
DPNRL/SNC 2%	1.60	-51.93	2.40	44.37	ENRL50/SNC 2%	2.40	-8.31	2.21	39.96
DPNRL/SNC 4%	2.38	-52.21	2.13	42.09	ENRL50/SNC 4%	2.88	-8.82	2.23	37.27
DPNRL/SNC 6%	2.74	-49.85	1.93	40.05	ENRL50/SNC 6%	3.78	-9.55	1.94	36.83
DPNRL/SNC 8%	3.83	-49.68	1.89	37.91	ENRL50/SNC 8%	6.19	-8.11	1.69	34.11

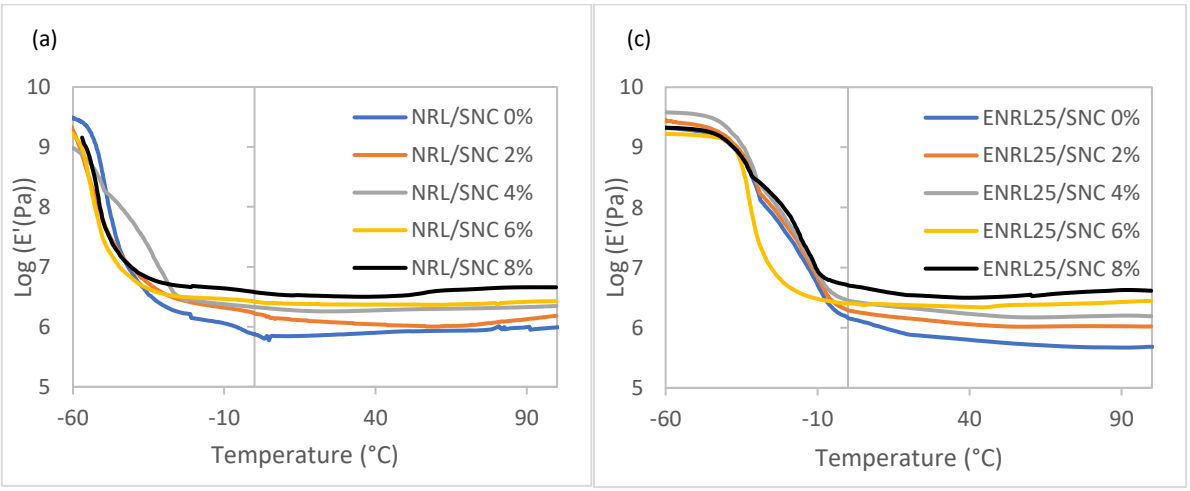

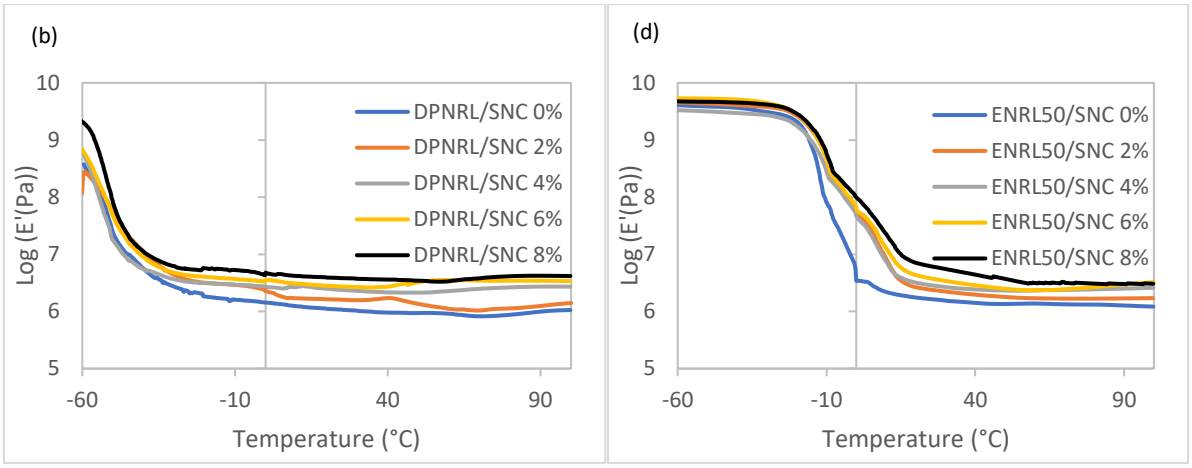

Figure 4.17: Plot of logarithm of storage modulus against temperature for SNC reinforced (a) NRL (b) DPNRL (c) ENRL25 and (d) ENRL50 nanocomposites films

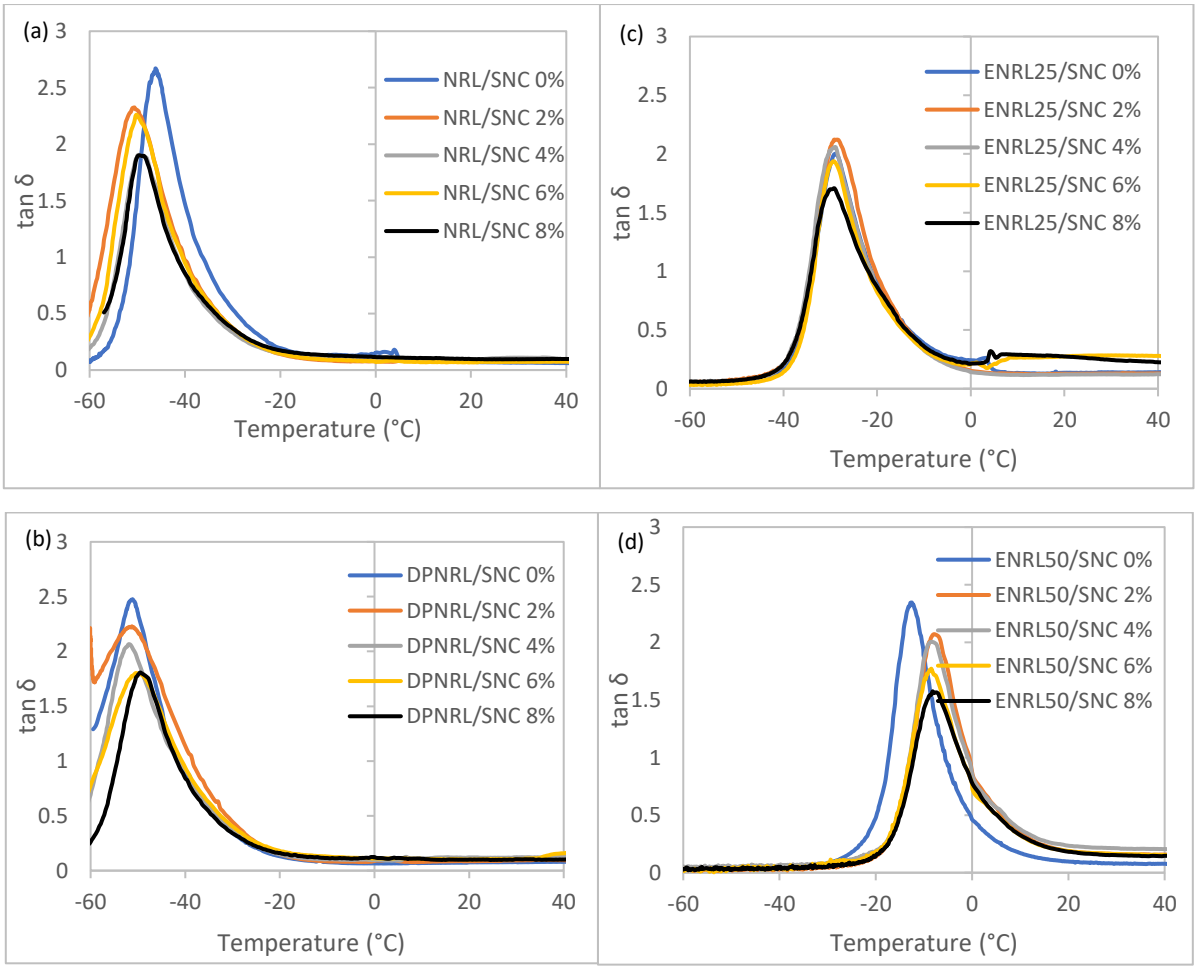

Figure 4.18: Plot of tan α against temperature for SNC reinforced (a) NRL (b) DPNRL (c) ENRL25 and (d) ENRL50 nanocomposites films

4.3.5 Mechanical properties of SNC/rubber composites films

Nanomaterials are an excellent reinforcing filler for NR due to their high surface area to volume ratio which allows stronger interaction with polymer matrix. High crystallinity imparts great stiffness and strength made SNC a promising reinforcing material for rubber. Report suggested that SNC is a suitable candidate to replace the conventional carbon black due to its capability for reinforcement in terms of strength, stiffness and elasticity (Rajisha *et al.*, 2015). Rubber/SNC composites both derived from renewable sources have extra advantages such as non-toxic, easy availability, good biocompatibility and ease of mechanical modification made them an interesting prospect over the typical carbon black filled rubber. The tensile mechanical properties of waxy maize SNC reinforced rubber composites films were evaluated at room temperature. Tensile tests revealed that all rubber nanocomposites films exhibited the behaviour of a typical amorphous polymer displaying elastic non-linear response at $T > T_g$. The evolution of nominal stress for various rubber latexes films is plotted in Figure 4.19 as a function of nominal strain. It was shown that the tensile strength and modulus of all rubber nanocomposites films constantly increased with increasing SNC content. Moreover, the stress increased regularly with strain until breaking of the rubber nanocomposites films. As expected, the tensile strength and modulus increased while elongation at break decreased with increasing starch content. This is because the incorporation of SNC into rubber matrix developed a stiffer rubber nanocomposites films with more resistant to deformation which subsequently caused the material to be more brittle and possessed decreased ability to deform before breaking. Similar findings had been reported elsewhere with the incorporation of nanofiller into different kind of matrices (González *et al.*, 2015; Chen *et al.*, 2019; Mujtaba *et al.*, 2019; Dai *et al.*, 2021).

According to Figure 4.19, the mechanical properties of rubber nanocomposites films improved remarkably with the addition of SNC into rubber matrices. Tensile strength corresponding to all rubber nanocomposites films with 8% SNC content increased by at least 2-fold when compared with unfilled rubber matrix as revealed in Table 4.8. This obvious increment in tensile strength of all rubber nanocomposites films resembles the significant reinforcing effect of SNC. It indicated the formation of intra and intermolecular interactions between SNC and rubber matrix forming a stronger rubber nanocomposites films (Kristo and Biliaderis, 2007). The homogenous dispersion of SNC even at the highest content of 8% shown in Figure 4.15 in Section 4.3.1 suggested the raise of possible rubber-SNC interaction which enhanced the tensile strength of rubber nanocomposites films. A composite material with well dispersed particles and appropriate interfacial bonding between filler and matrix can facilitate stress transfer through shear mechanism from matrix to particles that effectively bear the load thus enhancing the strength of the composite material (Wetzel, Haupert and Zhang, 2003; Abdelmouleh *et al.*, 2005; Brown and Ellyin, 2005). Additionally, it is believed that SNC forms rigid

three-dimensional network resulting in strong interfacial adhesion such as hydrogen bonding between fillers in the structure of the films. The improved tensile strength as observed from tensile test gives clear evidence about the presence of three-dimensional network within the rubber nanocomposites films. Moreover, addition of SNC increased the crosslink density of rubber nanocomposites films after vulcanization process as observed from Table 4.5. This increment in crosslink density enhanced the tensile strength of rubber nanocomposites films which agrees with the interpretation regarding the formation of stronger rubber structure with higher crosslink density.

From Table 4.9, it was disclosed that all unfilled rubber films exhibited the lowest tensile strength whereas all rubber nanocomposites films with 8% SNC content have the highest tensile strength among their respective rubber latex types. Furthermore, tensile strength and modulus increased linearly with SNC content ranging from 2-8%. This is in agreement with the outcome presented at Table 4.8 where storage modulus of the rubber nanocomposites constantly increased with SNC loading. Similar trend with varying SNC content has been reported elsewhere on NR nanocomposites films (Angellier, Molina-Boisseau and Dufresne, 2005, 2006; Gao *et al.*, 2014; Rajisha *et al.*, 2014, 2015). Within the context of 8% SNC content, DPNRL and ENRL25 showed the highest and lowest tensile strength of 10.6 MPa and 9.0 MPa respectively. This finding is identical to the one discussed at Section 4.2.4 where NRLs have higher tensile strength than ENRLs based films. This is mainly due to the reduced capability of ENR to exhibit SIC that directly contributed to tensile strength of the rubber films. The upper and lower bound value for NRLs based nanocomposites films are 10.6MPa (DPNRL/SNC 8%) and 4.2MPa (NRL/SNC 2%). On the other hand, ENRL50/SNC 2% and ENRL50/SNC 8% recorded tensile strength of 4.5MPa and 9.3MPa are the lower and upper limit of ENRLs based nanocomposites films. In terms of elastic properties, the diminution of elongation at break is not more than 200% for all rubber nanocomposites films when comparing unfilled matrix and rubber nanocomposites films with 8% SNC content. Although the incorporation of SNC slightly reduced the elongation at break, all rubber nanocomposites films still exhibited elongation at break of more than 700%. Ultimately, SNC proved to be an excellent filler for NRLs and ENRLs based on its effect on improving the mechanical properties while maintaining the elastic behaviour of rubber nanocomposites films.

The reinforcing effect of SNC is compared to the other classical fillers for NR such as fly ash, carbon black and chitin nanocrystals. It was found out that 8% of SNC content presented comparable tensile strength and improved elongation at break than 40% fly ash (Dasaesamoh, Osotchan and Subannajui, 2019). This scenario might be ascribed to the higher crystallinity, better compatibility and nano-dimension of SNC that enhanced the surface chemistry between filler and NR. Furthermore, SNC is clearly an excellent substitute to the conventional carbon black because the incorporation of 8% SNC has similar reinforcing effect in terms of tensile strength to 26.6% carbon black (Arroyo, López-

Manchado and Herrero, 2003). Besides, SNC seems to preserve the elastic behaviour of NR nanocomposites film even at 8% content contrarily to carbon black. Comparing with bio-based chitin nanocrystals, SNC possessed better ultimate properties which included both tensile strength and elongation at break (Liu *et al.*, 2018). This is due to the rod-like geometry of chitin nanocrystals that proved to have lower percolation threshold in NR nanocomposites.

Table 4.9: Stress-strain relationship of SNC reinforced rubber composites films

Samples	Tensile Strength (MPa)	Elongation at break (%)	Samples	Tensile Strength (MPa)	Elongation at break (%)
NRL/SNC 0%	3.3 ± 0.2	894.0 ± 41.1	ENRL25/SNC 0%	3.4 ± 0.3	935.9 ± 29.6
NRL/SNC 2%	4.2 ± 0.1	822.4 ± 21.0	ENRL25/SNC 2%	4.8 ± 0.1	924.4 ± 15.5
NRL/SNC 4%	5.5 ± 0.2	838.9 ± 16.7	ENRL25/SNC 4%	6.2 ± 0.3	907.0 ± 48.2
NRL/SNC 6%	8.1 ± 0.3	777.9 ± 22.4	ENRL25/SNC 6%	7.9 ± 0.3	918.2 ± 13.4
NRL/SNC 8%	10.1 ± 0.3	752.4 ± 38.3	ENRL25/SNC 8%	9.0 ± 0.1	827.2 ± 24.2
DPNRL/SNC 0%	4.9 ± 0.5	983.8 ± 25.3	ENRL50/SNC 0%	3.2 ± 0.5	960.0 ± 20.2
DPNRL/SNC 2%	5.5 ± 0.3	949.1 ± 20.3	ENRL50/SNC 2%	4.5 ± 0.3	892.6 ± 13.2
DPNRL/SNC 4%	6.7 ± 0.1	914.0 ± 15.9	ENRL50/SNC 4%	6.0 ± 0.2	907.0 ± 23.8
DPNRL/SNC 6%	8.2 ± 0.4	883.1 ± 13.7	ENRL50/SNC 6%	7.4 ± 0.3	888.6 ± 12.0
DPNRL/SNC 8%	10.6 ± 0.3	783.9 ± 28.5	ENRL50/SNC 8%	9.3 ± 0.3	871.5 ± 31.4

Remarks: Data were presented as average value ± standard deviation

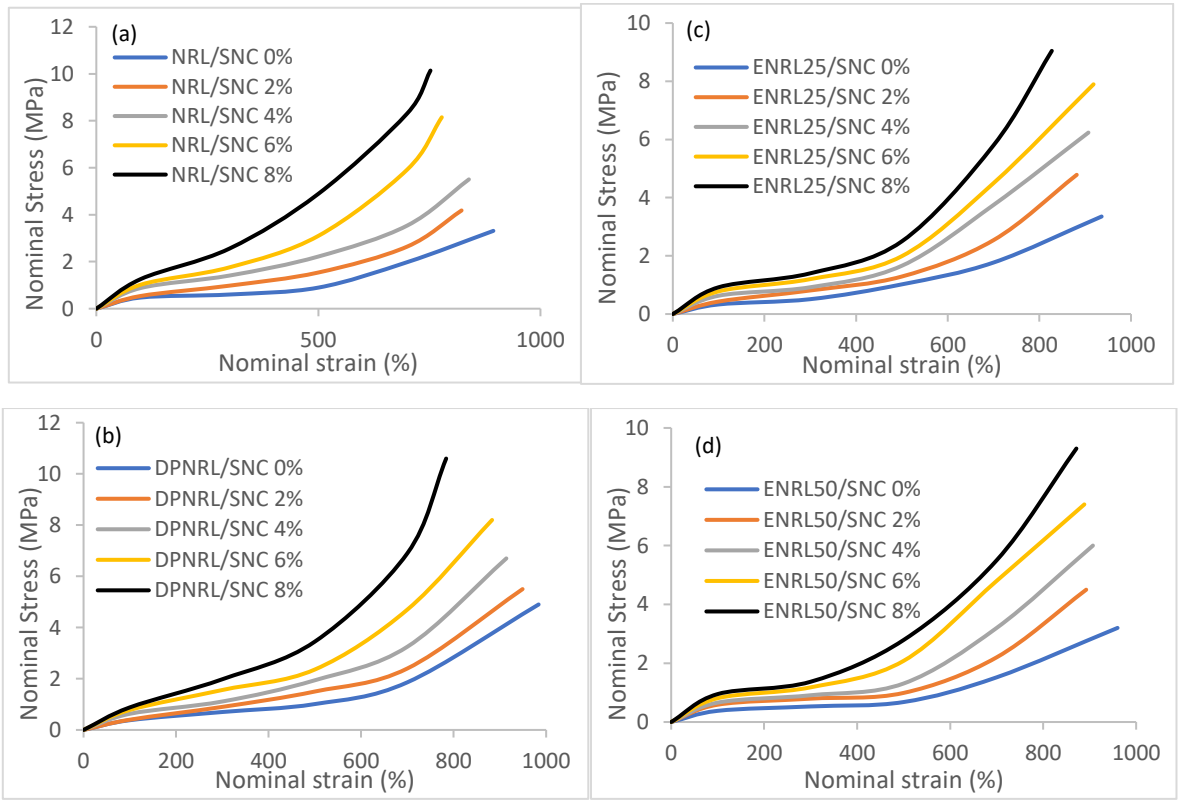

Figure 4.19: Plots of nominal stress against nominal strain for SNC reinforced (a) NRL (b) DPNRL (c) ENRL25 (d) ENRL50 composites films

4.3.6 Thermal stability of SNC/rubber composites films

Thermal stability of rubber vulcanizates is important to ensure the performance and reliability of the material over a wide range of applications and environmental conditions. Therefore, TGA was performed from 50 – 600 °C under nitrogen atmosphere for the rubber nanocomposites films to examine their thermal decomposition characteristics. Figure 4.20 depicts the TGA thermograms while Figure 4.21 shows the DTG of the rubber nanocomposites films. The beginning of the major degradation is signaled by the onset temperature (T_{on}). Temperature at which 50% decomposition (T_{50}) occurs indicates the thermal stability index of rubber vulcanizates (Košíková *et al.*, 2007). T_{on} and T_{50} are calculated by extrapolation from raw data of TGA. The maximum rate change of mass is reflected through the major peak in DTG curve and characterized by peak degradation temperature (T_p). These characteristics temperatures of the rubber nanocomposites films are summarized as in Table 4.10.

From Figure 4.20, it was shown that there is only one major turn in every of the TGA thermograms suggesting one significant decomposition step in all of the rubber nanocomposites films. However, Figure 4.21 displayed one shallow peak before the major decomposition peak hinting that the actual degradation process of rubber nanocomposites films consists of two weight loss maxima. Similar observations had been reported on modified starch filled NR composites (Wu *et al.*, 2018). These two peaks correspond to the degradation of SNC at lower temperature and rubber matrix at higher temperature. As unveiled by Figure 4.20, there is no mass loss before 200 °C stipulating the absence of water moisture in the rubber nanocomposites films. This implied that all moisture content in the rubber nanocomposites films was evaporated during the vulcanization process. The first slight weight loss step that took place at temperatures between 250 – 300 °C is related to the degradation of SNC. This reaffirmed the findings presented at Section 4.1.3 regarding the degradation temperature of SNC. The presence of SNC in the rubber nanocomposites films is validated through this event. Furthermore, this interpretation is favoured by the DTG plots showing rubber nanocomposites films incorporated with 8% SNC content have the most significant dip in peak at degradation temperature of SNC. On the other hand, the major mass loss of approximately 80% reflected through TGA thermograms and second weight loss step in DTG plots are related to the degradation of rubber matrices as RL is the main composition in the rubber mixture. These scenarios happened at temperature between 300 – 450 °C ascribed the decomposition of rubber molecular chains which is primarily initiated by thermal scissions of C=C and C-C bonds accompanying with a transfer of hydrogen at the site of scission in NR and ENR (Valodkar and Thakore, 2010; Wang *et al.*, 2010).

Table 4.10 shows the T_{on}, T_{50}, and T_p of all rubber nanocomposites films involved in TGA. It was noted that the incorporation of SNC in NRLs and ENRLs does not significantly improve nor deteriorate

the thermal stability of all rubber nanocomposites films. This is because the difference in T_{50} of neat rubber and every SNC filled rubber film does not exceed 8 °C while rubber degrades over a wide temperature ranging between 300 – 450 °C. The reasons behind might be due to (i) the low loading of SNC (maximum content is 8%) that may not possess noticeable impact on thermal stability of rubber films, (ii) the relatively lower degradation temperature of SNC (250 – 300 °C) than of rubber matrix (300 – 450 °C). Moreover, the addition of SNC had no considerable influence on T_{on} and T_p of all rubber nanocomposites. This is aligned with the discovery from other literatures about thermal stability of nanofiller filled polymer composites (Zamri *et al.*, 2017; Maciejewska and Sowińska, 2021). T_{on} of NRLs based films is in the range of 300 – 334 °C whereas ENRL based films exhibited T_{on} between 322 – 357 °C. Subsequently, T_{50} and T_p of ENRLs based films are higher than their NRLs counterpart suggesting the improved thermal stability of ENRLs. Such outcome is reported on carbon nanotubes filled ENR30 nanocomposites (Chuayjuljit, Mungmeechai and Boonmahitthisud, 2017). This is due to the introduction of epoxide groups that reduced the numbers of unsaturated C=C bonds allowing ENR to be less susceptible to heat degradation at elevated temperature.

Table 4.10: Characteristics degradation temperatures of rubber nanocomposites films

Samples	T_{on} (°C)	T_{50} (°C)	T_p (°C)	Samples	T_{on} (°C)	T_{50} (°C)	T_p (°C)
NRL/SNC 0%	322.1	383.1	377.3	ENRL25/SNC 0%	333.3	387.4	384.1
NRL/SNC 2%	327.2	381.4	376.5	ENRL25/SNC 2%	350.3	395.3	383.9
NRL/SNC 4%	328.6	381.2	377.9	ENRL25/SNC 4%	335.4	393.9	384.7
NRL/SNC 6%	333.4	381.7	378.7	ENRL25/SNC 6%	339.7	387.9	384.2
NRL/SNC 8%	323.7	378.7	374.1	ENRL25/SNC 8%	356.9	389.5	384.9
DPNRL/SNC 0%	310.6	376.4	373.5	ENRL50/SNC 0%	342.6	398.1	401.2
DPNRL/SNC 2%	309.5	372.9	373.9	ENRL50/SNC 2%	329.7	400.2	401.5
DPNRL/SNC 4%	305.8	380.5	378.7	ENRL50/SNC 4%	348.1	402.6	395.7
DPNRL/SNC 6%	300.1	376.6	378.9	ENRL50/SNC 6%	321.8	402.4	390.2
DPNRL/SNC 8%	305.4	376.8	380.3	ENRL50/SNC 8%	322.3	403.8	407.5

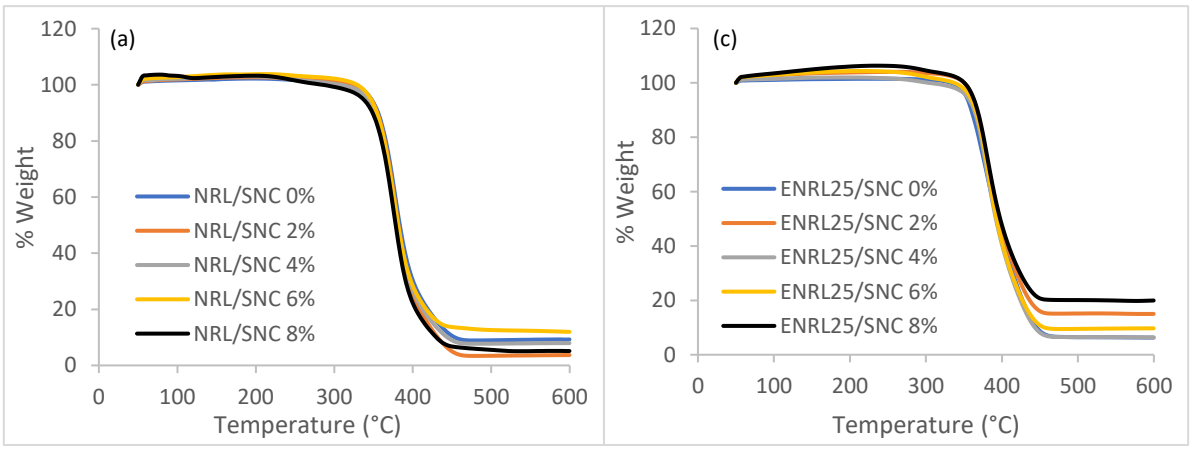

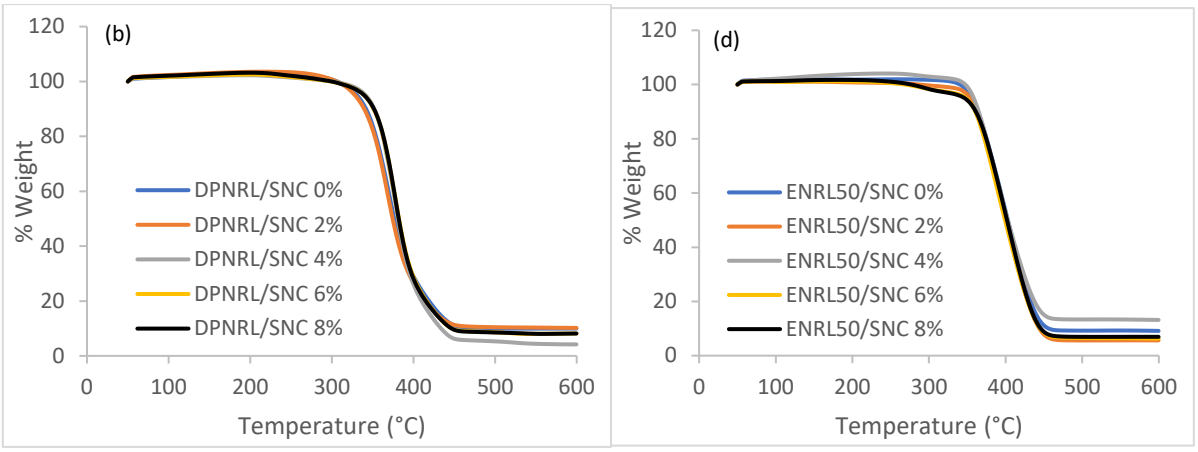

Figure 4.20: TGA curves for SNC reinforced (a) NRL (b) DPNRL (c) ENRL25 (d) ENRL50 composites films

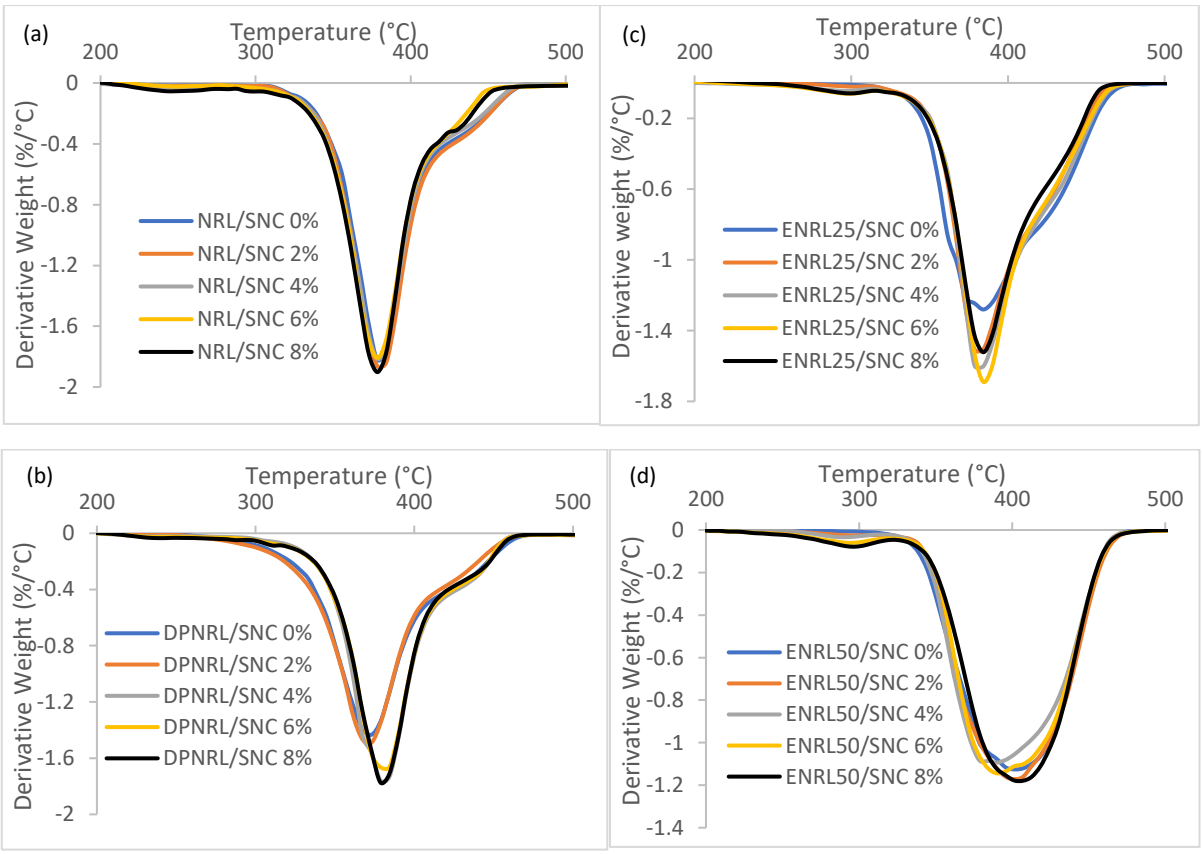

Figure 4.21: DTG curves for SNC reinforced (a) NRL (b) DPNRL (c) ENRL25 and (d) ENRL50 composites films

4.4 Summary of Chapter 4

Chapter 4 generally deals with objective 1 of the research which involves results for characterization of SNC, evaluation of physical and mechanical characteristics of sulphur-cured rubber films and SNC reinforced rubber composite films. Section 4.1 suggests that SNC is well dispersed in aqueous solution and has dimension in nano-scale. Moreover, SNC has higher crystallinity, higher T_m, better thermal stability while possessing similar degradation temperature to native starch. Section 4.2 presents the findings of physical and mechanical characteristics of sulphur-cured rubber films. The crosslink density and tensile strength increased with sulphur loading for all kinds of RL films but compensated with decreased elongation at break due to a stiffer rubber structure. Nonetheless, all rubber films can still be deformed to more than 700%. Toluene penetrability decreased with increasing sulphur loadings while ENRLs based films have better toluene resistance than their NRLs counterpart. The epoxide groups caused a decrease in chain mobility which contributed to an increase in T_g of ENRLs based films. Section 4.3 discussed the physical and mechanical characteristics of SNC reinforced rubber composite films. SNC is well dispersed in the rubber matrices within the range of 2-8%. The crosslink density increased with SNC content due to increased physical entanglements and additional chemical crosslinks. The incorporation of SNC increased the water uptake but decreased the toluene uptake of all rubber nanocomposite films. Moreover, the addition of SNC enhanced the mechanical properties and maintained the materials' deformability. SNC reinforced rubber composite films have comparable T_g to unfilled matrix and lower area under tan δ curve suggesting the rubber nanocomposite films have more capability to store energy. For thermal properties, there are two weight loss steps discovered corresponding to degradation of SNC at lower temperature rubber degradation at higher temperature.

Chapter 5

5.0 Shape Memory Behaviour and Energy Storage Capacity of Smart Rubbers

5.1 Development of Smart Rubbers

5.1.1 Shape memory behaviour of sulphur-cured rubber films

Smart materials, also known as responsive materials, refer to materials that have the ability to sense and respond to changes in their environment in a controlled manner. These materials exhibit unique behaviour that can be triggered by external stimuli such as temperature. Rubber has tremendous potential to be classified as smart material due to their exceptional molecular arrangement and physical properties. Reversible crosslinked network that enables rubber to deform when stress is applied and return to their original shape upon stress removal is a crucial characteristic for SME. Moreover, findings from Section 4.2 such as (i) being able to stay at the rubbery state for wide range of temperature and (ii) excellent mechanical properties which includes the capability to store extremely large strain of at least 700% aided in the potential for rubber to be exhibit shape memory behaviour. However, preliminary shape memory tests indicated that ENRLs based films failed to develop any SME due to their inability to fix the temporary shape when stress is removed. This might be due to interference of epoxy groups which hindered its ability to align and form ordered crystalline structure when elongated (Wang *et al.*, 2016). Thus, the ability of ENRLs based films to strain-crystallize especially at high elongation is diminished leading to the exclusion of them in further shape memory testing.

In the case of NRL and DPNRL films, the rubber matrix is an amorphous polymer at room temperature that forms crystals upon strain and returns to its original shape immediately when releasing the stretching force while vanishing crystals in the process. Moreover, T_g of NR at significantly below room temperature determined from Section 4.2.3 hinders the prerequisite properties for it to display SME. However, crosslinking of NR at the borderline between thermoplastic and elastomer allows the formation of stable SIC at room temperature where it is able to fix the temporary network at high state of elongation and fully recovers to the initial shape at temperature around 37 °C. It has been widely accepted that formation of pseudo networking of NR chain from non-rubber components assisted in SIC (Kaang *et al.*, 2006; Liu *et al.*, 2015). Moreover, due to the heterogeneity of crosslinked network points, short chain structure of the crosslinked region preferentially generates crystals that grow continuously in the process of tensile deformation (Tosaka *et al.*, 2004). All these elements make NR the first SMP that is able to be programmed without any initial heat treatment.

The shape memory behaviour of these SMRs presented at this section relates to only axial deformation and accounts for one-way SME. Table 5.1 presented the shape memory behaviour of NRLs based films which included the results of S_f and S_r. As shown, the crosslink density has a strong impact on SME of the rubber films. Higher crosslink density reflected a lower percentage of S_f in the sulphur-cured rubber films. This is because high crosslinking develops a tightly interconnected network that resists the applied stretching force and tends to pull the rubber films back to its original shape imparting strong elastic properties to the material. In fact, it was disclosed that the crystallinity index decreased almost linearly with crosslink density reducing the crystallizable sequence due to the disturbance from increasing chemical crosslinks (Femina *et al.*, 2023). Therefore, highly crosslinked NRL 2.0 and DPNRL 2.0 restored their original shape instantly after stretching force is released, thus no S_f is recorded. Owing to the similar reason, rubber films with 0.3 and 0.4phr sulphur possessed lower S_f than 0.2phr. On the other hand, uncrosslinked rubbers referring to NRL 0.0 and DPNRL 0.0 possessed certain degree of SME as revealed in Table 5.1. The presence of end-linked network originates from functional groups exist at both ends of the rubber chains forms linkage with natural impurities facilitates the occurrence of SIC (Toki *et al.*, 2009, 2013). The absence of crosslinks in NRL 0.0 and DPNRL 0.0 impeded full recovery of the material as part of the strain had been converted to permanent plastic deformation. As shown in Figure 5.1, the best overall SME is achieved with NRL 0.2 and DPNRL 0.2 both displaying 76.7% S_f and 100% S_r. This proposed that 0.2phr is the ideal sulphur content for crosslinking between thermoplastic and elastomer to induce SIC which kept a huge part of the material constrained in the stretched state with no plastic flow upon initiation of shape recovery (Tan *et al.,* 2024a). The entropy changes upon stretching promotes SIC and formation of crystals with low surface energy. This low surface energy crystallites usually feature a high T_m transcending room temperature which contributed to existence of SIC for development of SMR (Cavicchi, 2015). In general, the shape memory results indicated that lightly-crosslinked rubber and naturally occurring SIC are the essential qualities required to develop SMR.

Table 5.1: S_f and S_r of sulphur-cured rubber films

Samples	S_f (%)	S_r (%)
NRL 0.0	47.5 ± 3.5	89.6 ± 3.0
NRL 0.2	76.7 ± 2.4	100.0 ± 0.0
NRL 0.3	57.5 ± 1.2	100.0 ± 0.0
NRL 0.4	45.0 ± 4.7	100.0 ± 0.0
NRL 2.0	0.0 ± 0.0	-
DPNRL 0.0	40.0 ± 2.4	85.8 ± 3.5
DPNRL 0.2	75.8 ± 1.2	100.0 ± 0.0
DPNRL 0.3	64.2 ± 3.5	100.0 ± 0.0
DPNRL 0.4	37.5 ± 5.9	100.0 ± 0.0
DPNRL 2.0	0.0 ± 0.0	-

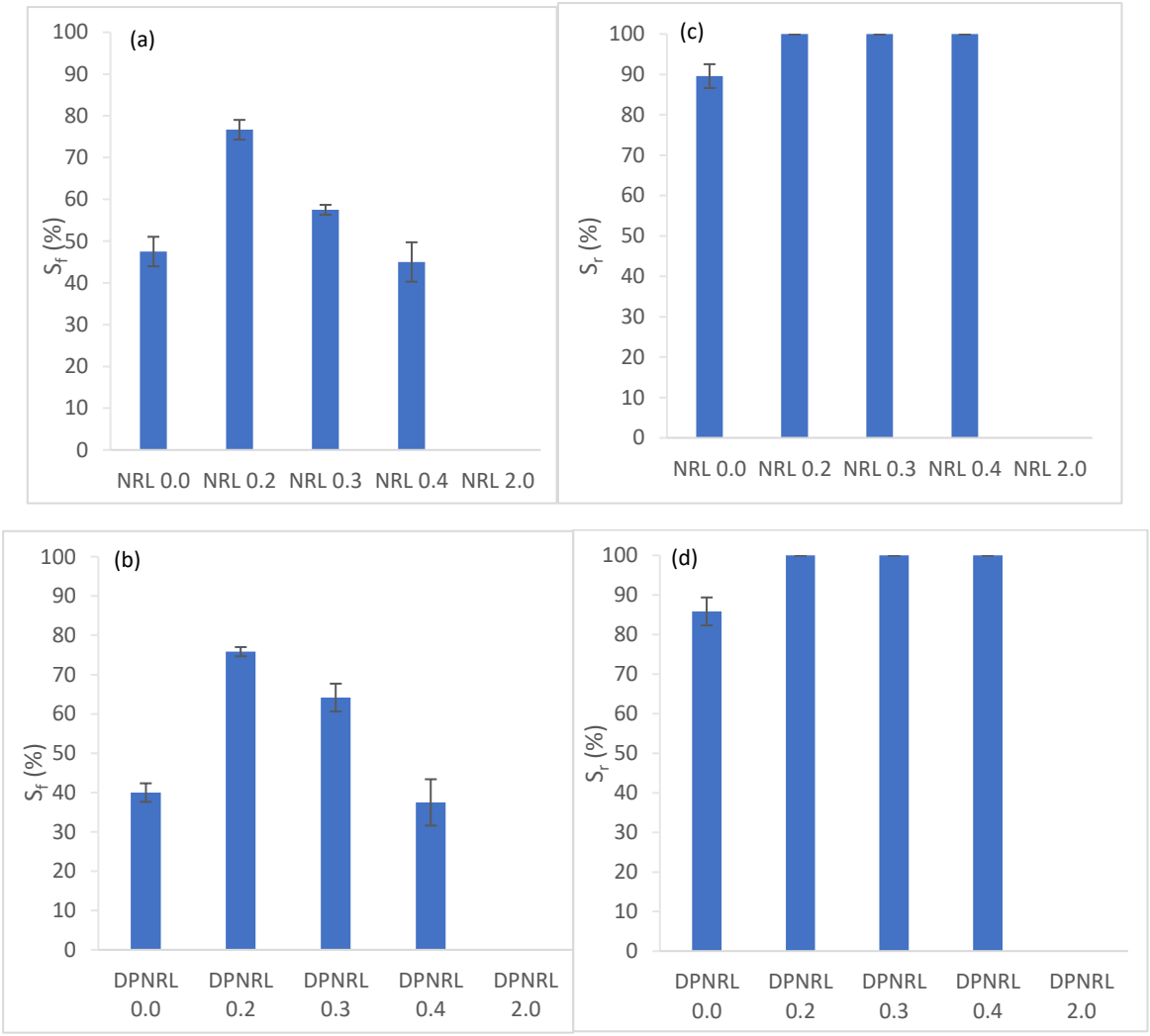

Figure 5.1: SME of sulphur-cured rubber films (a) S_f of NRL (b) S_f of DPNRL (c) S_r of NRL and (d) S_r of DPNRL films

5.1.2 Shape memory behaviour of SNC/rubber composites films

From Section 5.1.1, it was realized that lightly cross-linked NRL 0.2 and DPNRL 0.2 demonstrated the best overall SME among the other sulphur-cured rubber films. Therefore, all rubber nanocomposites films with varying SNC contents were cured with 0.2phr sulphur. Discussion from Section 4.3 showed that incorporation of SNC in various RL films (i) improved its resistance towards solvents penetration (ii) possessed better elasticity with higher energy storage capability (iii)remarkably enhanced the mechanical properties through filler-matrix interaction and formation three-dimensional filler network and (iv) exhibited comparable thermal stability with high degradation temperature. Several studies had indicated that the incorporation of nanoparticles impart positive impact in SIC of NR (Nie *et al.*, 2011; Hernández *et al.*, 2013). Thus, it is worth evaluating the effectiveness of SNC in shape memory behaviour of rubber nanocomposites films. Similarly to Section

5.1.1, ENRLs based nanocomposites films showed no SME due to their inability to possess any shape fixation during the programming stage. The shape memory parameters of the NRL and DPNRL nanocomposites films were derived from one full shape memory cycle for each specimen. Moreover, all shape memory behaviour of the rubber nanocomposite films was derived from axial deformation relating to only one-way SME. An interesting phenomenon was observed visually during the programing stage of the shape memory cycle shown in Figure 5.2. The colour of the rubber nanocomposite films changed from yellowish to opaque white at deformation strain of 600% resembling the appearance of large domains comparable to emergence of vast nematic domain in liquid crystals or stress induced whitening in semi crystalline polymer (Kojima, 1981; Wei *et al.*, 2019). This coincided with strain hardening of the rubber nanocomposite films as evident by the slope increase with deformation in stress-strain curve revealed in Figure 4.19. Moreover, the appearance of opaque white region indicated the formation of crystallites reflecting the presence of SIC that is an essential quality for the rubber nanocomposite films to exhibit shape memory behaviour (Meng, Jiang and Anthamatten, 2016). Moreover, the rubber nanocomposite film exhibited some "wrinkling" in the deformed shape. This is due to the entropy increase during heating causing the rubber molecules to become more disordered and tangled which resulted in some creasing of the rubber nanocomposite film (Geethamma and Sampath, 2019). All investigated smart rubbers possessed this phenomenon and the effect on S_f is deemed to be negligible as the creasing of the rubber nanocomposite films is considered minor. Figure 5.3 shows the development of S_f and S_r for NRL and DPNRL nanocomposites films programmed at room temperature while Table 5.2 lists the data of the shape memory parameters.

From Figure 5.3(a) and (b), it was realized that the incorporation of SNC enhanced S_f of the rubber nanocomposites films. This is mainly due to the dramatic improvement of SIC in SNC reinforced rubber composites films arising from the increased crystallinity of the material. Moreover, two well-defined crystallization mechanism was observed for rubber nanocomposites films during deformation contrarily to a single crystallization step for unfilled rubber films (Carretero-Gonzalez *et al.*, 2008a; Carretero-González *et al.*, 2008b; Weng *et al.*, 2010). The first step was related to the orientation of nanofillers during deformation while the second step was attributed to the conventional SIC of rubber matrix. Therefore, SNC can act as effective nucleation sites for the formation of crystallites in rubber due to their strong orientation at the direction of stretching. This favours the alignment of rubber chain along the deformation direction facilitating the growth of crystals which induced a more orderly arranged macroscopic structure thus resulted in enhanced SIC that improved the S_f of rubber nanocomposites films. Such observation was also reported on carbon nanodots and layered silicate filled NR nanocomposites (Hernández *et al.*, 2013; Liu *et al.*, 2019). Moreover, it is believed that

crosslink density plays a part in the improved SIC of rubber nanocomposites films. As revealed at Section 4.3.2 in Table 4.6, crosslink density increased with the content of SNC. Higher crosslink density might indeed aided in the SIC at large deformation due to faster reaching of the limit chain extensibility (Candau *et al.*, 2023). This statement is proved by the lower elongation at break of SNC reinforced rubber composites films shown at Section 4.3.5 in Table 4.9. In fact, all rubber nanocomposites films are lightly-crosslinked by sulphur where the increased in crosslink density is due to the interfacial interaction between filler and matrix. Therefore, these crosslinks promotes chain alignment upon deformation as they prevent loss of orientation by chain relaxation (Le Gac *et al.*, 2014). Furthermore, the dispersion level of SNC in rubber matrix also contributed to the SIC of the rubber nanocomposites films (Qu *et al.*, 2009). From Figure 4.15 at Section 4.3.1, SNC was uniformly dispersed throughout the rubber matrix. The homogeneous distribution of SNC encouraged higher level of filler-matrix interaction triggers the orientation of rubber chains as a result from the highly aligned SNC in the stretching direction. Therefore, the higher number of highly orientated stretched polymer chains supports the nucleation mechanism for more strain-induced crystals.

Owing to all the factors above, increasing content of SNC enhanced SIC that eventually improved S_f of the rubber nanocomposites films. From Table 5.2, all SNC filled rubber nanocomposites films manifested higher S_f than unfilled rubber films within the investigated content of SNC. The upper limit of S_f was recorded to be 93.3% achieved by NRL/SNC 8% and DPNRL/SNC 8%. As a result, the incorporation of 8% SNC to NRL and DPNRL improved the S_f by 35% and 23% respectively. Meanwhile, from Figure 5.3(c) and (d) no detrimental outcome was observed on S_r of the rubber nanocomposites films. Unfilled and filled rubber films exhibited 100% S_r over one full shape memory cycle resembling no plastic deformation was in presence during the process. Therefore, the incorporation of SNC maintains excellent elasticity of the rubber nanocomposites films associated to homogenous nanofiller dispersion and good filler-rubber interaction. These traits prevented the occurrence of slippage between SNC and rubber chains during stretching, thus preserving the elastic properties of rubber nanocomposites films. Since all rubber nanocomposites films exhibited improved S_f, ε_{stored} of the smart rubbers was then identified to quantify the real stored elongation before triggering the recovery of the specimen. This parameter is seldom acknowledged in the previous literature where it is also known as recoverable strain (Voit *et al.*, 2010). Figure 5.4(a) and (b) show the ε_{stored} of SNC reinforced NRL and DPNRL composites films under one complete shape memory cycle. It was noted that ε_{stored} of all smart rubbers is above 400% irrespective of SNC content. The incorporation of SNC to NRL and DPNRL increased the ε_{stored} of the rubber nanocomposites films where NRL/SNC 8% and DPNRL/SNC 8% achieved 550% and 560% stored elongation. Indeed, S_f of the rubber nanocomposites films contributed directly to the ε_{stored} thus the capability of storing strain increased with SNC content.

ε_{stored} values is higher (850%) in other literature as the rubber films is programmed to a higher strain of 920% while similar trend about the relationship between S_f and ε_{stored} was reported (Heuwers *et al.*, 2013). Moreover, full S_r is achieved for all rubber nanocomposites films indicating all ε_{stored} is able to recover to their permanent shape resembling the recoverable strain is equivalent to ε_{stored}. Therefore, the ability to store several 100% strain makes these SMR a suitable candidate for energy storage application. A comprehensive discussion about the energy storage capability of the smart rubbers will be presented at Section 5.2.

Table 5.2: S_f, S_r and ε_{stored} of SNC/rubber composites films

Samples	S_f (%)	S_r (%)	ε_{stored} (%)
NRL/SNC 0%	69.2 ± 3.5	100.0 ± 0.0	415.0 ± 21.2
NRL/SNC 2%	76.7 ± 2.4	100.0 ± 0.0	460.0 ± 14.1
NRL/SNC 4%	82.5 ± 1.2	100.0 ± 0.0	495.0 ± 7.1
NRL/SNC 6%	88.3 ± 4.7	100.0 ± 0.0	530.0 ± 0.0
NRL/SNC 8%	93.3 ± 2.4	100.0 ± 0.0	550.0 ± 7.1
DPNRL/SNC 0%	75.8 ± 3.5	100.0 ± 0.0	455.0 ± 21.1
DPNRL/SNC 2%	82.5 ± 1.2	100.0 ± 0.0	495.0 ± 7.1
DPNRL/SNC 4%	85.0 ± 0.0	100.0 ± 0.0	510.0 ± 0.0
DPNRL/SNC 6%	89.2 ± 1.2	100.0 ± 0.0	535.0 ± 7.1
DPNRL/SNC 8%	93.3 ± 2.4	100.0 ± 0.0	560.0 ± 14.1

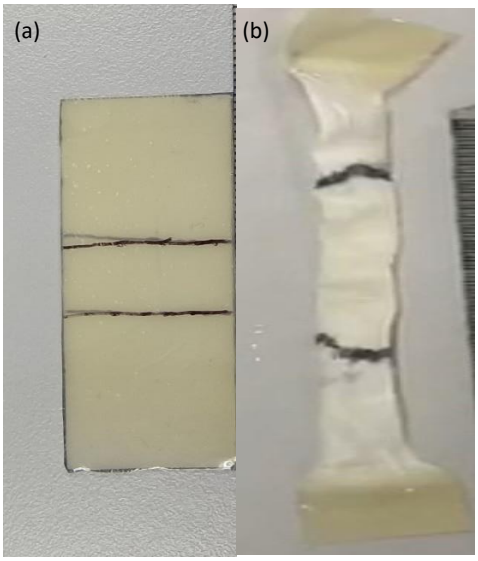

Figure 5.2: Appearance of NRL/SNC composite film (a) before and (b) after shape programming during a shape memory cycle

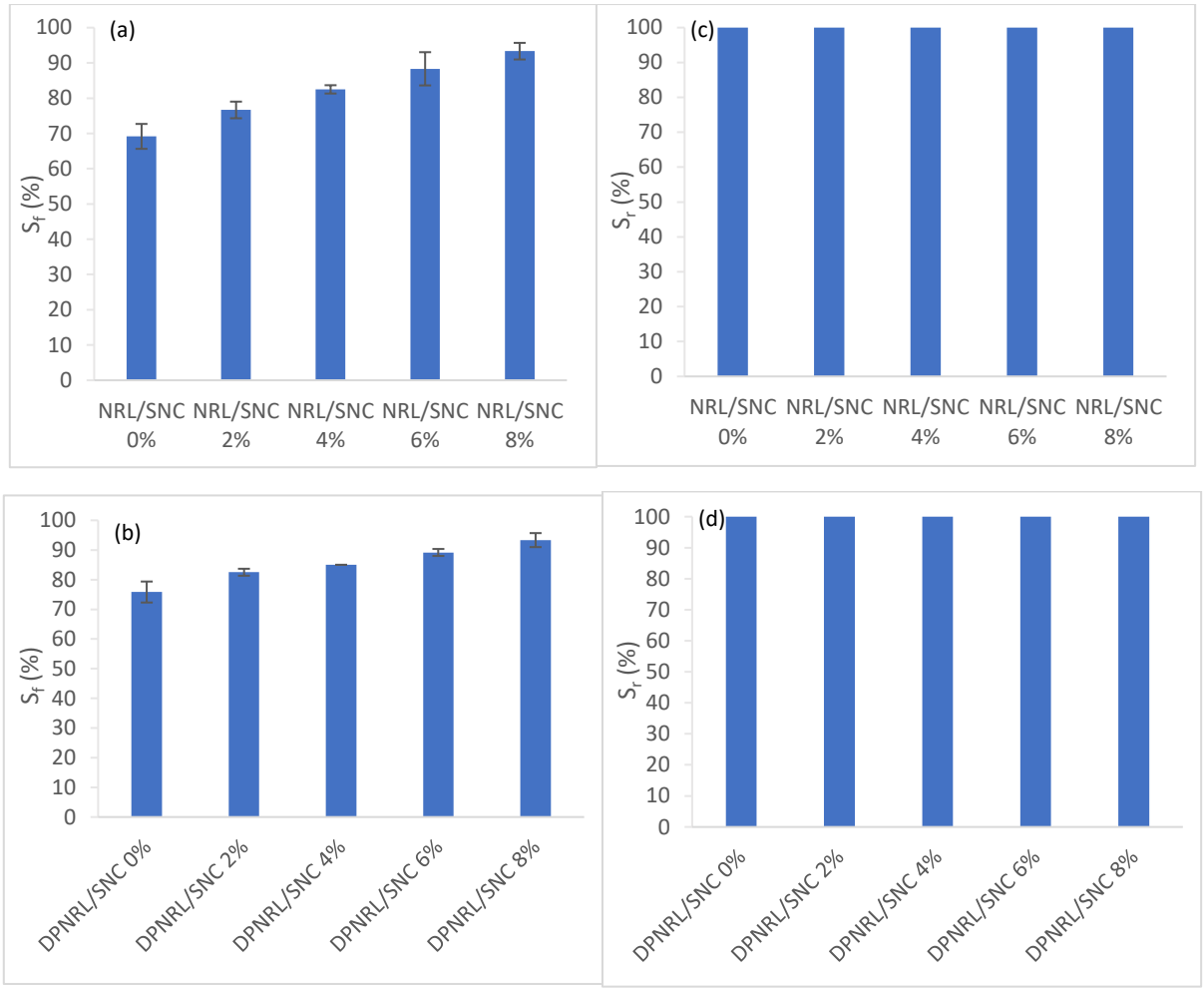

Figure 5.3: SME of rubber nanocomposites films (a) S_f of SNC reinforced NRL composites (b) S_f of SNC reinforced DPNRL composites (c) S_r of SNC reinforced NRL composites and (d) S_r of SNC reinforced DPNRL composites films

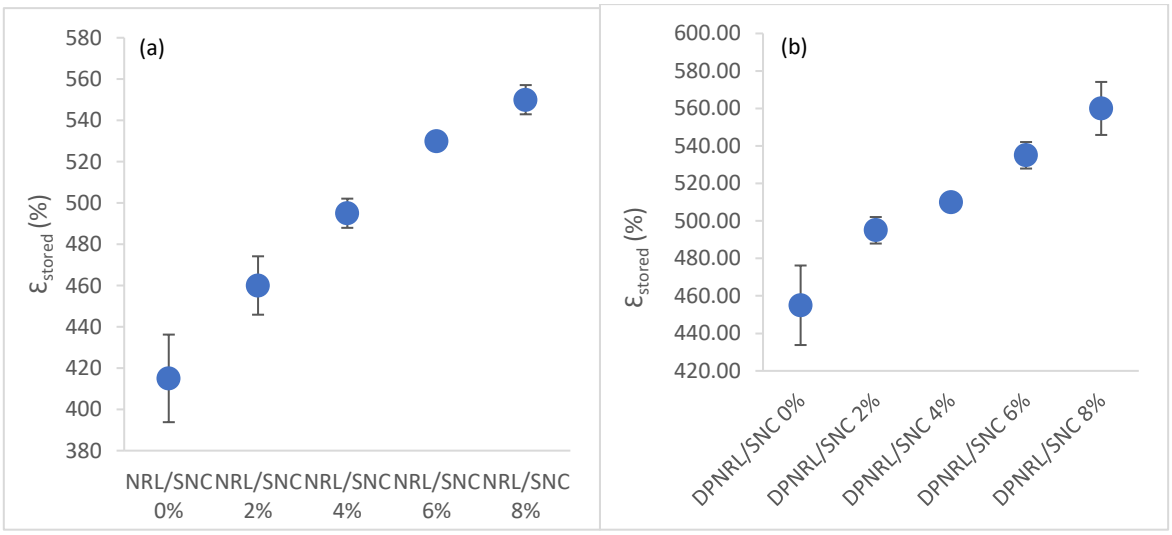

Figure 5.4: ε_{stored} of (a) NRL nanocomposites films (b) DPNRL nanocomposites films

5.2 Evaluation of energy storage capability of smart rubbers

5.2.1 Energy storage capacity of SNC reinforced rubber composite films

From the discussion of Section 5.1.2, it was realized that higher SNC content reflects improved shape memory behaviour. Therefore, the capability of storing strain indicated that there will be energy stored within the rubber nanocomposite films during fixing of the shape. Investigation regarding energy storage capacity of the rubber nanocomposite films was done by calculating the bounded area under unloading curve based on the value of ε_{stored} previously determined from shape memory tests. Figure 5.5 shows an exemplary of a loading-unloading curve where area under the loading curve reflected by the red lines indicates $E_{Applied}$ whereas the area under the unloading curve shown by the green lines corresponds to E_{Stored} during a shape memory cycle. It is affirmed that some part of $E_{Applied}$ is stored within the rubber nanocomposite films due to the fact that SMPs not only store strain but also stress that translated to a certain amount of energy (Heuwers *et al.*, 2013). Furthermore, Figure 5.6 shows the relationship between each energy involved during a loading-unloading cycle. It was originally assumed that all $E_{Applied}$ was stored entirely by the rubber nanocomposite films. As shown in Figure 5.6, shape fixing of the rubber nanocomposite films has a positive role towards energy storage suggesting the ability of a material to remain at a temporary mechanical deformation is crucial towards the storing of elastic elongation work energy which will then be released as thermal dissipation during the recovery of original shape. On the other hand, the non-fixation part due to retraction of the rubbery material and rubber hysteresis which is a result of energy loss due to friction occurring inside the rubber films have a negative impact towards energy storage capability within the rubber nanocomposite films.

Figure 5.7 (a) and (b) show the first cycle of loading-unloading curves for SNC reinforced NRL and DPNRL composite films. It was realized that the loading-unloading curves for both NRL/SNC and DPNRL/SNC exhibited a similar pattern where tensile strength and modulus of the rubber nanocomposite films increased with SNC loadings within the elongation range of 0-600%. This is aligned to the result presented in Section 4.3.5. Moreover, the areas under loading and unloading curves suggested that $E_{Applied}$ and E_{stored} of the rubber nanocomposite films increased with SNC content. This indicated that the incorporation of SNC benefited the energy storage capability of the rubber nanocomposite films. As expected, NRL and DPNRL nanocomposite films showed almost identical amount of $E_{Applied}$ and E_{stored} with respect to the same loading of SNC. This is because the tensile stress applied and the obtained ε_{stored} at similar content of SNC reflected in Section 4.4.2 are comparable. Subsequently, Figure 5.8 shows the loading-unloading curves of DPNRL/SNC 8% for three cycles. Other investigated rubber nanocomposite films exhibited similar plot pattern and trend as DPNRL/SNC 8%. It was first discovered that the required stress to achieve the same strain decreased from the first to

the third cycle. This phenomena is associated to the stress softening of rubber network which known as the Mullins effect (Diani, Fayolle and Gilormini, 2009). Moreover, there is a significant hysteresis loop enclosed by the first loading-unloading cycle proposing that the energy loss due to the friction for the first cycle is high. Besides, the area enclosed by the hysteresis loop decreased drastically from the first to the second cycle and more gradually from the second to the third cycle. This observation is similar to the findings of previous literature (Carleo *et al.*, 2020; Yang *et al.*, 2022). In this rubber nanocomposite film, energy dissipation of each cycle drops as the number of cycles increased with the most significant energy dissipation happened at the first cycle. In another word, substantial stress softening occurs in the first cycle of loading and progressive softening happens gradually in the following cycles. It is because repeated stretching caused the untangling of rubber molecular chains, the breakdown of interaction between filler and rubber, and the disruption of three-dimensional network among fillers which consequently resulted in decrease of Mullins effect (Fu *et al.*, 2019).

SNC reinforced rubber composite films do not only store strain which has been discussed in Section 4.4.2. In fact, they have the ability to store stress which corresponds to the storage of a certain amount of energy. Figure 5.9 (a) and (b) show the E_{stored} of NRL/SNC and DPNRL/SNC with 0%, 4% and 8% SNC content for cycle 1 and cycle 3. It was shown that the incorporation of SNC increased the E_{stored} for both NRL and DPNRL based rubber nanocomposite films within the number of cycles performed. This is due to the higher stress applied to achieve the required strain and not to mention the higher ε_{stored} resulting from enhanced S_f determined from shape memory test presented in Section 4.4.2. Moreover, for both NRL/SNC and DPNRL/SNC rubber nanocomposites films, the E_{Stored} slightly decreased with the number of cycles. This is mainly because of the lower stress applied to the rubber nanocomposite films upon elongation to the required strain as shown in Figure 5.8. The upper limit for E_{stored} was achieved by DPNRL/SNC 8% recording 20.91 MJ/m^3 at the first cycle while the lower limit for E_{stored} was valued at 6.36 MJ/m^3 by NRL/SNC 0% at the third cycle. Figure 5.10 (a) and (b) show the $E_{efficiency}$ of SNC reinforced NRL and DPNRL composite films with 0%, 4% and 8% loading for the first and third cycles. Similar to the findings of E_{stored}, $E_{efficiency}$ increased with the content of SNC for both the first and third cycles. This is mainly attributed to the higher E_{stored} for rubber nanocomposite films with higher loading of SNC. Besides, $E_{efficiency}$ increased from cycle 1 to cycle 3 for both NRL/SNC and DPNRL/SNC rubber nanocomposite films irrespective of the loading of SNC. This increment is the result of decreased Mullins effect where lesser energy is required to compensate for energy loss due to rubber hysteresis when the number of cycles increased. Thus, the highest $E_{efficiency}$ is achieved by DPNRL/SNC 8% at cycle 3 recording 79.95% whereas the lowest $E_{efficiency}$ is calculated at 29.65% attained by NRL/SNC 0% at cycle 1.

Table 5.3 and 5.4 tabulated the calculated values of energy parameters which included $E_{Applied}$, E_{stored}, $E_{retract}$, hysteresis and $E_{efficiency}$ for the investigated rubber nanocomposite films for cycle 1 and cycle 3 respectively. It was manifested from Table 5.3 and Table 5.4 that $E_{Applied}$ increased with SNC loading for both NRL/SNC and DPNRL/SNC rubber nanocomposite films. The increment of $E_{Applied}$ is due to the higher tensile stress required to elongate the stiffer rubber nanocomposite films with higher SNC content to the required length. Hence, E_{stored} which stores part of the energy provided follows the same relationship as $E_{Applied}$ where the reasons have been discussed above. The maximal value of E_{stored} by DPNRL/SNC 8% is similar to another previously reported SMP (Cooper *et al.*, 2021). The rubber nanocomposite film's high extensibility coupled with its high recoverable energy gives this material large E_{stored} of 20.91 MJ/m^3 that is approximately six times greater than previous recorded highest energy density presented by an SMP (Zhang and Li, 2013). Additionally, the low density of rubber nanocomposite films (1.1g/cm^3) results in a significant specific energy density of 19.01 J/g which is roughly 487 times greater than energy density of skeletal muscle, measured at 0.039 J/g (Madden *et al.*, 2004). On the other hand, $E_{retract}$ decreased with the loading of SNC for both types of rubber nanocomposite films. This is related to the lower S_f that resulted in lower ε_{stored} that caused the rubber nanocomposite films to incline towards spontaneous retraction to the original shape. Furthermore, the values of rubber hysteresis are comparable between each rubber nanocomposite film with varying SNC content for both NRL/SNC and DPNRL/SNC. This indicated that the incorporation of SNC has little to no effect towards stress softening of the material. However, as mentioned above, the number of cycles has a great impact towards rubber hysteresis. Therefore, presented in Table 5.3 and Table 5.4, the calculated values of cycle 1 and cycle 3 have some differences between them as the energy loss due to hysteresis is significantly lesser in cycle 3. Generally, the energies considered for the rubber nanocomposite films obey the energy conservation law where energy is neither created nor destroyed but transformed from one form to another. After all, NRL/SNC and DPNRL/SNC rubber nanocomposite films exhibited the same trend and comparable values for all the energy parameters investigated.

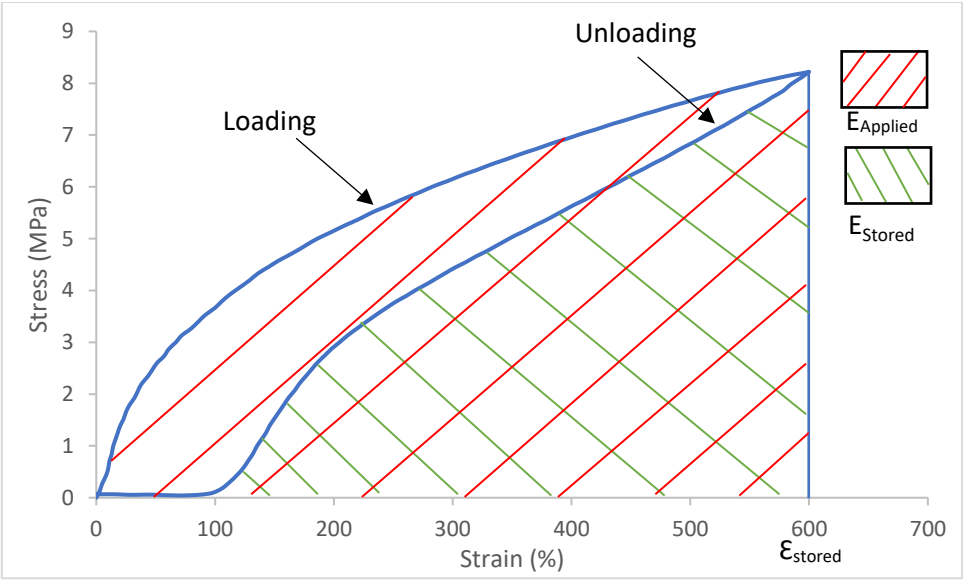

Figure 5.5: Plot of stress vs strain for a typical loading-unloading curve

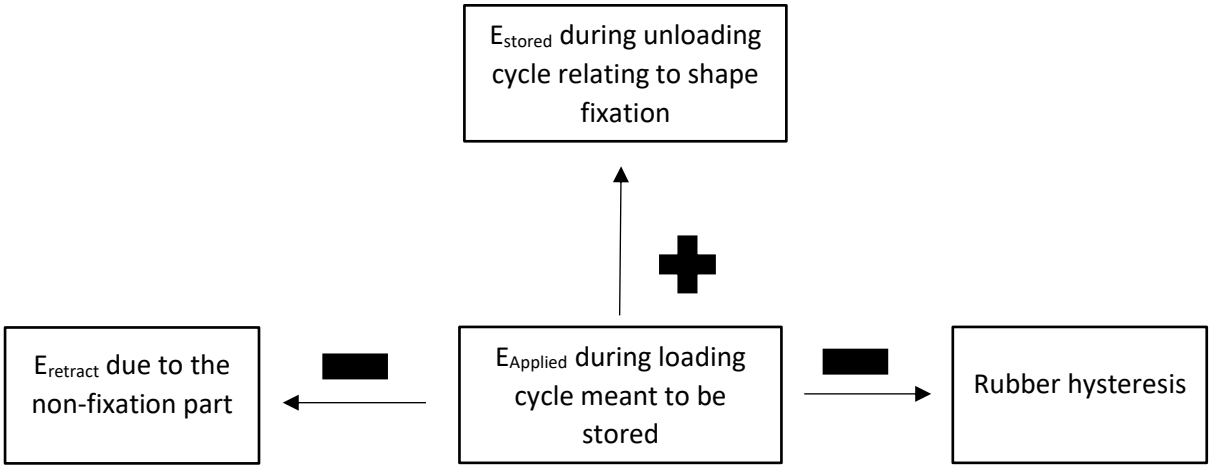

Figure 5.6: Schematic diagram of the types of energy involved during a loading-unloading cycle and their relationship to $E_{Applied}$ which was assumed to be stored entirely (+) positive role (-) negative role

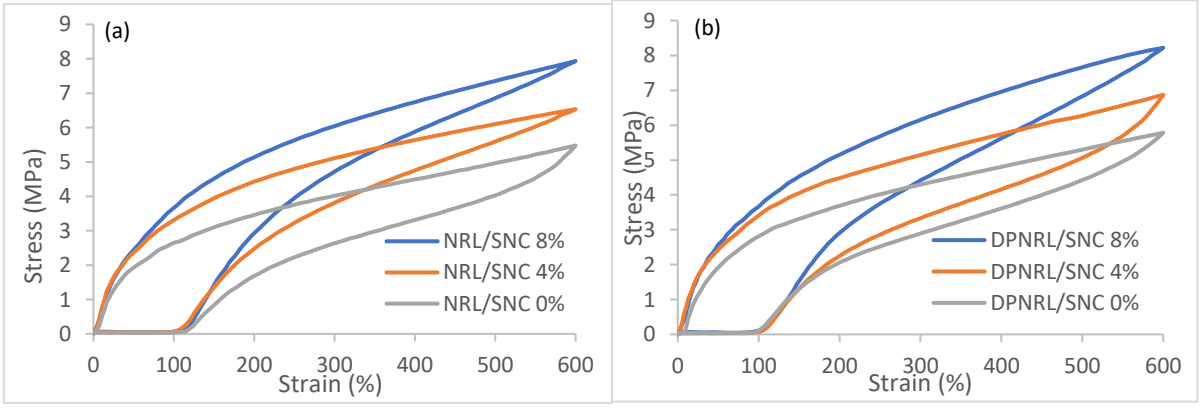

Figure 5.7: First cycle of the loading-unloading curves for SNC reinforced (a) NRL composite films and (b) DPNRL composite films

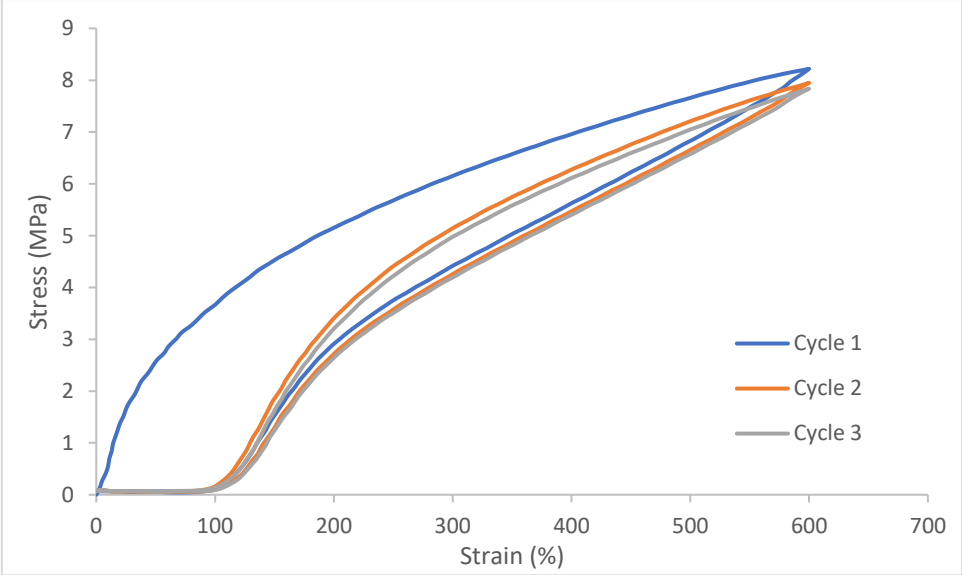

Figure 5.8: Three cycles loading-unloading curves of DPNRL/SNC 8%

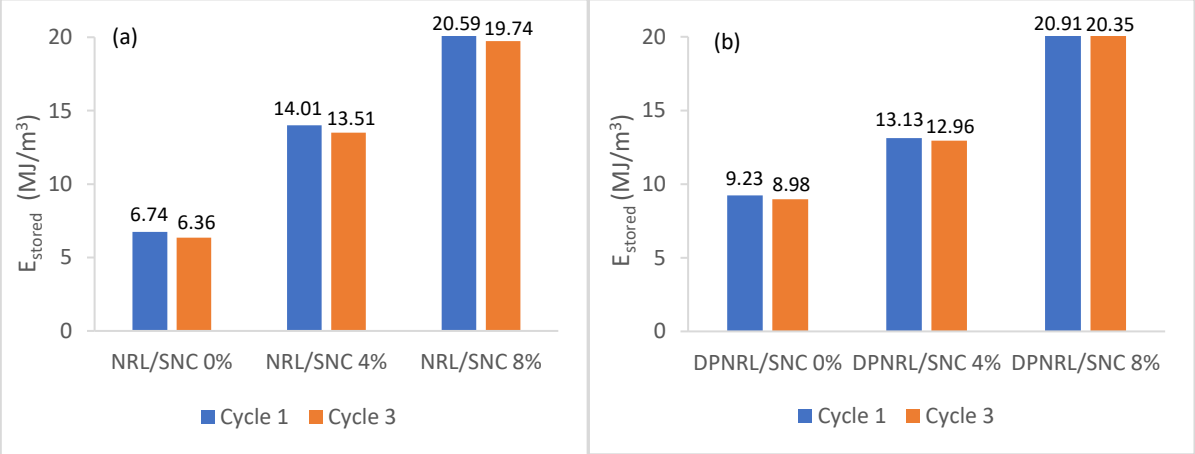

Figure 5.9: E_{stored} of (a) NRL/SNC rubber nanocomposite films and (b) DPRNL/SNC rubber nanocomposite films

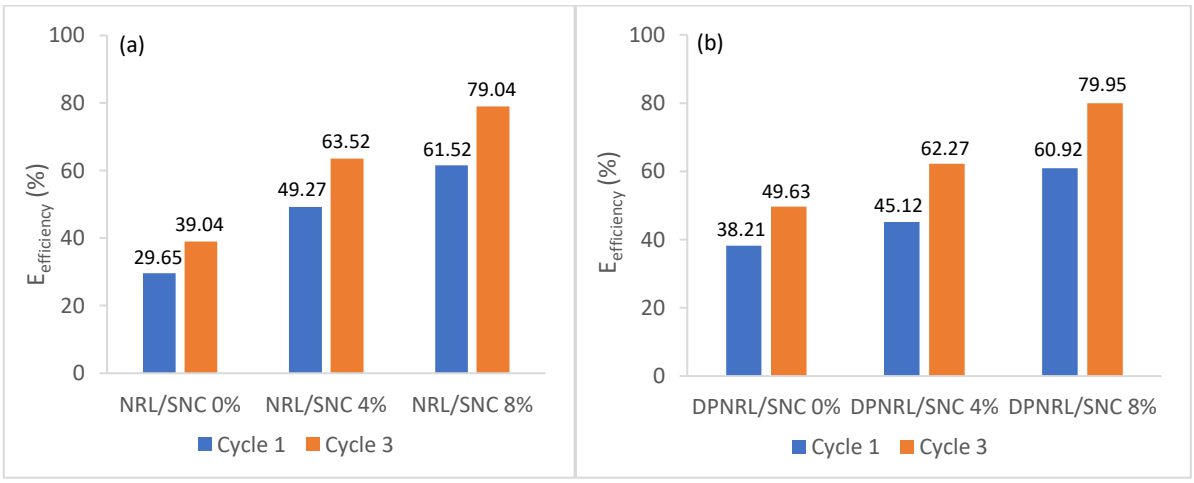

Figure 5.10: $E_{efficiency}$ of (a) NRL/SNC rubber nanocomposite films and (b) DPNRL/SNC rubber nanocomposite films

Table 5.3: Calculated energy parameters of the first cycle for the investigated rubber nanocomposite films

Specimens	$E_{Applied}$ (MJ/m^3)	E_{Stored} (MJ/m^3)	$E_{retract}$ (MJ/m^3)	Hysteresis (MJ/m^3)	$E_{efficiency}$ (%)
NRL/SNC 0%	22.74	6.74	7.55	8.45	29.65
NRL/SNC 4%	28.44	14.01	6.04	8.38	49.27
NRL/SNC 8%	33.46	20.59	3.82	9.05	61.52
DPNRL/SNC 0%	24.16	9.23	6.78	8.14	38.21
DPNRL/SNC 4%	29.09	13.13	5.12	10.85	45.12
DPNRL/SNC 8%	34.32	20.91	3.08	10.33	60.92

Table 5.4: Calculated energy parameters of the third cycle for the investigated rubber nanocomposite films

Specimens	$E_{Applied}$ (MJ/m^3)	E_{Stored} (MJ/m^3)	$E_{retract}$ (MJ/m^3)	Hysteresis (MJ/m^3)	$E_{efficiency}$ (%)
NRL/SNC 0%	16.30	6.36	7.45	2.49	39.04
NRL/SNC 4%	21.27	13.51	5.89	1.87	63.52
NRL/SNC 8%	24.97	19.74	3.70	1.54	79.04
DPNRL/SNC 0%	18.09	8.98	6.57	2.54	49.63
DPNRL/SNC 4%	20.81	12.96	4.70	3.15	62.27
DPNRL/SNC 8%	25.46	20.35	2.44	2.66	79.95

5.2.2 Demonstration of energy stored within the rubber nanocomposite films by manual experiment

As discussed in Section 5.2.1, the investigated rubber nanocomposite films are capable of storing certain amount of energy during a shape memory cycle. This happens when the applied stress is removed, the rubber nanocomposite film retains a large amount of fixed strain thereby storing elastic deformation energy. The E_{stored} will then be released upon the recovery process of its original shape. The extent of recoverable elastic energy is constrained by the amount of reversible work performed by the rubber nanocomposite film. The whole energy storing process mirrors the shape memory cycle which involves temperature change. The principle of the thermomechanical energy storage system is shown in Figure 5.11. The sample is stretched at ambient temperature before undergoing cooling process. Instead of immediately returning to its original shape, it stays at the elongated shape after cooling at low temperature thus storing elastic deformation energy. After heating at an elevated temperature, the sample can locally release mechanical energy during entropy driven recoiling where the sample retracts, therefore a load can be lifted. At this stage, the elastic energy stored within the smart rubber during the shape fixing step is released as mechanical energy where work is done by lifting a load in the vertical direction.

To this extent, an idea had been developed to showcase the utilization of E_{stored} within the rubber nanocomposite films by lifting a load with the conversion of E_{stored} to mechanical energy. Here, the demonstration of rubber nanocomposite film as a potential high strength, high extensibility and soft one-way actuator had been conducted. Figure 5.12(a) and (b) show a prestrained rubber nanocomposite film that possessed a weight of approximately 1g had the capability of lifting loads weighing 40g. The loads were raised by 4.5cm upon initiation of its S_r at ambient temperature. This demonstrated the that the rubber nanocomposite film lifted 40 times of its own weight with a specific work output of 0.02 J/g. Compared to other shape memory based actuator (Krajovic and Anthamatten, 2021), this rubber nanocomposite film achieved both a larger actuation displacement and work output. It is crucial to highlight that the rubber nanocomposite film functioning as a one-way actuator requires reprogramming after each cycle thus restricting its potential applications when compared to other reversible actuators that do not necessitate reprogramming throughout the cycling process. This demonstration suggested that rubber nanocomposite film exhibited energy storage potential with high stretchability as well as excellent S_r.

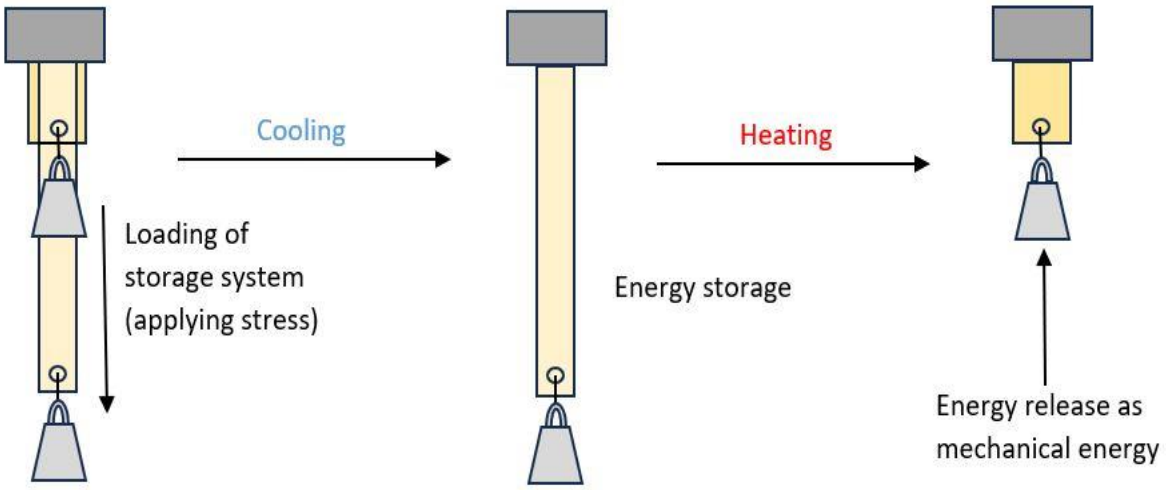

Figure 5.11: Principle of the thermomechanical energy storage system of the rubber nanocomposite film

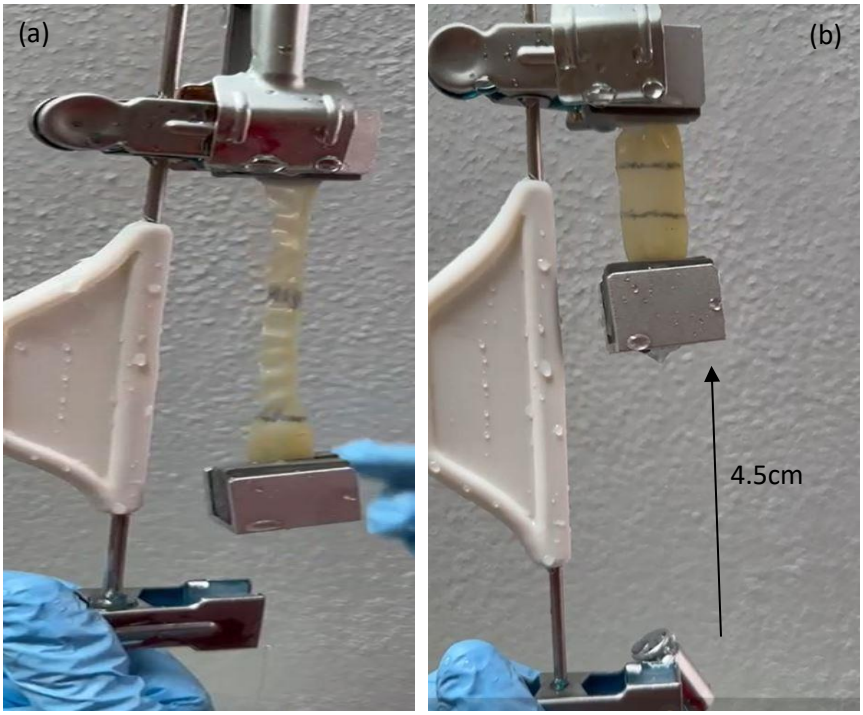

Figure 5.12: (a,b) a prestrained rubber nanocomposite film lifting a load of 40g by 4.5cm

5.3 Summary of Chapter 5

Chapter 5 addresses objective 2 and objective 3 of the research: investigating the SME of smart rubbers including sulphur-cured rubber films and SNC reinforced rubber composite films and evaluating the energy storage potential of the smart rubbers through experimental analysis and manual demonstration. Chapter 5.1 highlights that ENRLs based films do not exhibit any SME while NRLs based films with 0.2 phr sulphur loadings has the best SME achieving 76.7% S_f and 100% S_r. SME of the smart rubbers increased with SNC loadings where NRL/SNC 8% and DPNRL/SNC 8% both achieving 93.3% S_f and 100% S_r showing the effectiveness of SNC in enhancing the shape memory behavior of the rubber nanocomposite films. This is mainly due to the increase in crystallinity of the material that favours the alignment of rubber chains which facilitates the growth of strain-induced crystals. Moreover, ε_{stored} of the smart rubbers achieved more than 500% indicating the potential for energy storage application. Chapter 5.2 shows the energy storage potential of the smart rubbers. E_{Stored} of the rubber nanocomposite films increased with the amount of SNC where the upper limit achieved is 20.91 MJ/m^3 accounting for DPNRL/SNC 8% while NRL/SNC composite films have comparable values. The rubber hysteresis decreased with the number of loading-unloading cycles due to reduced Mullins effect. The highest $E_{efficiency}$ achieved among the smart rubbers is 79.95%. Furthermore, manual demonstration validates that there are energy stored within the rubber nanocomposite films where the smart rubber is capable of lifting a weight of 40g in the vertical direction.

Chapter 6

6.0 Conclusion and Future Works

6.1 Conclusion

The objectives layout in Chapter 1 had been met through detailed analysis and original experimental works. The outcomes of this research were listed as below:

1. Synthesis and characterization of SNC as well as evaluating the physical and mechanical characteristics of sulphur-cured rubber films and SNC reinforced rubber composite films:

   1.1 Synthesis and characterization of SNC

   The synthesizing method of SNC by acid hydrolysis is effective. It is because SNC was observed to be well dispersed in aqueous solution with dimension in nanoscale. SNC was found to possess A-type crystalline structure with higher relative crystallinity than native starch. This was reaffirmed by the higher and sharper 2Θ diffraction peaks of SNC in the diffractogram. Due to the increase in crystallinity of SNC, an obvious shift to the right was noticed from DSC thermogram suggesting SNC has higher melting temperature than native starch. Moreover, thermal degradation of SNC occurs at 300 °C which is similar to native starch but with higher remaining solid residue indicating that SNC is more thermally stable when compared to its native counterpart.

   1.2 Physical and mechanical characteristics of sulphur-cured rubber films

   The crosslink density and tensile strength of sulphur-cured rubber films increased with sulphur loading. However, this is accompanied with a reduction in elongation at break because of the development of stiffer rubber structure. Furthermore, toluene penetrability was found to decrease with higher sulphur loading due to the reduction in free volumes between rubber chain resulted from the increase in crosslink density. ENRLs based rubber films have lower swelling percentage in toluene than its NRLs counterpart. The presence of epoxide groups that contain oxirane rings reduced the affinity towards non-polar solvents thus improving its resistance against toluene. It was also noted that epoxide groups caused a reduced in chain mobility which contributed to the increased in T_g of ENRLs based rubber films. The increasing amount of epoxide groups is directly related to the conformational flexibility of the rubber chain. Therefore, ENRL50 have the highest T_g among the investigated RL films.

1.3 Physical and mechanical characteristics of SNC reinforced rubber composite films

Morphological study showed that SNC is well dispersed in rubber nanocomposites films even at the highest content of 8%. Homogeneity in dispersion of nanofiller is crucial in enhancing the mechanical properties of the nanocomposites. Crosslink density of the rubber nanocomposites films was found to increase with higher SNC content. The well dispersed SNC tends to develop more physical entanglements and chemical crosslinks with the rubber chain. The increased in crosslink density is inclined towards the formation of a stiffer rubber structure that reduced the chain mobility which governs T_g of a material. Interestingly, this case is not reflected in SNC reinforced rubber nanocomposites reflected from DMA. In another way, the interaction between SNC and rubber matrix enhanced the mechanical properties but does not have significant influence on chain mobility of the rubber nanocomposites films. The incorporation of SNC in rubber matrix increased the water uptake but decreased it susceptibility to toluene swelling. This is because the high hydrophilicity of hydroxyl groups presented in SNC allowing them to bind easily with water molecules. On the other hand, the formation of three-dimensional network of SNC that acts as physical barrier hinders the permeability of toluene into the composites network. Similarly to the sulphur-cured rubber films, ENRLs based rubber nanocomposites films have better toluene resistance than NRLs. In terms of reinforcing capability, SNC was found to improve the mechanical properties of rubber nanocomposites films while maintained the materials' deformability. Moreover, SNC proved to be a good substitute to the conventional carbon black as it imparted similar reinforcing strength with a lower content. T_g of the of the rubber nanocomposites is comparable to the unfilled matrix suggesting that SNC has little to no effect on occurrence of glass-rubber transition of the material. However, the I_α peaks of rubber nanocomposites films were observed to be lower than neat rubber suggesting the material acts more elastic and have more potential to store energy rather dissipating it. There are two weight loss steps corresponding to the degradation of SNC at lower temperature and rubber matrix at higher temperature for the rubber nanocomposites films.

2. To induce SME in sulphur-cured rubber films and investigate the effectiveness SNC on SME of the rubber nanocomposite films:

All shape memory behaviour of the SMR was performed through axial deformation accounting for only one-way SME. From the result of shape memory testing, ENRLs-based rubber films do not demonstrate any SME due to their inability to fix the temporary shape while NRLs-based

rubber films with 0.2phr sulphur exhibited the best overall SME achieving a S_f of 76.7% and S_r of 100.0%. SME of the rubber films is mainly induced by SIC with crosslinking between the borderline of thermoplastic and elastomer. Therefore, sulphur dosage of 0.2phr was applied to all SNC reinforced rubber nanocomposites films to further evaluate the shape memory behaviour. It was found that the SME of rubber nanocomposites films improved with SNC content. This is mainly due to the increased crystallinity of the material that favours the alignment of rubber chain along the deformation direction facilitating the growth of crystals which induced a more orderly arranged macroscopic structure thus resulted in enhanced SIC. The finest achievable SME of rubber nanocomposites films within the investigated range are NRL/SNC 8% and DPNRL/SNC 8% where both achieved S_f of 93.3% and S_r of 100.0%. Moreover, it was revealed that the ε_{stored} of the aforementioned rubber nanocomposite films is 550% and 560% respectively suggesting the capability of storing large strain which translated to the potential for energy storage application.

3. To evaluate the energy storage potential of smart rubber through experimental analysis and manual experiment.

   It was realized that higher SNC content reflects improved shape memory behaviour of the rubber nanocomposite films. The energy storage potential through experimental analysis of the rubber nanocomposite films were evaluated by cyclic loading-unloading tests. It was shown that the incorporation of SNC increased the E_{stored} for both NRL and DPNRL based rubber nanocomposite films within the number of cycles performed. The upper limit for E_{stored} was achieved by DPNRL/SNC 8% recording 20.91 MJ/m^3 at the first cycle while the lower limit for E_{stored} was valued at 6.36 MJ/m^3 by NRL/SNC 0% at the third cycle. Additionally, the low density of rubber nanocomposite films (1.1g/cm^3) results in a significant specific energy density of 19.01 J/g which is approximately 487 times greater than energy density of skeletal muscle, measured at 0.039 J/g. Similar to the findings of E_{stored}, $E_{efficiency}$ increased with the content of SNC for both the first and third cycles. The highest $E_{efficiency}$ is achieved by DPNRL/SNC 8% at cycle 3 recording 79.95% whereas the lowest $E_{efficiency}$ is calculated at 29.65% attained by NRL/SNC 0% at cycle 1. The demonstration of rubber nanocomposite film as a potential high strength, high extensibility and soft one-way actuator had been conducted by manual experiment. The rubber nanocomposite film weighing about 1g has the capability to lift a load of 40g by 4.5cm. This demonstrated the that the rubber nanocomposite film lifted 40 times of its own weight with a specific work output of 0.02 J/g. This demonstration suggested that rubber nanocomposite film exhibited energy storage potential with high

stretchability as well as excellent S_r. This aligns well with the growing needs of various industries for flexible high-performance and efficient energy storage solutions.

6.2 Contributions of the work

- The physical and mechanical characteristics such as barrier properties, mechanical properties and mechanical behaviour of sulphur-cured SPNRL are known
- The physical and mechanical characteristics including barrier properties, mechanical properties, mechanical behaviour and thermal properties of SNC reinforced NRL, DPNRL, ENRL25 and ENRL50 are uncovered
- SME in sulphur-cured rubber films is successfully induced and the optimum sulphur dosage is found
- SME in SNC reinforced rubber composite films is successfully enhanced with improved mechanical properties
- Discovered and quantified the energy storage potential of rubber nanocomposite films
- Validation of the energy storage potential through practical experiment is successful
- Design of self-made elongation device and manual demonstration is purely original

6.3 Future works

Based on the findings of the experimental results, more work can be done on inducing SME in ENRL as ENRL do not possess any SME in the current work. This may be achieved by incorporating other material who have moderate phase transition temperature as SME of any polymer is mainly governs by T_m or T_g of the composite. This will aid in extending the undiscovered potential of novel SPNR latex in many applications. Moreover, further improvement can be work on establishing SME in NRL and DPNRL with higher sulphur or SNC content without affecting the flexibility of the rubber films. The suggestion will certainly develop stronger rubber films with higher tensile strength that can improve E_{stored} within the material. This research generally achieved one-way SME with excellent S_f and S_r in rubber films, investigation towards the development of multiple-way SME in rubber film remains an interesting area to be explored. It can greatly increase the market usage of rubber in the future as this material has its gifted advantages such as excellent elasticity, durability, low-cost while being always abundant and sustainable.

The shape memory test and manual demonstration were conducted using self-made elongation device. In order to obtain a more accurate set of stress-strain data, a reliable automated testing equipment that have the capability of elongating material to large strain with rapid cooling and heating features is highly recommended. Furthermore, enhancement on the $E_{efficiency}$ of the rubber

films can be realized by reducing the energy loss due to hysteresis. Modifications such as changes to the rubber vulcanizing method, filler type and improvement on filler-rubber interactions can be done to overcome this matter. The threshold load that can be lifted by the current rubber nanocomposite film to achieve the maximum work output without compromising the SME obtained can also be evaluated in future research. The energy storage capability of this rubber nanocomposite films presents an exciting future prospect to be integrated in smart systems, 3D or 4D printing, lithium batteries, supercapacitors and as a part in energy transformation technology.

References

A.J. Jeffrey (2020) *Determining Glass Transition Temperature Using DMA*, *The Madison Group*. Available at: https://madisongroup.com/determining-glass-transition-temperature-using-dma/ (Accessed: 12 December 2022).

Abdelmouleh, M. *et al.* (2005) 'Modification of cellulose fibers with functionalized silanes: Effect of the fiber treatment on the mechanical performances of cellulose-thermoset composites', *Journal of Applied Polymer Science*, 98(3), pp. 974–984. doi: 10.1002/app.22133.

Aggarwal, P. and Dollimore, D. (1998) 'A thermal analysis investigation of partially hydrolyzed starch', *Thermochimica Acta*, 319(1–2), pp. 17–25. doi: 10.1016/s0040-6031(98)00355-4.

Ahmad, H. S., Ismail, H. and Rashid, A. A. (2017) 'Hardness and swelling behaviour of epoxidized natural rubber/recycled acrylonitrile-butadiene rubber (ENR 50/NBRr) blends', *AIP Conference Proceedings*, 1865(1). doi: 10.1063/1.4993344.

Ahmed, J. (2017) 'Thermal Properties of Polylactides and Stereocomplex', in *Glass Transition and Phase Transitions in Food and Biological Materials*. Wiley, pp. 261–279. doi: 10.1002/9781118935682.ch12.

Akhil, A. *et al.* (2015) *DOE/EPRI Electricity Storage Handbook in Collaboration with NRECA.* Albuquerque, NM, and Livermore, CA (United States). doi: 10.2172/1170618.

Al-Maamori, M. H. and Hamza, A. F. (2018) 'Effect of sulfur and Nano- carbon black on the mechanical properties of hard rubber', *Journal of University of Babylon, Engineering Sciences*, 26(2), pp. 127–134.

Alakrach, A. M. *et al.* (2018) 'The Effect of Epoxidized Natural Rubber as A Compatibilizer on the Properties of Standard Malaysian Rubber/Ethylene Propylene Diene Monomer Blends', *Journal of Physics: Conference Series*, 1019(1). doi: 10.1088/1742-6596/1019/1/012068.

Albouy, P. A. *et al.* (2012) 'A stroboscopic X-ray apparatus for the study of the kinetics of strain-induced crystallization in natural rubber', *Polymer*, 53(15), pp. 3313–3324. doi: 10.1016/j.polymer.2012.05.042.

Albouy, P. A. *et al.* (2014) 'The impact of strain-induced crystallization on strain during mechanical cycling of cross-linked natural rubber', *Polymer*, 55(16), pp. 4022–4031. doi: 10.1016/j.polymer.2014.06.034.

Ali, A. *et al.* (2023) 'Recent progress in energy harvesting systems for wearable technology', *Energy Strategy Reviews*, 49, p. 101124. doi: 10.1016/j.esr.2023.101124.

Anand, K. *et al.* (2018) 'Effect of starch nanocrystals on natural rubber latex vulcanizate properties', *Progress in Rubber, Plastics and Recycling Technology*, 34(2), pp. 75–87. doi: 10.1177/147776061803400201.

Aneke, M. and Wang, M. (2016) 'Energy storage technologies and real life applications – A state of the art review', *Applied Energy*, 179, pp. 350–377. doi: 10.1016/j.apenergy.2016.06.097.

Angellier, H. *et al.* (2004) 'Optimization of the preparation of aqueous suspensions of waxy maize starch nanocrystals using a response surface methodology', *Biomacromolecules*, 5(4), pp. 1545–1551. doi: 10.1021/bm049914u.

Angellier, H., Molina-Boisseau, S., Dufresne, A., *et al.* (2005) 'Processing and Structural Properties of Waxy Maize Starch Nanocrystals Reinforced Natural Rubber', *Macromolecules*, 38(9), pp. 3783–

3892. doi: 10.1021/ma0512399.

Angellier, H., Molina-Boisseau, S., Lebrun, L., *et al.* (2005) 'Processing and Structural Properties of Waxy Maize Starch Nanocrystals Reinforced Natural Rubber', *Macromolecules*, 38(9), pp. 3783–3792. doi: 10.1021/ma050054z.

Angellier, H., Putaux, J. L., *et al.* (2005) 'Starch nanocrystal fillers in an acrylic polymer matrix', *Macromolecular Symposia*, 221, pp. 95–104. doi: 10.1002/masy.200550310.

Angellier, H., Molina-Boisseau, S., Belgacem, M. N., *et al.* (2005) 'Surface chemical modification of waxy maize starch nanocrystals', *Langmuir*, 21(6), pp. 2425–2433. doi: 10.1021/la047530j.

Angellier, H. (2005) *Waxy maize starch nanocrystals for composite applications*. Joseph Fourier University. Available at: https://tel.archives-ouvertes.fr/tel-00010699.

Angellier, H., Molina-Boisseau, S. and Dufresne, A. (2005) 'Mechanical properties of waxy maize starch nanocrystal reinforced natural rubber', *Macromolecules*, 38(22), pp. 9161–9170. doi: 10.1021/ma0512399.

Angellier, H., Molina-Boisseau, S. and Dufresne, A. (2006) 'Waxy maize starch nanocrystals as filler in natural rubber', *Macromolecular Symposia*, 233, pp. 132–136. doi: 10.1002/masy.200690009.

Arcos-Vargas, A., Canca, D. and Nunez, F. (2021) *Mathematical Modelling of Contemporary Electricity Markets*. 1st edn, *Mathematical Modelling of Contemporary Electricity Markets*. 1st edn. Elsevier. doi: 10.1016/C2019-0-04254-9.

Ariyawiriyanan, W. *et al.* (2013) 'The mechanical properties of vulcanized deproteinized natural rubber', *Energy Procedia*, 34, pp. 728–733. doi: 10.1016/j.egypro.2013.06.806.

Arroyo, M., López-Manchado, M. A. and Herrero, B. (2003) 'Organo-montmorillonite as substitute of carbon black in natural rubber compounds', *Polymer*, 44(8), pp. 2447–2453. doi: 10.1016/S0032-3861(03)00090-9.

Asar, A. *et al.* (2022) 'Self-sensing shape memory polymer composites reinforced with functional textiles', *Composites Science and Technology*, 221, p. 109219. doi: 10.1016/j.compscitech.2021.109219.

Ashby, M. F. (2016) *Materials and Sustainable Development*. 2nd edn. Oxford: Elsevier. doi: 10.1016/C2014-0-01670-X.

ASTM D412 (2016) *Standard Test Methods for Vulcanized Rubber and Thermoplastic Elastomer-Tension*. West Conshohocken, PA: ASTM International. doi: 10.1520/D0412-16.2.

Aydoɬdu, Y. *et al.* (2016) 'The effects of thermal procedure on transformation temperature, crystal structure and microstructure of Cu-Al-Co shape memory alloy', *Journal of Physics: Conference Series*, 667(1). doi: 10.1088/1742-6596/667/1/012010.

De Azeredo, H. M. C. *et al.* (2014) *The use of biomass for packaging films and coatings*, *Advances in Biorefineries: Biomass and Waste Supply Chain Exploitation*. doi: 10.1533/9780857097385.2.819.

Babal, A. S. *et al.* (2015) 'Depression in glass transition temperature of multiwalled carbon nanotubes reinforced polycarbonate composites: effect of functionalization', *RSC Advances*, 5(54), pp. 43462–43472. doi: 10.1039/C5RA05825B.

Bahl, S. *et al.* (2020) 'Smart materials types, properties and applications: A review', *Materials Today: Proceedings*, 28, pp. 1302–1306. doi: 10.1016/j.matpr.2020.04.505.

Barik, S. K. and Rao, P. S. (2019) 'Shape Memory Alloys A Great Boon for the Industrial Application',

International Journal of Engineering Research & Technology, 7(03), pp. 1–7.

Bauer, T. *et al.* (2012) 'Thermal Energy Storage Materials and Systems', *Annual Review of Heat Transfer*, 15(15), pp. 131–177. doi: 10.1615/annualrevheattransfer.2012004651.

Behl, M., Razzaq, M. Y. and Lendlein, A. (2010) 'Multifunctional shape-memory polymers', *Advanced Materials*, 22(31), pp. 3388–3410. doi: 10.1002/adma.200904447.

Bel Haaj, S. *et al.* (2016) 'Starch nanocrystals and starch nanoparticles from waxy maize as nanoreinforcement: A comparative study', *Carbohydrate Polymers*, 143, pp. 310–317. doi: 10.1016/j.carbpol.2016.01.061.

Bespalko, S., Miranda, A. M. and Halychyi, O. (2018) 'Overview of the existing heat storage technologies: Sensible heat', *Acta Innovations*, (28), pp. 82–113. doi: 10.32933/ActaInnovations.28.8.

Biliaderis, C. G. *et al.* (1985) 'Thermal behavior of amylose-lipid complexes', *Carbohydrate Polymers*, 5(5), pp. 367–389. doi: 10.1016/0144-8617(85)90044-X.

Blackley, D. C. (1997) 'Latex-dipping processes', in *Polymer Latices*. 2nd edn. Chapman & Hall, pp. 155–228.

Bloemendal, M. and Olsthoorn, T. N. (2018) 'The effect of a density gradient in groundwater on ATES system efficiency and subsurface space use', *Advances in Geosciences*, 45, pp. 85–103. doi: 10.5194/adgeo-45-85-2018.

Bokobza, L. (2007) 'Multiwall carbon nanotube elastomeric composites: A review', *Polymer*, 48(17), pp. 4907–4920. doi: 10.1016/j.polymer.2007.06.046.

Boonkerd, K., Deeprasertkul, C. and Boonsomwong, K. (2016) 'Effect of sulfur to accelerator ratio on crosslink structure, reversion, and strength in natural rubber', *Rubber Chemistry and Technology*, 89(3), pp. 450–464. doi: 10.5254/rct.16.85963.

Bouthegourd, E. *et al.* (2011) 'Natural rubber latex/potato starch nanocrystal nanocomposites: Correlation morphology/electrical properties', *Materials Letters*, 65(23–24), pp. 3615–3617. doi: 10.1016/j.matlet.2011.07.069.

Brostowitz, N. R., Weiss, R. A. and Cavicchi, K. A. (2014) 'Facile fabrication of a shape memory polymer by swelling cross-linked natural rubber with stearic acid', *ACS Macro Letters*, 3(4), pp. 374–377. doi: 10.1021/mz500131r.

Brown, G. M. and Ellyin, F. (2005) 'Assessing the predictive capability of two-phase models for the mechanical behavior of alumina/epoxy nanocomposites', *Journal of Applied Polymer Science*, 98(2), pp. 869–879. doi: 10.1002/app.22188.

Bülbül, Ş. (2020) 'Improving the crosslink density and the mechanical properties after vulcanization for an iron oxide layer (scale) and SBR/rubber masterbatch', *Materiali in Tehnologije*, 54(1), pp. 71–78. doi: 10.17222/mit.2019.129.

Buléon, A. *et al.* (1997) 'Starches from A to C: Chlamydomonas reinhardtii as a model microbial system to investigate the biosynthesis of the plant amylopectin crystal', *Plant Physiology*, 115(3), pp. 949–957. doi: 10.1104/pp.115.3.949.

Burfield, D. R., Lim, K. -L and Law, K. -S (1984) 'Epoxidation of natural rubber latices: Methods of preparation and properties of modified rubbers', *Journal of Applied Polymer Science*, 29(5), pp. 1661–1673. doi: 10.1002/app.1984.070290520.

C.S.L Baker and I.R Gelling (1989) 'Epoxidized natural rubber', *NR technology*, 20(3), pp. 56–63. doi:

10.1007/978-94-009-3435-1_3.

Cairns, P. *et al.* (1997) 'Determination of the polymorphic composition of smooth pea starch', *Carbohydrate Polymers*, 32(3–4), pp. 275–282. doi: 10.1016/S0144-8617(96)00115-4.

Le Cam, J. B. (2017) 'Energy storage due to strain-induced crystallization in natural rubber: The physical origin of the mechanical hysteresis', *Polymer*, 127, pp. 166–173. doi: 10.1016/j.polymer.2017.08.059.

Candau, N. *et al.* (2019) 'Characteristic-time of strain induced crystallization of crosslinked natural rubber To cite this version : HAL Id : hal-00743306'.

Candau, N. *et al.* (2023) 'Elastocaloric Waste/Natural Rubber Materials with Various Crosslink Densities', *Polymers*, 15(11), p. 2566. doi: 10.3390/polym15112566.

Cao, F. and Jana, S. (2007) 'Nanoclay-tethered shape memory polyurethane nanocomposites', *Polymer*, 48(13), pp. 3790–3800. doi: 10.1016/j.polymer.2007.04.027.

Carleo, F. *et al.* (2020) 'Modeling the full time-dependent phenomenology of filled rubber for use in anti-vibration design', *Polymers*, 12(4), pp. 1–16. doi: 10.3390/POLYM12040841.

Carretero-Gonzalez, J. *et al.* (2008) 'Real-time crystallization of organoclay nanoparticle filled natural rubber under stretching', *Macromolecules*, 41(7), pp. 2295–2298. doi: 10.1021/ma7028506.

Carretero-González, J. *et al.* (2008) 'Effect of nanoclay on natural rubber microstructure', *Macromolecules*, 41(18), pp. 6763–6772. doi: 10.1021/ma800893x.

Cataldo, F. (1992) 'Chlorination and bromination of epoxidized natural rubber (ENR)', *Journal of Applied Polymer Science*, 45(10), pp. 1705–1710. doi: 10.1002/app.1992.070451003.

Cataldo, F. (2002) 'Preparation of silica-based rubber compounds without the use of a silane coupling agent through the use of epoxidized natural rubber', *Macromolecular Materials and Engineering*, 287(5), pp. 348–352. doi: 10.1002/1439-2054(20020501)287:5<348::AID-MAME348>3.0.CO;2-1.

Cavicchi, K. A. (2015) 'Shape Memory Polymers from Blends of Elastomers and Small Molecule Additives', *Macromolecular Symposia*, 358(1), pp. 194–201. doi: 10.1002/masy.201500064.

Chang, Y. *et al.* (2006) 'Thermomechanical properties and shape memory effect of epoxidized natural rubber crosslinked by 3-amino-1,2,4-triazole', *Polym Int*, 56(July 2007), pp. 694–698. doi: 10.1002/pi.2203.

Chen, G. *et al.* (2008) 'Simultaneous reinforcing and toughening: New nanocomposites of waterborne polyurethane filled with low loading level of starch nanocrystals', *Polymer*, 49(7), pp. 1860–1870. doi: 10.1016/j.polymer.2008.02.020.

Chen, H. *et al.* (2009) 'Progress in electrical energy storage system: A critical review', *Progress in Natural Science*, 19(3), pp. 291–312. doi: 10.1016/j.pnsc.2008.07.014.

Chen, Q. J. *et al.* (2019) 'The preparation and characterization of nanocomposite film reinforced by modified cellulose nanocrystals', *International Journal of Biological Macromolecules*, 132, pp. 1155–1162. doi: 10.1016/j.ijbiomac.2019.04.063.

Chen, Y. *et al.* (2008) 'Comparative study on the films of poly(vinyl alcohol)/pea starch nanocrystals and poly(vinyl alcohol)/native pea starch', *Carbohydrate Polymers*, 73(1), pp. 8–17. doi: 10.1016/j.carbpol.2007.10.015.

Cho, J. W. *et al.* (2004) 'Improved mechanical properties of shape-memory polyurethane block

copolymers through the control of the soft-segment arrangement', *Journal of Applied Polymer Science*, 93(5), pp. 2410–2415. doi: 10.1002/app.20747.

Chuayjuljit, S. *et al.* (2006) 'Oil resistance and physical properties of in situ epoxidized natural rubber from high ammonia concentrated latex', *Journal of Applied Polymer Science*, 100(5), pp. 3948–3955. doi: 10.1002/app.22998.

Chuayjuljit, S., Mungmeechai, P. and Boonmahitthisud, A. (2017) 'Mechanical properties, thermal behaviors and oil resistance of epoxidized natural rubber/multiwalled carbon nanotube nanocomposites prepared via in situ epoxidation', *Journal of Elastomers & Plastics*, 49(2), pp. 99–119. doi: 10.1177/0095244316639634.

Clark, G. L. *et al.* (1940) 'Hysteresis in Crystallization of Stretched Vulcanized Rubber from X-Ray Data Correlation with Stress-Strain Behavior and Resilience', *Industrial & Engineering Chemistry*, 32(11), pp. 1474–1477. doi: 10.1021/ie50371a016.

Colonna, P. and Buleon, A. (2009) 'Thermal transitions of starches', in *Starches: Characterization, Properties, and Applications*. 1st edn. Boca Raton: CRC Press, pp. 71–103. doi: https://doi.org/10.1201/9781420080247.

Cooper, C. B. *et al.* (2021) 'High Energy Density Shape Memory Polymers Using Strain-Induced Supramolecular Nanostructures', *ACS Central Science*, 7(10), pp. 1657–1667. doi: 10.1021/acscentsci.1c00829.

Coran, A. Y. (2013) *Vulcanization*, *The Science and Technology of Rubber*. doi: 10.1016/B978-0-12-394584-6.00007-8.

Le Corre, D. *et al.* (2012) 'Optimization of the batch preparation of starch nanocrystals to reach daily time-scale', *Starch/Staerke*, 64(6), pp. 489–496. doi: 10.1002/star.201100145.

Le Corre, D., Bras, J. and Dufresne, A. (2010) 'Starch nanoparticles: A review', *Biomacromolecules*, 11(5), pp. 1139–1153. doi: 10.1021/bm901428y.

Correa-Pinilla, D. E. *et al.* (2022) 'Agroecological and South American leaf blight escape zones for rubber cultivation in Colombia', *Agronomy Journal*, 114(5), pp. 2830–2844. doi: 10.1002/agj2.21068.

Cramm, J. *et al.* (2011) *Investigating the feasibility of Implementing Pavegen energy - harvesting piezoelectric floor tiles in the new SUB*. British Columbia. doi: 10.14288/1.0108404.

Crəciunescu, C. and Ercuta, A. (2015) 'Modulated interaction in double-layer shape memory-based micro-designed actuators', *Science and Technology of Advanced Materials*, 16(6). doi: 10.1088/1468-6996/16/6/065003.

Dai, L. *et al.* (2021) 'Preparation and characterization of cross-linked starch nanocrystals and self-reinforced starch-based nanocomposite films', *International Journal of Biological Macromolecules*, 181, pp. 868–876. doi: 10.1016/j.ijbiomac.2021.04.020.

Danwanichakul, D. *et al.* (2014) 'Extraction of protein from skim natural rubber latex using PEG as a surfactant via low speed centrifugation and continuous flow', *Journal of Applied Polymer Science*, 131(4), pp. 1–9. doi: 10.1002/app.39900.

Darji, D. *et al.* (2020) 'Epoxidised natural rubber (ENR) latex: an alternative raw material for latex dipped products', *Journal of Rubber Research*, 23(4), pp. 375–385. doi: 10.1007/s42464-020-00065-5.

Darko, C. (2022) 'The link between swelling ratios and physical properties of EPDM rubber compound having different oil amounts', *Journal of Polymer Research*, 29(8). doi: 10.1007/s10965-022-03179-z.

Das, A., Basu, D. and Heinrich, G. (2020) 'Encyclopedia of Polymeric Nanomaterials', *Encyclopedia of Polymeric Nanomaterials*, pp. 1–5. doi: 10.1007/978-3-642-36199-9.

Dasaesamoh, A., Osotchan, T. and Subannajui, K. (2019) 'Mechanical strength of natural rubber filled fly ash', *IOP Conference Series: Materials Science and Engineering*, 625(1). doi: 10.1088/1757-899X/625/1/012013.

Davies, C. K. L. *et al.* (1983) 'Strain crystallization in random copolymers produced by epoxidation of cis 1,4-polyisoprene', *Polymer*, 24(1), pp. 107–113. doi: 10.1016/0032-3861(83)90090-3.

Davino, D. (2021) 'Smart Materials and Devices for Energy Harvesting', *Materials*, 14(16), p. 4738. doi: 10.3390/ma14164738.

Dehghani-Sanij, A. R. *et al.* (2019) 'Study of energy storage systems and environmental challenges of batteries', *Renewable and Sustainable Energy Reviews*, 104(January), pp. 192–208. doi: 10.1016/j.rser.2019.01.023.

Dhanasekaran, R. *et al.* (2018) 'Shape Memory Materials for Bio-medical and Aerospace Applications', *Materials Today: Proceedings*, 5(10), pp. 21427–21435. doi: 10.1016/j.matpr.2018.6.551.

Diani, J., Fayolle, B. and Gilormini, P. (2009) 'A review on the Mullins effect', *European Polymer Journal*, 45(3), pp. 601–612. doi: 10.1016/j.eurpolymj.2008.11.017.

Dieu, T. V. *et al.* (2023) 'Review: Natural rubber – Improvement of properties', *Vietnam Journal of Chemistry*, 61(3), pp. 269–283. doi: 10.1002/vjch.202200225.

Dome, K. *et al.* (2020) 'Changes in the Crystallinity Degree of Starch Having Different Types of Crystal Structure after Mechanical Pretreatment', *Polymers*, 12(3), p. 641. doi: 10.3390/polym12030641.

Dufresne, A. (2000) 'Plasticized Starch/Tunicin Whiskers Nanocomposites. 1. Structural Analysis', pp. 8344–8353.

Dufresne, A. (2006) 'Comparing the mechanical properties of high performances polymer nanocomposites from biological sources', *Journal of Nanoscience and Nanotechnology*, 6(2), pp. 322–330. doi: 10.1166/jnn.2006.906.

Dufresne, A. (2008a) 'Polysaccharide nano crystal reinforced nanocomposites', *Canadian Journal of Chemistry*, 86(6), pp. 484–494. doi: 10.1139/v07-152.

Dufresne, A. (2008b) 'Polysaccharide nanocrystal reinforced nanocomposites', *Canadian Journal of Chemistry*, 86(6), pp. 484–494. doi: 10.1139/V07-152.

Dufresne, A. (2010) 'Natural Rubber Green Nanocomposites', in Thomas, S. and Stephen, R. (eds) *Rubber Nanocomposites: Preparation, Properties and Applications*. 1st edn. Wiley, pp. 113–145. doi: 10.1002/9780470823477.

Dufresne, A. and Cavaillé, J. Y. (1998) 'Clustering and percolation effects in microcrystalline starch-reinforced thermoplastic', *Journal of Polymer Science, Part B: Polymer Physics*, 36(12), pp. 2211–2224. doi: 10.1002/(SICI)1099-0488(19980915)36:12<2211::AID-POLB18>3.0.CO;2-2.

Dye, D. (2015) 'Shape memory alloys: Towards practical actuators', *Nature Materials*, 14(8), pp. 760–761. doi: 10.1038/nmat4362.

Evans, I. D. and Haisman, D. R. (1982) 'The Effect of Solutes on the Gelatinization Temperature Range of Potato Starch', *Starch - Stärke*, 34(7), pp. 224–231. doi: 10.1002/star.19820340704.

Fatimah Rubaizah, M. R. *et al.* (2018) 'Specialty latex material for sustainable product applications',

Rubber World, 259(2), pp. 32–36.

Favier, V. *et al.* (1997) 'Mechanical Percolation in Cellulose Whisker Nanocomposites', *POLYMER ENGINEERING AND SCIENCE*, 37(10), pp. 1732–1739.

Femina, G. *et al.* (2023) 'X-ray diffraction study of strain-induced crystallization of hydrogenated nitrile-butadiene rubbers: Effect of crosslink density', *Polymer*, 271(January), p. 125782. doi: 10.1016/j.polymer.2023.125782.

Flanigan, C. M. *et al.* (2012) 'Comparative study of silica, carbon black and novel fillers in tread compounds', *Rubber World*.

Flory, P. J. (1947) 'Thermodynamics of Crystallization in High Polymers. I. Crystallization Induced by Stretching', *The Journal of Chemical Physics*, 15(6), pp. 397–408. doi: 10.1063/1.1746537.

Flory, P. J. and Rehner, J. (1943) 'Statistical mechanics of cross-linked polymer networks II. Swelling', *The Journal of Chemical Physics*, 11(11), pp. 521–526. doi: 10.1063/1.1723792.

Fried, J. R. (2014) 'Polymer Structure', in *Polymer Science and Technology*. 3rd edn. New Jersey: Prentice Hall, p. 86.

Fu, W. *et al.* (2019) 'Mechanical Properties and Mullins Effect in Natural Rubber Reinforced by Grafted Carbon Black', *Advances in Polymer Technology*, 2019, pp. 1–11. doi: 10.1155/2019/4523696.

Le Gac, P. Y. *et al.* (2014) 'Role of strain induced crystallization and oxidative crosslinking in fracture properties of rubbers', *Polymer*, 55(10), pp. 2535–2542. doi: 10.1016/j.polymer.2014.03.023.

Gao, Y. J. S. *et al.* (2014) 'Reinforcement of natural rubber latex film by starch nanocrystal', *Applied Mechanics and Materials*, 543–547, pp. 3886–3891. doi: 10.4028/www.scientific.net/AMM.543-547.3886.

Geethamma, V. G. and Sampath, V. (2019) 'Rubber as an Aid to Teach Thermodynamics', *Resonance*, 24(2), pp. 217–238. doi: 10.1007/s12045-019-0772-x.

Gent, A. N. and Zhang, L. Q. (2002) 'Strain-induced crystallization and strength of rubber', *Rubber Chemistry and Technology*, 75(5), pp. 923–933. doi: 10.5254/1.3547692.

GlobeNewswire (2021) 'Global Starch Market to Reach 160.3 Million Metric Tons by 2026', *GLOBE NEWSWIRE*, 12 July. Available at: https://www.globenewswire.com/news-release/2021/07/12/2261007/0/en/Global-Starch-Market-to-Reach-160-3-Million-Metric-Tons-by-2026.html.

González-Jiménez, A. *et al.* (2022) 'Shape-Memory Composites Based on Ionic Elastomers', *Polymers*, 14(6), p. 1230. doi: 10.3390/polym14061230.

González, K. *et al.* (2015) 'Starch and cellulose nanocrystals together into thermoplastic starch bionanocomposites', *Carbohydrate Polymers*, 117, pp. 83–90. doi: 10.1016/j.carbpol.2014.09.055.

Gopalan Nair, K. and Dufresne, A. (2003) 'Crab shell chitin whisker reinforced natural rubber nanocomposites. 1. Processing and swelling behavior', *Biomacromolecules*, 4(3), pp. 657–665. doi: 10.1021/bm020127b.

Gopinath, S. *et al.* (2021) 'Shape-Memory Polymer Nanocomposites of Poly(ϵ-caprolactone) with the Polystyrene- block-polybutadiene- block-polystyrene-tri- block Copolymer Encapsulated with Metal Oxides', *ACS Omega*, 6(9), pp. 6261–6273. doi: 10.1021/acsomega.0c05839.

Gravity power (2014) *Grid scale energy storage*, *Gravity Power*. Available at:

https://www.gravitypower.net/ (Accessed: 20 September 2022).

Groves, R. and Routh, A. F. (2017) 'Film deposition and consolidation during thin glove coagulant dipping', *Journal of Polymer Science, Part B: Polymer Physics*, 55(22), pp. 1633–1648. doi: 10.1002/polb.24290.

Grundy, A. (2021) 'IEA: Global power demand to jump 4.5% as renewables remain "largely immune" to COVID-19 impacts', *Current*, 21 April. Available at: https://www.current-news.co.uk/news/iea-global-power-demand-to-jump-4-5-as-renewables-remain-largely-immune-to-covid-19-impacts.

Guney, M. S. and Tepe, Y. (2017) 'Classification and assessment of energy storage systems', *Renewable and Sustainable Energy Reviews*, 75(February 2016), pp. 1187–1197. doi: 10.1016/j.rser.2016.11.102.

H. Alenius, K. Turjanmaa, T, P. (2016) 'Natural rubber latex allergy', *Disease-a-Month*, 62(1), pp. 5–17. doi: 10.1016/j.disamonth.2015.11.002.

Habib, N. A. *et al.* (2021) 'Crosslinking Density Characteristics of a Nanocomposite Elastomer', *Journal of Physics: Conference Series*, 1795(1). doi: 10.1088/1742-6596/1795/1/012072.

Haris, N. I. N. *et al.* (2022) 'Dynamic mechanical properties of natural fiber reinforced hybrid polymer composites: a review', *Journal of Materials Research and Technology*, 19, pp. 167–182. doi: 10.1016/j.jmrt.2022.04.155.

Hashim, A. S. and Ong, S. K. (2017) 'Natural Rubber and its Derivatives', *Elastomers*. doi: 10.5772/intechopen.69661.

Hassanzadeh-Aghdam, M. K., Ansari, R. and Mahmoodi, M. J. (2019) 'Thermo-mechanical properties of shape memory polymer nanocomposites reinforced by carbon nanotubes', *Mechanics of Materials*, 129, pp. 80–98. doi: 10.1016/j.mechmat.2018.11.009.

Heard, B. P. *et al.* (2017) 'Burden of proof: A comprehensive review of the feasibility of 100% renewable-electricity systems', *Renewable and Sustainable Energy Reviews*, 76(September 2016), pp. 1122–1133. doi: 10.1016/j.rser.2017.03.114.

Hemsri, S. *et al.* (2015) 'Improvement of toughness and water resistance of bioplastic based on wheat gluten using epoxidized natural rubber', *IOP Conference Series: Materials Science and Engineering*, 87(1). doi: 10.1088/1757-899X/87/1/012049.

Heng, T. S. and Joo, G. K. (2017) 'Crop Systems', *Encyclopedia of Applied Plant Sciences*. 2nd edn. Elsevier.

Henry, F. *et al.* (2013) 'The effect of agglomeration on the emission of particles from nanopowders flow', *Chemical Engineering Transactions*, 31, pp. 811–816. doi: 10.3303/CET1331136.

Henze, V. (2021) 'Global Energy Storage Market Set to Hit One Terawatt-Hour by 2030', *BloombergNEF*, 15 November. Available at: https://about.bnef.com/blog/global-energy-storage-market-set-to-hit-one-terawatt-hour-by-2030/.

Hernández, M. *et al.* (2013) 'Structure and segmental dynamics relationship in natural rubber/layered silicate nanocomposites during uniaxial deformation', *Macromolecules*, 46(8), pp. 3176–3182. doi: 10.1021/ma4002353.

Heuwers, B. *et al.* (2012) 'Stress-induced melting of crystals in natural rubber: A new way to tailor the transition temperature of shape memory polymers', *Macromolecular Rapid Communications*, 33(18), pp. 1517–1522. doi: 10.1002/marc.201200313.

Heuwers, B. *et al.* (2013) 'Shape-memory natural rubber: An exceptional material for strain and

energy storage', *Macromolecular Chemistry and Physics*, 214(8), pp. 912–923. doi: 10.1002/macp.201200649.

Hiemenz, P. C. and Lodge, T. P. (2007) 'Networks, Gels and Rubber Elasticity', in *Polymer Chemistry*. 2nd edn. Boca Raton: Taylor & Francis, pp. 381–418. doi: https://doi.org/10.1201/9781420018271.

Hiranobe, C. T. *et al.* (2021) 'Cross-linked density determination of natural rubber compounds by different analytical techniques', *Materials Research*, 24(S1), pp. 1–9. doi: 10.1590/1980-5373-MR-2021-0041.

Ho, C. C. and Khew, M. C. (2000) 'Low Glass Transition Temperature (T g) Rubber Latex Film Formation Studied by Atomic Force Microscopy', *Langmuir*, 16(6), pp. 2436–2449. doi: 10.1021/la990192f.

Hossain, E. *et al.* (2020) 'A Comprehensive Review on Energy Storage Systems: Types, Comparison, Current Scenario, Applications, Barriers, and Potential Solutions, Policies, and Future Prospects', *Energies*, 13(14), p. 3651. doi: 10.3390/en13143651.

Hua, Z. *et al.* (2008) 'Structure and Properties of Starch Nanocrystal-Reinforced Soy Protein Plastics', *Polymers and Polymer Composites*, 16(2), pp. 101–113. doi: 10.1002/pc.

Huang, W. M. (1998) *Shape memory alloys and their application to actuators for deployable structures*. University of Cambridge.

Huang, W. M. *et al.* (2010) 'Thermo-moisture responsive polyurethane shape-memory polymer and composites: A review', *Journal of Materials Chemistry*, 20(17), pp. 3367–3381. doi: 10.1039/b922943d.

Van Humbeeck, J. and Kustov, S. (2005) 'Active and passive damping of noise and vibrations through shape memory alloys: Applications and mechanisms', *Smart Materials and Structures*, 14(5). doi: 10.1088/0964-1726/14/5/001.

Huneau, B. (2011) 'Strain-Induced Crystallization of Natural Rubber : a Review of X-ray Diffraction Investigations To cite this version : HAL Id : hal-01007326 STRAIN-INDUCED CRYSTALLIZATION OF NATURAL RUBBER : A REVIEW OF X-RAY DIFFRACTION INVESTIGATIONS', *Rubber chemistry and technology*, 84, p. 425–452.

Ibrahim, M. A. (2022) 'Synthetic polymers', in *Synthetic Engineering Materials and Nanotechnology*. 1st edn. Amsterdam: Elsevier, pp. 33–58. doi: https://doi.org/10.1016/C2020-0-01204-1.

Imberty, A. and Perez, S. (1988) 'A revisit to the three-dimensional structure of B-type starch', *Biopolymers*, 27(8), pp. 1205–1221. doi: 10.1002/bip.360270803.

IRENA (2020) *Global Renewables Outlook 2020: Summary*. Available at: www.irena.org.

Jahid, M. A., Hu, J. and Zhuo, H. (2018) *Stimuli-responsive polymers in coating and laminating for functional textile*, *Smart Textile Coatings and Laminates*. Elsevier Ltd. doi: 10.1016/B978-0-08-102428-7.00007-9.

Jenkins, P. J. *et al.* (1994) 'In situ simultaneous small and wide angle x-ray scattering: A new technique to study starch gelatinization', *Journal of Polymer Science Part B: Polymer Physics*, 32(8), pp. 1579–1583. doi: 10.1002/polb.1994.090320829.

Jeong, H. M., Ahn, B. K. and Kim, B. K. (2001) 'Miscibility and shape memory effect of thermoplastic polyurethane blends with phenoxy resin', *European Polymer Journal*, 37(11), pp. 2245–2252. doi: 10.1016/S0014-3057(01)00123-9.

Jiang, D. D. *et al.* (1999) 'TGA/FTIR studies on the thermal degradation of some polymeric sulfonic

and phosphonic acids and their sodium salts', *Polymer Degradation and Stability*, 63(3), pp. 423–434. doi: 10.1016/S0141-3910(98)00123-2.

Jimenez, G. and Jana, S. (2009) 'Composites of Carbon Nanofibers and Thermoplastic Polyurethanes With Shape-Memory Properties Prepared by Chaotic Mixing', *POLYMER ENGINEERING AND SCIENCE*, 49(10), pp. 2020–2030. doi: 10.1002/pen.21442.

Joseph, A. *et al.* (2015) 'Current status of sulphur vulcanization and devulcanization chemistry: process of vulcanization', *Rubber Science*, 28(1), pp. 82–121.

Júnior, H. L. O. *et al.* (2022) 'Smart Fabric Textiles: Recent Advances and Challenges', *Textiles*, 2(4), pp. 582–605. doi: 10.3390/textiles2040034.

Kaang, S. *et al.* (2006) 'A test method to measure fatigue crack growth rate of rubbery materials', *Polymer Testing*, 25(3), pp. 347–352. doi: 10.1016/j.polymertesting.2005.12.005.

Kaewsakul, W. *et al.* (2021) 'Natural rubber and epoxidized natural rubber in combination with silica fillers for low rolling resistance tires', in *Chemistry, Manufacture, and Applications of Natural Rubber*. 2nd edn. Elsevier, pp. 247–316. doi: 10.1016/B978-0-12-818843-9.00009-6.

Kalita, H. (2018) 'Shape Memory Polymers', in *Shape Memory Polymers: Theory and Application*. 1st edn. Berlin: Walter de Gruyter, pp. 1–39.

Kalita, H. and Karak, N. (2014) 'Bio-Based Hyperbranched Polyurethane/Multi-WalledCarbon Nanotube Nanocomposites as ShapeMemory Materials', *Polymers and Polymer Composites*, 35(4), pp. 636–643. doi: 10.1002/pc.22705.

Kang, H. *et al.* (2017) 'Fabrication of graphene/natural rubber nanocomposites with high dynamic properties through convenient mechanical mixing', *Composites Part B: Engineering*, 112, pp. 1–7. doi: 10.1016/j.compositesb.2016.12.035.

Katzenberg, F., Heuwers, B. and Tiller, J. C. (2011) 'Superheated rubber for cold storage', *Advanced Materials*, 23(16), pp. 1909–1911. doi: 10.1002/adma.201100408.

Kausar, A. (2022) 'Shape memory polymer/graphene nanocomposites: State-of-the-art', *e-Polymers*, 22(1), pp. 165–181. doi: 10.1515/epoly-2022-0024.

Khadivi, P. *et al.* (2019) 'Fabrication of microphase-separated polyurethane/cellulose nanocrystal nanocomposites with irregular mechanical and shape memory properties', *Applied Physics A: Materials Science and Processing*, 125(11), pp. 1–10. doi: 10.1007/s00339-019-3082-y.

Khan, Ibrahim, Saeed, K. and Khan, Idrees (2019) 'Nanoparticles: Properties, applications and toxicities', *Arabian Journal of Chemistry*, 12(7), pp. 908–931. doi: 10.1016/j.arabjc.2017.05.011.

Kim, B. K. *et al.* (2000) 'Shape-Memory Behavior of Segmented Polyurethanes with an Amorphous Reversible Phase: The Effect of Block Length and Content', *Journal of Polymer Science, Part B: Polymer Physics*, 38(20), pp. 2652–2657. doi: 10.1002/1099-0488(20001015)38.

Kim, B. K., Lee, S. Y. and Xu, M. (1996) 'Polyurethanes having shape memory effects', *Polymer*, 37(26), pp. 5781–5793. doi: 10.1016/S0032-3861(96)00442-9.

Kim, D. Y. *et al.* (2020) 'Correlation between the crosslink characteristics and mechanical properties of natural rubber compound via accelerators and reinforcement', *Polymers*, 12(9), pp. 1–14. doi: 10.3390/polym12092020.

Kim, H. Y. *et al.* (2012) 'Characterization of nanoparticles prepared by acid hydrolysis of various starches', *Starch/Staerke*, 64(5), pp. 367–373. doi: 10.1002/star.201100105.

Kim, J. Y., Park, D. J. and Lim, S. T. (2008) 'Fragmentation of waxy rice starch granules by enzymatic hydrolysis', *Cereal Chemistry*, 85(2), pp. 182–187. doi: 10.1094/CCHEM-85-2-0182.

Kim, S. Y., Noh, Y. J. and Yu, J. (2014) 'Improved thermal conductivity of polymeric composites fabricated by solvent-free processing for the enhanced dispersion of nanofillers and a theoretical approach for composites containing multiple heterogeneities and geometrized nanofillers', *Composites Science and Technology*, 101, pp. 79–85. doi: 10.1016/j.compscitech.2014.06.028.

Kinasih, N. A., Fathurrohman, M. I. and Winarto, D. A. (2017) 'Swelling behaviour in n-pentane and mechanical properties of epoxidized natural rubber with different epoxide content', *IOP Conference Series: Materials Science and Engineering*, 223(1). doi: 10.1088/1757-899X/223/1/012002.

Kleinhans, G. and Heidenhain, F. (1986) 'Actively moving polymers', *Kunststoffe*, 76, pp. 1069–1072.

Koerner, H. *et al.* (2004) 'Remotely actuated polymer nanocomposites - Stress-recovery of carbon-nanotube-filled thermoplastic elastomers', *Nature Materials*, 3(2), pp. 115–120. doi: 10.1038/nmat1059.

Kojima, M. (1981) 'Stress whitening in crystalline propylene-ethylene block copolymers', *Journal of Macromolecular Science, Part B*, 19(3), pp. 523–541. doi: 10.1080/00222348108015316.

KÖK, M. *et al.* (2019) 'Akıllı Malzemeler üzerine derleme: araştırmalar ve uygulamaları', *El-Cezeri Fen ve Mühendislik Dergisi*, (September). doi: 10.31202/ecjse.562177.

Kolesov, I. *et al.* (2009) 'Kinetics and dynamics of thermally-induced shape-memory behaviour of crosslinked short-chain branched polyethylenes', *Polymer*, 50(23), pp. 5490–5498.

Košíková, B. *et al.* (2007) 'Role of lignin filler in stabilization of natural rubber–based composites', *Journal of Applied Polymer Science*, 103(2), pp. 1226–1231. doi: 10.1002/app.24530.

Kow, Y. Y., Chai, A. B. and Ho, J. H. (2020a) 'Development of shape memory natural rubber through prevulcanisation method', *IOP Conference Series: Earth and Environmental Science*, 442(1). doi: 10.1088/1755-1315/442/1/012009.

Kow, Y. Y., Chai, A. B. and Ho, J. H. (2020b) 'Relationships between swelling temperature and shape memory properties of palmitic acid-based shape memory natural rubber', *Journal of Rubber Research*, 23(1), pp. 13–22. doi: 10.1007/s42464-019-00031-w.

Kow, Y. Y., Chai, A. B. and Ho, J. H. (2020c) 'The effect of palmitic acid loadings on the shape memory cycle of shape memory natural rubber', *IOP Conference Series: Earth and Environmental Science*, 442(1). doi: 10.1088/1755-1315/442/1/012010.

Krajovic, D. M. and Anthamatten, M. (2021) 'Melt-Processable Shape-Memory Elastomers Containing Bisurea Segments', *ACS Applied Polymer Materials*, 3(4), pp. 2082–2087. doi: 10.1021/acsapm.1c00129.

Kristo, E. and Biliaderis, C. G. (2007) 'Physical properties of starch nanocrystal-reinforced pullulan films', *Carbohydrate Polymers*, 68(1), pp. 146–158. doi: 10.1016/j.carbpol.2006.07.021.

Krukanont, P. and Prasertsan, S. (2004) 'Geographical distribution of biomass and potential sites of rubber wood fired power plants in Southern Thailand', *Biomass and Bioenergy*, 26(1), pp. 47–59. doi: 10.1016/S0961-9534(03)00060-6.

Kruželák, J., Sýkora, R. and Hudec, I. (2016) 'Sulphur and peroxide vulcanisation of rubber compounds-overview', *Chemical Papers*, 70(12), pp. 1533–1555. doi: 10.1515/chempap-2016-0093.

Kumar, A. P. *et al.* (2009) 'Nanoscale particles for polymer degradation and stabilization-Trends and future perspectives', *Progress in Polymer Science (Oxford)*, 34(6), pp. 479–515. doi:

10.1016/j.progpolymsci.2009.01.002.

Lacayo-pineda, J. (2015) *Encyclopedia of Polymeric Nanomaterials*, *Encyclopedia of Polymeric Nanomaterials*. doi: 10.1007/978-3-642-29648-2.

Laghmach, R. *et al.* (2015) 'Phase field modelling of strain induced crystal growth in an elastic matrix', *Journal of Chemical Physics*, 142(24). doi: 10.1063/1.4923226.

Lan, X. *et al.* (2009) 'Fiber reinforced shape-memory polymer composite and its application in a deployable hinge', *Smart Materials and Structures*, 18(2). doi: 10.1088/0964-1726/18/2/024002.

Lazim, M. *et al.* (2015) 'Production of Hollow Toy Product From Radiation Prevulcanized Natural', p. 6. Available at: https://inis.iaea.org/collection/NCLCollectionStore/_Public/45/102/45102268.pdf.

Lecorre, D., Bras, J. and Dufresne, A. (2011a) 'Ceramic membrane filtration for isolating starch nanocrystals', *Carbohydrate Polymers*, 86(4), pp. 1565–1572. doi: 10.1016/j.carbpol.2011.06.064.

Lecorre, D., Bras, J. and Dufresne, A. (2011b) 'Evidence of micro- and nanoscaled particles during starch nanocrystals preparation and their isolation', *Biomacromolecules*, 12(8), pp. 3039–3046. doi: 10.1021/bm200673n.

Lecorre, D., Bras, J. and Dufresne, A. (2012) 'Influence of native starch's properties on starch nanocrystals thermal properties', *Carbohydrate Polymers*, 87(1), pp. 658–666. doi: 10.1016/j.carbpol.2011.08.042.

LeCorre, D., Bras, J. and Dufresne, A. (2011) 'Influence of botanic origin and amylose content on the morphology of starch nanocrystals', *Journal of Nanoparticle Research*, 13(12), pp. 7193–7208. doi: 10.1007/s11051-011-0634-2.

Lecorre, D. S., Bras, J. and Dufresne, A. (2012) 'Influence of the botanic origin of starch nanocrystals on the morphological and mechanical properties of natural rubber nanocomposites', *Macromolecular Materials and Engineering*, 297(10), pp. 969–978. doi: 10.1002/mame.201100317.

LeCorre, D. S., Bras, J. and Dufresne, A. (2012) 'Influence of the Botanic Origin of Starch Nanocrystals on the Morphological and Mechanical Properties of Natural Rubber Nanocomposites', *Macromolecular Materials and Engineering*, 297(10), pp. 969–978. doi: 10.1002/mame.201100317.

Lee, K. S. (2010) 'A review on concepts, applications, and models of aquifer thermal energy storage systems', *Energies*, 3(6), pp. 1320–1334. doi: 10.3390/en3061320.

Lendlein, A. and Langer, R. (2002) 'Biodegradable, elastic shape-memory polymers for potential biomedical applications', *Science*, 296(5573), pp. 1673–1676. doi: 10.1126/science.1066102.

Leng, J. *et al.* (2009) 'Shape-memory polymers - A class of novel smart materials', *MRS Bulletin*, 34(11), pp. 848–855. doi: 10.1557/mrs2009.235.

Li, H. *et al.* (2018) 'Relations between chain-length distribution, molecular size, and amylose content of rice starches', *International Journal of Biological Macromolecules*, 120, pp. 2017–2025. doi: 10.1016/j.ijbiomac.2018.09.204.

Lifshitz, E. M., Kosevich, A. M. and Pitaevskii, L. P. (1986) *Theory of Elasticity*. 3rd edn. Oxford: Elsevier. doi: 10.1016/C2009-0-25521-8.

Lin, N. *et al.* (2011) 'Preparation, modification, and application of starch nanocrystals in nanomaterials: A review', *Journal of Nanomaterials*, 2011. doi: 10.1155/2011/573687.

Liu, B. *et al.* (2019) 'Promoted strain-induced crystallization of cis-1, 4-polyisoprene with functional carbon nanodots', *Advanced Industrial and Engineering Polymer Research*, 2(1), pp. 25–31. doi:

10.1016/j.aiepr.2019.01.002.

Liu, C. *et al.* (2002) 'Chemically Cross-Linked Polycyclooctene : Synthesis , Characterization , and Shape Memory Behavior', *Macromolecules*, 35(27), pp. 9868–9874.

Liu, C. *et al.* (2020) 'Using epoxidized solution polymerized styrene-butadiene rubbers (ESSBRs) as coupling agents to modify silica without volatile organic compounds', *Polymers*, 12(6). doi: 10.3390/POLYM12061257.

Liu, C. and Mather, P. T. (2002) 'Proceedings of the Annual Technical Conference - Society of Plastics Engineers, 60th (Vol. 3)', in. Brookfield: Society of Plastics Engineers, pp. 2685–2689.

Liu, C., Qin, H. and Mather, P. T. (2007) 'Review of progress in shape-memory polymers', *Journal of Materials Chemistry*, 17(16), pp. 1543–1558. doi: 10.1039/b615954k.

Liu, J. *et al.* (2015) 'New evidence disclosed for networking in natural rubber by dielectric relaxation spectroscopy', *Soft Matter*, 11(11), pp. 2290–2299. doi: 10.1039/c4sm02521k.

Liu, X. *et al.* (2010) 'Kinetics and mechanism of thermal decomposition of cornstarches with different amylose/amylopectin ratios', *Starch/Staerke*, 62(3–4), pp. 139–146. doi: 10.1002/star.200900202.

Liu, Y. *et al.* (2016) 'High Performance Shape Memory Epoxy/Carbon Nanotube Nanocomposites', *ACS Applied Materials and Interfaces*, 8(1), pp. 311–320. doi: 10.1021/acsami.5b08766.

Liu, Y. *et al.* (2018) 'Liquid Crystalline Behaviors of Chitin Nanocrystals and Their Reinforcing Effect on Natural Rubber', *ACS Sustainable Chemistry and Engineering*, 6(1), pp. 325–336. doi: 10.1021/acssuschemeng.7b02586.

Loos, K. *et al.* (2020) 'Strain-induced crystallisation in natural rubber: a thermodynamically consistent model of the material behaviour using a multiphase approach', *Continuum Mechanics and Thermodynamics*, 32(2), pp. 501–526. doi: 10.1007/s00161-019-00859-y.

Low, B. (2022) 'MRC TO REVIVE RUBBER INDUSTRY', *The Star*, 3 June.

Luo, X. and Mather, P. T. (2010) 'Conductive shape memory nanocomposites for high speed electrical actuation', *Soft Matter*, 6(10), pp. 2146–2149. doi: 10.1039/c001295e.

Maciejewska, M. and Sowińska, A. (2021) 'Influence of fillers and ionic liquids on the crosslinking and performance of natural rubber biocomposites', *Polymers*, 13(10). doi: 10.3390/polym13101656.

Madden, J. D. W. *et al.* (2004) 'Artificial Muscle Technology: Physical Principles and Naval Prospects', *IEEE Journal of Oceanic Engineering*, 29(3), pp. 706–728. doi: 10.1109/JOE.2004.833135.

Mager, D. M. and Thomas, A. D. (2011) 'Extracellular polysaccharides from cyanobacterial soil crusts: A review of their role in dryland soil processes', *Journal of Arid Environments*, 75(2), pp. 91–97. doi: 10.1016/j.jaridenv.2010.10.001.

Mahmoud, M. *et al.* (2020) 'A review of mechanical energy storage systems combined with wind and solar applications', *Energy Conversion and Management*, 210(December 2019), p. 112670. doi: 10.1016/j.enconman.2020.112670.

Manaila, E., Daniela, M. and Craciu, G. (2012) 'Aspects Regarding Radiation Crosslinking of Elastomers', *Advanced Elastomers - Technology, Properties and Applications*, (July 2015). doi: 10.5772/47747.

Marković, G. *et al.* (2020) 'Crosslinking of Polymers: Rubber Vulcanization', in *Reactive and Functional Polymers Volume Two*. 1st edn. Springer, Cham, pp. 117–134. doi: 10.1007/978-3-030-45135-6_5.

Martins, P. C., Latorres, J. M. and Martins, V. G. (2022) 'Impact of starch nanocrystals on the physicochemical, thermal and structural characteristics of starch-based films', *LWT*, 156, p. 113041. doi: 10.1016/j.lwt.2021.113041.

Materne, T., Corvasce, F. and Leitz, P. (2000) 'EP 0 995 775 A1', *European Patent Office*. Available at: https://patentimages.storage.googleapis.com/5d/82/12/62aadb34714746/EP0995775A1.pdf.

Mélé, P. *et al.* (2011) 'Reinforcing Mechanisms of Starch Nanocrystals in a Nonvulcanized Natural Rubber Matrix', *Biomacromolecules*, 12(5), pp. 1487–1493. doi: 10.1021/bm101443a.

Meng, H. and Li, G. (2016) 'Controlled Activation Schemes of SMPs for Aerospace Appplications', in *Shape-Memory Polymers for Aerospace Applications*. 1st edn. Lancaster, Pennsylvania: DEStech Publications, Inc, pp. 1–25.

Meng, Q. and Hu, J. (2009) 'A review of shape memory polymer composites and blends', *Composites Part A: Applied Science and Manufacturing*, 40(11), pp. 1661–1672. doi: 10.1016/j.compositesa.2009.08.011.

Meng, Y., Jiang, J. and Anthamatten, M. (2016) 'Body temperature triggered shape-memory polymers with high elastic energy storage capacity', *Journal of Polymer Science, Part B: Polymer Physics*, 54(14), pp. 1397–1404. doi: 10.1002/polb.23990.

Miguel Martín-Martínez, J. (2002) 'Rubber base adhesives', in Dillard, D. A., Pocius, A. V., and Chaudhury, M. (eds) *Adhesion Science and Engineering*. Elsevier, pp. 573–675. doi: 10.1016/B978-044451140-9/50013-5.

Mishra, J. (2017) 'Smart Materials-Types SS and their Application: A Review', *International Journal of Mechanical And Production Engineering*, (5), pp. 2321–2071. Available at: http://www.iraj.in/journal/journal_file/journal_pdf/2-427-15173758871-3.pdf.

Mitali, J., Dhinakaran, S. and Mohamad, A. A. (2022) 'Energy storage systems : A review', *Energy Storage and Saving*, pp. 0–161. doi: 10.1016/j.enss.2022.07.002.

Mooney, M. (1940) 'A theory of large elastic deformation', *Journal of Applied Physics*, 11(9), pp. 582–592. doi: 10.1063/1.1712836.

Mudzviti, S. and Matai, J. (2019) 'Rubber from Euphorbia Matebelensis Latex', in Chirisa, I. (ed.) *The Sustainable Ethic in the Management of the Physical, Infrastructural and Natural Resources of Zimbabwe*. 1st edn. Langaa RPCIG, pp. 399–422.

Mujtaba, M. *et al.* (2019) 'Production of novel chia-mucilage nanocomposite films with starch nanocrystals; An inclusive biological and physicochemical perspective', *International Journal of Biological Macromolecules*, 133, pp. 663–673. doi: 10.1016/j.ijbiomac.2019.04.146.

Musto, P. (2013) 'Grand challenges in polymer chemistry: Energy, environment, health', *Frontiers in Chemistry*, 1(December), pp. 31–34. doi: 10.3389/fchem.2013.00031.

Nabavitabatabayi, M. *et al.* (2014) 'Numerical analysis of a thermally enhanced domestic hot water tank', *Applied Energy*, 129, pp. 253–260. doi: 10.1016/j.apenergy.2014.04.081.

Nadeem, F. *et al.* (2019) 'Comparative review of energy storage systems, their roles, and impacts on future power systems', *IEEE Access*, 7, pp. 4555–4585. doi: 10.1109/ACCESS.2018.2888497.

Nair, A. B. and Joseph, R. (2014) *Eco-friendly bio-composites using natural rubber (NR) matrices and natural fiber reinforcements*, *Chemistry, Manufacture and Applications of Natural Rubber*. doi: 10.1533/9780857096913.2.249.

Nair, K. G. *et al.* (2003) 'Crab shell chitin whiskers reinforced natural rubber nanocomposites. 3.

Effect of Chemical Modification of chitin whiskers', *Biomacromolecules*, 4(6), pp. 1835–1842. doi: 10.1021/bm030058g.

Namathoti, S. and Vakkalagadda, M. R. K. (2023) 'Mechanical and Shape Recovery Characterization of MWCNTs/HNTs-Reinforced Thermal-Responsive Shape-Memory Polymer Nanocomposites', *Polymers*, 15(3), p. 710. doi: 10.3390/polym15030710.

Namazi, H. and Dadkhah, A. (2008) 'Surface Modification of Starch Nanocrystals Through Ring-Opening Polymerization of e-Caprolactone and Investigation of Their Microstructures', *Journal of Applied Polymer Science*, 110(5), pp. 2405–2412. doi: 10.1002/app.

Namazi, H. and Dadkhah, A. (2010) 'Convenient method for preparation of hydrophobically modified starch nanocrystals with using fatty acids', *Carbohydrate Polymers*, 79(3), pp. 731–737. doi: 10.1016/j.carbpol.2009.09.033.

Nara, S. and Komiya, T. (1983) 'Studies on the Relationship Between Water-satured State and Crystallinity by the Diffraction Method for Moistened Potato Starch', *Starch - Stärke*, 35(12), pp. 407–410. doi: 10.1002/star.19830351202.

Navarro-Baena, I. *et al.* (2016) 'Design of biodegradable blends based on PLA and PCL: From morphological, thermal and mechanical studies to shape memory behavior', *Polymer Degradation and Stability*, 132, pp. 97–108. doi: 10.1016/j.polymdegradstab.2016.03.037.

Neus Angles, M. and Dufresne, A. (2000) 'Plasticized starch/tuniein whiskers nanocomposites. 1. Structural analysis', *Macromolecules*, 33(22), pp. 8344–8353. doi: 10.1021/ma0008701.

Ngudsuntear, K. *et al.* (2022) 'Mechanical and Aging Properties of Hydrogenated Epoxidized Natural Rubber and Its Lifetime Prediction', *ACS Omega*, 7(41), pp. 36448–36456. doi: 10.1021/acsomega.2c04225.

Nie, Y. *et al.* (2011) 'Structural evolution during uniaxial deformation of natural rubber reinforced with nano-alumina', *Polymers for Advanced Technologies*, 22(12), pp. 2001–2008. doi: 10.1002/pat.1709.

Nie, Y. *et al.* (2017) 'Features of strain-induced crystallization of natural rubber revealed by experiments and simulations', *Polymer Journal*, 49(3), pp. 309–317. doi: 10.1038/pj.2016.114.

Nocil, L. (2010) 'NR Latex & Latex Products', *Technical Note: NR-Latex & Latex Products*, pp. 1–56.

Nsitem, N. (2024) *Global Energy Storage Market Records Biggest Jump Yet*, *BloombergNEF*. Available at: https://about.bnef.com/blog/global-energy-storage-market-records-biggest-jump-yet/ (Accessed: 11 September 2024).

Olabi, A. G. *et al.* (2021) 'Critical review of energy storage systems', *Energy*, 214, p. 118987. doi: 10.1016/j.energy.2020.118987.

Olabi, A. G. and Grunwald, A. (2008) 'Design and application of magnetostrictive materials', *Materials and Design*, 29(2), pp. 469–483. doi: 10.1016/j.matdes.2006.12.016.

Onions, A. (2020) *Rubber Compounding*, *MacLellan rubber*. Available at: https://maclellanrubber.com/blog/article/rubber-compounding (Accessed: 3 May 2022).

Osada, Y. (1995) 'Heat-sensitive Reversible Shape-memory Hydrogels'. Jpn.

Osman, A. I. *et al.* (2023) 'Cost, environmental impact, and resilience of renewable energy under a changing climate: a review', *Environmental Chemistry Letters*, 21(2), pp. 741–764. doi: 10.1007/s10311-022-01532-8.

Ou, S.-F. *et al.* (2023) 'Effects of superelasticity and shape memory ability of NiTi-based alloys on deposition efficiency of ultrasonic-assisted coating', *Journal of Alloys and Compounds*, 937, p. 168189. doi: 10.1016/j.jallcom.2022.168189.

Ouyang, Q. *et al.* (2021) 'Structural changes of A-, B- and C-type starches of corn, potato and pea as influenced by sonication temperature and their relationships with digestibility', *Food Chemistry*, 358, p. 129858. doi: 10.1016/j.foodchem.2021.129858.

Owen, M. J. (2001) 'Elastomers: Siloxane', *Encyclopedia of Materials: Science and Technology*. 2nd edn. Elsevier. Available at: https://doi.org/10.1016/B0-08-043152-6/00448-4.

Oyama, T. (2014) 'Cross-Linked Polymer Synthesis Syntheses of Chemically Cross-Linked Polymers Formation of Cross-Linked Structure by Polymerization', pp. 1–11. doi: 10.1007/978-3-642-36199-9.

Özdemir, T. (2020) 'Elastomeric micro- and nanocomposites for neutron shielding', *Micro and Nanostructured Composite Materials for Neutron Shielding Applications*, pp. 125–137. doi: 10.1016/b978-0-12-819459-1.00005-2.

Pan, Q. and Cho, N. (2007) 'The investigation of a shape memory alloy micro-damper for MEMS applications', *Sensors*, 7(9), pp. 1887–1900. doi: 10.3390/s7091887.

Paris, M. *et al.* (1999) 'Crystallinity and structuring role of water in native and recrystallized starches by 13C CP-MAS NMR spectroscopy. 1: Spectral decomposition', *Carbohydrate Polymers*, 39(4), pp. 327–339. doi: 10.1016/S0144-8617(99)00022-3.

Piyada, K., Waranyou, S. and Thawien, W. (2013) 'Mechanical, thermal and structural properties of rice starch films reinforced with rice starch nanocrystals', *International Food Research Journal*, 20(1), pp. 439–449.

Poh, B. T. and Tan, B. K. (1991) 'Mooney scorch time of epoxidized natural rubber', *Journal of Applied Polymer Science*, 42(5), pp. 1407–1416. doi: 10.1002/app.1991.070420525.

Poh, G. K. X., Chew, I. M. L. and Tan, J. (2019) 'Life Cycle Optimization for Synthetic Rubber Glove Manufacturing', *Chemical Engineering and Technology*, 42(9), pp. 1771–1779. doi: 10.1002/ceat.201800476.

Ponnamma, D. *et al.* (2013) *Rubber Nanocomposites: Latest Trends and Concepts*. doi: 10.1007/978-3-642-20928-4_3.

Pradhan, S. *et al.* (2022) 'An insight into mechanical & thermal properties of shape memory polymer reinforced with nanofillers; a critical review', *Materials Today: Proceedings*, 50, pp. 1107–1112. doi: 10.1016/j.matpr.2021.07.504.

Princi, E. (2019) '8. Manufacturing and transformation technologies', *Rubber*, pp. 147–164. doi: 10.1515/9783110640328-008.

Putaux, J. L. *et al.* (2003) 'Platelet nanocrystals resulting from the disruption of waxy maize starch granules by acid hydrolysis', *Biomacromolecules*, 4(5), pp. 1198–1202. doi: 10.1021/bm0340422.

Qader, I. N., Kök, M. and Dağdelen, F. (2019) 'Effect of heat treatment on thermodynamics parameters, crystal and microstructure of (Cu-Al-Ni-Hf) shape memory alloy', *Physica B: Condensed Matter*, 553(October 2018), pp. 1–5. doi: 10.1016/j.physb.2018.10.021.

Qu, L. *et al.* (2009) 'Remarkable reinforcement of natural rubber by deformation-induced crystallization in the presence of organophilic montmorillonite', *Acta Materialia*, 57(17), pp. 5053–5060. doi: 10.1016/j.actamat.2009.07.007.

Quitmann, D. *et al.* (2013) 'Solvent-sensitive reversible stress-response of shape memory natural

rubber', *ACS Applied Materials and Interfaces*, 5(9), pp. 3504–3507. doi: 10.1021/am400660f.

Quitmann, D. *et al.* (2014) 'Environmental memory of polymer networks under stress', *Advanced Materials*, 26(21), pp. 3441–3444. doi: 10.1002/adma.201305698.

Quitmann, D. *et al.* (2015) 'Programming of shape memory natural rubber for near-discrete shape transitions', *ACS Applied Materials and Interfaces*, 7(3), pp. 1486–1490. doi: 10.1021/am507184c.

Rabiei, S. and Shojaei, A. (2016) 'Vulcanization kinetics and reversion behavior of natural rubber/styrene-butadiene rubber blend filled with nanodiamond - The role of sulfur curing system', *European Polymer Journal*, 81, pp. 98–113. doi: 10.1016/j.eurpolymj.2016.05.021.

Rad, F. M. and Fung, A. S. (2016) 'Solar community heating and cooling system with borehole thermal energy storage - Review of systems', *Renewable and Sustainable Energy Reviews*, 60, pp. 1550–1561. doi: 10.1016/j.rser.2016.03.025.

Rajisha, K. R. *et al.* (2014) 'Preparation and characterization of potato starch nanocrystal reinforced natural rubber nanocomposites', *International Journal of Biological Macromolecules*, 67, pp. 147–153. doi: 10.1016/j.ijbiomac.2014.03.013.

Rajisha, K. R. *et al.* (2015) 'Preparation and Characterization of Corn Starch Nanocrystal Reinforced Natural Rubber Nanocomposites via Co-coagulation Process', *InCIEC 2014*. doi: 10.1007/978-981-287-290-6.

Raksaksri, L. *et al.* (2017) 'Use of TBzTD as Noncarcinogenic Accelerator for ENR/SiO2 Nanocomposites: Cured Characteristics, Mechanical Properties, Thermal Behaviors, and Oil Resistance', *International Journal of Polymer Science*, 2017, pp. 12–18. doi: 10.1155/2017/9721934.

Ralon, P. *et al.* (2017) *Electricity storage and renewables: Costs and markets to 2030*, *International Renewable Energy Agency*. Available at: http://irena.org/publications/2017/Oct/Electricity-storage-and-renewables-costs-and-markets%0Ahttps://www.irena.org/-/media/Files/IRENA/Agency/Publication/2017/Oct/IRENA_Electricity_Storage_Costs_2017.pdf.

Ramezani, M. and Ripin, Z. M. (2012) 'Characteristics of elastomer materials', in *Rubber-Pad Forming Process*. 1st edn. Swaston: Woodhead, pp. 43–64.

Ramli, R. *et al.* (2020) 'Preliminary study on epoxidized natural rubber latex composites intended for shoe soles applic', *International Journal of Emerging Trends in Engineering Research*, 8(1 1.2 Special Issue), pp. 122–131. doi: 10.30534/ijeter/2020/1781.22020.

Ramli, R. *et al.* (2022) 'PREPARATION AND CHARACTERIZATION OF SPECIALTY NATURAL RUBBER LATEX CONCENTRATE', *Rubber Chemistry and Technology*, 95(1), pp. 101–118. doi: 10.5254/RCT.21.79945.

Rapp, S. and Baier, H. (2010) 'Determination of recovery energy densities of shape memory polymers via closed-loop, force-controlled recovery cycling', *Smart Materials and Structures*, 19(4). doi: 10.1088/0964-1726/19/4/045018.

Ratna, D. and Karger-Kocsis, J. (2008) 'Recent advances in shape memory polymers and composites: A review', *Journal of Materials Science*, 43(1), pp. 254–269. doi: 10.1007/s10853-007-2176-7.

Ratner, B. D. (2012) 'Polymeric Implants', in *Polymer Science: A Comprehensive Reference*. Elsevier, pp. 397–411. doi: 10.1016/B978-0-444-53349-4.00230-2.

Rattanasom, N., Prasertsri, S. and Ruangritnumchai, T. (2009) 'Comparison of the mechanical properties at similar hardness level of natural rubber filled with various reinforcing-fillers', *Polymer Testing*, 28(1), pp. 8–12. doi: 10.1016/j.polymertesting.2008.08.004.

Reghunadhan, A. *et al.* (2021) 'Shape Memory Materials from Rubbers', *Materials*, 14(23), pp. 1–19. doi: 10.3390/ma14237216.

Rehman, S., Al-Hadhrami, L. M. and Alam, M. M. (2015) 'Pumped hydro energy storage system: A technological review', *Renewable and Sustainable Energy Reviews*, 44, pp. 586–598. doi: 10.1016/j.rser.2014.12.040.

Ren, X. *et al.* (2022) 'Sustainable Epoxidized Guayule Natural Rubber, Blends and Composites with Improved Oil Resistance and Greater Stiffness', *Materials*, 15(11), pp. 1–14. doi: 10.3390/ma15113946.

Rezende, R. *et al.* (2019) 'NUMERICAL MODELING OF ELASTOMERIC SUPPORT DEVICES IN BRIDGE', (November).

Riffat SB, M. A. (2015) 'Building Energy Consumption and Carbon dioxide Emissions: Threat to Climate Change', *Journal of Earth Science & Climatic Change*, s3, pp. 1–3. doi: 10.4172/2157-7617.s3-001.

Rivlin, R. . (1948) 'Large Elastic Deformations of Isotropic Materials IV. Further Development of the General Theory', *Philosophical Transactions of the Royal Society of London*, 240, pp. 459–490.

Roberts, A. D. (ed.) (1988) *Natural Rubber Science and Technology*. Oxford: Oxford University Press.

Robertson, C. G. and Hardman, N. J. (2021) 'Nature of carbon black reinforcement of rubber: Perspective on the original polymer nanocomposite', *Polymers*, 13(4), pp. 1–28. doi: 10.3390/polym13040538.

Rousseau, I. A. (2008) 'Challenges of Shape Memory Polymers: A Review ofthe Progress Toward Overcoming SMP's Limitations', *POLYMER ENGINEERING AND SCIENCE*, 48, pp. 2075–2089. doi: 10.1002/pen.21213.

Saadoun Al Azzawi, W. (2023) 'Analytical and Experimental Analysis of the Shape Recovery Behavior of Continuous Fiber Reinforced Shape Memory Polymer', *Diyala Journal of Engineering Sciences*, pp. 49–58. doi: 10.24237/djes.2023.160404.

Sadequl, A. M., Poh, B. T. and Ishiaku, U. S. (1999) 'Effect of filler loading on the mechanical properties of epoxidized natural rubber (ENR 25) compared with natural rubber (SMR L)', *International Journal of Polymeric Materials and Polymeric Biomaterials*, 43(3–4), pp. 261–278. doi: 10.1080/00914039908009689.

Saeb, M. R., Ramezani-Dakhel, H. and Esteki, B. (2012) 'Correlation between the crosslink density and mechanical properties of the natural rubber nanocomposites', *AIP Conference Proceedings*, 1459(1), pp. 83–85. doi: 10.1063/1.4738405.

Bin Samsuri, A. and Abdullahi, A. A. (2017) 'Degradation of Natural Rubber and Synthetic Elastomers', in *Reference Module in Materials Science and Materials Engineering*. Amsterdam: Elsevier. doi: 10.1016/B978-0-12-803581-8.09212-2.

Santoro, M., Nicolay, O. F. and Cangialosi, T. J. (2001) 'Pseudoelasticity and thermoelasticity of nickel-titanium alloys: A clinically oriented review. Part I: Temperature transitional ranges', *American Journal of Orthodontics and Dentofacial Orthopedics*, 119(6), pp. 587–593. doi: 10.1067/mod.2001.112446.

Sarbu, I. and Sebarchievici, C. (2016) 'Thermal Energy Storage', in *Solar Heating and Cooling Systems: Fundamentals, Experiments and Applications*. 1st edn. Elsevier, pp. 99–138.

Sasitaran, M. *et al.* (2016) 'Preparation and Characterisation of crosslinked nr and enr blends 2017', *ASEAN Journal on Science and Technology for Development*, 34(2), pp. 106–118.

Schaefer, R. J. (2002) 'Mechanical Properties of Rubber', in Piersol, A. G. and Paez, T. (eds) *Harris' Shock and Vibration Handbook*. 6th edn. New York: McGraw Hill.

Schwartz, M. (2016) 'Elastomers', in *Encyclopedia and Handbook of Materials, Parts and Finishes*. 3rd edn. Boca Raton: Taylor & Francis, pp. 283–321.

Seo, G. *et al.* (2017) 'Reinforcement of Rubber Properties by Carbon Black and Silica Fillers : A Review', 52(2), pp. 1–17. Available at: http://www.koreascience.kr/article/JAKO201722647668600.pdf.

Sessini, V., Navarro-Baena, I., *et al.* (2018) 'Effect of the addition of polyester-grafted-cellulose nanocrystals on the shape memory properties of biodegradable PLA/PCL nanocomposites', *Polymer Degradation and Stability*, 152, pp. 126–138. doi: 10.1016/j.polymdegradstab.2018.04.012.

Sessini, V., Brox, D., *et al.* (2018) 'Thermally activated shape memory behavior of copolymers based on ethylene reinforced with silica nanoparticles', *Nanocomposites*, 4(2), pp. 19–35. doi: 10.1080/20550324.2018.1472723.

Setyadewi, N. M. and Indrajati, I. N. (2019) 'Shape Memory Behavior of Shape Memory Natural Rubber', *IOP Conference Series: Materials Science and Engineering*, 553(1). doi: 10.1088/1757-899X/553/1/012050.

Shirole, A. *et al.* (2018) 'Tailoring the Properties of a Shape-Memory Polyurethane via Nanocomposite Formation and Nucleation', *Macromolecules*, 51(5), pp. 1841–1849. doi: 10.1021/acs.macromol.7b01728.

Shoji, S. and Masui, K. (2015) *Encyclopedia of Polymeric Nanomaterials*, *Encyclopedia of Polymeric Nanomaterials*. doi: 10.1007/978-3-642-29648-2.

Shrivastava, A. (2018) 'Introduction to Plastics Engineering', *Introduction to Plastics Engineering*, pp. 1–16. doi: 10.1016/b978-0-323-39500-7.00001-0.

Šimkovic, I. and Jakab, E. (2001) 'Thermogravimetry/mass spectrometry study of weakly basic starch-based ion exchanger', *Carbohydrate Polymers*, 45(1), pp. 53–59. doi: 10.1016/S0144-8617(00)00230-7.

Sina Ebnesajjad (2016) *Introduction To Plastics*, *Chemical Resistance of Commodity Thermoplastics*. Elsevier Inc. doi: 10.1016/b978-075065148-6/50001-5.

Sisanth, K. S. *et al.* (2017) 'General introduction to rubber compounding', in *Progress in Rubber Nanocomposites*. 1st edn. Swaston: Woodhead, pp. 1–39. doi: https://doi.org/10.1016/C2014-0-03997-4.

Small IV, W. *et al.* (2005) 'Laser-activated shape memory polymer intravascular thrombectomy device', *Optics Express*, 13(20), p. 8204. doi: 10.1364/opex.13.008204.

Socaciu, L. (2012) 'Seasonal thermal energy storage.', *Applied Mathematics and Mechanics*, 55(IV), pp. 775–784. doi: 10.1299/jsmemag.97.912_937.

Soliman, A. A. A., El-Shinnawy, N. A. and Mobarak, F. (1997) 'Thermal behaviour of starch and oxidized starch', *Thermochimica Acta*, 296(1–2), pp. 149–153. doi: 10.1016/S0040-6031(97)00040-3.

Somseemee, O. *et al.* (2022) 'Enhanced interfacial interaction between modified cellulose nanocrystals and epoxidized natural rubber via ultraviolet irradiation', *Scientific Reports*, 12(1), pp. 1–13. doi: 10.1038/s41598-022-10558-5.

Spanner, K. and Koc, B. (2016) 'Piezoelectric motors, an overview', *Actuators*, 5(1). doi: 10.3390/act5010006.

Sun, H. *et al.* (2011) 'Influence of amount of sulfur on mechanical, dynamic, and shape-memory properties of trans-1,4-polyisoprene', *Journal of Macromolecular Science, Part B: Physics*, 50(5), pp. 871–879. doi: 10.1080/00222348.2010.497034.

Surya, I., Sukeksi, L. and Hayeemasae, N. (2018) 'Studies on cure index, swelling behaviour, tensile and thermooxidative properties of natural rubber compounds in the presence of alkanolamide', *IOP Conference Series: Materials Science and Engineering*, 309(1). doi: 10.1088/1757-899X/309/1/012060.

Svihus, B., Uhlen, A. K. and Harstad, O. M. (2005) 'Effect of starch granule structure, associated components and processing on nutritive value of cereal starch: A review', *Animal Feed Science and Technology*, 122(3–4), pp. 303–320. doi: 10.1016/j.anifeedsci.2005.02.025.

Swinkels, J. J. M. (1985) 'Composition and Properties of Commercial Native Starches', *Starch - Stärke*, 37(1), pp. 1–5. doi: 10.1002/star.19850370102.

Tan, Y. W. *et al.* (2024a) 'Effectiveness of Starch Nanocrystals on Mechanical and Shape Memory Behaviour of Smart Rubber', *International Journal of Nanoelectronics and Materials (IJNeaM)*, 17(June), pp. 61–68. doi: 10.58915/ijneam.v17iJune.836.

Tan, Y. W. *et al.* (2024b) 'Energy Storage Capacity of Shape Memory Natural Rubber Nanocomposite Films', in *Material Strength and Applied Mechanics*. IOS Press, pp. 277–283. doi: 10.3233/ATDE240556.

Tanaka, Y. *et al.* (1996) 'DEPROTEINIZED NATURAL RUBBER LATEX AND ITS PRODUCTION PROCESS'. Japan: United States Patent. Available at: https://patentimages.storage.googleapis.com/74/29/86/05b990b2080ffd/US5569740.pdf.

Tang, L.-C. *et al.* (2019) 'Mechanical Properties of Rubber Nanocomposites Containing Carbon Nanofillers', in Yaragalla, S., Mishra, R. K., and Maria, H. J. (eds) *Carbon-Based Nanofillers and Their Rubber Nanocomposites*. 1st edn. Amsterdam: Elsevier, pp. 367–423. doi: https://doi.org/10.1016/C2018-0-02522-0.

Tanrattanakul, V. *et al.* (2003) 'In situ epoxidized natural rubber: Improved oil resistance of natural rubber', *Journal of Applied Polymer Science*, 90(1), pp. 261–269. doi: 10.1002/app.12706.

Terai, T. (2002) 'Reversible Thermal Recording Media Comprising Shape Memory Polymers and Showing Good Image Storability'. Jpn.

Thakur, S. (2016) *Shape Memory Polymers for Smart Textile Applications*. 1st edn. Edited by B. Kumar. London: IntechOpen. doi: 10.5772/66015.

Thielemans, W., Belgacem, M. N. and Dufresne, A. (2006) 'Starch nanocrystals with large chain surface modifications', *Langmuir*, 22(10), pp. 4804–4810. doi: 10.1021/la053394m.

Toki, S. *et al.* (2004) 'Strain-induced molecular orientation and crystallization in natural and synthetic rubbers under uniaxial deformation by in-situ synchrotron X-ray study', *Rubber Chemistry and Technology*, 77(2), pp. 317–335. doi: 10.5254/1.3547826.

Toki, S. *et al.* (2009) 'New insights into the relationship between network structure and strain-induced crystallization in un-vulcanized and vulcanized natural rubber by synchrotron X-ray diffraction', *Polymer*, 50(9), pp. 2142–2148. doi: 10.1016/j.polymer.2009.03.001.

Toki, S. *et al.* (2013) 'Entanglements and networks to strain-induced crystallization and stress-strain relations in natural rubber and synthetic polyisoprene at various temperatures', *Macromolecules*, 46(13), pp. 5238–5248. doi: 10.1021/ma400504k.

Toki, S., Fujimaki, T. and Okuyama, M. (2000) 'Strain-induced crystallization of natural rubber as

detected real-time by wide- angle X-ray diffraction technique', *Polymer*, 41(14), pp. 5423–5429. doi: 10.1016/S0032-3861(99)00724-7.

Toozandehjani, M. (2018) 'Conventional and Advanced Composites in Aerospace Industry: Technologies Revisited', *American Journal of Aerospace Engineering*, 5(1), p. 9. doi: 10.11648/j.ajae.20180501.12.

Tosaka, M. *et al.* (2004) 'Orientation and Crystallization of Natural Rubber Network As Revealed by WAXD Using Synchrotron Radiation', *Macromolecules*, 37(9), pp. 3299–3309. doi: 10.1021/ma0355608.

Trabelsi, S., Albouy, P. A. and Rault, J. (2003) 'Crystallization and Melting Processes in Vulcanized Stretched Natural Rubber', *Macromolecules*, 36(20), pp. 7624–7639. doi: 10.1021/ma030224c.

Tsai, Y. C. and Chiu, C. C. (2022) 'Solute Diffusivity and Local Free Volume in Cross-Linked Polymer Network: Implication of Optimizing the Conductivity of Polymer Electrolyte', *Polymers*, 14(10). doi: 10.3390/polym14102061.

Ushak, S., Fernández, A. G. and Grageda, M. (2015) *Using molten salts and other liquid sensible storage media in thermal energy storage (TES) systems*, *Advances in Thermal Energy Storage Systems: Methods and Applications*. Woodhead Publishing Limited. doi: 10.1533/9781782420965.1.49.

Utrilla-Coello, R. G. *et al.* (2014) 'Acid hydrolysis of native corn starch: Morphology, crystallinity, rheological and thermal properties', *Carbohydrate Polymers*, 103(1), pp. 596–602. doi: 10.1016/j.carbpol.2014.01.046.

Valodkar, M. and Thakore, S. (2010) 'Thermal and mechanical properties of natural rubber and starch nanobiocomposites', *International Journal of Polymer Analysis and Characterization*, 15(6), pp. 387–395. doi: 10.1080/1023666X.2010.500543.

Vazquez, S. *et al.* (2010) 'Energy storage systems for transport and grid applications', *IEEE Transactions on Industrial Electronics*, 57(12), pp. 3881–3895. doi: 10.1109/TIE.2010.2076414.

Viguié, J., Molina-Boisseau, S. and Dufresne, A. (2007) 'Processing and characterization of waxy maize starch films plasticized by sorbitol and reinforced with starch nanocrystals', *Macromolecular Bioscience*, 7(11), pp. 1206–1216. doi: 10.1002/mabi.200700136.

Voit, W. *et al.* (2010) 'High-strain shape-memory polymers', *Advanced Functional Materials*, 20(1), pp. 162–171. doi: 10.1002/adfm.200901409.

Wan, N. Y., Chin, K. P. and Saad, C. S. M. (2010) 'Comparison of epoxidised natural rubber (enr) 37.5 and enr 25/ enr 50 physical blend: Specialty polymer for "green tyre" application', *IOP Conference Series: Materials Science and Engineering*, 11, p. 012004. doi: 10.1088/1757-899x/11/1/012004.

Wang, M., Guo, L. and Sun, H. (2019) 'Manufacture of Biomaterials', *Encyclopedia of Biomedical Engineering*. 1st edn. Elsevier. Available at: https://doi.org/10.1016/B978-0-12-801238-3.11027-X.

Wang, Q. *et al.* (2023) 'Nano-crosslinked dynamic hydrogels for biomedical applications', *Materials Today Bio*, 20, p. 100640. doi: 10.1016/j.mtbio.2023.100640.

Wang, W. *et al.* (2016) 'Novel Slide-Ring Material/Natural Rubber Composites with High Damping Property', *Scientific Reports*, 6(February), pp. 1–13. doi: 10.1038/srep22810.

Wang, W. *et al.* (2023) 'Development and Prospect of Smart Materials and Structures for Aerospace Sensing Systems and Applications', *Sensors*, 23(3), p. 1545. doi: 10.3390/s23031545.

Wang, Z. F. *et al.* (2010) 'Thermal stability and mechanical properties of modified starch/NR

composite', *Journal of Polymer Materials*, 27(3), pp. 283–292.

Wee, J. S. H., Chai, A. B. and Ho, J. H. (2017) 'Fabrication of shape memory natural rubber using palmitic acid', *Journal of King Saud University - Science*, 29(4), pp. 494–501. doi: 10.1016/j.jksus.2017.09.003.

Wei, B. *et al.* (2015) 'Thermal degradation behavior of hypochlorite-oxidized starch nanocrystals under different oxidized levels', *Carbohydrate Polymers*, 124, pp. 124–130. doi: 10.1016/j.carbpol.2015.01.081.

Wei, P. *et al.* (2019) 'Unique Stress Whitening and High-Toughness Double-Cross-Linked Cellulose Films', *ACS Sustainable Chemistry & Engineering*, 7(1), pp. 1707–1717. doi: 10.1021/acssuschemeng.8b05485.

Weng, G. *et al.* (2010) 'Large-scale orientation in a vulcanized stretched natural rubber network: Proved by in situ synchrotron x-ray diffraction characterization', *Journal of Physical Chemistry B*, 114(21), pp. 7179–7188. doi: 10.1021/jp100920g.

Wetzel, B., Haupert, F. and Zhang, M. Q. (2003) 'Epoxy nanocomposites with high mechanical and tribological performance', *Composites Science and Technology*, 63(14), pp. 2055–2067. doi: 10.1016/S0266-3538(03)00115-5.

Whitby, G. S. and Simmons, H. E. (1925) 'Vulcanization Accelerators-I', *Industrial and Engineering Chemistry*, 17(9), pp. 931–935. doi: 10.1021/ie50189a021.

Wongvasana, B. *et al.* (2022) 'Comparative Structure–Property Relationship between Nanoclay and Cellulose Nanofiber Reinforced Natural Rubber Nanocomposites', *Polymers*, 14(18), p. 3747. doi: 10.3390/polym14183747.

Wu, J. *et al.* (2018) 'Preparation and Physical Properties of Porous Starch/Natural Rubber Composites', *Starch/Staerke*, 70(11–12), pp. 1–8. doi: 10.1002/star.201700296.

Wu, L., Jin, C. and Sun, X. (2011) 'Synthesis, properties, and light-induced shape memory effect of multiblock polyesterurethanes containing biodegradable segments and pendant cinnamamide groups', *Biomacromolecules*, 12(1), pp. 235–241. doi: 10.1021/bm1012162.

Wu, M., McIntosh, J. and Liu, J. (2016) 'Current prevalence rate of latex allergy: Why it remains a problem?', *Journal of Occupational Health*, 58(2), pp. 138–144. doi: 10.1539/joh.15-0275-RA.

Wu, W. *et al.* (2019) 'Strengthened, recyclable shape memory rubber films with a rigid filler nano-capillary network', *Journal of Materials Chemistry A*, 7(12), pp. 6901–6910. doi: 10.1039/c9ta01266d.

Xia, Y. *et al.* (2021) 'A Review of Shape Memory Polymers and Composites: Mechanisms, Materials, and Applications', *Advanced Materials*, 33(6), pp. 1–33. doi: 10.1002/adma.202000713.

Xie, T. (2011) 'Recent advances in polymer shape memory', *Polymer*, 52(22), pp. 4985–5000. doi: 10.1016/j.polymer.2011.08.003.

Xu, Y. *et al.* (2014) 'Morphological, structural, and thermal properties of starch nanocrystals affected by different botanic origins', *Cereal Chemistry*, 91(4), pp. 383–388. doi: 10.1094/CCHEM-10-13-0222-R.

Yadav, V., Pal, D. and Poonia, A. K. (2024) 'Nanofillers as a potential key for shaping the future of the industries', *Hybrid Advances*, 7, p. 100340. doi: 10.1016/j.hybadv.2024.100340.

Yang, T. T. *et al.* (2022) 'Effect of cyclic straining with various rates on stress softening/hysteresis and structural evolution of filled rubber: A time-resolved SANS study', *Composites Part B: Engineering*,

242(June), p. 110100. doi: 10.1016/j.compositesb.2022.110100.

Yin, J. *et al.* (2022) 'Facile fabrication of high nanofiller-content natural rubber nanocomposites for reversible plasticity shape memory polymers', *Composites Science and Technology*, 221, p. 109349. doi: 10.1016/j.compscitech.2022.109349.

Yong, Z. *et al.* (2006) 'Effect of Cationic Group Content on Shape MemoryEffect in Segmented Polyurethane Cationomer', *Journal of Applied Polymer Science*, 103(5), pp. 545–556. doi: 10.1002/app.24820.

Yoo, H. J. *et al.* (2006) 'Polyurethane-carbon nanotube nanocomposites prepared by in-situ polymerization with electroactive shape memory', *Journal of Macromolecular Science, Part B: Physics*, 45 B(4), pp. 441–451. doi: 10.1080/00222340600767471.

Zamri, S. F. M. *et al.* (2017) 'Exploration on effects of 15 nm SiO2 filler on miscibility, thermal stability and ionic conductivity of PMMA/ENR 50 electrolytes', *AIP Conference Proceedings*, 1809(March 1996). doi: 10.1063/1.4975464.

Zare, M. *et al.* (2019) 'Thermally-induced two-way shape memory polymers: Mechanisms, structures, and applications', *Chemical Engineering Journal*, 374(May), pp. 706–720. doi: 10.1016/j.cej.2019.05.167.

Zende, R., Ghase, V. and Jamdar, V. (2023) 'A review on shape memory polymers', *Polymer-Plastics Technology and Materials*, 62(4), pp. 467–485. doi: 10.1080/25740881.2022.2121216.

Zhang, H. *et al.* (2009) 'A novel type of shape memory polymer blend and the shape memory mechanism', *Polymer*, 50(6), pp. 1596–1601. doi: 10.1016/j.polymer.2009.01.011.

Zhang, J. *et al.* (2012) 'Unique multifunctional thermally-induced shape memory poly(p-dioxanone)-poly(tetramethylene oxide)glycol multiblock copolymers based on the synergistic effect of two segments', *Journal of Physical Chemistry C*, 116(9), pp. 5835–5845. doi: 10.1021/jp211953q.

Zhang, P. and Li, G. (2013) 'Structural relaxation behavior of strain hardened shape memory polymer fibers for self-healing applications', *Journal of Polymer Science Part B: Polymer Physics*, 51(12), pp. 966–977. doi: 10.1002/polb.23295.

Zhang, X. *et al.* (2015) 'Sustainable shape memory polymers based on epoxidized natural rubber cured by zinc ferulate via oxa-Michael reaction', *International Journal of Smart and Nano Materials*, 6(4), pp. 195–210. doi: 10.1080/19475411.2015.1129368.

Zhang, X. *et al.* (2019) 'The Pathway to Intelligence: Using Stimuli-Responsive Materials as Building Blocks for Constructing Smart and Functional Systems', *Advanced Materials*, 31(11), pp. 1–48. doi: 10.1002/adma.201804540.

Zhong, Z. and Sun, X. S. (2005) 'Thermal characterization and phase behavior of cornstarch studied by differential scanning calorimetry', *Journal of Food Engineering*, 69(4), pp. 453–459. doi: 10.1016/j.jfoodeng.2004.07.023.

Zhu, J. *et al.* (2022) 'Bubblegum inspired epoxidized natural rubber composites for superior mechanical and electrical properties', *Polymer*, 257(September), p. 125286. doi: 10.1016/j.polymer.2022.125286.

Zou, Y. *et al.* (2023) 'Biobased Recyclable Rubbers With Shape Memory, Self-welding, and Damping Properties by Cross-Linking Epoxidized Natural Rubber with Succinic Anhydride', *ACS Sustainable Chemistry & Engineering*, 11(51), pp. 18123–18130. doi: 10.1021/acssuschemeng.3c07063.

Zunic, B. and Peter, S. (2018) 'World ' s largest Science , Technology & Medicine Open Access book publisher', (2016), pp. 267–322.